Recognition of orthoflaviviral RNA in mosquitoes and viral countermeasures

Doctoral thesis

to obtain a doctorate (PhD)

from the Faculty of Medicine

of the University of Bonn

Anja vom Hemdt

from Aachen

2024

Written with authorization of

the Faculty of Medicine of the University of Bonn

First reviewer: PD Dr. rer. nat. Beate Mareike Kümmerer

Second reviewer: Prof. Dr. rer. nat. Martin Schlee

Day of oral examination: 12.01.2024

From the Institute of Virology

Director: Prof. Dr. med. Hendrik Streeck

Table of Contents

List of abbreviations

%	Percent
°C	Degree Celsius
2'-O-MTase	2'-O-methyltransferase
aa	Amino acid
Ago1	Argonaute-1
Ago2	Argonaute-2
AMP	Antimicrobial peptide
arbovirus	Arthropod-borne virus
ATP	Adenosine triphosphate
Aub	Aubergine
BHK	Baby hamster kidney
BSA	Bovine serum albumin
BSL	Biosafety Level
C3PO	Component 3 Promoter of RISC
$CaCl_2$	Calcium chloride
Cas9	CRISP-associated protein 9
CHIKV	Chikungunya virus
CIP	Calf intestinal alkaline phosphatase
CRISPR	Clustered regularly interspaced short palindromic repeats
D. melanogaster	*Drosophila melanogaster*
Dcr-1	Dicer-1
Dcr-2	Dicer-2
DENV	Dengue virus
DMEM	Dulbecco's Modified Eagle Medium
DMSO	Dimethyl sulfoxide
DNA	Deoxyribonucleic acid
dNTP	Deoxynucleotide triphosphate
Dome	Domeless
DPBS	Dulbecco's Phosphate-Buffered Saline
dsRNA	Double-stranded RNA
DUF	Domain of unknown function
E. coli	Escherichia coli
e.g.	For example
EDTA	Ethylenediamine tetra acidic acid
EIP	Extrinsic incubation period
ER	Endoplasmic reticulum
et al.	And others
EtBr	Ethidium bromide
exo-siRNA	Exogenous siRNA
FADD	Fas-associated death domain
FBS/FCS	Fetal bovine serum

FFU	Focus-forming units
FMDV	Foot-and-mouth disease virus
for	Forward
g	Gram
GMP	Guanosine monophosphate
GTase	Guanylyltransferase
GTP	Guanosine triphosphate
h	Hour
Hop	Hopscotch
ICA	Infectious Center Assay
ICTV	International Committee on Taxonomy of Viruses
IMD	Immune deficiency
IVT	*In vitro* transcription
JAK/STAT	Janus kinase/signal transducer
JEV	Japanese encephalitis virus
k.o.	Knockout
Kb	Kilobase
L-15	Leibovitz's L-15 Medium
LB	Lysogeny broth
LVP	Liverpool
m^7G cap	N-7-methylguanosine cap
MEM	Minimum Essential Medium
$MgCl_2$	Magnesium chloride
min	Minute
miRNA	Micro RNA
MOI	Multiplicity of infection
MyD88	Myeloid differentiation primary response 88
N-7-MTase	Guanine-methyltransferase
NaCl	Sodium chloride
$NaHCO_3$	Sodium bicarbonate
NaOH	Sodium hydroxide
NEAA	Non-essential amino acids
NF-κB	Nuclear factor -κB
NS	Non-structural protein
ns	Not significant
nt	Nucleotide
PAMP	Pathogen-associated molecular pattern
PBS	Dulbecco's Phosphate-Buffered Saline
PCR	Polymerase chain reaction
Pen/Strep	Penicillin/streptomycin
PFU	Plaque-forming units
PGRP	Peptidoglycan recognition receptor

pH	Potential of hydrogen
PIAS	Protein inhibitor of activated STAT
piRNA	PIWI-interacting RNA
PIWI	P-element-induced wimpy testis
poly(I:C)	Polyinosinic:polycytidylic acid
pPseAsibi	Pseudo-Asibi
pre-miRNA	Precursor miRNA
pri-miRNA	Primary miRNA
Pub	Polyubiquitin
qRT-PCR	Quantitative real-time PCR
rev	Reverse
RIG-I	Retinoic acid-inducible gene I
RISC	RNA-induced-silencing-complex
RLR	RIG-I-like receptor
Rluc	Relative luciferase
RNA	Ribonucleic acid
RNAi	RNA interference
RNase	Ribonuclease
ROS	Reactive oxygen species
rpm	Revolutions per minute
RT	Room temperature
SAM	S-adenosyl-L-methionine
SD	Standard deviation
SDS	Sodium dodecyl sulfate
sec	Second
SEM	Standard error of the mean
sfRNA	Subgenomic flaviviral RNA
SFV	Semliki Forest virus
SINV	Sindbis virus
siRNA	Small interfering RNA
SNP	Single nucleotide polymorphism
SOC	Super Optimal broth with Catabolite repression
SP	Structural protein
Spz	Spätzle
ssRNA	Single-stranded RNA
TAE	Tris-acetate-EDTA
TB	Terrific broth
$TCID_{50}$	Tissue culture infectious dose 50
TE	Transposable element
TPB	Tryptose Phosphate Broth
TRAF	TNF receptor-associated factor
Upd	Unpaired

UTR	Untranslated region
vpiRNA	Virus-specific piRNA
VRP	Virus replicon particle
VSR	Viral suppressor of RNAi
WNV	West Nile virus
Wt	Wild-type
YFV	Yellow fever virus
YF-VRP	Yellow fever virus replicon particles
ZIKV	Zika virus
Zuc	Zucchini

1. Introduction

1.1 Orthoflaviviruses

In 1984, the International Committee on Taxonomy of Viruses (ICTV) classified *Flaviviridae* as a new family of viruses. The virus family includes four genera, which until recently were named as follows: *Flavivirus*, *Hepacivirus*, *Pegivirus,* and *Pestivirus* (Westaway *et al.*, 1985; Stapleton *et al.*, 2011; Simmonds *et al.*, 2017). In April 2023*,* the genus name *Flavivirus* was changed to *Orthoflavivirus* by the ICTV to reduce ambiguity, as the taxon names *Flaviviridae* and *Flavivirus* both contained “flavi” (Postler *et al.*, 2023). Viruses belonging to the genus *Orthoflavivirus* are mainly transmitted to humans by biting arthropods such as ticks or mosquitoes and are thus also called vector-borne orthoflaviviruses (van Leur *et al.*, 2021). The genus comprises more than 70 members that can be further subdivided into the following ecological groups: I) mosquito-borne orthoflaviviruses transmitting between vertebrates and mosquitoes; II) tick-borne orthoflaviviruses transmitting between vertebrates and ticks; III) no known vector orthoflaviviruses that only infect vertebrates via horizontal transmission; IV) insect-specific orthoflaviviruses transmitted vertically between insects (Slonchak *et al.*, 2022).

Mosquito-borne orthoflaviviruses, like yellow fever virus (YFV), dengue virus (DENV), Zika virus (ZIKV), and West Nile virus (WNV), profoundly affect public health worldwide by causing various infectious diseases. It is estimated that around 400 million DENV infections and 200,000 YFV infections emerge each year (Gershman *et al.*, 2012; Bhatt *et al.*, 2013). Even though diseases caused by mosquito-borne orthoflaviviruses are commonly acute in vertebrates, the innate and adaptive immune response counteracts and eliminates the viral infection. Recent studies indicate that some orthoflaviviruses induce persistent infections in vertebrates (McGee *et al.*, 2011; Randall *et al.*, 2017). Interestingly, the mosquito immune system does not eliminate the viral pathogen but controls it. Thus, arthropod-borne viral (arboviral) infections in mosquitoes are persistent and associated with minor fitness costs. Due to different selective pressures on arboviruses, the virulence in mosquitoes highly depends on the transmission route. Vertical transmission is less virulent than horizontal transmission (Lambrechts *et al.*, 2009; Goic *et al.*, 2016).

1.1.1 Genome organization

Orthoflaviviruses are enveloped, spherical viruses with a diameter of 50 nm. A host-derived lipid bilayer containing 180 subunits each of the envelope proteins E and M surrounds the nucleocapsid (Kuhn *et al.*, 2002; Mukhopadhyay *et al.*, 2005). Two virion forms have been characterized: the intracellular one, containing only prM and E, and the extracellular infectious one, containing predominantly M and E (Chambers *et al.*, 1990). Cleavage of prM to M occurs during the maturation process after transporting the virion to the trans-Golgi (Lorenz *et al.*, 2002). Ninety E dimers are incorporated on the surface of a mature virion, whereby the dimers are arranged antiparallel (Kuhn *et al.*, 2002) (Figure 1A).

Orthoflaviviruses harbor an 11 kb RNA genome with positive polarity. The infectious genomic RNA has a type I cap at its 5' end (m^7GpppAmG), no poly-A tail at the 3' end, and encodes for one open-reading frame flanked by a 5' and a 3' untranslated region (UTR) (Chambers *et al.*, 1990). Instead of the poly-A tail, mosquito-borne orthoflaviviruses terminate with the conserved dinucleotide CU (Wengler *et al.*, 1981). Following the translation of the genomic RNA into a single polyprotein, the latter is co- and post-translationally cleaved by cellular and viral proteases into the three structural proteins (SP) C, prM, E, and the seven non-structural (NS) proteins NS1-NS5 (Figure 1B).

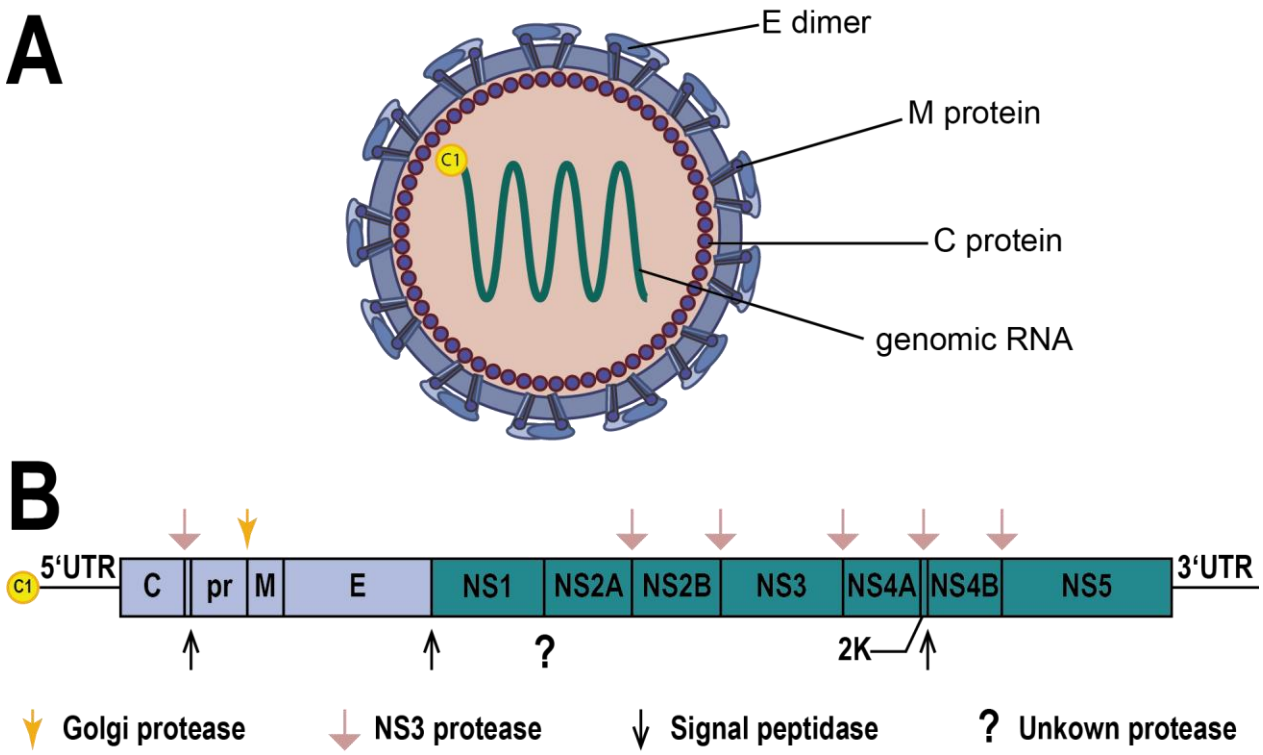

Figure 1: Virion structure and genome organization of orthoflaviviruses.
A) The spherical capsid contains the viral genome and is surrounded by a lipid bilayer in which the envelope proteins M and E are embedded. B) The polyprotein derived from the single open reading frame of the orthoflaviviral RNA is cleaved by viral and cellular proteases, resulting in three structural (C, prM, E) and seven non-structural proteins (NS1-NS5).

1.1.2 Life cycle

The first step in the orthoflaviviral life cycle involves binding of the envelope protein to a host receptor on the plasma membrane surface (Figure 2). Not all orthoflaviviruses use the same receptors for binding, which might be linked to different envelope protein sequences. In addition, it has been observed that one orthoflavivirus species can infect different cell types, suggesting that one species can bind multiple attachment proteins (Fishburn *et al.*, 2022). After binding to a host factor, most orthoflaviviruses enter cells via clathrin-mediated endocytosis. Using single-particle tracking of DENV, it was shown that viral particles are captured at the cell surface by pre-existing clathrin-coated pits. After clathrin-dependent internalization, the particles were transported to the early endosomes, which mature into late endosomes (van der Schaar *et al.*, 2008; Fishburn *et al.*, 2022). Interestingly, the wild-type YFV-Asibi strain also enters host cells via a clathrin-dependent route, while the vaccine strain YFV-17D, derived from YFV-Asibi by serial passaging in

mouse and chicken embryo tissues, enters mammalian cells via a clathrin-independent route (Fernandez-Garcia *et al.*, 2016). Following endocytosis, protons are pumped from the cytoplasm into the endosome's lumen, which reduces the endosomal pH. The acidified environment leads to a conformational change in the envelope protein, causing the endosome membrane and viral membrane to fuse. A fusion pore is formed through which the nucleocapsid is released into the cytosol (Smit *et al.*, 2011; Fishburn *et al.*, 2022). The nucleocapsid stabilizes and protects the viral RNA but also prevents translation. Thus, the viral RNA needs to be uncoated before translation, which is mediated by ubiquitination of the capsid protein by the host enzyme UBA1, resulting in subsequent disassembly of the nucleocapsid (Fishburn *et al.*, 2022).

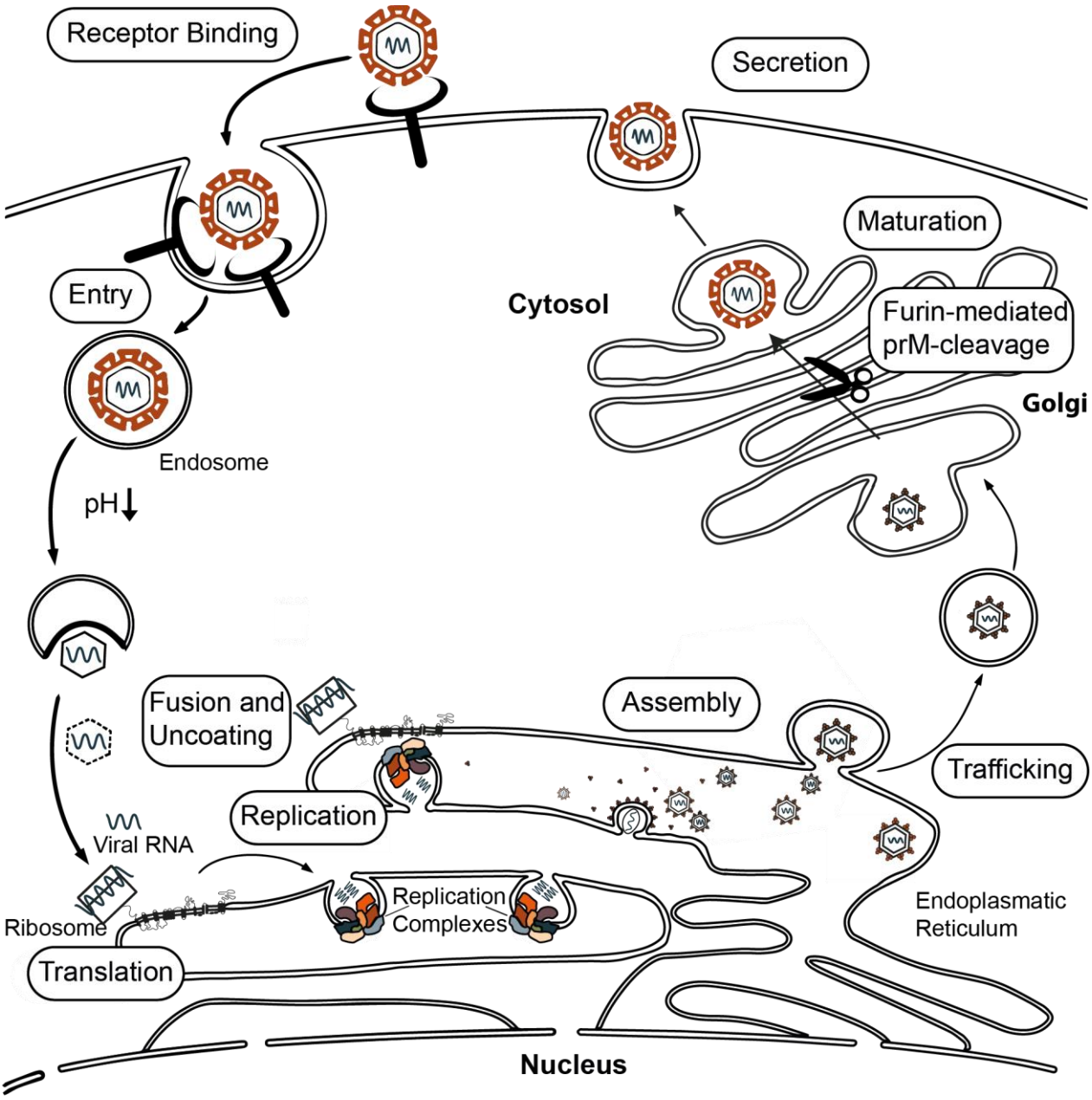

Figure 2: Orthoflavivirus replication cycle.
Most orthoflaviviruses enter the host cell by clathrin-dependent endocytosis. The pH is decreased within the endosome, resulting in the fusion of the viral envelope with the endosomal membrane. Upon fusion, the viral genome is released and uncoated. Host ribosomes translate the viral RNA into one polyprotein, which is co- and post-translationally processed by host and viral proteases. The transmembrane proteins are inserted into the endoplasmatic reticulum (ER), and the polyprotein is cleaved by host and viral proteases. The viral RNA is replicated within replication complexes consisting of non-structural proteins. The viral structural proteins assemble, are loaded with genomic RNAs at the ER, and enter the *trans*-Golgi network. Within the Golgi network, the immature virions are cleaved by furin protease, resulting in mature virions released by exocytosis. Picture adapted from (Fishburn *et al.*, 2022).

Translation into a single polyprotein begins after successful entry, fusion, and uncoating of the viral RNA. As previously mentioned, the orthoflaviviral genome is capped (m^7GpppAmG) at the 5' end. The cap structure leads to the recruitment of cellular ribosomal subunits, which initiate translation by scanning the genome until they reach the AUG start codon (Chiu *et al.*, 2005; Barrows *et al.*, 2018). Termination of the translation occurs when the stop codon is reached. All three types of stop codons (UAA, UAG, and UGA) are represented in the different orthoflavivirus members, indicating that the stop sequence is not conserved between orthoflaviviruses (Chambers *et al.*, 1990). While it is still highly discussed whether the translation initiates on ER-associated ribosomes, it is known that polyprotein synthesis occurs in association with ER membranes (Barrows *et al.*, 2018). The first quarter of the resulting polyprotein comprises the structural proteins, while the non-structural proteins are located on the remaining protein.

Once the polyprotein is translated, it is cleaved by cellular and viral proteases into ten mature proteins that are incorporated into the ER membrane. The incorporation is initiated via a signal peptide sequence located at the C-terminus of the capsid protein (Barrows *et al.*, 2018). The signal sequence is known as the anchor and spans the ER membrane. Cleavage of the anchor sequence is mediated by a two-step process, starting with the NS3 protease and followed by a cellular signalase (Barrows *et al.*, 2018; He *et al.*, 2020). After cleavage, the mature capsid is released into the cytosol, and a small part remains in the ER membrane. The host signal peptidase cleaves between C-prM, prM-E, E-NS1, and 2K-NS4B and the virus-encoded NS3 protease cleaves between NS2A-NS2B, NS2B-NS3, NS3-NS4A, NS4A-2K, and NS4B-NS5 (Figure 2B) (Barrows *et al.*, 2018). The non-structural proteins can be divided into two groups according to their size. The large proteins NS1, NS3, and NS5 are highly conserved, and the smaller proteins NS2A, NS2B, NS4A, and NS4B share the feature that they are hydrophobic (Rice *et al.*, 1985; Chambers *et al.*, 1990).

The non-structural proteins form a replication complex on ER membranes (Welsch *et al.*, 2009). As a first replication intermediate, the RNA-dependent RNA polymerase encoded in the NS5 protein catalyzes the minus-strand synthesis. The minus-strand subsequently serves as a template for plus-strand synthesis. Since replication occurs in the cytoplasm and cellular capping enzymes are not present here, orthoflaviviruses encode their own

methyltransferase in the NS5 protein, which caps the newly synthesized viral plus-strand RNAs (Rice *et al.*, 1985; Bartholomeusz *et al.*, 1999). Assembly of newly synthesized and capped viral RNAs with structural proteins at the ER results in membrane invagination and the formation of immature virions. During the transport of the immature virions through the Golgi apparatus, the membrane proteins are glycosylated, and prM is processed to pr and M by the enzyme furin. This process allows the envelope proteins to detach from the prM proteins and dimerize. Infectious particles are formed and released at the cell surface by exocytosis (van den Elsen *et al.*, 2021; Fishburn *et al.*, 2022).

1.1.3 Cap structure

Cellular mRNAs in higher eukaryotes undergo modifications that are essential in many cellular and biological processes (Boo *et al.*, 2020). One of the most important is the modification at the 5' end of the mRNA, named N-7-methylguanosine (m^7G) cap (Figure 3). The addition of the cap structure in higher eukaryotes occurs via three different enzymes in the nucleus: I) removal of the γ-phosphate from the 5' triphosphate by the RNA triphosphatase to generate 5' diphosphate RNA; II) transfer of a guanosine monophosphate (GMP) group from guanosine triphosphate (GTP) by the RNA guanylyltransferase to the 5' diphosphate to create GpppNp-RNA; III) transfer of the methyl group from S-adenosyl-L-methionine (SAM) to the cap guanine to create the cap0 structure ($m^7GpppNp$). In the last step, the m^7G-specific 2'-O-methyltransferase methylates the ribose-2'-O position of the first nucleotide, generating the cap1 structure (m^7GpppN_m) (Decroly *et al.*, 2012; Ramanathan *et al.*, 2016). The cap structure has different roles depending on the location of the RNA. In the nucleus, the cap structure prevents mRNA degradation by 5' exoribonucleases and facilitates the export out of the nucleus. In the cytoplasm, the cap ensures efficient translation, prevents degradation by 5' exoribonucleases, and marks the mRNA as "self" (Netzband *et al.*, 2020).

Given the importance of cap structures in mammalian cells, it is not surprising that many viruses also cap their RNA. However, since orthoflaviviruses replicate in the cytoplasm and the mammalian capping machinery is located in the nucleus, they need to encode their own capping enzymes. Capping of viral RNA is mediated by only two proteins, namely NS3 and NS5. The two proteins encode at least four enzymes responsible for catalyzing the capping reaction (Ruggieri *et al.*, 2021). The NS3 protein encodes the

triphosphatase, and the NS5 protein the RNA guanylyltransferase (GTase), the RNA guanine-methyltransferase (N-7-MTase), and the 2'-O-methyltransferase (2'-O-MTase) (Li *et al.*, 1999; Ray *et al.*, 2006; Issur *et al.*, 2009). The capping reaction takes place on (+) strand RNAs and starts with the triphosphatase that removes the 5' phosphate, resulting in a di-phosphorylated RNA (Issur *et al.*, 2009). Subsequently, the GTase transfers a GMP moiety from GTP to the 5' end of the di-phosphorylated RNA to form a base cap structure. Finally, the base cap structure is first methylated at the guanine N-7 position by the N-7-MTase, and then the 2'-O-MTase methylates the RNA at the ribose 2'-O position of the first nucleotide. Following these reactions, a cap1 structure is formed at the 5' end of the viral genome (Saeedi *et al.*, 2013; Ruggieri *et al.*, 2021).

By comparing structures and sequences of different viral 2'-O-MTases, a conserved motif consisting of the amino acids NS5-K61-D146-K182-E218 was discovered. This tetrad forms the active site of the 2'-O-methyltransfer reaction (Egloff *et al.*, 2002). Using substitution experiments, Ray and colleagues (2006) could show for WNV that all four residues are essential for 2'-O-MTase activity, but only D146 is essential for N-7-MTase activity. Further, they were able to rescue viruses containing the K61A, K182A, or E218A substitution, indicating an important but not essential role for 2'-O-MTase activity. In contrast, no virus was recovered when RNA containing the D146A mutation was transfected, indicating the essential role of the N-7-MTase activity (Ray *et al.*, 2006; Zhou *et al.*, 2007).

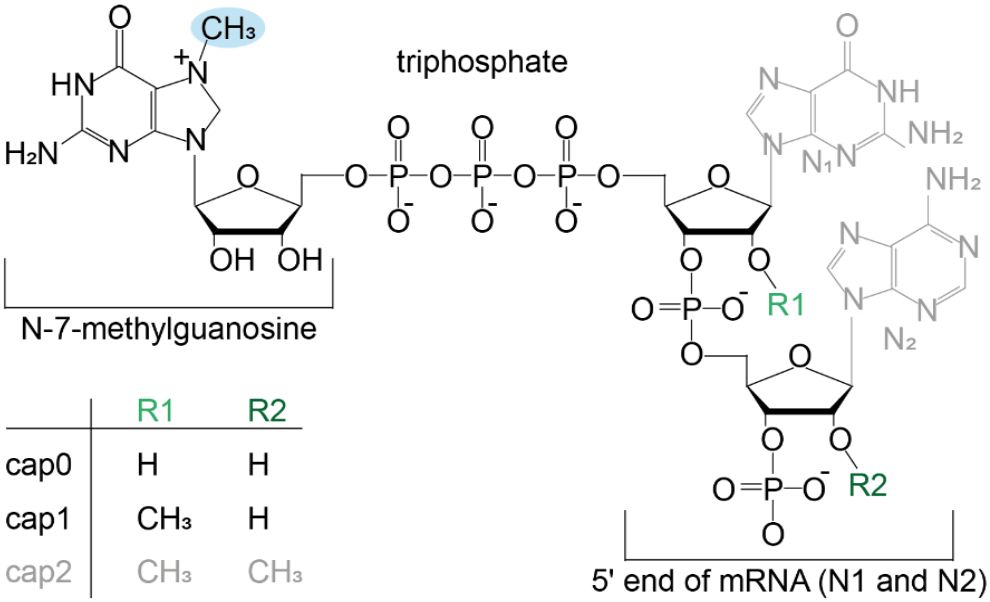

Figure 3: mRNA cap structure.
The orthoflaviviral cap structure is N-7-methylated (highlighted in blue) and 2'-O-methylated at the first ribose (R1). In higher eukaryotes, the first (R1) and sometimes, in addition, the second ribose (R1 and R2) are 2'-O-methylated, forming a cap1 or cap2 structure, respectively.

1.1.4 Transmission cycle of mosquito-borne orthoflaviviruses

The transmission of arboviruses can be divided into four different cycles: I) urban cycle; II) sylvatic cycle; III) epizootic cycle; IV) zoonotic cycle (Figure 4) (Ong *et al.*, 2014). Usually, humans are considered dead-end hosts for arboviruses. However, in rare cases, the viruses are sufficiently amplified, resulting in an urban epidemic cycle where the virus is directly transmitted between humans and mosquitoes. In the sylvatic cycle, arboviruses circulate between non-human primates, birds, and rodents. This cycle takes place in areas that are not inhabited. The circulation of arboviruses between domestic animals and mosquitoes is called an epizootic cycle. Rarely, an epizootic cycle may result in a zoonotic cycle. Here, arboviruses are directly transmitted from non-human animals to humans (Weaver *et al.*, 2004; Ong *et al.*, 2014; Sacchetto *et al.*, 2020). While YFV can be transmitted via the urban, sylvatic, or epizootic cycle, DENV is mainly transmitted via the urban cycle and rarely via the sylvatic cycle (Figueiredo, 2019; Sacchetto *et al.*, 2020).

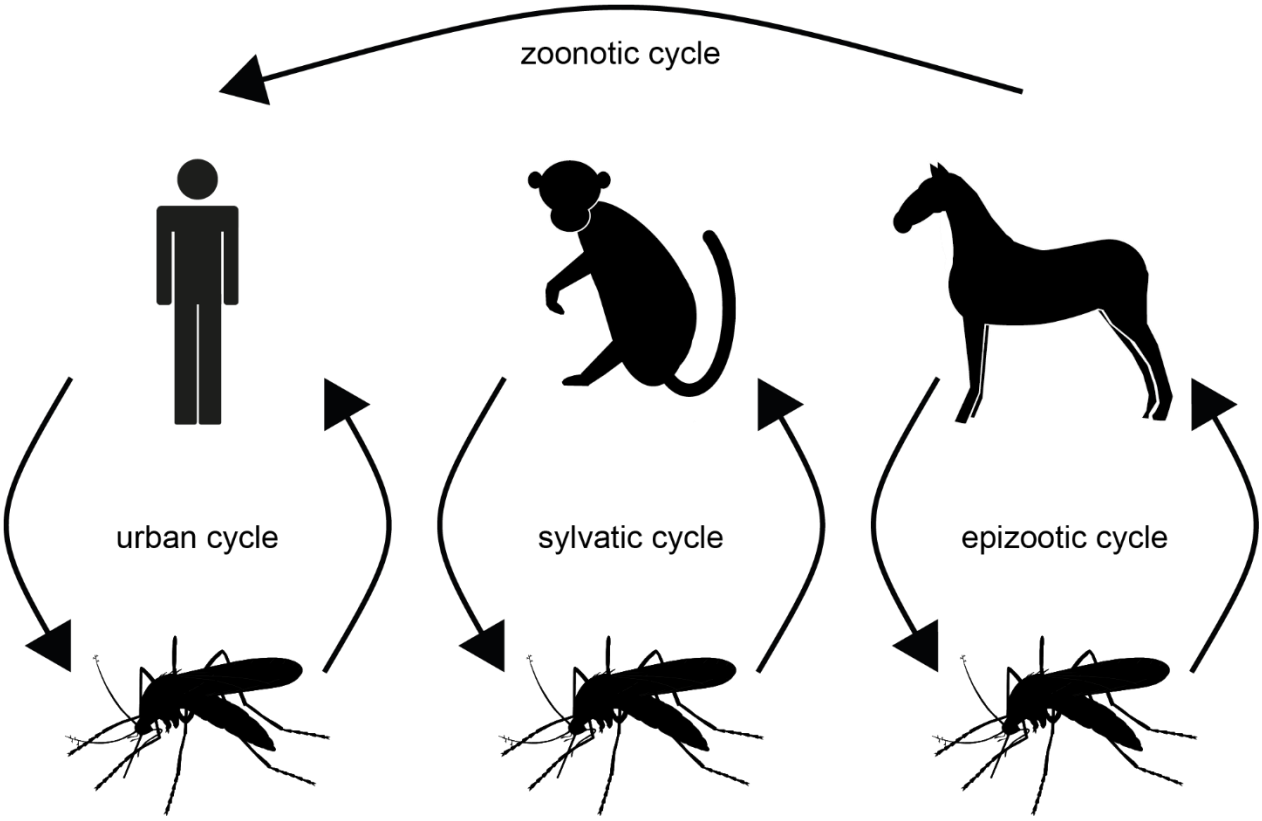

Figure 4: Transmission cycles of orthoflaviviruses.
Orthoflaviviruses can be either transmitted via the urban cycle (left), sylvatic cycle (middle), or epizootic cycle (right). Rarely, orthoflaviviruses can be transmitted via the zoonotic (top) cycle, which involves direct transmission from a non-human animal to a human.

1.1.5 Dissemination of mosquito-borne orthoflaviviruses in mosquitoes

Mosquitoes ingest mosquito-borne orthoflaviviruses with a blood meal, which allows viral transmission to the midgut (Figure 5). The virus needs to establish an efficient infection in the mosquito midgut upon transmission. This infection is highly dependent on the viral titer and the diversity of the viral population. Both factors support viral replication in the midgut cells (Patterson *et al.*, 2018; Weaver *et al.*, 2021). The midgut consists of a single-layered epithelium surrounded by muscle cells, tracheoles, and fibroblasts. It can be divided into two regions: the anterior and the posterior midgut. While the anterior midgut is mainly responsible for carbohydrate digestion, the posterior midgut is mainly responsible for blood meal digestion. A recent single-cell RNA-seq study of *Aedes aegypti* midguts revealed that the mosquito midgut comprises 20 different cell-type clusters, including, among others, intestinal stem cells, enteroblasts, and enteroendocrine cells (Cui *et al.*,

2020). Once the virus establishes an efficient replication in the epithelial cells of the midgut, it passes the basal lamina and escapes into the hemolymph. However, as proposed by Girard and colleagues, the virus might require a threshold of midgut infection before it is able to escape the midgut barrier (Girard *et al.*, 2004). The hemocoel is an open cavity where the hemolymph circulates (Lee *et al.*, 2019). Thus, the virus spreads from the hemolymph throughout the mosquito body to the fat body, muscles, saliva glands, and neural tissue (Cheng *et al.*, 2016; Rückert *et al.*, 2018). As soon as the virus passes the basal lamina surrounding the salivary glands, it also needs to establish efficient replication in this organ. Following efficient viral replication in the salivary glands, the virus can be transmitted to a new vertebrate host by saliva injection during mosquito probing (Weaver *et al.*, 2021).

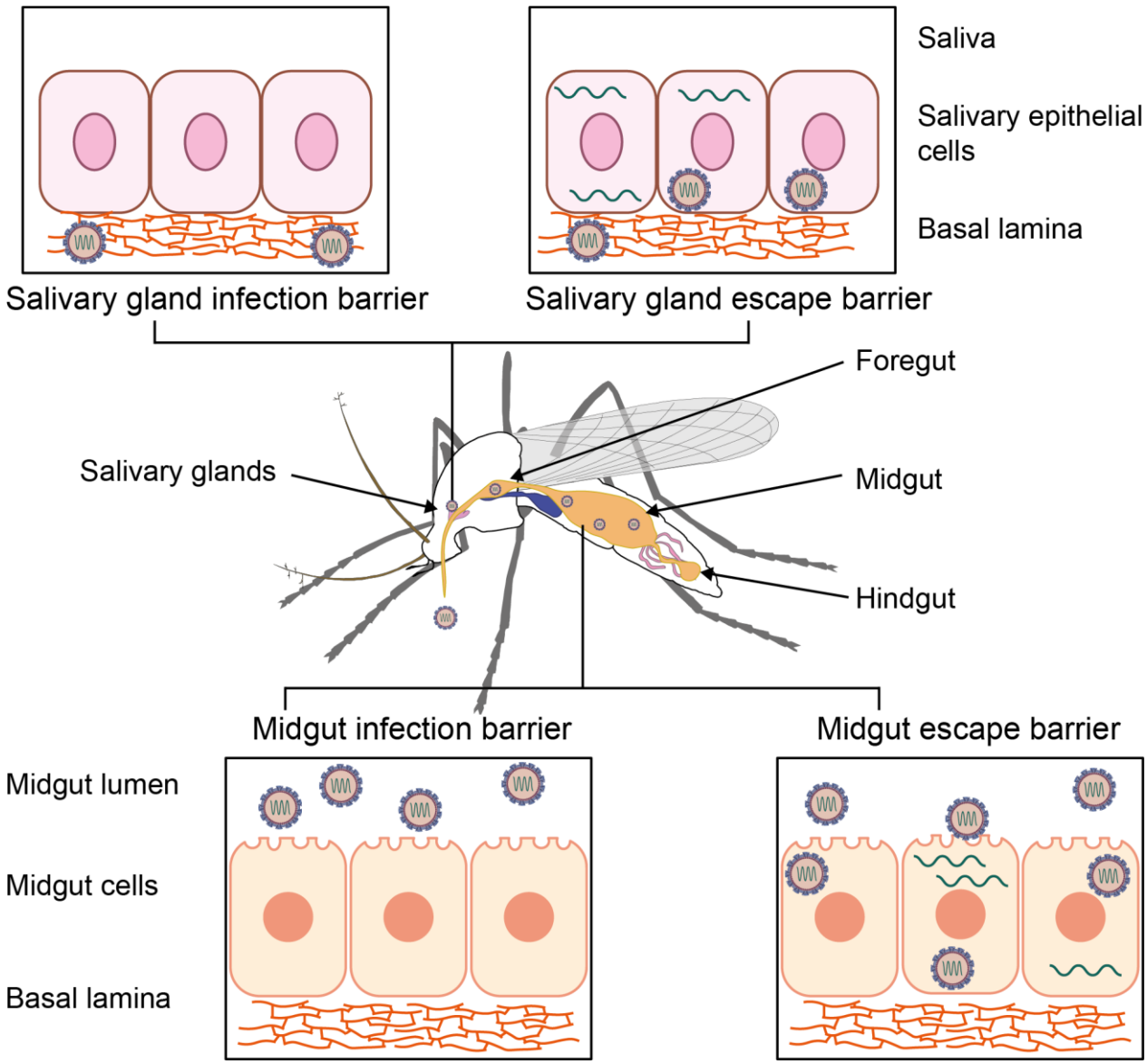

Figure 5: Virus infection and dissemination in mosquitoes.
After mosquitoes ingest an infectious blood meal, viruses must overcome four barriers before being further transmitted. The first barrier is the midgut infection barrier (bottom left), which refers to the inability of viruses to establish replication in the midgut. The second barrier is called the midgut escape barrier (bottom right) and describes the inability of viruses to disseminate into secondary organs. If the virus can disseminate to the salivary glands but does not replicate in the salivary glands, the third barrier, the salivary gland infection barrier (top right), is reached. Lastly, the salivary gland escape barrier (top right) refers to the inability of viruses to escape into the saliva. Picture adapted from (Carpenter *et al.*, 2023).

1.2 Innate immune defense of mosquitoes

Comparable to vertebrates, the first line of immune defense in mosquitoes is the innate immunity. The mosquito immune response mainly occurs during the extrinsic incubation period, which is the time between ingesting an infected blood meal by a mosquito and the time until the mosquito becomes capable of transmitting the virus. The immune response shapes the outcome of the infection and virus transmission. In total, five different major pathways are known: I) RNA interference pathway (RNAi); II) Janus kinase/signal transducer (JAK/STAT) pathway; III) Toll pathway; IV) immunodeficiency pathway; V) mitogen-activated protein kinase (MAPK) pathway. From these pathways, RNAi is considered to be the most crucial antiviral pathway in mosquitoes (Tikhe *et al.*, 2021).

1.2.1.1 RNA interference pathway (RNAi)

In the early 1990s, RNAi was first described as a plant defense mechanism against the tobacco etch virus and was initially termed RNA-mediated virus resistance or post-transcriptional gene silencing (Lindbo *et al.*, 2005). Further research revealed dsRNA as the trigger for RNAi in *Caenorhabditis elegans* and shortly after, the same trigger was identified for RNAi in *Drosophila melanogaster*. As *D. melanogaster* is the model organism for insects, most knowledge about RNAi derives from research performed with *D. melanogaster* (Blair, 2011). The RNAi pathway involves the distinct degradation of target RNAs, and depending on the origin of the RNA, three classes of RNAi machinery are differentiated: I) small interfering RNA (siRNA) pathway; II) micro RNA (miRNA) pathway; III) P-element-induced wimpy testis (PIWI)-interacting (piRNA) pathway (Figure 6) (Tikhe *et al.*, 2021).

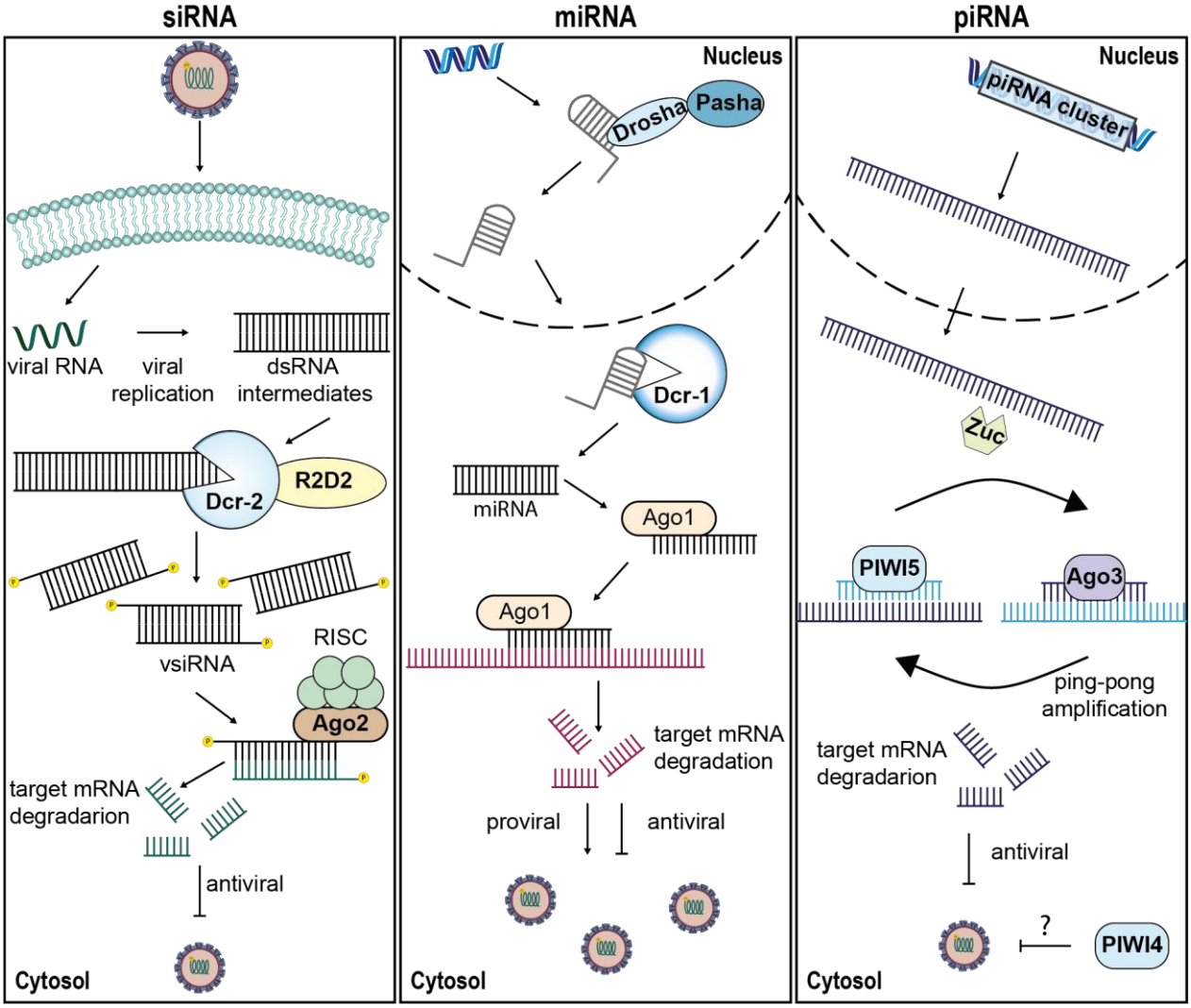

Figure 6: Schematic presentation of the three major RNAi pathways.
(left): siRNA pathway. Depending on the origin of the dsRNA, the siRNA pathway can be divided into endogenous and exogenous siRNA pathways. Depicted is the exogenous siRNA pathway. Viral dsRNAs, formed as intermediates during viral replication, are cleaved by the RNase III-like enzyme Dcr-2 and its co-factor R2D2 into small 21 nt siRNAs. siRNAs are loaded onto Argonaute-2 within the RISC. The passenger strand is removed from the complex, and the guide strand binds complementary RNAs to target them for degradation. (middle): miRNA pathway. RNA polymerase II transcripts fold back into partially double-stranded pri-miRNAs. The transcripts are cleaved into 70 nt pre-miRNAs by the ribonuclease Drosha and then transported into the cytoplasm. Subsequently, the pre-miRNAs are cut into 22 nt miRNA/miRNA* duplexes by Dcr-1. The duplexes are loaded onto Ago1, a part of the RISC, where one strand (miRNA*) is degraded. The other serves as a target sequence to degrade (partially) complementary mRNA. (right): piRNA pathway. Precursor RNAs are transcribed from piRNA clusters and transported into the cytoplasm, where they are cleaved into 25-27 nt pre-piRNAs by the endonuclease Zuc. Those pre-piRNAs are further amplified through a ping-pong amplification loop. Viral piRNAs can be amplified in a ping-pong loop consisting of the proteins Ago3 and Piwi5. Picture adapted from (Tikhe *et al.*, 2021).

siRNA pathway: Depending on the origin of the double-stranded target RNA, the siRNA pathway can be divided into two branches: the endogenous siRNA pathway and the exogenous siRNA (exo-siRNA) pathway. Endogenous double-stranded RNA (dsRNA) is produced through bidirectional transcription of the same genomic segment, transcription of structured loci such as hairpin RNAs, or transposon sequences (Czech *et al.*, 2008; Okamura *et al.*, 2008; Adelman *et al.*, 2012). The origin of exogenous dsRNA highly depends on the genomic structure of the invading virus. While the genomic RNA of double-stranded RNA viruses itself serves as a target for the exo-siRNA pathway, single-stranded RNA (ssRNA) viruses form dsRNA as replication intermediates. DNA viruses also produce double-stranded RNA, formed by the hybridization of overlapping transcripts (Bronkhorst *et al.*, 2014). The exo-siRNA pathway is considered to be the primary antiviral immune response in mosquitoes (Figure 6). The viral dsRNA is cleaved by the RNase III-like enzyme Dicer-2 (Dcr-2) into small interfering RNAs with a length of 21 nucleotides (Galiana-Arnoux *et al.*, 2006). The resulting siRNAs are 5’ phosphorylated and have a single-strand overhang of 2 nucleotides at both 3’ ends (Blair *et al.*, 2015). Interestingly, the DExD/H-box helicase domain of the Dicer and the retinoic acid-inducible gene I (RIG-I) enzymes are structurally closely related. RIG-I is a mammalian sensor of viral infections and mediates the type-1 interferon response upon viral infection (Deddouche *et al.*, 2008). Once the dsRNA is cleaved into siRNAs, the dsRNA binding protein R2D2 partners with Dcr-2 to load the siRNAs onto Argonaute-2 (Ago2) within the RNA-induced-silencing-complex (RISC) (Liu *et al.*, 2003; Blair *et al.*, 2015). Ago2 is an Mg^{2+}-dependent RNA endonuclease, cleaving together with the endonuclease Component 3 Promoter of RISC (C3PO), the passenger strand of the siRNA and thus triggers the dissociation of this strand from the RISC (Matranga *et al.*, 2005). The decision of which strand becomes the guide strand and which becomes the passenger strand depends on the thermodynamic stability of the siRNA duplex. R2D2 binds the thermodynamically more stable 5’ end (passenger strand), allowing Dcr-2 to load the retaining strand into Ago2 (guide strand) (Tomari *et al.*, 2004). Following this binding, the RNA methyltransferase Hen1 2’-O-methylates the 3’ terminal nucleotide of the guide strand to finalize the maturation of an siRNA-loaded RISC (Yang *et al.*, 2006; Schuster *et al.*, 2019). The guide strand binds to complementary viral target RNAs via Watson-Crick base pairing, and subsequently, this target RNA is sequence-specific degraded by Ago2 (Blair *et al.*, 2015).

miRNA pathway: The miRNA pathway is mainly involved in post-transcriptional gene regulation, but recent studies also suggest an antiviral function of miRNAs in mosquitoes (Figure 6) (Feng *et al.*, 2018). miRNAs are short dsRNAs (~ 22 nt) found in animals, plants, and even viruses. They are derived from RNA polymerase II transcripts that fold back into partial dsRNA structures and form a hairpin structure called primary miRNA (pri-miRNAs) (Yang *et al.*, 2011; Donald *et al.*, 2012). Pri-miRNAs are cleaved into 70 nt precursor miRNAs (pre-miRNAs) with 2- to 3-nt ssRNA overhangs by the enzymes Drosha and Pasha (Tikhe *et al.*, 2021). The pre-miRNAs are transported from the nucleus to the cytoplasm by the protein exportin-5 before Dicer-1 (Dcr-1) cleaves the pre-miRNA into mature ~ 22 nt miRNA/miRNA* duplexes. Unlike siRNA, the miRNA/miRNA* duplexes are not entirely double-stranded. The duplex is loaded onto Argonaute-1 (Ago1), a component of the miRISC complex. Here, one strand (known as miRNA*) is degraded or loaded into another miRISC complex. The mature miRNA guides the miRISC to the target mRNA, leading to the degradation, repression of translation, or increased stability of the target RNA (Donald *et al.*, 2012; Blair *et al.*, 2015).

Recent studies showed that miRNAs play an essential role in viral replication. It was shown that the miRNA aae-miR-2940 leads to an upregulation of a metalloprotease in *Aedes albopictus*, which is important for WNV replication. Conversely, a reduction of aae-miR-2940 can lead to a reduced expression of the metalloprotease and thus restricts the replication of WNV (Slonchak *et al.*, 2014). The endosymbiont *Wolbachia* was suggested to use a host miRNA to reduce expression of the methyltransferase AaDnmt2 in *Aedes aegypti*, which is relevant for DENV replication. Through this miRNA, *Wolbachia* can suppress the replication of DENV in their mosquito host (Zhang *et al.*, 2013).

piRNA pathway: The piRNAs are the most recently discovered class of animal small RNAs (Figure 6). In contrast to siRNAs and miRNAs, which derive from at least partially double-stranded precursors, piRNAs are single-stranded. They have a border size spectrum of 24 – 30 nt and are processed independently of the RNase III enzyme Dicer (Grivna *et al.*, 2006; Siomi *et al.*, 2011). Most knowledge about this pathway is derived from *D. melanogaster*, but some distinct differences exist between the piRNA pathway between *Drosophila* and mosquitoes. The following describes the piRNA pathway of *Drosophila* before some essential differences are presented.

The primary function of the piRNA pathway in *Drosophila* is to control transposable elements (TEs) mobilization by silencing them. Transposable elements are DNA sequences that can change their position within a genome to transfer genetic and epigenetic material to the offspring. However, TEs threaten the germline genome integrity (Duc *et al.*, 2019). The piRNA pathway can be divided into two branches: the primary and secondary pathways (Siomi *et al.*, 2011; Liu *et al.*, 2019). First, long, single-stranded precursor antisense RNAs are transcribed from genomic transposon-rich clusters and are transported into the cytoplasm. There, they are cut into 24–27 nt piRNAs by the endonuclease Zucchini (Zuc). These piRNAs have a sequence bias for uridine at the first nucleotide position (U1). The piRNAs are loaded into either a Piwi- or Aubergine (Aub)-containing effector complex, where they are truncated, 2'-O-methylated, and thus matured (Varjak *et al.*, 2018; Liu *et al.*, 2019). In the primary pathway, Piwi-loaded piRNAs translocate to the nucleus, where they transcriptionally silence transposons. The secondary piRNA pathway includes piRNAs loaded onto the Aub-containing effector complex. These piRNAs are amplified in the cytoplasm through a ping-pong loop by binding complementary sense transposon RNAs, which Aub cuts. The resulting antisense RNAs have a sequence bias for adenine at the 10th position (A10) and associate with Ago3. In turn, the piRNA-Ago3 complex targets and slices antisense transposons, which are again bound by Piwi- or Aub-containing effector complexes. These piRNAs can then re-enter the ping-pong replication cycle (Varjak *et al.*, 2018; Liu *et al.*, 2019).

As mentioned above, the piRNA pathways between *Drosophila* and mosquitoes differ. piRNAs with the specific ping-pong signature (U1 and A10) are only expressed in germline tissues in *Drosophila* but also in somatic tissues in *Aedes aegypti* during chikungunya virus (CHIKV) infection. These findings indicate that the non-canonical piRNA pathway in the mosquitoes' soma might act redundantly to a siRNA-driven immune response (Morazzani *et al.*, 2012). The main players of the piRNA pathway in *Drosophila* are Piwi, Ago3, and Aub, all of which belong to the PIWI protein family. While there is a direct orthologue for Ago3 in mosquitoes, several orthologues were found for the Piwi and Aub proteins. Two Ago3 and nine PIWI (Piwi1-9) proteins were found in *Aedes albopictus*, and one Ago3 and seven PIWI proteins (Piwi1-7) in *Aedes aegypti* (Campbell *et al.*, 2008; Schnettler *et al.*, 2013; Wang *et al.*, 2018). The *Aedes aegypti*-derived Ago3 and Piwi4-6 are expressed in somatic tissues, whereas Piwi1-3 are germline-specific. Both

Aedes albopictus-derived Ago3 proteins and Piwi1-7 could be detected in female mosquitoes, but only Piwi5-7 and the Ago3 proteins in the midgut. Piwi8-9 appear to be present only in embryos of *Aedes albopictus* (Varjak *et al.*, 2018).

Ago and Piwi proteins share two important domains: the PAZ and the PIWI domains. The PIWI domain is structurally similar to RNase H and contains a catalytic structure known as DxDH. In *D. melanogaster*, Ago1-3 encode such a motif, but Piwi does not. By contrast, this motif was found in all Ago and Piwi proteins in *Aedes aegypti*, indicating that all proteins are capable of cleaving RNA (Varjak *et al.*, 2018).

Virus-specific piRNAs (vpiRNAs) from various viruses have been found in mosquitoes. These include alphaviruses (e.g., CHIKV and Sindbis virus (SINV)) and orthoflaviviruses (e.g., DENV, ZIKV). The single-stranded RNA of these viruses serves as a substrate for producing vpiRNAs. To date, it is still being determined how Piwi proteins distinguish viral and host RNAs (Miesen, Joosten, *et al.*, 2016). Interestingly, orthoflavivirus vpiRNAs are not distributed throughout the viral genome but can only be mapped to specific regions (hotspots). Thus, DENV vpiRNAs were mapped mainly to the 3’ end of the NS5 protein, and they did not show a characteristic ping-pong signature (U1 and A10) but were 2’-O-methylated at their 3’ end (Wang *et al.*, 2018). Knockdown of Piwi5, Ago3, and to a lesser extent Piwi6 in the *Aedes aegypti*-derived cell line Aag2 resulted in a reduction of DENV vpiRNA levels (Miesen, Ivens, *et al.*, 2016). The fact that vpiRNAs can be found for various viruses in mosquitoes suggests that the piRNA pathway might exhibit a potential antiviral role in this organism (Varjak *et al.*, 2018).

1.2.1.2 JAK/STAT pathway

Mosquitoes, like other insects, possess efficient innate immunity. Part of this immunity is the highly conserved JAK/STAT pathway, which activates transcription factors that directly induce the expression of various effector genes (Figure 7). The pathway is activated by a ligand that binds to the monomeric receptor Domeless (Dome). The binding leads to the subsequent dimerization of Dome and its activation. The conformational change of Dome induced by the dimerization leads to the autophosphorylation of the tyrosine kinase Hopscotch (Hop), which subsequently phosphorylates Dome. Due to this phosphorylation, Dome forms a docking site for cytoplasmic STATs. Bound STAT is phosphorylated and dimerized. The dimerized STAT can translocate to the nucleus through a RanGTP-

dependent mechanism. Once in the nucleus, STAT can activate the transcription of specific target genes (Souza-Neto *et al.*, 2009; Tikhe *et al.*, 2021). In vertebrates, a wide variety of cytokines and growth factors lead to the activation of the JAK/STAT pathway. In 1998, the secreted proteins Unpaired (Upd) Upd1, Upd2, and Upd3 were described as ligands for the JAK/STAT pathway in *Drosophila* (Harrison *et al.*, 1998). In contrast, the ligands activating the pathway in mosquitoes are yet unknown (Tikhe *et al.*, 2021). In one study, the secreted peptide Vago was shown to lead to a JAK/STAT-dependent reduction of WNV infection in *Culex* cells (Paradkar *et al.*, 2012). Two Vago genes exist in *Aedes aegypti*, Vago1 and Vago2. In contrast, Russell and colleagues could not see the induction of Vago2 after infection of Aag2 cells with the insect-specific cricket paralysis virus or stimulation with poly(I:C). Moreover, they could also not measure the induction of Vago1 in stimulated or unstimulated cells (Russell *et al.*, 2020).

The antiviral role of the JAK/STAT pathway was mainly studied for DENV infection in transgenic *Aedes aegypti* mosquitoes. Knockdown experiments of the positive regulators for the JAK/STAT pathway Dome and Hop led to increased viral DENV loads. In contrast, the knockdown of the negative regulator protein inhibitor of activated STAT (PIAS) led to decreased viral loads (Souza-Neto *et al.*, 2009). Further experiments showed that overexpression of Dome and Hop in the *Aedes aegypti* midgut decreased DENV infection and dissemination. In contrast, ZIKV infection intensity was not altered after overexpression of Hop, and the dissemination was only reduced at seven days post-infection and absent 14 days post-infection (Jupatanakul *et al.*, 2017). A different study showed that depletion of PIAS in female *Aedes aegypti* led to decreased viral loads of ZIKV (Angleró-Rodríguez *et al.*, 2017). These results indicate that different orthoflaviviruses are differentially affected by the JAK/STAT pathway in mosquitoes, and further research is needed to unravel the exact mechanisms.

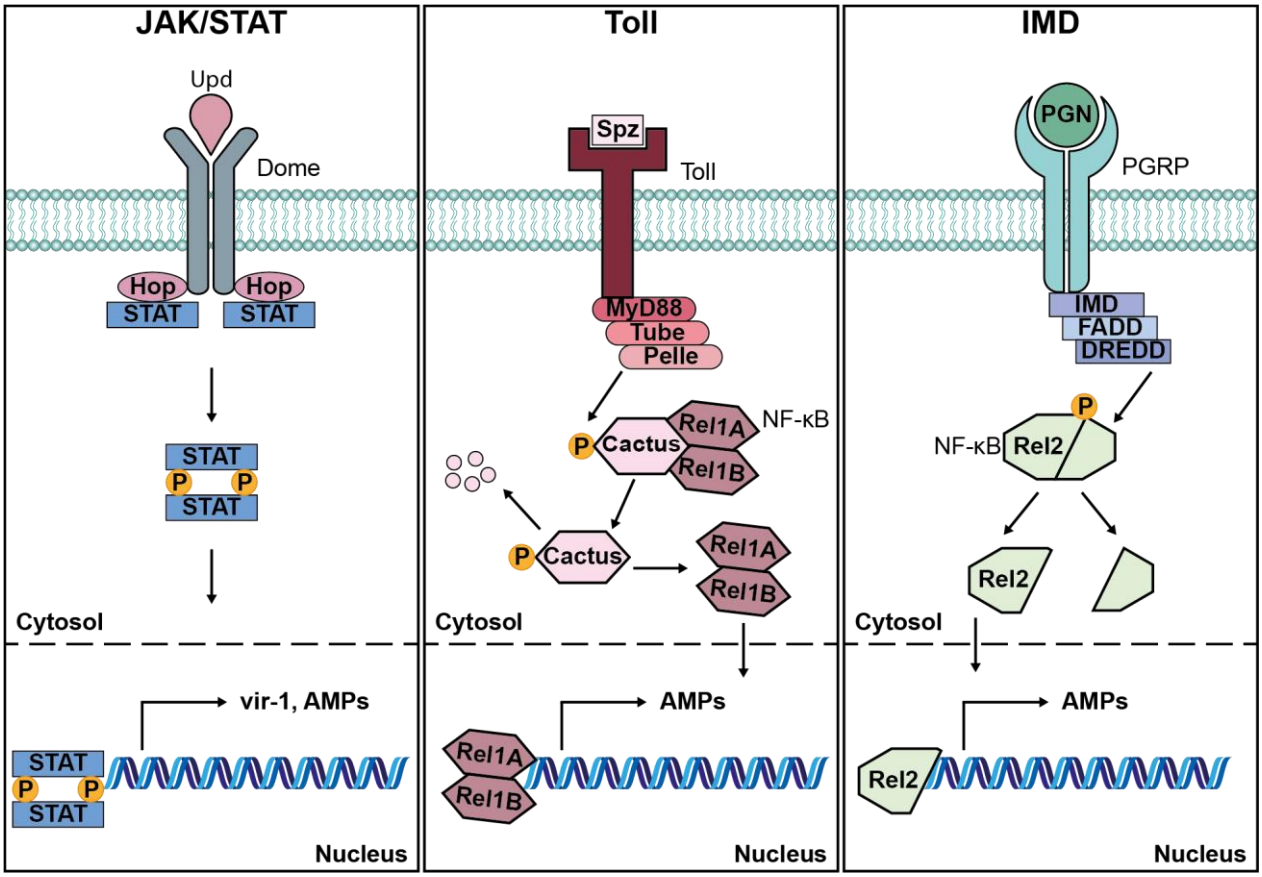

Figure 7: Major signal transduction pathways in insects.
(left): JAK/STAT pathway. The binding of a ligand (in *Drosophila*: Upd) to the receptor Dome leads to the subsequent dimerization of Dome and the autophosphorylation of Hop. Phosphorylated Hop then phosphorylates Dome, leading to the formation of a binding pocket for STAT. Bound STAT is also phosphorylated, leading to its dimerization and translocation into the nucleus, which induces the expression of antimicrobial peptides (AMPs). (middle): Toll pathway. Recognition of pathogen-associated molecular patterns (PAMPs) leads to the cleavage and activation of the precursor cytokine Spz. Spz binds to the Toll receptor, resulting in the dimerization of Toll and the recruitment of the proteins MyD88, Tube, and Pelle. The protein kinase Pelle phosphorylates the negative regulator Cactus, resulting in the release of Rel1A and Rel1B. They translocate into the nucleus, where they induce the expression of AMPs. (right): IMD pathway. The binding of peptidoglycans to their receptor leads to the oligomerization of the intracellular receptor domain and the recruitment of IMD, FADD, and DREDD. DREDD cleaves the transcription factor Rel2, resulting in the translocation of the N-terminal domain of Rel2 into the nucleus, where it induces the expression of AMPs. Picture adapted from (Tikhe *et al.*, 2021).

1.2.1.3 Toll pathway

The Toll pathway was initially discovered in *Drosophila* as a defense mechanism against fungi and Gram-positive bacteria (Hoffmann *et al.*, 2002). Comparative genomic analysis of *Anopheles gambiae* mosquitoes and *Drosophila* showed that genes belonging to the Toll pathway are highly conserved (Christophides *et al.*, 2002). The Toll pathway is activated by recognizing pathogen-associated molecular patterns (PAMPs). Recognition of PAMPs triggers an extracellular proteolytic cascade that results in cleavage and activation of the inactive precursor cytokine pro-Spätzle (Spz) (Figure 7). Activated Spz binds to the Toll receptor, which thereby dimerizes and activates. Toll recruits the death domain-containing proteins myeloid differentiation primary response 88 (MyD88), Tube, and Pelle. The protein kinase Pelle phosphorylates the negative regulator Cactus, which binds the NF-κB-like transcription factor Rel1. In *Aedes aegypti*, unlike *Anopheles gambiae*, two isoforms of Rel are present, called Rel1A and Rel1B (Sang *et al.*, 2005). Cactus undergoes ubiquitin-mediated degradation, thereby releasing Rel1A and its co-activator Rel1B. They translocate into the nucleus to induce the expression of various AMPs (Russell *et al.*, 2020; Tikhe *et al.*, 2021).

The antiviral effect of the Toll pathway was demonstrated in several *in vivo* studies. In 2008, a study showed that gene silencing of the negative regulator Cactus resulted in a 4-fold reduction of DENV viral titers in the midgut of *Aedes aegypti*. Using transcriptional analysis, the authors were also able to provide evidence for induced expression of Rel1 and downstream AMPs upon DENV infection (Xi *et al.*, 2008). Gene silencing of MyD88 resulted in increased levels of DENV virus particles in *Aedes aegypti*. Since mosquitoes from the Rockefeller laboratory strain were used in this experiment, the authors also performed a gene-silencing study in field mosquitoes. Again, inhibition of MyD88 resulted in increased DENV virus particle production (Ramirez *et al.*, 2010). Interestingly, the transcriptional analysis showed that genes relevant to the Toll pathway are also upregulated following ZIKV infection (Angleró-Rodríguez *et al.*, 2017).

Infections of mosquitoes with the maternally transmitted symbiotic bacteria *Wolbachia* showed that infection leads to increased levels of reactive oxygen species (ROS), which can activate the Toll pathway. The activated Toll pathway produces AMPs that lead to the inhibition of DENV in mosquitoes infected with *Wolbachia* (Pan *et al.*, 2012).

In contrast to the *in vivo* data, experiments performed in cell culture showed controversial results. Russell and colleagues could not detect a Toll-induced immune response in the *Aedes aegypti*-derived cell line Aag2 after stimulation with Gram-positive bacteria, Gram-negative bacteria, or viral PAMP dsRNA (Russell *et al.*, 2020). In contrast, another study showed that although pro-Spz1C could not stimulate Aag2 cells, Aag2 cells were stimulated by Spz1C, resulting in the expression of AMPs. This suggests that the Toll pathway in mosquito cells is only functional after administering an active ligand (Saucereau *et al.*, 2022).

1.2.1.4 Immunodeficiency pathway

The immune deficiency (IMD) pathway is a nuclear factor -κB (NF-κB) regulated pathway. Recognition of peptidoglycans, which are part of the bacterial cell wall, activates the IMD pathway. The peptidoglycans bind to the peptidoglycan recognition receptors (PGRPs) (Figure 7). *Aedes aegypti* encodes seven different PGRPs (Wang *et al.*, 2015). The ligand binding to the receptor leads to the oligomerization of the intracellular receptor domain and the recruitment of IMD, Fas-associated death domain (FADD), and DREDD. DREDD cleaves the transcription factor Rel2 in a phosphorylation-dependent manner (Sim *et al.*, 2014). The N-terminal NF-κB domain of Rel2 translocates into the nucleus and activates AMP gene expression. The C-terminal domain of Rel2 remains in the cytosol (Russell *et al.*, 2020).

The antiviral role of the IMD pathway is unknown, but some studies suggest that viral infections lead to the induction of the IMD pathway. Russell and colleagues demonstrated that in the *Aedes aegypti*-derived cell line Aag2, Rel2-inducible genes were upregulated dose-dependent after stimulation with dsRNA and cricket paralysis virus (Russell *et al.*, 2020). In another study, infection of the *Culex quinquefasciatus*-derived cell line Hsu with WNV was shown to result in Dcr-2-dependent activation of Vago (Paradkar *et al.*, 2014). The authors found that Dcr-2 activated the TNF receptor-associated factor (TRAF), which triggered the cleavage of Rel2. Cleavage of Rel2 allowed translocation of the N-terminal domain of Rel2 into the nucleus and binding to the NF-κB binding site in the promoter region upstream of the Vago gene. The inducible expression of Vago led to stimulation of the JAK/STAT pathway (Paradkar *et al.*, 2014).

1.3 Viral evade mechanisms

Viral infections lead to the activation of the host immune system. In order to establish an efficient infection, orthoflaviviruses have evolved several mechanisms to counteract the vertebrate and invertebrate immune systems. Several mechanisms described in the literature depict how orthoflaviviruses evade the vertebrate immune system, which they mainly do through their non-structural proteins. In contrast, little is known about how viruses evade the mosquito immune system. In the following, some examples of viral evade mechanisms are given.

One of the orthoflaviviruses' best-studied mechanisms to block the insect immune system is the generation of non-coding subgenomic flaviviral RNAs (sfRNAs). sfRNAs are generated by the degradation of viral genomic RNA by the 5' → 3' exoribonuclease XRN1/Pacman. XRN1 stalls at conserved structured elements in the 3'UTR of orthoflaviviruses, which leads to the accumulation of sfRNAs (Göertz *et al.*, 2016). Already in 2012, WNV sfRNA was shown to inhibit *in vitro* cleavage of Dicer in the *Aedes albopictus*-derived cell line U4.4 and the *D. melanogaster*-derived cell line S2, thereby inhibiting siRNA- and miRNA-induced RNAi signaling (Schnettler *et al.*, 2012). Further studies showed that not only WNV sfRNA but also DENV sfRNA and Kunjin virus sfRNA interact with Dicer and Ago2, and it was hypothesized that large amounts of sfRNA lead to binding and short-term sequestration of Dicer and Ago2, resulting in mild suppression of RNAi machinery in human and mosquito cells (Moon *et al.*, 2015). *In vivo* experiments with sfRNA-deficient WNV lowered infection and transmission rates after oral infection but not after intrathoracic injection, indicating that sfRNA is relevant for escaping the midgut infection barrier (Göertz *et al.*, 2016). In addition, higher levels of DENV sfRNA were measured in the salivary glands than in the midgut and carcass, suggesting that sfRNA is important for overcoming the midgut barrier and plays a role in the salivary glands (Pompon *et al.*, 2017). Similar results were shown by sfRNA-deficient ZIKV, suggesting high conservation of the function of sfRNA (Slonchak *et al.*, 2020). In addition, ZIKV sfRNA appears to have an anti-apoptotic effect, as ZIKV sfRNA production resulted in altered expression of mosquito genes belonging to cell death pathways (Slonchak *et al.*, 2020). ZIKV sfRNA binds to mosquito DEAD/H-box helicase ME31B, thereby supporting replication and virion production (Göertz *et al.*, 2019). However, in the

same study, ZIKV sfRNA was not shown to suppress the induction of Toll or JAK/STAT signaling.

In addition to the critical role of sfRNA in counteracting the mosquito immune system, orthoflaviviruses exploit several more mechanisms to counteract the mosquito immune system. These include interactions with the JAK/STAT and the NF-κB pathway. WNV NS1 and NS5 were described to target STAT for degradation in *Culex* mosquitoes by inducing the E3 ubiquitin ligase Cullin4 (Paradkar *et al.*, 2015). In the *Aedes albopictus*-derived cell line U4.4, infection with Japanese encephalitis virus (JEV) reduced STAT phosphorylation (Lin *et al.*, 2004). DENV infection of *Aedes aegypti* cells led to the downregulation of four AMPs (Sim *et al.*, 2010). Additionally, co-culturing of Gram-negative bacteria in DENV-infected cells increased bacterial growth, indicating a reduced expression of AMPs from the Toll and IMD pathways. These data suggest that DENV inhibits the immune response in the infected cells (Sim *et al.*, 2010).

While it is known that many orthoflaviviral non-structural proteins antagonize the vertebrate immune system, the precise antagonistic effects of the NS proteins in mosquitoes are not well described. Nevertheless, recent studies showed that NS4B of all four DENV serotypes acts as a suppressor of the RNAi response but does not bind dsRNA. However, the data was generated in Sf21 cells (fall armyworm) and not mosquito cells (Kakumani *et al.*, 2013). Further, it was shown that DENV NS2A functions as a viral suppressor of RNAi (VSR) in insect and vertebrate cells. The VSR activity of DENV-NS2A can be suppressed by introducing a point mutation at position 135 (K135A). DENV-NS2A-K135A replicated less strongly in immunocompetent Aag2 cells than the wild-type virus but comparably to the wild-type virus in RNAi incompetent C6/36 cells (Qiu *et al.*, 2020).

A protein that acts as a suppressor of the RNAi response has also been discovered for YFV. The YFV capsid can bind long double-stranded RNA with high affinity, preventing the RNA from being cut by Dicer (Samuel *et al.*, 2016). The full-length capsid protein of ZIKV could support the replication of an alphavirus, but the observed effect was Dcr-2 independent (Varjak, Donald, *et al.*, 2017).

1.4 Aim of this study

2’-O-methylation at the first nucleotide (N1) of the 5’ end of RNAs has been identified as one of the most important RNA modifications in vertebrates to mark RNA as “self”.

Previous studies showed that YFV-17D exploits this mechanism and 2'-O-methylates its viral RNA to form a cap1 structure, thereby escaping recognition by the vertebrate immune system (Schuberth-Wagner *et al.*, 2015). Considering that mosquito-borne orthoflaviviruses need to replicate efficiently in vertebrates and mosquitoes, this thesis aimed to investigate whether orthoflaviviruses use the 2'-O-methylation of their RNA to evade the mosquito immune recognition as well.

For this purpose, a 2'-O-methyltransferase deficient YFV-17D cap0 virus was established and growth curve analyses of this virus in comparison to its cap1 counterpart were performed on different mosquito cells, including Dcr-2 knockout cells. The latter cell line allowed insights into whether Dcr-2 is involved in recognizing the cap0 structure. In addition, an infectious clone of wild-type YFV-Asibi was generated to study the importance of the 2'-O-methylation for replication not only *in vitro* but also *in vivo* in mosquitoes. Different *in vivo* infection methods were used to narrow down at which level the differentiation between 2'-O-methylated and unmethylated viruses occurs.

Since the 2'-O-methyltransferase is highly conserved between orthoflaviviruses, it was further aimed to study the significance of the 2'-O-methylation in DENV and ZIKV for replication in mosquito cells.

2. Materials and Methods

2.1 Materials

2.1.1 Instruments, reagents, and consumables

Table 1: Equipment/instruments used in this thesis

Equipment/instruments	Manufacturer
Agarose gel documentation	Bioscience Inc., Santa Clara (USA)
Avanti® J-E (rotors: JA-14, JA-25.50)	Beckman Coulter GmbH, Krefeld (Germany)
Blue light transilluminator Visi-BlueTM VB-26	UVP Laboratory Products, Upland (Germany)
Centrifuge Eppendorf 5424	Eppendorf, Hamburg (Germany)
Centrifuge Eppendorf 5424 R	Eppendorf, Hamburg (Germany)
Climate test cabinet MKKL 200/1200	Flohr Instrumenten & Apparatenbouw, Nieuwegein (Netherlands)
Combs for agarose gels (12er, 6er)	Peqlab Biotechnologie GmbH, Erlangen (Germany)
Fluorescence microscope, Axio Imager M1	Carl Zeiss, Oberkochen (Germany)
Galaxy® 170S (incubator)	New Brunswick/Eppendorf, Hamburg (Germany)
Gene Amp PCR System 2400	Applied Biosystems, Thermo Fisher Scientific, Dreieich (Germany)
Gene Pulser Xcell™ electroporation system	Bio-Rad Laboratories GmbH, Munich (Germany)
Glass plate (75 x 50 mm)	Fisherbrand, Schwerte (Germany)
Glassware (flasks, measuring cylinder)	Schott AG, Mainz; Fisherbrand, Schwerte (Germany)
Hemotek membrane feeding device	Hemotek Ltd., Blackburn (UK)
HERAcell™ 240 (cell culture)	Heraeus Holding GmbH, Hanau (Germany)
Heraeus Kelvitron®	Heraeus Holding GmbH, Hanau (Germany)
Heraeus Megafuge 1.0R	Heraeus Holding GmbH, Hanau (Germany)
Heraeus™ B6200 (bacteria)	Heraeus Holding GmbH, Hanau (Germany)
Ice machine AF100	Scotsman Ice Systems, Vernon Hills (USA)
Inverse microscope AE20/AE21 Tension	Motic Deutschland GmbH, Wetzlar (Germany)

Table 1: Equipment/instruments used in this thesis (continued)

Equipment/instruments	Manufacturer
Leica DMS1000 stereomicroscope	Leica, Wetzlar, (Germany)
LightCycler® 480 Instrument II	Roche Molecular Systems, Inc., Mannheim (Germany)
L7-75 Ultracentrifuge	Beckman Coulter GmbH, Krefeld (Germany)
Mastercycler® EP Pro S	Eppendorf, Hamburg (Germany)
Mastercycler® EP Gradient S	Eppendorf, Hamburg (Germany)
Mastercycler® Pro	Eppendorf, Hamburg (Germany)
MilliQ® water processing system	Merck Millipore, Darmstadt (Germany)
NanoDrop 2000c	Thermo Fisher Scientific, Dreieich (Germany)
Nanoject II device	Drummond Scientific Company, Broomall, PA (USA)
Neubauer counting chamber improved	Brand GmbH + Co. KG, Wertheim (Germany)
Pipette boy, accu-jet® pro	Brand GmbH + Co. KG, Wertheim (Germany)
Pipettes, Eppendorf research plus	Eppendorf, Hamburg (Germany)
Power supply Standard Power Pack P25	Biometra GmbH, Göttingen (Germany)
SANYO CO_2 incubator (virus)	SANYO, Moriguchi (Japan)
Scale Kern PNJ 3000-2M	KERN & Sohn GmbH, Balingen (Germany)
Scale TP-3002	Denver Instruments, Göttingen (Germany)
Shaker Certomat S	Sartorius AG, Göttingen (Germany)
Swinging-Bucket Rotor SW 32 Ti	Beckman Coulter GmbH, Krefeld (Germany)
SynergyTM 2 Multi-Detection Microplate Reader	BioTek Instruments, Inc., Winooski (USA)
Thermo printer P93D	Mitsubishi Electric, Erlangen (Germany)
Tissue Lyser	Qiagen, Hilden (Germany)
Vortex-Shaker VV3	VWR, Darmstadt (Germany)
Water bath	Gesellschaft für Labortechnik, Burgwedel (Germany)

Table 2: Chemicals and reagents

Chemicals/reagents	Manufacturer
Acetone	Carl Roth GmbH & Co. KG, Karlsruhe (Germany)
Acedic acid	Carl Roth GmbH & Co. KG, Karlsruhe (Germany)
Adenosine triphosphate (ATP)	Sigma-Aldrich, Munich (Germany)
Agar-agar	Carl Roth GmbH & Co. KG, Karlsruhe (Germany)
Agarose	Biozym Scientific, Hessich Oldendorf (Germany)
Ampuwa® H_2O	Fresenius Kabi, Bad Homburg (Germany)
Arabinose	Merck Millipore, Darmstadt (Germany)
Bovine serum albumin (BSA)	Merck Millipore, Darmstadt (Germany)
Bromphenol blue	Carl Roth GmbH & Co. KG, Karlsruhe (Germany)
Calciumchlorid ($CaCl_2$)	Carl Roth GmbH & Co. KG, Karlsruhe (Germany)
Carbenicillin	Sigma-Aldrich, Munich (Germany)
Chloramphenicol	Sigma-Aldrich, Munich (Germany)
Chloroform	Carl Roth GmbH & Co. KG, Karlsruhe (Germany)
Crystal violet	Merck Millipore, Darmstadt (Germany)
Deoxynucleotide Triphosphates (dNTPs)	Thermo Fisher Scientific, Dreieich (Germany)
Ethanol absolut	AppliChem GmbH (Darmstadt)
Ethidium bromide 1% (EtBr)	Carl Roth GmbH & Co. KG, Karlsruhe (Germany)
Ethylenediamine tetra acidic acid (EDTA) disodium salt (Na_2EDTA)	Carl Roth GmbH & Co. KG, Karlsruhe (Germany)
Ethylenediaminetetraacetic acid (EDTA)	Carl Roth GmbH & Co. KG, Karlsruhe (Germany)
Ficoll® 400	Carl Roth GmbH & Co. KG, Karlsruhe (Germany)
Formaldehyde 37%	AppliChem GmbH, Darmstadt (Germany)
Isopropanol	AppliChem GmbH, Darmstadt (Germany)
Lipofectamine™ 2000	Thermo Fisher Scientific, Dreieich (Germany)
Lysogeny broth (LB) medium (Luria Miller)	Carl Roth GmbH & Co. KG, Karlsruhe (Germany)
Magnesium chloride ($MgCl_2$)	Qiagen, Hilden (Germany)

Table 2: Chemicals and reagents (continued)

Chemicals/reagents	Manufacturer
Magnesium sulfate	Sigma-Aldrich, Munich (Germany)
Methanol	AppliChem GmbH, Darmstadt (Germany)
Midori Green Advance DNA Stain	Genetics Europe GmbH, Düren (Germany)
Sodium bicarbonate ($NaHCO_3$)	Carl Roth GmbH & Co. KG, Karlsruhe (Germany)
Pilomann 1%	Bausch-Lomb, Rochester, NY, (USA)
Potassium acetate	Carl Roth GmbH & Co. KG, Karlsruhe (Germany)
RNase free H_2O	Invitrogen™, Thermo Fisher Scientific, Dreieich (Germany)
Sheep blood, defibrinated	Fiebig, Xebios Diagnostics GmbH, Düsseldorf (Germany)
Sodium chloride (NaCl)	Carl Roth GmbH & Co. KG, Karlsruhe (Germany)
Sodium chloride solution (sterile)	Braun, Melsungen (Germany).
Sodium dodecyl sulfate (SDS)	Carl Roth GmbH & Co. KG, Karlsruhe (Germany)
Sodium hydroxide (NaOH)	Carl Roth GmbH & Co. KG, Karlsruhe (Germany)
Sucrose	Carl Roth GmbH & Co. KG, Karlsruhe (Germany)
Super Optimal broth with Catabolite repression (SOC) medium	Invitrogen™, Thermo Fisher Scientific, Dreieich (Germany)
Terrific broth (TB) Medium	Carl Roth GmbH & Co. KG, Karlsruhe (Germany)
TRIS	Carl Roth GmbH & Co. KG, Karlsruhe (Germany)
TRIS PUFFERAN® ≥ 99,9%	Carl Roth GmbH & Co. KG, Karlsruhe (Germany)
Tris-hydrochloride (Tris-HCl)	Carl Roth GmbH & Co. KG, Karlsruhe (Germany)
TRIzol™ Reagent	Invitrogen™, Thermo Fisher Scientific, Dreieich (Germany)
Trypanblau	Carl Roth GmbH & Co. KG, Karlsruhe (Germany)
Xylene cyanole	Carl Roth GmbH & Co. KG, Karlsruhe (Germany)
Zeocin	InvivoGen, San Diego, CA (USA)

Table 3: Consumables used in this thesis

Consumables	Manufacturer
4titude® 96 Well Semi-Skirted PCR Plate	Azenta, Burlington, Massachusett (USA)
Cell culture dish (p150)	TPP, Trasadingen (Switzerland)
Cell culture flasks with/without filter(T25, T75, T175)	Corning/Fisher Scientific GmbH, Schwerte (Germany)
Cell culture plates (6-, 24-, 48-, 96-wells)	TPP, Trasadingen (Switzerland)
Centrifuge tubes NalgeneTM (250 ml)	Thermo Fisher Scientific, Dreieich (Germany)
Electroporation cuvette (2 mm)	VWR International GmbH, Langenfeld (Germany)
Eppendorf Safe-Lock™ Tube (1.5 ml, 2 ml)	Eppendorf Vertrieb Deutschland GmbH, Wesseling (Germany)
Glass capillary	Drummond Scientific Company, Broomall, PA (USA)
Greiner LUMITRAC™ 600 microplate (96 well)	Greiner Bio-One GmbH, Frickenhausen (Germany)
Inoculation loop	VWR International GmbH, Langenfeld (Germany)
PCR-reaction tubes (0.2 ml)	Sarstedt AG & Co. KG, Nümbrecht (Germany)
Pipet tips with filter (10 µl, 20 µl, 100 µl, 200 µl, 1000 µl)	STARLAB GmbH, Hamburg (Germany)
Pipet tips without filter	STARLAB GmbH, Hamburg (Germany)
Precellys zirconium oxide beads (1.4 mm diameter)	Bertin Technologies, Montigny-le-Bretonneux (France)
Precision tweezers DUMONT	Carl Roth GmbH & Co. KG, Karlsruhe (Germany)
Reaction tubes (0.5 ml, 1.5 ml, 2.0 ml)	Sarstedt AG & Co. KG, Nümbrecht (Germany)
Screw cap tubes (15 ml, 50 ml)	STARLAB GmbH, Hamburg (Germany)
Serological pipets (1 ml, 2 ml, 5 ml, 10 ml, 25 ml)	Sarstedt AG & Co. KG, Nümbrecht (Germany)
Spring steel tweezers, pointed	Carl Roth GmbH & Co. KG, Karlsruhe (Germany)
Sterican® Gr. 20 cannula	B. Braun SE, Melsungen (Germany)

2.1.2 Kits and enzymes

Table 4: Kits used in this thesis

Description	Manufacturer
mMESSAGE mMACHINE™ T7 Transcription Kit	Invitrogen™, Thermo Fisher Scientific, Dreieich (Germany)
mMESSAGE mMACHINE™ SP6 Transcription Kit	Invitrogen™, Thermo Fisher Scientific, Dreieich (Germany)
Phusion® High-Fidelity PCR Kit	Thermo Fisher Scientific, Dreieich (Germany)
SuperScript® III One-Step RT-PCR System with Platinum® Taq DNA Polymerase Kit	Invitrogen™, Thermo Fisher Scientific, Dreieich (Germany)
SuperScript™ III Reverse Transcriptase	Invitrogen™, Thermo Fisher Scientific, Dreieich (Germany)
KAPA SYBR® FAST One-Step	Roche Molecular Systems, Inc., Mannheim (Germany)
NucleoBond® Xtra Midi Kit	Macherey-Nagel, Düren (Germany)
NucleoSpin® Plasmid	Macherey-Nagel, Düren (Germany)
NucleoSpin® Gel and PCR Clean-up Kit	Macherey-Nagel, Düren (Germany)
NucleoSpin® RNA Virus	Macherey-Nagel, Düren (Germany)
Monarch® DNA Gel Extraction Kit	New England Biolabs GmbH, Frankfurt a.M. (Germany)
Renilla Luciferase Assay System	Promega GmbH, Walldorf (Germany)
Rapid DNA Ligation Kit	Thermo Fisher Scientific, Dreieich (Germany)
Lipofectamine™ 2000 Transfection Reagent	Invitrogen™, Thermo Fisher Scientific, Dreieich (Germany)

Table 5: Enzymes and antibodies

Description	Manufacturer
Calf intestinal alkaline phosphatase (CIP)	New England Biolabs GmbH, Frankfurt a.M. (Germany)
T4 ligase	Thermo Fisher Scientific, Dreieich (Germany)
Restriction enzymes	New England Biolabs GmbH, Frankfurt a.M. (Germany)
Trypsin-EDTA (0.05%)	Thermo Fisher Scientific, Dreieich (Germany)
Anti-Flavivirus Group Antigen Antibody (MAB10216)	Merck Millipore, Darmstadt (Germany)

Table 5: Enzymes and antibodies (continued)

Description	Manufacturer
Alexa Fluor® 555 goat anti-mouse (A21424)	Invitrogen™, Thermo Fisher Scientific, Dreieich (Germany)

2.1.3 Buffers and solutions

Table 6: Buffers and solutions

Description	Composition
P1 resuspension buffer	0.5 M EDTA (pH 6) 1 M Tris-HCl (pH 8) RNase A (10 mg/ml) ad H_2O
P2 lysis buffer	200 mM NaOH 1% SDS ad H_2O
P3 neutralization buffer	3M K-acetate (pH 5.4) ad H_2O
50x Tris-acetate-EDTA (TAE)-buffer	242 g Tris 100 ml Na_2EDTA (0.5 M, pH 8) 57.1 ml acetic acid ad 1 L H_2O
Crystal violet staining solution	0.2% crystal violet in 20% EtOH
Trypan blue (working solution)	0.5% Trypan blue in DPBS
2x MEM	9.87 g MEM-powder 2.2 g $NaHCO_3$ ad 470 ml H_2O, sterile-filtered 20 ml FCS 10 ml Pen/Strep

2.1.4 Oligonucleotides and plasmids

Oligonucleotide primers were purchased from IDT (Coralville, Iowa, USA). The sequences are presented in the 5'-3' direction, and primers in sense orientation are labeled as forward (for) and primers in antisense orientation as reverse (rev).

Table 7: Oligonucleotides

Primer name	Orientation	Sequence (5'-3')
Bo87	for	ATGCCCTGTCAGGCTCCCAG
Bo166	rev	TAGGAGATGTGAGTGGGTTTGAC
Bo222	rev	CAGGGCCAGTACTCTGATAGTGG
Bo286	for	ACGAGAGAGATGATAGGGTCTGC
Bo443	for	AGGTTCAGACGAACGGACCTTG
Bo618	rev	GATAGATCCATCGCAGTCTATGGTGTA
Bo619	for	GAAAAACCCTGGGCGTTAACATGGTACGACGAGGAGTTC
Bo620	rev	GAACTCCTCGTCGTACCATGTTAACGCCCAGGGTTTTTC
Bo650	for	TCAGGGTTATTGTCTCATGAGCGG
Bo721	for	TCAACAAAGCCACGTTGTGT
Bo795	rev	CAATGACAATAGTCATGCTG
Bo927	for	TTCGAGCTCACGCGTAAATTTAATACGACTCACTATAGAGT TGTTAG
Bo944	for	ACATTGATTGCTGGTGCTAT
Bo1023	rev	CTGCACTTGAGATGTCCTGTGAAGAG
Bo1149	for	CCTGGTGCTGCGTCTCCGCGGTGGCATGGTGAGCAAGG GCGAGGAGGATA
Bo1150	rev	TATCCTCCTCGCCCTTGCTCACCATGCCACCGCGGAGAC GCAGCACCAGG
Bo1151	for	CGGCGGCATGGACGAGCTGTACAAGAACTTTGATTTATTA AAATTAGCAG
Bo1152	rev	CTGCTAATTTTAATAAATCAAAGTTCTTGTACAGCTCGTCC ATGCCGCCG
Bo1181	rev	CATATGGCACGGCTTCCCTTTGC
Bo1307	for	CCAGGAATTCCACTCATGCCATGTACTACGTGTCTGGAGC
Bo1308	rev	GCTCCAGACACGTAGTACATGGCATGAGTGGAATTCCTGG
Bo1309	for	GGAGGGATCTTTTTATTCTTGATGA
Bo1310	rev	ACATGTACCATATGGCTCTGCTGCC
Bo1311	for	TCACGAAACTCCACACATGCCATGTACTGGGTATCCAATG
Bo1312	rev	CATTGGATACCCAGTACATGGCATGTGTGGAGTTTCGTGA

Table 7: Oligonucleotides (continued)

Primer name	Orientation	Sequence (5'-3')
Bo1313	for	TCCCGCAACTCTACACATGCCATGTACTGGGTCTCTGGAG
Bo1314	rev	CTCCAGAGACCCAGTACATGGCATGTGTAGAGTTGCGGA
Bo1315	for	ATTGACCCCCAAGTGGAGAAAAAGA
Bo1316	rev	TAATCCCAGCCCTTCAACACCACCT
Bo1346	for	GGTGAATTGTGTGAAGACAC
Bo1401	for	ATGAAAGGCGTGGAACGCCT
Bo1402	rev	AGGCGTTCCACGCCTTTCAT
Bo1403	for	TTTAGAGACTCTGATGACTG
Bo1404	rev	CAGTCATCAGAGTCTCTAAA
Bo1405	for	CTGTGAAGCTTGCATCAATA
Bo1406	rev	TATTGATGCAAGCTTCACAG
Bo1407	for	AAAACGAGGTAGACATTTCT
Bo1408	rev	AGAAATGTCTACCTCGTTTT
Bo1415	for	CTTTTGTACCATGGTTATCA
Bo1416	rev	TGATAACCATGGTACAAAAG
Bo1417	for	AAGAGGTCCAGTTGATCGCT
Bo1418	rev	AGCGATCAACTGGACCTCTT
Bo1419	for	GGCCACTTCGTATCTCCGCA
Bo1420	rev	TGCGGAGATACGAAGTGGCC
Bo1436	for	CATCCAAGATAACCAAGTGG
Bo1437	rev	CCACTTGGTTATCTTGGATG
Bo1440	for	CAAAGGATTCACTCTTGGAA
Bo1441	rev	TTCCAAGAGTGAATCCTTTG
Bo1442	for	GAACATCATTACCTTCAAGG
Bo1443	rev	CCTTGAAGGTAATGATGTTC
Bo1467	for	GGCATGATGGTCCTCGCGATGGTGAGA
Bo1468	rev	TCTCACCATCGCGAGGACCATCATGCC
Bo1475	rev	GGCTGCTCTCTCCAGTTCCA
Bo1493	for	CTAGGAGTTGGGGCGGATCAAGGATGCGCC
Bo1494	rev	GGCGCATCCTTGATCCGCCCCAACTCCTAG
Bo1511	for	GACGTGGAGGAGAACCCTGGACCTATGTCTGGTCGTAAA GCTCAGGGA
Bo1512	rev	TCCCTGAGCTTTACGACCAGACATAGGTCCAGGGTTCTCC TCCACGTC
Bo1542	for	GTGAGCTTATCTGAAACACC
Bo1543	rev	GGTGTTTCAGATAAGCTCAC

Table 7: Oligonucleotides (continued)

Primer name	Orientation	Sequence (5'-3')
Bo1578	for	AAAACTGGACGCCGGGGGAG
Bo1581	rev	CTCCCCCGGCGTCCAGTTTT
Bo1602	for	GCAACAAAGGTCCATCCAAG
Bo1603	rev	CTTGGATGGACCTTTGTTGC
Bo1663	for	GAAGGTAGGAGGGGAGCTGC
Bo1664	rev	GCAGCTCCCCTCCTACCTTC

Table 8: PCR primers for SYBR green qPCR

Name	Sequence (5' - 3')
Bo1528 vir-1 for	GGAGGACATCAGTAAGCACATAG
Bo1529 vir-1 rev	TAAACGGAACGGTTGGACG
Bo1530 Ago2 for	GTAGCCTCGTTCGCAATGTA
Bo1531 Ago2 rev	CTCAACAAGAAGCACCCTGA
Bo1532 MyD88 for	GCGACTGGTGGTTGTTATTTC
Bo1533 MyD88 rev	TTATACCCTGCGTGTACGAAC
Bo1536 Dcr-1 for	GTCACCCTGTGAGTGACAGTT
Bo1537 Dcr-1 rev	ATATCGTGCGCTTGGCTGAA
Bo1234 ACT for	CGTTCGTGACATCAAGGAAA
Bo1235 ACT rev	GAACGATGGCTGGAAGAGAG

Table 9: qPCR primers and probes

Name	Sequence (5' - 3')	5' reporter dye/quencher
Bo1590 YFV qPCR for	TCCCTGAGCTTTACGACCAGA	-
Bo1591 YFV qPCR rev	AATCGAGTTGCTAGGCAATAAACAC	-
Bo1592 YFV Probe	ATCGTTCGT/ZEN/TGAGCGATTAGCAG	5'-FAM 3'-3IABkFQ
Bo1396 DENV qPCR for	GGATAGACCAGAGATCCTGCTGT	-
Bo1397 DENV 1-3 qPCR rev	CATTCCATTTTCTGGCGTTC	-
Bo1398 DENV 4 qPCR rev	CAATCCATCTTGCGGCGCTC	-
Bo1394 DENV Probe 1	CAGCATCAT/ZEN/TCCAGGCACAG	5'-FAM 3'-3IABkFQ
Bo1395 DENV Probe 2	CAACATCAA/ZEN/TCCAGGCACAG	5'-FAM 3'-3IABkFQ

Table 10: Plasmids

Name	Description and source
pACNR/FLYF-17Dx	Full-length infectious cDNA clone of the YFV vaccine strain 17D. Contains an ampicillin resistance gene for propagation in bacteria and an SP6 promoter for *in vitro* transcription (Bredenbeek *et al.*, 2003). Kindly provided by Charles M. Rice, Rockefeller University, New York, USA.
pD2/IC-30P-A-DEN2-FL	Full-length infectious cDNA clone of the DENV-2 strain 16681. Contains an ampicillin resistance gene and a T7 promoter for *in vitro* transcription (Kinney *et al.*, 1997). Kindly provided by Richard M. Kinney, Centers for Disease Control and Prevention, Fort Collins, Colorado, USA.
pCCI-SP6-ZIKV	Full-length infectious cDNA clone of the ZIKV isolate BeH819015 from Brazil. Contains a chloramphenicol resistance gene for propagation in bacteria and an SP6 promoter for *in vitro* transcription (Mutso *et al.*, 2017). Kindly provided by Andres Merits, University of Tartu, Tartu, Estonia.
pIZ/V5	Small vector for expression of proteins in insect cells. Contains a zeocin resistance gene for propagation in bacteria and cell cultures. Kindly provided by Esther Schnettler, Bernhard-Nocht-Institute for Tropical Medicine, Hamburg, Germany.
YF Replicon *Renilla*	Yellow fever virus replicon expressing a *Renilla* luciferase. Contains an ampicillin resistance gene and an SP6 promoter for *in vitro* transcription (Schuberth-Wagner *et al.*, 2015). Kindly provided by Beate Kümmerer, University Hospital Bonn, Bonn, Germany.
YF Replicon *Renilla*-E218A	YFV replicon expressing a *Renilla* luciferase and with abrogated 2'-O-methylation activity of NS5 (E218A mutation). Contains an ampicillin resistance gene and an SP6 promoter for *in vitro* transcription (Schuberth-Wagner *et al.*, 2015). Kindly provided by Beate Kümmerer, University Hospital Bonn, Bonn, Germany.
pCHIKV-mCherry	Full-length infectious cDNA clone of the CHIKV isolate FJ959103 from Mauritius with a mCherry protein in the nsP3 protein. Contains a kanamycin resistance gene and a T7 promoter for *in vitro* transcription (Kümmerer *et al.*, 2012). Kindly provided by Beate Kümmerer, University Hospital Bonn, Bonn, Germany.

Table 10: Plasmids (continued)

Name	Description and source
pPseAsibi	Full-length infectious cDNA clone of a pseudo-Asibi (pPseAsibi). The cDNA clone includes most nucleotide exchanges between YFV-17D and YFV-Asibi. Contains an ampicillin resistance gene and an SP6 promoter for *in vitro* transcription. Kindly provided by Beate Kümmerer, University Hospital Bonn, Bonn, Germany.
YFVR-Gluc	YFV replicon expressing a *Gaussia* luciferase. Contains an ampicillin resistance gene and an SP6 promoter for *in vitro* transcription (Lücke *et al.*, 2022). Kindly provided by Beate Kümmerer, University Hospital Bonn, Bonn, Germany.

2.1.5 Cell lines

Table 11: Cells lines used in this thesis

Name	Description and source
BHK-21/J	Adherent fibroblast cell line that arose from a Syrian hamster. Baby Hamster Kidney (BHK)-21/J cells are a laboratory-passaged derivate of BHK-21 cells. Cells were kindly provided by Charles M. Rice, Rockefeller University, New York, USA (Stoker *et al.*, 1964; Lindenbach *et al.*, 1997).
A549	Adherent cell line isolated from lung tissue of a Caucasian male with lung cancer (Giard *et al.*, 1973). Cells were kindly provided by Ute Winke, University Hospital Bonn, Bonn, Germany.
A549 IFIT1 k.o.	A549 derived IFIT1 negative cell line using the CRISPR-Cas9 technology (Tsukamoto *et al.*, 2023). Cells were kindly provided by Yuta Tsukamoto, University Hospital Bonn, Bonn, Germany.
Vero B4	Adherent cell line established from the kidney of an African green monkey (Ammerman *et al.*, 2009). Cells were kindly provided by Ute Winke, University Hospital Bonn, Bonn, Germany.
C6/36	*Aedes albopictus* cell line from freshly hatched larva origin (Singh, 1967). Cells were obtained from ATCC.
Aag2	*Aedes aegypti* cell line from embryonic origin (Peleg, 1968). Cells were kindly provided by Sandra Junglen, Charité Berlin, Germany.
Aag2 AF5	Single cell-derived clonal cell line from Aag2, negative for Phasi Charoen-like virus (Fredericks *et al.*, 2019). Cells were kindly provided by Kevin Maringer, University of Surrey, United Kingdom.
Aag2 AF319	AF5-derived Dcr-2 negative cell line created using the CRISPR-Cas9 technology (Varjak, Maringer, *et al.*, 2017). Cells were kindly provided by Kevin Maringer, University of Surrey, United Kingdom.

Table 11: Cells lines used in this thesis (continued)

Name	Description and source
Aag2 C3PC12	Aag2 cell clone derivates, which are cleared of the persistently infecting viruses cell fusing agent virus, Phasi Charoen-like virus, and Culex Y virus (Machado *et al.*, 2022). Cells were kindly provided by Ronald van Rij, Radboud Institute for Molecular Life Science in Nijmegen, Netherlands.
U4.4	*Aedes albopictus* cell line from larvae origin (Singh, 1967; Condreay *et al.*, 1986). Cells were kindly provided by Sandra Junglen, Charité Berlin, Germany.
CCL-125	*Aedes aegypti* cell line from larva origin (Singh, 1967). Cells were kindly provided by Sandra Junglen, Charité Berlin, Germany.

2.1.6 Bacterial strains

Table 12: Bacterial strains

Name	Description	Source
MC1061	Chemically competent *Escherichia coli* (*E. coli*) bacteria used for general cloning procedures.	Kindly provided by Charles M. Rice, Rockefeller University, New York, USA.
Top10	Chemically competent *E. coli* bacteria used for cloning procedures with the vector pIZ/V5.	Thermo Fisher Scientific, Dreieich (Germany)
Stbl3	Chemically competent *E. coli* bacteria used for cloning procedures with the vector pIZ/V5.	Kindly provided by Martin Schlee, University Hospital Bonn, Bonn, Germany.
EPI300	Chemically competent *E. coli* bacteria with a mutant *trfA* gene under the control of an inducible promoter for CopyControl clones. EPI300 cells were used for the propagation of the pCC1BAC plasmid.	Kindly provided by Andres Merits, University of Tartu, Tartu, Estonia.

2.1.7 Cell culture medium and supplements

Table 13: Cell culture medium and supplements used in this thesis

Description	Manufacturer
Minimum Essential Medium (MEM)	Gibco Thermo Fisher Scientific, Dreieich (Germany)
Dulbecco's Modified Eagle Medium (DMEM)	Gibco Thermo Fisher Scientific, Dreieich (Germany)

Table 13: Cell culture medium and supplements used in this thesis (continued)

Description	Manufacturer
Leibovitz's L-15 Medium (L-15)	Gibco Thermo Fisher Scientific, Dreieich (Germany)
Fetal bovine serum (FCS/FBS)	Sigma-Aldrich, Munich (Germany)
Non-Essential Amino Acids (NEAA) (100x)	Gibco Thermo Fisher Scientific, Dreieich (Germany)
L-Glutamin (100x)	Gibco Thermo Fisher Scientific, Dreieich (Germany)
Tryptose Phosphate Broth (TPB)	Gibco Thermo Fisher Scientific, Dreieich (Germany)
0.05% Trypsin-EDTA	Gibco Thermo Fisher Scientific, Dreieich (Germany)
Dimethyl sulfoxide (DMSO)	Carl Roth GmbH & Co. KG, Karlsruhe (Germany)
Dulbecco's Phosphate-Buffered Saline (DPBS)	Gibco Thermo Fisher Scientific, Dreieich (Germany)
OptiPRO™ SFM	Gibco Thermo Fisher Scientific, Dreieich (Germany)
Opti-MEM	Gibco Thermo Fisher Scientific, Dreieich (Germany)
Penicillin/Streptomycin (Pen/Strep) (100x)	Gibco Thermo Fisher Scientific, Dreieich (Germany)
Poly-L-Lysine	Gibco Thermo Fisher Scientific, Dreieich (Germany)

2.1.8 Software

Table 14: Software

Description	Developer
Adobe Illustrator (version 27.5)	Adobe Inc., San José, California (USA)
Gen5 Microplate Reader	BioTek Instruments, Inc., Winooski (USA)
Geneious Prime® (version 2019.2.3)	Biomatters Ltd., Auckland (New Zealand)
LightCycler® 480 Software LCS480 1.5.1.62	Roche Molecular Systems, Inc., Mannheim (Germany)
Mendeley Desktop (version 1.19.8)	Elsevier, Amsterdam (Netherlands)
Microsoft Office 2016 (version 16.0.4266.1001)	Microsoft Corporation, Redmond (USA)
Prism (version 9.5.1)	GraphPad, La Jolla (USA)

2.2 Methods

2.2.1 Cell culture

2.2.1.1 Cell culture of vertebrate cells

All vertebrate cells were cultured in the respective medium (Table 15) at 37 °C and 5% CO_2 under sterile conditions. Cells were subcultured twice (Vero B4, A549) or three times (BHK-21/J) a week. Therefore, the old medium was removed, cells were washed twice with PBS, and detached by adding trypsin-EDTA onto the cells. Following 5 min incubation at 37 °C, the trypsin reaction was stopped by adding four times the volume of medium containing serum. Depending on the split ratio, the appropriate volume of cells was transferred into a new flask, and the corresponding medium was added.

Table 15: Composition of the vertebrate cell culture medium

Cell line	Medium	Supplements
BHK-21/J	MEM	7.5% FBS 1% NEAA 1% L-Glut
A549/Vero B4	DMEM	10% FBS

2.2.1.2 Cell culture of insect cells

All insect cells were cultured in the respective medium (Table 16) at 28 °C without CO_2. The cells were subcultured twice a week to a ratio of 1:2 to 1:4, depending on their confluency. For Aag2, C6/36, and U4.4 cells, the old medium was removed, fresh medium was added, and the cells were mechanically detached from the flask with a cell scraper. CCL-125 cells were washed twice with PBS before they were detached by adding trypsin-EDTA for 5 min at 28 °C. The reaction was stopped by adding four times the volume of medium containing serum. Depending on the split ratio, the appropriate volume of cells was transferred into a new flask, and the corresponding medium was added. To seed Aag2 cells for further experiments, they were trypsinized as described for CCL-125 cells.

Table 16: Composition of the insect cell culture medium

Cell line	Medium	Supplements
C6/36	L-15	10% FBS
Aag2 (wt, AF5, AF319)	L-15	10% FBS 10% TPB 1% NEAA
CCL-125	L-15	20% FBS
U4.4	L-15	20% FBS 2% TPB 1% NEAA

2.2.1.3 Cell counting and seeding

Cells were counted using a Neubauer counting chamber to seed them with the desired concentration. The detached cells were mixed 1:1 with trypan blue (0.5% in DPBS), a non-membrane permeable substance that only non-living cells can absorb. The viable cells of four chamber squares were counted using a transmitted-light microscope, and the average cell number was calculated. The total number of cells per ml was calculated using the following formula:

$$\frac{number\ of\ counted\ cells}{number\ of\ counted\ squares} * dilution\ factor * 10^4 = {}^{cells}/_{ml}$$

The required volume of cells per well was calculated with the following formula:

$$\frac{{}^{desired\ cells}/_{well}}{{}^{avaible\ cells}/_{ml}} * 1000 = x\ \mu l\ cells\ per\ well$$

The cells were seeded in a total volume of 200 µl in 96-well plates, 1 ml in 24-well plates, and 2 ml in 6-well plates.

2.2.1.4 Electroporation of vertebrate cells

This study used electroporation to introduce *in vitro* transcribed RNA into BHK-21/J cells by an electrical pulse. 24 h prior to electroporation, the cells were split to a ratio of 1:2 to ensure exponential growth. Cells were suspended (2.2.1.1) according to the protocol for electroporation, and the cell number was determined. The suspended cells were pelleted by centrifugation, the supernatant discarded, and the cells washed twice with 10 ml ice-cold OptiPRO™ SFM medium. All centrifugation steps were performed at 1200 rpm and

4 °C for 10 min. After the last washing step, the cells were set to a final concentration of 2 x 10^7 cells/ml and kept on ice until further use. Next, the *in vitro* transcribed RNA was thawed on ice, and a 2 µl RNA aliquot was transferred to a fresh 1.5 ml reaction tube. In a second reaction tube, 50 µl OptiPRO™ SFM medium was mixed with 50 µl cell suspension (≙ 10^6 cells). The 100 µl cell suspension was pipetted onto the RNA, mixed gently, transferred to a 2 mm electroporation cuvette, and placed in the ShockPod cuvette chamber. The cells were subjected to an electric pulse of 140 V for 25 ms using a Gene Pulser Xcell™ electroporator. Following the electric pulse, the cells were incubated for 10 min at room temperature (RT) and then transferred to 1.25 ml BHK-21/J medium using a Pasteur pipette. Depending on the subsequent application, all cells were seeded in a T25 flask and/or used for an infectious center assay (2.2.4.2).

2.2.1.5 Electroporation of insect cells

Insect cells were likewise electroporated to introduce *in vitro* transcribed RNA into the cells by an electrical impulse. This study used C6/36 and Aag2 cells for electroporation experiments. Due to the lower doubling time of insect cells, they were not split prior to electroporation. The cells were suspended in PBS using a cell scraper, the cell number was determined, and the cells were pelleted by centrifugation. The supernatant was discarded, and the cells were washed twice with 10 ml PBS. All centrifugation steps were performed at 1200 rpm for 10 min. Following the last washing step, the cells were set to a final concentration of 2 x 10^7 cells/ml. The *in vitro* transcribed RNA was thawed on ice, and a 2 µl aliquot was transferred to a new 1.5 ml reaction tube. A volume of 500 µl cells (≙ 10^7 cells) was added to the RNA, mixed gently, and then transferred to a 2 mm electroporation cuvette. The cuvette was placed in the ShockPod cuvette chamber, and the cells were subjected twice to an electric pulse of 400 V, 25 µF, and 800 Ω using a Gene Pulser Xcell™ electroporator. The cells were incubated for 1 min at RT before they were transferred to 1 ml C6/36 or Aag2 medium. The cells were seeded in 24-well plates at a concentration of 5 x 10^5 cells/well or in T25 flasks at a concentration of 5 x 10^6 cells, depending on the subsequent application.

2.2.1.6 Transfection of cells

In this study, chemical transfection was used to introduce *in vitro* transcribed RNA into Vero E6 cells. The cells were seeded 24 h prior to transfection at a final concentration of

8×10^4 cells/well in a 24-well plate. For each well, two mixtures were prepared. The first one contained 2 µl RNA diluted in 150 µl Opti-MEM and the second one 5 µl Lipofectamine 2000 diluted in 150 µl Opti-MEM. The latter was added to the diluted RNA and incubated for 15 min at RT. Before adding 300 µl RNA-lipid complexes to the cells, the cell culture medium was exchanged with 1 ml fresh medium. The transfected cells were incubated at 37 °C and 5% CO_2 for 8 h before the cell culture medium was again exchanged, and the FCS concentration was reduced to 2%. The cells were incubated for another ten days before the virus was harvested.

2.2.2 Microbiological methods

2.2.2.1 Transformation

Depending on the used plasmids, different chemically competent *E. coli* cells (MC1061, Stbl3, or EPI300) were used for transformation (Table 17). All cells were thawed on ice and diluted 1:10 with 0.1 M $CaCl_2$-solution. Afterward, 100 µl cells were mixed with 10 µl ligation mixture and incubated on ice for 20 min (MC1061, Stbl3) or 35 min (EPI300). Heat shock was performed for the MC1061 and Stbl3 cells at 43.5 °C for 45 sec and for the EPI300 cells at 42 °C for 2 min. Following the heat shock, the cells were placed on ice for 2 min. After adding 200 µl LB medium (MC1061, Stbl3) or 200 µl SOC medium (EPI300), the cells were incubated at 37 °C and 300 rpm for 30 to 60 min. The reaction mixtures were plated on agar plates (MC1061, Stbl3: LB plates; EPI300: TB plates) containing the appropriate antibiotic (Table 17) and incubated at 37 °C overnight.

Table 17: Vector, bacteria, and antibiotics used in this study

Vector	*E. coli* cells	Antibiotic	Concentration
pACNR/FLYF-17Dx	MC1061	Carbenicillin	50 mg/ml
pBR322-DEN2-FL	MC1061	Carbenicillin	50 mg/ml
pIZ/V5	Stbl3	Zeocin	25 µg/ml
pCC1BAC	EPI300	Chloramphenicol	12.5 µg/ml

2.2.2.2 Plasmid isolation

Mini preparation and plasmid isolation: Single MC1061 or Stbl3 colonies from the agar plate were inoculated with 5 ml LB medium containing the appropriate antibiotic and incubated overnight at 37 °C and 180 rpm. Isolation and purification of the plasmids were performed using the NucleoSpin® Plasmid kit according to the manufacturer's instructions,

except for the following steps: for low copy plasmids, 2 x 2 ml cultivated bacteria were harvested via centrifugation at 11,000 rpm for 5 min, and the plasmid DNA was eluted with 30 µl pre-warmed (70 °C) AE buffer. Single EPI300 colonies were inoculated with 10 ml TB medium containing chloramphenicol and incubated overnight at 37 °C and 180 rpm. The next day, the 10 ml pre-culture was used to inoculate 40 ml TB medium containing chloramphenicol and 0.1% arabinose. This culture was incubated at 37 °C and 180 rpm for 5 h. The cultivated bacteria were centrifuged at 5,000 rpm for 10 min before they were suspended in 10 ml P1 buffer. The same amount of lysis buffer P2 was added and incubated for 5 min at RT. Finally, the lysis reaction was stopped by carefully adding 10 ml neutralization buffer P3. The lysate was clarified by centrifugation (15,000 rpm, 30 min, RT), and the clear supernatant was passed through an organza fabric before 0.6 volumes of isopropanol were added. The DNA was precipitated by centrifugation at 15,000 rpm for 30 min and 4 °C. The supernatant was removed, and the precipitated DNA was isolated a second time using the NucleoSpin® Plasmid kit as described above. All isolated plasmids were control digested (2.2.3.5) with specific restriction enzymes to verify the resulting band sizes.

Midi preparation and plasmid isolation: 150 – 200 µl MC1061 or Stbl3 mini cultures were used to inoculate 150 – 200 ml LB medium containing the appropriate antibiotics. The midi cultures were incubated overnight at 37 °C and 180 rpm. The bacteria were harvested by centrifugation of the liquid culture at 5,000 rpm for 30 min, and the plasmids were isolated using the NucleoBond® Xtra Midi kit according to the manufacturer's instructions except for the following steps: the precipitated DNA was washed with 1.5 ml 70% EtOH, and the dried DNA was reconstituted using 50 µl H_2O at 37 °C. For Epi300 cells, 50 µl mini culture was used to inoculate 50 ml TB medium containing 12.5 µg/ml chloramphenicol. The culture was incubated overnight at 37 °C and 180 rpm before the 50 ml culture was used to inoculate 450 ml TB medium containing 12.5 µg/ml chloramphenicol and 0.1% arabinose. This culture was incubated for 5 h at 37 °C and 180 rpm. The bacteria were collected by centrifugation at 4,000 g for 15 min. The liquid was removed, and the bacteria were suspended in 30 ml P1 buffer. The bacterial suspension was then divided into two tubes, and 15 ml lysis buffer P2 was added to each tube. The solutions were incubated at RT for 5 min before adding 15 ml neutralization buffer P3. The lysates were cleared by centrifugation at 15,000 g for 30 min and then

passed through an organza fabric. 0.6 volumes of isopropanol were added, and the DNA was precipitated by centrifugation at 15,000 g, 30 min, and 4 °C. The liquid was removed, and the precipitated DNA was isolated a second time using the NucleoBond® Xtra Midi kit according to the manufacturer's instructions as described above. The resulting DNA concentrations were photometrically measured using the NanoDrop 200c, and the concentration was set to 1 µg/µl. 100 ng plasmid DNA was used to perform a control digest (2.2.3.5).

2.2.3 Molecular methods

2.2.3.1 Polymerase Chain Reaction (PCR)

DNA fragments were amplified using the Phusion™ High-Fidelity DNA Polymerase kit in a total volume of 25 or 50 µl. The composition of the PCR can be found in Table 18. The annealing temperature was adapted depending on the primers' melting temperature, and the elongation time depended on the length of the fragment to be amplified. The amplification program can be found in Table 19. The sizes of the resulting DNA fragments were verified by applying 1 µl PCR mixture to gel electrophoresis (2.2.3.3).

Table 18: Phusion PCR reaction mixture

Component	25 µl rxn	50 µl rxn
5x Phusion™ HF Buffer	5	10
10 mM dNTPs	0.5	1
10 mM primer forward	0.5	1
10 mM primer reverse	0.5	1
Phusion polymerase	0.5	1
Template DNA (50-100 ng)	0.5	1
H_2O	17	35.5

Table 19: Phusion cycling profile

Cycle step	Temperature	Time	Cycles
Initial Denaturation	98 °C	30''	1
Denaturation	98 °C	10''	35
Annealing	52 – 58 °C	10''	
Extension	72 °C	15 – 30''/kb	
Final Extension	72 °C	5'	1
Hold	4 °C	Hold	1

2.2.3.2 Site-directed mutagenesis through fusion PCR technology

Site-directed mutagenesis through fusion PCR technology can be used to modify DNA fragments precisely. For this purpose, overlapping primers were designed to include the desired mutation centrally (Figure 8). Two additional primers (downstream and upstream) were then used to insert the desired mutation by performing two PCR reactions, one with the primers f1 and r2 and one PCR with primers f2 and r1. The resulting fragments carried the desired mutation and were complementary at their ends. In order to receive the extended PCR product, the first two amplicons were purified (2.2.3.4). These amplicons were then used in a third PCR reaction called fusion PCR. Since the two amplicons were complementary, they hybridized, and the whole fragment was amplified using the primers f1 and r1. The generated double-stranded DNA was first purified and then used for molecular cloning. Schematic illustrations of all constructed plasmids can be found in the appendix (10.2).

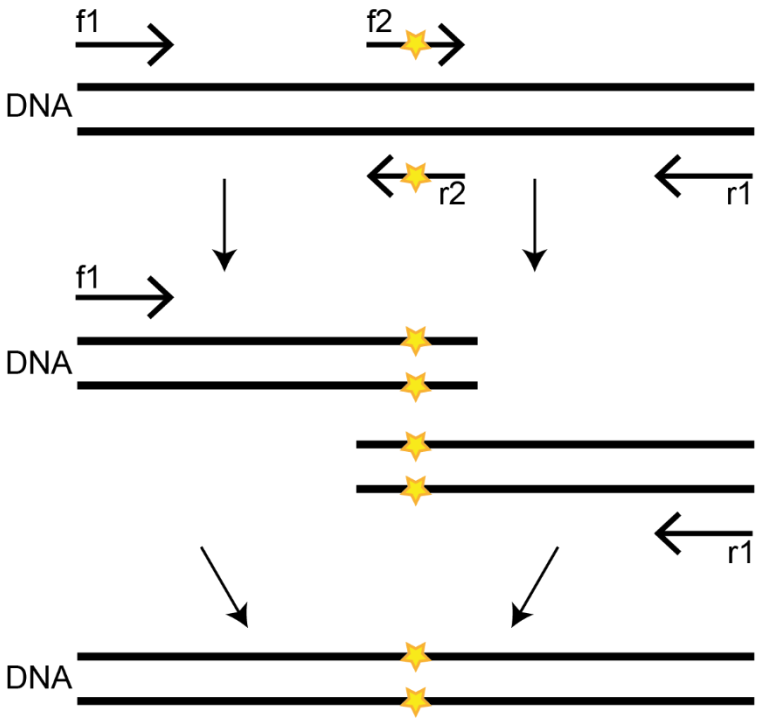

Figure 8: Site-directed mutagenesis through fusion PCR.
The desired mutation is located at the center of primers f2 and r2. In two independent reactions with one upstream and one downstream primer (f1, r1), overlapping fragments with the desired mutations were generated. The two fragments were fused in a third PCR reaction.

2.2.3.3 Agarose gel electrophoresis

Agarose gel electrophoresis was used to visualize DNA or RNA and to separate DNA fragments by size. Standard electrophoresis was conducted in 1% agarose gels prepared in TAE buffer and stained with Midori Green (0.1 µl/ml) for DNA or with EtBr (1 µg/ml) for RNA. The agarose concentration was reduced for larger DNA fragments and increased for smaller fragments. The samples were diluted with 6x loading dye, and a 1 kb plus ladder was used as a marker. Electrophoresis was carried out at 140 V for 20-25 min. DNA and RNA fragments were visualized under UV light.

2.2.3.4 Purification of DNA fragments

PCR purification was performed when a single band was visible after gel electrophoresis. The NucleoSpin® Gel and PCR Clean-up kit was used according to the manufacturer's instructions, except for the last step. Here, the elution buffer was pre-warmed to 70 °C. If more than one band was visible, the DNA was extracted using the Monarch® Gel Extraction kit. Therefore, the whole reaction mixture (PCR or enzymatic) was applied on a 1% agarose gel as described under 2.2.3.3, and the desired DNA fragment was excised from the gel. The excised gel slice was then purified according to the manufacturer's instructions, except for the last step. The elution buffer was pre-warmed to 50 °C, and the centrifugation was carried out at 11,000 rpm. All purified fragments were electrophoretically verified before further use.

2.2.3.5 DNA restriction

DNA restrictions were performed prior to ligation, to analyze plasmid DNA or to linearize plasmid DNA. For a restriction digest, approximately 1 µg vector and 5 – 10 µl PCR fragment were digested with the enzymes for 1 h in a total volume of 30 µl. The digestion time was increased up to 12 h, depending on the efficiency of the used enzymes. The digest was verified by gel electrophoresis. Once the vector and insert were completely digested, the vector was dephosphorylated for 10 min by adding 1.5 U CIP for 10 min at 37 °C. Preparative gel electrophoresis was used to isolate and purify the correct bands. For test digests, approximately 100 ng DNA was digested for 30 min in a total volume of 10 µl, and for linearization 2 µg DNA for 1 h in a total volume of 30 µl. The band sizes were also electrophoretically verified. The standard compositions for all digests are listed in Table 20.

Table 20: Reaction mixtures for restriction and test digest

Component	Restriction digest [µl]	Test digest [µl]	Linearization [µl]
Buffer	3	1	3
Enzyme I	0.7	0.2	0.7
Enzyme II	0.7	0.2	-
DNA	x	x	x
H_2O	ad 30	ad 10	ad 30

2.2.3.6 Ligation

DNA fragments with complementary ends were connected using the Rapid DNA Ligation Kit, whereby a T4 ligase catalyzed the ligation reaction. Vector and insert were used in a ratio of 1:3 and the exact volumes were estimated according to the results from the gel electrophoresis. The standardized composition of a ligation reaction is listed in Table 21. A vector control was included for each ligation to exclude re-ligation of the vector despite dephosphorylation. Here, the vector was used in a ligation reaction without the insert. Ligation was performed for 10 min at RT, and then both ligation mixtures were used for bacterial transformation (2.2.2.1).

Table 21: Ligation reaction mixture

component	Ligation [µl]	Vector control [µl]
Vector	x	x
Insert	x	-
Buffer	2	2
T4 ligase	0.3	0.3
H_2O	ad 10	ad 10

2.2.3.7 Sanger sequencing

Plasmids and PCR reactions were sequenced up to and across cloning junctions to validate the accuracy of the introduced mutations in each construct. Therefore, the plasmids were sent with a suitable forward or reverse primer to Eurofins Scientific (Luxembourg City, Luxembourg). Each sequencing reaction contained 500 ng plasmid DNA or 20 – 400 ng PCR product and 25 µM primer in a total volume of 10 µl. The sequences were analyzed using Geneious Prime®.

2.2.3.8 DNA precipitation and *in vitro* transcription

To rescue viruses from cDNA clones, plasmid DNA was linearized as described in 2.2.3.5 to generate an authentic 3' end upon transcription. The linearization was verified via gel electrophoresis before the linearized DNA was precipitated for 1 h at -80 °C or overnight at -20 °C by adding 70 µl H_2O, 12.5 µl 2 M potassium acetate (pH 5.6), and 250 µl 100% ethanol. The precipitated DNA was pelleted via centrifugation at 14,000 rpm for 15 min at 4 °C, washed once with 200 µl 70% ethanol, and centrifuged at 14,000 rpm for 10 min at RT. The precipitated and pelleted DNA was resolved in 4.3 µl RNase-free H_2O, and 0.3 µl DNA was analyzed via gel electrophoresis. Depending on the promoter present in the cDNA construct, 2 µl linearized and precipitated DNA was *in vitro* transcribed using the SP6 or T7 mMESSAGE mMACHINE™ kit. The standard composition of an *in vitro* transcription (IVT) reaction is listed in Table 22. The reaction was incubated at 37 °C for 2 h before the transcription efficiency was verified by running 0.2 µl RNA on an ethidium bromide gel. The resulting RNA was stored until further use at -80 °C.

Table 22: *In vitro* transcription reaction mixture

Component	Amount for one IVT reaction [µl]
2x NTP/Cap	5
10x reaction buffer	1
GTP	1
Enzyme mix (SP6/T7)	1
Linearized and precipitated DNA	2

2.2.3.9 Isolation of viral RNA

Viral RNA was isolated using the NucleoSpin® RNA Virus Kit from Macherey-Nagel, according to the manufacturer's instructions. Briefly, either 75 µl cell culture supernatant or 140 µl shredded mosquito was lysed in 300 µl RAV1 containing carrier RNA and heated at 70 °C for 10 min. Each sample was mixed with 300 µl ethanol (100%) and loaded onto a column. The loaded silica membranes were washed with 500 µl RAW, 600 µl RAV3, and 200 µl RAV3. The first and second washing steps were performed at 8,000 rpm for 1 min and the third at 11,000 rpm for 5 min. RNA was eluted in 60 µl RNase-free H_2O (pre-heated to 70 °C) and incubated for 2 min. Isolated RNAs were stored at -80 °C until further use.

2.2.3.10 Isolation of cellular RNA

Cellular RNA was isolated with TRIzol™. Therefore, the cell culture supernatant was removed, and the cells were washed once with PBS before 500 µl TRIzol™ was added. The homogenized cells were transferred to a new 1.5 ml reaction tube and incubated at RT for 5 min. Next, 100 µl chloroform was added, the mixture was vortexed for 15 sec and then incubated for 10 min at RT. The samples were centrifuged at 12,000 rpm for 5 min to separate the phases: three phases form, a lower phenol-chloroform phase, an interphase, and a colorless upper phase. The upper phase contained the RNA and was transferred to a new 1.5 ml reaction tube. The RNA was precipitated by adding 250 µl isopropanol and subsequent centrifugation at 12,000 rpm for 15 min at 4 °C. The supernatant was removed, and the RNA pellet was washed twice with 75% EtOH. After each washing step, the RNA was vortexed and centrifuged at 12,000 rpm for 10 min at 4 °C. The washed RNA was air-dried and dissolved in 20 µl pre-heated H_2O (55 °C).

2.2.3.11 Probe-based quantitative real-time PCR

The probe-based quantitative real-time PCR (qRT-PCR) method was used to quantify specific amounts of YFV or DENV RNAs. All qRT-PCR reactions were performed with probes and primers specific for the viruses in a total volume of 20 µl for YFV and 25 µl for DENV. The used primers and probes are listed in Table 9. Amounts of viral RNA were quantified using a known standard serially diluted 1:10 in H_2O. The qRT-PCRs were prepared in sealed 96-well plates and measured using a LightCycler® 480 Instrument II. Table 23 to 26 show the exact compositions and the cycling conditions for the LightCycler®.

Table 23: YFV qRT-PCR reaction mixture

Component	Amount for one qRT-PCR rxn [µl]
2x RXn	10
10 mM primer forward	0.5
10 mM primer reverse	0.5
10 mM probe	0.5
50 mM $MgSo_4$	1
SSIII RT Platinum Taq	0.4
H_2O	4.1
RNA	3

Table 24: YFV qRT-PCR cycling profile

Cycle step	Temperature	Time	Cycles
Reverse transcription	45 °C	30’	1
Initial denaturation	95 °C	5’	1
Amplification	95 °C	10’’	45
Read out	57 °C	30’’	

Table 25: DENV qRT-PCR reaction mixture

Component	Amount for one qRT-PCR rxn [µl]
2x RXn	12.5
10 mM primer forward	0.5
10 mM primer reverse	1
10 mM probe	0.5
BSA (1 mg/ml)	1
50 mM $MgSo_4$	1.3
SSIII RT Platinum Taq	1
H_2O	2.2
RNA	5

Table 26: DENV qRT-PCR cycling profile

Cycle step	Temperature	Time	Cycles
Reverse transcription	45 °C	30’	1
Initial denaturation	95 °C	5’	1
Amplification	95 °C	5’’	45
Read out	57 °C	35’’	
Cooling	40 °C	30’’	

2.2.3.12 SYBR green quantitative real-time PCR

SYBR green qRT-PCRs were used to quantify specific amounts of genes. A single reaction contained 100 ng RNA in a final volume of 10 µl. The composition of a single reaction is listed in Table 27, primers in Table 8, and the cycle program in Table 28. The qRT-PCRs were prepared in sealed 96-well plates and measured using a LightCycler® 480 Instrument II. Actin was used as a reference gene, and the resulting data was quantified using the ΔΔCT method described by Pfaffl and colleagues (Pfaffl *et al.*, 2004).

Table 27: KAPA SYBR® FAST One-Step qRT-PCR reaction mixture

Component	Amount for one qRT-PCR [µl]
KAPA SYBR qPCR Master Mix	5
10 mM dUTP	0.2
10 µM Primer for	0.2
10 µM Primer rev	0.2
50X Kapa RT Mix	0.2
H_2O	2.2
RNA	2

Table 28: KAPA SYBR® FAST One-Step qRT-PCR cycling program

Cycle step	Temperature	Time	Cycles
Reverse transcription	42 °C	5’	1
Enzyme activation	95 °C	3’	1
Denaturation	95 °C	10”	45
Annealing	60 °C	20”	
Read out	72 °C	20”	
Cooling	40 °C	10”	

2.2.4 Virological methods

Depending on the used viruses, virological work was performed either in a Biosafety Level-2 (BSL-2) or BSL-3 laboratory.

2.2.4.1 Production of infectious particles and virus replicon particles

All viral RNA genomes except for ZIKV were electroporated into BHK-21/J cells (2.2.1.4) to generate viral stocks. The electroporated cells were transferred into 1.25 ml medium and seeded into a T25 flask. The medium was filled up to 5 ml with BHK-21/J medium and incubated at 37 °C and 5% CO_2 for 72 h. For ZIKV, viral RNA was transfected (2.2.1.6) in duplicates into Vero E6 cells. The transfected cells were incubated at 37 °C and 5% CO_2 for ten days.

To generate virus replicon particles (VRPs), *in vitro* transcribed packaging construct RNA and replicon RNA were co-electroporated into BHK-21/J cells. Cells were then seeded into a T25 flask, filled up to 5 ml, and incubated at 32 °C and 5% CO_2 for 72 h.

The cell culture supernatant containing infectious particles or VRPs was harvested after the indicated incubation period. Cell debris was removed by centrifugation at 1200 rpm and 4 °C for 10 min. The viruses and VRPs were stored as aliquots at -80 °C until further use.

To generate viral stocks for *in vivo* experiments, supernatants from three electroporations were pooled. The cell culture supernatant containing virus was first centrifuged to remove the cell debris and then ultracentrifuged to concentrate the viral stocks. Therefore, the supernatants were centrifuged at 29,000 rpm and 4 °C for 1.5 h using a Beckman SW 32 Ti rotor. Each sample was dissolved in 200 µl BHK-21/J medium overnight at 4 °C. The aliquots were stored at -80 °C until further use.

2.2.4.2 Infectious Center Assay (ICA)

An infectious center assay was performed after electroporation to obtain a first overview of the infectivity and plaque morphology of the recovered virus. For this purpose, 150 µl of the cells previously adjusted to 2 x10^7 cells/ml were mixed with 12 ml BHK-21/J medium and seeded into a 6-well plate (2 ml/well). This plate was incubated for about 30 min at 37 °C and 5% CO_2. Then, 100 µl of the electroporated and previously with 1.25 ml BHK-21/J medium mixed cells was added to the first well. Another 100 µl of this mixture was diluted in 9.9 ml BHK-21/J medium. From this dilution, 1 ml was added to the second well, 200 µl to the third, 20 µl to the fourth, and 2 µl to the fifth. The sixth well served as a cell control. The cells were incubated for 4 to 6 h before the supernatant was carefully removed, and the cells were overlaid with 3 ml agarose overlay (1:1 1.2% agarose in H_2O: 2x MEM). Cells were incubated for an additional 72 h and were then fixed with 6% formaldehyde. The agarose was removed, and cells were stained with crystal violet.

2.2.4.3 Virus titration and plaque assay

Titration was performed to quantify the amount of virus present in a suspension. The plaque assay was used for viruses showing a cytopathic effect, and the titer is expressed in plaque-forming units per ml (PFU/ml). Depending on the virus to be titrated, two different methods of virus titration were used. For both methods, one 6-well plate of cells was seeded the day before titration for each sample to be titrated. For YFV samples, BHK-21/J cells were seeded at a concentration of 3 x 10^5 BHK-21/J cells/well. The next day, virus samples were serially diluted in 1:10 steps in 1% FCS in PBS. Viruses were titrated from -1

to -6 unless the virus stocks were previously concentrated by ultracentrifugation. In this case, dilution levels from -1 to -7 were prepared, but only dilutions -2 to -7 were used. The BHK-21/J medium of the 6-well plates was removed and replaced by 200 µl of the appropriate virus dilution. The cells were incubated for 1 h at 37 °C and 5% CO_2 before 3 ml overlay was added per well (1:1 1.2% agarose in H_2O: 2x MEM). Cells were incubated for three days at 5% CO_2 and 37 °C and then fixed in 6% formaldehyde for at least 30 min. The plates were rinsed with water, and the agarose was removed from the cells. The fixed cells were rinsed with water again and stained with crystal violet for at least 10 min. The staining solution was removed and the cells were washed with tap water and dried. The number of plaques was counted manually to calculate PFU/ml using the formula below.

$$counted\ plaques\ per\ well * 5 * 10^{dilution\ factor} = \frac{PFU}{ml}$$

For DENV samples, Vero B4 cells were seeded at a concentration of 3 x 10^5 cells/well. The next day, samples were serially diluted in 1:10 steps in 30% FCS in PBS. The viruses were titrated as described above, with one modification. After the one-hour incubation, the inoculum was removed before the agarose overlay was added to the cells due to the high FCS concentration in the virus dilutions. When the agarose overlay reached the gel form, 1 ml DMEM medium was added to the agarose overlay per well to prevent desiccation during incubation. Cells were incubated for 7 d at 37 °C and 5% CO_2 before they were fixed and stained as described above. The number of plaques was counted manually to calculate the PFU/ml using the abovementioned formula.

2.2.4.4 Tissue Culture Infectious Dose 50 ($TCID_{50}$)

Viral titers of non-cytopathic viruses were quantified via $TCID_{50}$ with immunofluorescence as a readout. Virus samples were serially diluted (1:10) with four replicates per dilution from -1 to -6 in DMEM without supplements. An equal amount of Vero B4 cell suspension (2 x 10^4) was mixed with the appropriate virus dilution in a 96-well plate. The cells were incubated at 37 °C and 5% CO_2 for four days. Following incubation, the virus was removed and the cells were washed once with 200 µl PBS. The PBS was exchanged by 200 µl acetone/methanol (1:1) and incubated at -20 °C for 20 min. Following fixation, the acetone/methanol solution was removed and the cells were dried for 5 - 10 min at RT.

Cells were rehydrated by adding 200 µl PBS for 5 min. Afterward, the antibody staining was performed. Therefore, 100 µl primary antibody (Table 5) was added in a 1:5000 dilution in PBS overnight at 4 °C. The cells were washed twice with 200 µl PBS before 100 µl secondary antibody was added in a 1:400 dilution in PBS (Table 5). After a 1 h incubation at 37 °C, the cells were washed twice with 200 µl PBS. The fluorescence was evaluated using a Zeiss microscope, and the focus-forming units (FFU/ml) were calculated using the $TCID_{50}$ calculator (Marco Binder, Dept. Infectious Diseases, Molecular Virology, Heidelberg University).

2.2.4.5 Viral infection of vertebrate and insect cells

Vertebrate or insect cells were infected with different viruses to generate comparative growth curves. Cells were seeded in 24-well plates (cell numbers listed in Table 29) 24 h before infection and were infected with a defined multiplicity of infection (MOI) the following day. The MOI indicates the ratio of infectious particles to cells. Based on the previously determined viral titer (2.2.4.3 and 2.2.4.4), the required virus volumes for the respective MOIs were calculated. Viral stocks were diluted to 300 µl/well in the appropriate cell medium without supplements. The cell culture medium was removed and exchanged for infection with 300 µl virus dilution. Vertebrate cells were incubated for 1 h at 37 °C and 5% CO_2, and insect cells at 28 °C without CO_2. Following infection, the inoculum was discarded, and cells were washed twice with 500 µl PBS and once with 500 µl medium without supplements. Lastly, the cells were covered with 1.5 ml standard medium and further incubated at 37 °C and 5% CO_2 or 28 °C. For growth curve analysis, supernatant samples of 100 µl were taken at defined time points and stored at -80 °C until further titration or RNA isolation.

Table 29: Cell numbers for different cell lines in 24-well plates

Cell line	Cell number per 24-well
BHK-21/J	8×10^4
Vero B4	8×10^4
A549	1×10^5
C6/36	2.5×10^5
Aag2 (AF5 and AF319)	2.5×10^5
CCL-125	4×10^5
U4.4	2×10^5

2.2.5 Mosquitoes

In this thesis, the *Aedes aegypti* strain Liverpool (LVP) was used. The mosquitoes were kept under standardized conditions at 28 °C and 80% humidity in a 12:12 h day/night cycle. The mosquitoes were kindly provided by Sanjay Basu (Pirbright Institute, UK).

2.2.5.1 Rearing of mosquitoes

Filter papers covered with mosquito eggs were placed in a plastic tray with approx. 1 l deionized water. For synchronized egg hatching, the plastic tray was placed inside a vacuum chamber, and the vacuum was applied for at least 60 min. Following the vacuum release, the hatched larvae were counted, and 300 – 400 larvae were placed in a new tray with the dimensions of 35 x 18 x 13 (width x depth x height) and filled with 1 l deionized water. The mosquito larvae were fed with crushed nutritionally balanced fish food. After three to five days, the water was upscaled to 2 l. Pupation began after 5 to 10 days. The pupae were counted and transferred to a new cage (dimension: 30 cm x 30 cm x 30 cm), where the mosquitoes hatched. The mosquitoes were fed twice a week with sheep blood (defibrinated, supplemented with 5 mM ATP) and 10% sucrose solution to maintain the colony.

2.2.5.2 Oral infection of mosquitoes

For oral infections, pupae were collected into one cage for 5 - 7 days to obtain the closest emerging date possible. Approximately 5 days post-eclosion and 48 h before the experiment, female mosquitoes were separated from the males. Therefore, all mosquitoes were collected from their cage using an aspirator. The mosquitoes were anesthetized by keeping them at -20 °C for 1 min. To maintain anesthesia, they were kept on ice during the separation process. Males and females were visually separated by examining their antennae. Male antennae are feathery, while female antennae are plain. Up to 20 females were collected per plastic tray covered with mesh. On average, the mosquitoes were 7 - 14 days old on the day of infection. Mosquitoes used for *in vivo* experiments were fed with 10% sucrose twice a week.

Oral infection experiments were performed in a BSL-3 laboratory. To allow mosquitoes to acclimate to the negative pressure in the BSL-3, they were moved to the laboratory at least 48 h before the experiment. Mosquitoes were starved for 24 hours and were then allowed to feed on blood supplemented with the respective virus for 1 hour. The blood

meal had a total volume of 3 ml and consisted of 50% blood and 50% virus supplemented with 5 mM ATP. The virus had a final concentration of 1×10^7 PFU/ml and was ultracentrifugated. Feeding was performed using a Hemotek membrane feeding device. Following feeding, mosquitoes were anesthetized on ice and visually inspected for blood uptake. Mosquitoes were transferred to new cylindrical containers covered with mesh and kept under standardized rearing conditions. They were monitored daily and fed with 10% sucrose.

2.2.5.3 Intrathoracic infection of mosquitoes

For intrathoracic infections, pupae were also collected into one cage for 5 - 7 days to obtain the closest emerging date possible. As described above, the mosquitoes were separated into males and females, and the females were moved to the BSL-3 laboratory at least 48 h prior to the experiment. A solution containing 300 PFU virus in 27.6 nl 0.9% sodium chloride solution was prepared for injection. The mosquitoes were anesthetized on ice and placed under a Leica DMS1000 microscope. Single mosquitoes were arranged on their site using forceps, and the virus was injected into the membranous area anterior to the mesepisternum. The injection was performed with fine glass capillaries using a NanoJect II device. Injected mosquitoes were transferred to new cylindrical containers covered with mesh and kept under standardized rearing conditions. They were monitored daily and fed with 10% sucrose.

2.2.5.4 Processing of mosquitoes and RNA isolation

Oral-infected mosquitoes were processed within 3 h post-infection or on days 3, 5, 7, 10, 14, or 21. Therefore, mosquitoes were anesthetized using ice and kept on ice until salvation. The mosquitoes were placed on their back to dissect the legs plus wings from the carcass. Legs plus wings were pooled and placed in tubes filled with 8 to 10 1.4 mm zirconium oxide beads. The mosquitoes' proboscides were inserted into a 10 µl pipette tip filled with 5 µl FCS to sample saliva. The tip of the pipette tip was cut off to facilitate the insertion of the proboscides. Salivation was forced by pipetting 1 µl pilocarpine hydrochloride (1%) to the mosquito thorax. Mosquitoes were allowed to salivate for 20 – 30 min before the pipette tip content was mixed with 15 µl MEM medium. Finally, the carcass was also placed in tubes filled with 8 to 10 1.4 mm zirconium oxide beads. Intrathoracic infected mosquitoes were not dissected, and the whole mosquito was placed

in tubes filled with 8 to 10 1.4 mm zirconium oxide beads at 0 or 7 days post-infection. All samples were stored at -80 °C.

The samples were thawed before RNA isolation, and 300 µl MEM medium without supplements was added. To ensure that the samples did not overheat during the shredding process, they were placed into a tissue lyser adaptor and stored at -20 °C for 5 - 8 min. The samples were shredded twice for 30 sec with a frequency of 30 Hz using a TissueLyser and subsequently centrifuged at 2,500 rpm for 10 min at 4 °C. For RNA isolation, 140 µl shredded supernatant was mixed with 300 µl RAV1 (+ carrier RNA) buffer, or 10 µl saliva was mixed with 300 µl RAV1. RNA isolation was performed as described above (2.2.3.9).

2.2.6 Statistics

Statistical significance was determined with GraphPad Prism 9. The significance of *in vitro* experiments was calculated using the Student's t-test, and the significance of *in vivo* experiments using the Mann–Whitney U-test or the unpaired t-test with Welch's correction. For all tests a $p < 0.05$ was considered significant (* $p < 0.05$; ** $p < 0.01$; *** $p < 0.001$; **** $p < 0.0001$; ns: not significant).

3. Results

Orthoflaviviruses transmitted by mosquitoes have the ability to replicate efficiently in vertebrates and insects. While many interactions between viruses and the vertebrate immune system are already known, little is known about the interactions between viruses and the mosquito immune system. Even though mosquitoes only exhibit innate immunity and no adaptive immunity, it is tempting to examine whether there are conserved mechanisms in viruses that they use to counteract the vertebrate and insect immune systems.

2'-O-methylation of the 5'-terminal nucleotide (N_1) of orthoflaviviral RNA, leading to the formation of a cap1 structure, is a well-known and essential mechanism orthoflaviviruses use to evade the vertebrate immune system. This mechanism relies on the 2'-O-methylation, leading to the formation of a cap1 (m^7GpppNm) or a cap2 (m^7GpppNmNm) structure in almost all eukaryotic cellular mRNAs (Dong *et al.*, 2014). The cap1 structure of eukaryotic mRNA is important for stability, translation, and marking the RNA as "self" (Furuichi *et al.*, 1976, 1977). Labeling RNA as "self" is particularly important for vertebrates since RNAs in the cytosol are distinguished as self or non-self by the receptor RIG-I. mRNAs with a cap1 structure are sensed as endogenous and do not trigger an immune response. However, the vertebrate immune response is activated if RIG-I recognizes exogenous RNA. To circumvent this immune response, orthoflaviviral RNA is methylated at the ribose 2'-O position of the first nucleotide. This methylation is catalyzed by the methyltransferase located at the N-terminal domain of the NS5 protein (Egloff *et al.*, 2002; Dong *et al.*, 2014). The methyltransferase is highly conserved among orthoflaviviruses and catalyzes the ribose 2'-O and the guanine N-7-methylation. While the 2'-O-methylation is critical for innate immune evasion, the N-7-methylation is essential for enhancing viral translation (Dong *et al.*, 2014). Responsible for the methyltransferase activity is the conserved K-D-K-E motif. All four amino acids are crucial for 2'-O-methylation, but only asparagine is essential for the N-7-methylation. Mutation of single amino acids from the K-D-K-E motif influences the replication ability of the virus to different extents. Viruses only deficient in 2'-O-methylation (K61A, K182A, or E218A) are attenuated in cell culture and a viral mutant (D146A) defective in 2'-O and N-7-methylation is lethal (Ray *et al.*, 2006; Zhou *et al.*, 2007).

Schuberth-Wagner and colleagues previously reported that mutation of the glutamine of the conserved K-D-K-E tetrad to alanine at position 218 (E218A) in NS5 of YFV-17D led to the abrogation of the 2'-O-methylation activity. Due to this, a cap0 structure is formed instead of a cap1 structure at the viral 5' end. In immune-competent cells, RIG-I recognizes this mutant virus and initiates an effective immune response, leading to a reduced replication of the cap0 virus compared to the cap1 virus (Schuberth-Wagner *et al.*, 2015).

In mosquitoes, the best-studied antiviral pathway is the siRNA pathway. It involves the recognition of double-stranded RNA by the enzyme Dcr-2 and the subsequent cleavage of the dsRNA into smaller dsRNA duplexes. Interestingly, the endonuclease Dcr-2 interacts, similar to RIG-I, with modified RNAs through its DExD/H box (Ahmad *et al.*, 2015). Therefore, it was interesting to analyze if Dcr-2 has a similar function in distinguishing self from non-self RNA.

This study aimed to analyze whether orthoflaviviruses also evade the insect immune system by modulating their 5' cap structure via 2'-O-methylation. Further, it was investigated whether Dcr-2 mediates the distinction between cap1 and cap0 orthoflaviviruses and what mechanisms viruses have evolved to counteract the discrimination mechanism of cap0 RNA.

3.1 Recognition of YFV-17D cap0 in mosquito cells

Since a previous study already successfully showed that the position E218 in the NS5 protein of YFV-17D is crucial for escaping the vertebrate immune system, this finding was used as a starting point for this study (Schuberth-Wagner *et al.*, 2015). To test whether orthoflaviviruses with an abrogated methyltransferase activity (cap0) also replicate to reduced titers in insect cells, different mosquito cell lines were infected with YFV-17D cap1 and cap0. In the infectious YFV-17D cap0 cDNA clone that Schuberth-Wagner and colleagues used, the codon for E218 (GAA) was mutated to GCA (alanine). To reduce the likelihood of spontaneous reversion, two nucleotides in the GAA codon were exchanged. The new infectious clone carried the GCC codon, leading to the E218A exchange (Figure 9A). This exchange was introduced using site-directed mutagenesis through fusion PCR technology (2.2.3.2). The obtained PCR fragment encompassing the desired mutations was cut with the restriction enzymes NgoMIV and XhoI and ligated into the YFV-17D cap1

backbone cut with the same set of enzymes. The successful introduction of the mutation was verified by Sanger sequencing. A schematic illustration of the construct can be found in the appendix (10.2). Next, the YFV-17D cap1 and cap0 cDNA clones were linearized with XhoI to generate an authentic 3' end upon transcription, precipitated, and *in vitro* transcribed. The RNA was electroporated into BHK-21/J cells to rescue both viruses.

Following the successful rescue of YFV-17D cap1 and cap0, the insect cell lines C6/36, Aag2, U4.4, and CCL-125 were infected in triplicates at an MOI of 0.01. Growth curves for the cell lines C6/36 and Aag2 were generated over ten days, whereas for the cell lines U4.4 and CCL-125, replication was assessed only on day five post-infection (Figure 9B-D).

As shown in Figure 9B, YFV-17D cap1 replicated to high titers in the *Aedes albopictus*-derived cell line C6/36. The cap1 virus reached its peak titer of 1×10^7 PFU/ml five days post-infection. In contrast, YFV-17D cap0 did not replicate in this cell line at any tested time point. In the *Aedes aegypti*-derived cell line Aag2, YFV-17D cap1 and cap0 replicated, but the replication of YFV-17D cap0 was reduced compared to the replication of cap1 (Figure 9C). The replication of YFV-17D cap1 was less than 1 $\log_{10}$ higher three days post-infection than the replication of YFV-17D cap0. This difference increased until day seven, when the replication of YFV-17D cap1 was 1.7 $\log_{10}$ higher than the YFV-17D cap0 replication. Between day seven and day ten post-infection, the viral titers of YFV-17D cap1 remained constant, and the titers of cap0 virus continued to increase, reducing the difference in viral titers between cap1 and cap0 virus at this time point (cap1: 8.5×10^5 PFU/ml; cap0: 1×10^5 PFU/ml). Likewise, YFV-17D cap1 and cap0 replicated to different titers in the *Aedes albopictus*-derived cell line U4.4 and in the *Aedes aegypti*-derived cell line CCL-125 five days post-infection (Figure 9D). Replication of YFV-17D cap0 was reduced in U4.4 cells, but this difference was not significant. In contrast, YFV-17D cap0 was unable to exceed the detection limit in CCL-125 cells at day five post-infection, and the cap1 virus only replicated to low titers (660 PFU/ml).

Collectively, replication of YFV-17D cap0 was reduced in all tested mosquito cell lines compared to the cap1 virus, indicating that the replication of this virus was unambiguously impaired.

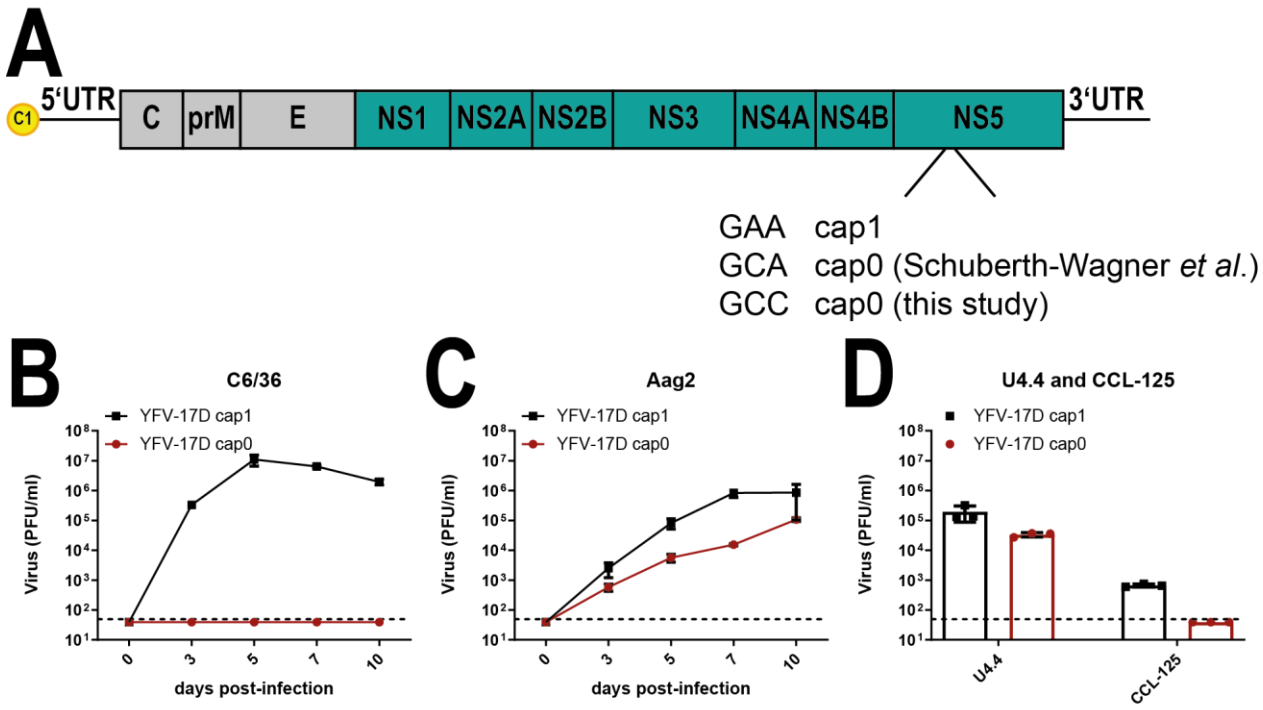

Figure 9: Growth kinetics of YFV-17D cap1 and cap0 in different mosquito cell lines. A) YFV genome: Boxes in grey indicate the structural proteins, and boxes in green the NS proteins. The capped (yellow dot) 5'UTR and the 3'UTR are depicted as black lines. The codons for the aa position 218 in NS5 of the cap1 and cap0 viruses used in this study are displayed under the NS5 protein. B) Growth kinetics of YFV-17D cap1 and cap0 in C6/36 (B) and Aag2 (C) cells. D) Replication of YFV-17D cap1 and cap0 five days post-infection in U4.4 and CCL-125 cells. Cells were infected at a multiplicity of infection (MOI) of 0.01, and viral titers were measured at days 0, 3, 5, 7, and 10 post-infection (C6/36, Aag2) or at day 5 post-infection (U4.4, CCL-125) by titration on BHK-21/J cells. Data represent Mean ± SD of triplicates. Dashed lines: detection limit.

3.2 Establishment and replication analysis of YFV-Asibi cap1 and cap0

In 1927, Stokes and colleagues first isolated the YFV from a patient suffering from yellow fever and named the virus after him – Asibi (Stokes *et al.*, 1928). Serial passaging of the virus in different cell types, including chicken embryos without nervous tissue, led to the discovery of the now well-known vaccine strain of YFV, called YFV-17D (Theiler *et al.*, 1937; Davis *et al.*, 2019). Since then, the YFV-17D strain has been highly studied and considered a safe model organism for YFV. Studies showed that YFV-17D infected the midgut of *Aedes aegypti*, but the virus was unable to disseminate to secondary tissues because of the midgut infection barrier (McElroy *et al.*, 2006b; Danet *et al.*, 2019). In contrast, YFV-Asibi quickly infected and disseminated in *Aedes aegypti* at high rates (Miller *et al.*, 1988; McElroy *et al.*, 2006b, 2008). In order to study the replication behavior of YFV cap1 and cap0 *in vivo*, an infectious cDNA clone of the YFV-Asibi strain was established. Besides the *in vivo* application, establishing an infectious cDNA clone allowed site-directed mutagenesis studies through fusion PCR.

3.2.1 Establishment of an infectious YFV-Asibi cDNA clone

The nucleotide sequence of our infectious YFV-17D clone was compared to one published sequence of YFV-Asibi to establish an infectious YFV-Asibi cDNA clone. As a reference for YFV-Asibi, the amino acid sequence of Hahn and colleagues was used (Hahn, Dalrymple, *et al.*, 1987), except for two nucleotides, which were not exchanged (nt position 2142 and 7319 according to aa 714 and 2440). The YFV-17D and YFV-Asibi sequences used in this study differ in 66 nt, resulting in the exchange of 31 amino acids (Figure 10A). The 5'UTRs do not harbor any exchanges, while the 3'UTRs differ in five nucleotides. All nucleotide and amino acid exchanges are listed in the appendix (Table S 1). A previously established pseudo-Asibi (pPseAsibi) infectious cDNA clone was used as the cloning vector to construct the infectious cDNA clone of YFV-Asibi. pPseAsibi already included most nucleotide exchanges between YFV-17D and YFV-Asibi. Ten nucleotide exchanges, leading to three amino acid exchanges, were missing. Those were introduced into the pPseAsibi to construct the full-length YFV-Asibi infectious cDNA clone. The nucleotide exchanges were inserted in three successive steps (Figure 10B).

In the first step, a fragment comprising partially the envelope protein to NS1 protein flanked by the restriction sites NsiI and MluI was generated. Four nucleotides were

exchanged within this fragment using fusion PCR technology (Table 30, Figure 10B). In the second step, three nucleotides were exchanged using fusion PCR technology. The resulting fragment partially comprised the NS proteins 1 to 4A flanked by the restriction sites KpnI and NgoMIV (Table 30, Figure 10B). In the last step, a fragment partially comprising the NS4A to NS5 proteins flanked by the restriction enzymes NgoMIV and AatII was generated (Table 30, Figure 10B). Here, three nucleotides were exchanged using fusion PCR technology. Following restriction digests, each fragment was sequentially cloned into the pre-existing infectious clone pPse-Asibi, replacing the equivalent fragment of pPseAsibi. A schematic illustration of the construct can be found in the appendix (10.2). The resulting plasmid was amplified in *E. coli* MC1061 cells, and the resulting plasmid DNA was sequenced up to and across cloning junctions of each fragment to verify the authenticity of the replaced mutations.

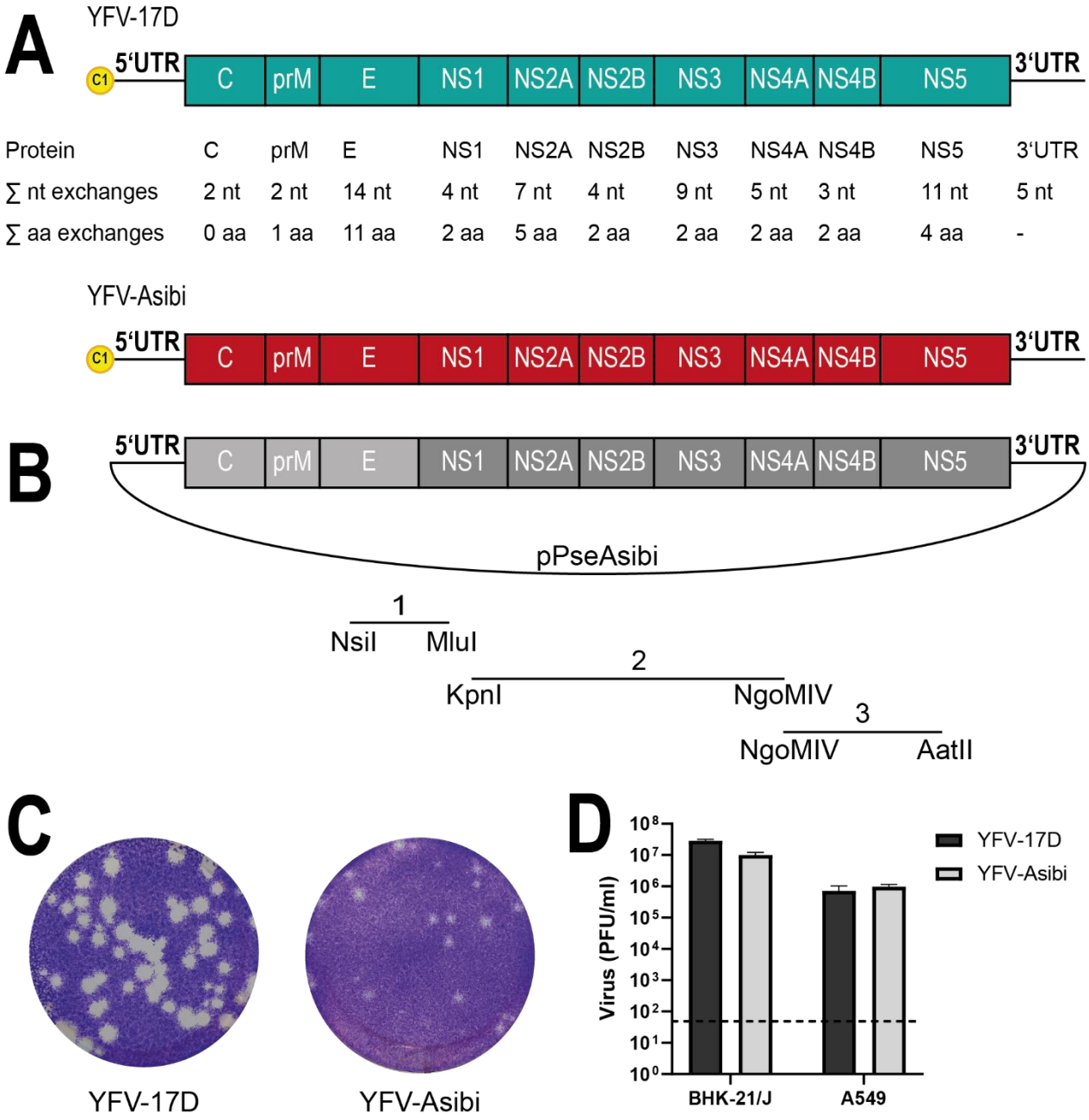

Figure 10: Generation of the infectious YFV-Asibi clone.
A) Schematic representation of YFV-17D (green) and -Asibi (red). The nucleotide and amino acid exchanges are depicted between the schematic representations. B) Construction scheme showing the three fragments containing mutations corresponding to YFV-Asibi, which were sequentially introduced into pPseAsibi via intermediate clones. C) Plaque morphology of YFV-17D and YFV-Asibi after performing an ICA on BHK-21/J cells. The cells were fixed three days after electroporation and stained with crystal violet. D) Comparison of YFV-17D and YFV-Asibi growth characteristics. BHK-21/J and A549 cells infected with YFV-17D cap1 and YFV-Asibi cap1 at an MOI of 0.01. Viral titers were measured at day 3 post-infection by titration on BHK-21/J cells. Data represent Mean ± SD of duplicates (BHK-21/J) or triplicates (A549). Dashed line: detection limit.

The obtained YFV-Asibi cDNA clone and the YFV-17D cDNA clone were linearized with XhoI to generate an authentic 3' end of the genomes for viral recovery. The linearized DNA was precipitated, *in vitro* transcribed from an SP6 promoter, and the generated RNA was electroporated into BHK-21/J cells. Three days post electroporation, the cell culture supernatants containing the infectious particles were harvested and titrated on BHK-21/J cells. The resulting viral titers of YFV-17D and YFV-Asibi were comparably high (YFV-17D: 5.5 x 10^6 PFU/ml; YFV-Asibi: 1.1 x 10^7 PFU/ml). Efficient replication of the rescued viruses was confirmed by infectious center assay (ICA) (Figure 10C). The plaque morphology revealed reduced plaque size of YFV-Asibi compared to YFV-17D, but both viruses showed plaques up to the same dilution (10^5). BHK-21/J and A549 cells were infected with the rescued viruses at an MOI of 0.01 for three days to compare the general replication ability of the two YF viruses. Both viruses replicated to high titers in BHK-21/J cells, but YFV-17D replicated 0.4 $\log_{10}$ higher than YFV-Asibi (Figure 10D). In A549 cells, YFV-Asibi replicated slightly higher than YFV-17D.

Overall, the infectious YFV-Asibi cDNA clone was successfully established, and replication-competent virus was rescued from the plasmid. This virus infected vertebrate cells with comparable efficiency as YFV-17D. The YFV-Asibi cDNA clone was used for subsequent experiments.

Table 30: Summary of differences between pPseAsibi and pYFV-Asibi.
Individual differences are summarized by fragment number. The nucleotide of pPseAsibi is always given first, followed by the one of pYFV-Asibi. If the nucleotide exchange led to an amino acid exchange, the amino acid of pPseAsibi is also indicated first, and then the one of pYFV-Asibi.

Fragment no.	Position	nt exchange	aa exchange
1	2193	C → T	Ala → Val
	2405	G → C	Cys → Ser
	2578	G → T	
	2704	G → A	
2	4025	G → A	Val → Met
	4864	A → G	
	5926	C → T	
3	6829	C → T	
	7945	T → C	
	8008	C → T	

3.2.2 Recognition of YFV-Asibi cap0 in vertebrate and mosquito cell lines

Following the successful rescue of YFV-Asibi cap1, YFV-Asibi cap0 was constructed to investigate whether the replication of this virus was inhibited to comparable means as observed with YFV-17D cap0. Therefore, the NS5 protein of YFV-Asibi cap1 was mutated at position E218A (glutamine to alanine exchange) using site-directed mutagenesis through fusion PCR technology (2.2.3.2). The resulting PCR fragment and the YFV-Asibi backbone were digested with the enzymes NgoMIV and AatII and subsequently ligated. A schematic illustration of the construct can be found in the appendix (10.2). The successful introduction of the mutation was verified by Sanger sequencing. YFV-Asibi cap1 and cap0 cDNA clones were linearized with XhoI, precipitated, and *in vitro* transcribed. Electroporation of the *in vitro* transcribed RNA into BHK-21/J cells revealed similar progeny virus titers for both viruses (YFV-Asibi cap1: 1.15 x 10^7 PFU/ml; YFV-Asibi cap0: 1.1 x 10^7 PFU/ml). Thus, vertebrate cells (BHK-21/J, A549) and insect cells (C6/36, Aag2) were infected in duplicates (BHK-21/J) or triplicates (A549, C6/36, Aag2) with YFV-Asibi cap1 and cap0 to monitor viral replication over time. Due to the greater doubling time of BHK-21/J cells, the growth curve of these cells was performed for four days, whereas it was performed for seven days for A549 cells and for ten days for the insect cell lines.

Both viruses showed comparable replication characteristics over time in BHK-21/J cells (Figure 11A). The viral replication of cap1 and cap0 virus peaked three days post-infection with titers of 10^7 PFU/ml and replicated stable until day four. Despite the absence of the 2'-O-methylation at the 5' cap structure of YFV-Asibi (cap0), the cap0 virus showed no disadvantage in the production of progeny virus in cells lacking a functional immune response.

Schuberth-Wagner *et al*. showed that YFV-17D cap0 replicated less efficiently in A549 cells than the corresponding cap1 virus due to a RIG-I-induced immune response (Schuberth-Wagner *et al.*, 2015). To confirm that the same applies to YFV-Asibi, the vertebrate cell line A549 was infected with YFV-Asibi cap1 and cap0 to investigate the effect of the RIG-I-induced immune response on viral replication. Concordantly, YFV-Asibi cap1 and the methyltransferase deficient cap0 mutant showed similar replication behavior in A549 cells compared to their respective YFV-17D counterparts. Both YFV-Asibi viruses showed efficient replication in the cells, but replication of YFV-Asibi cap0 was strongly

reduced compared to the replication of the cap1 virus (Figure 11B). The most notable difference was visible three days post-infection, where the replication of YFV-Asibi cap0 was reduced by 1.7 $\log_{10}$ compared to YFV-Asibi cap1. The replication of both viruses peaked on day five (cap1: 3 x 10^6 PFU/ml; cap0: 1.4 x 10^5 PFU/ml) and decreased slightly until day seven.

One member of the interferon-induced protein with tetratricopeptide repeats (IFIT) family, namely IFIT1, has been reported to specifically bind to 2'-O-unmethylated RNAs (Daffis *et al.*, 2010; Habjan *et al.*, 2013). To indirectly confirm that the generated YFV-Asibi cap0 virus was lacking the 2'-O-methylation, A549 IFIT1 knockout (k.o.) cells and parental A549 cells were infected with YFV-Asibi cap1 and cap0 at an MOI of 0.01. At 72 h post-infection, the amount of virus released into the supernatant was determined using plaque assay (Figure 11C). The replication of YFV-Asibi cap0 was slightly reduced compared to cap1 in the IFIT1 k.o. cells, but this difference was not significant. In contrast, the replication of YFV-Asibi cap0 was significantly reduced in the A549 wild-type cells by 2.5 $\log_{10}$. This data indicates that the replication of YFV-Asibi cap0 was distinctly downregulated in the wild-type cells due to IFIT1 binding to 2'-O-unmethylated RNA.

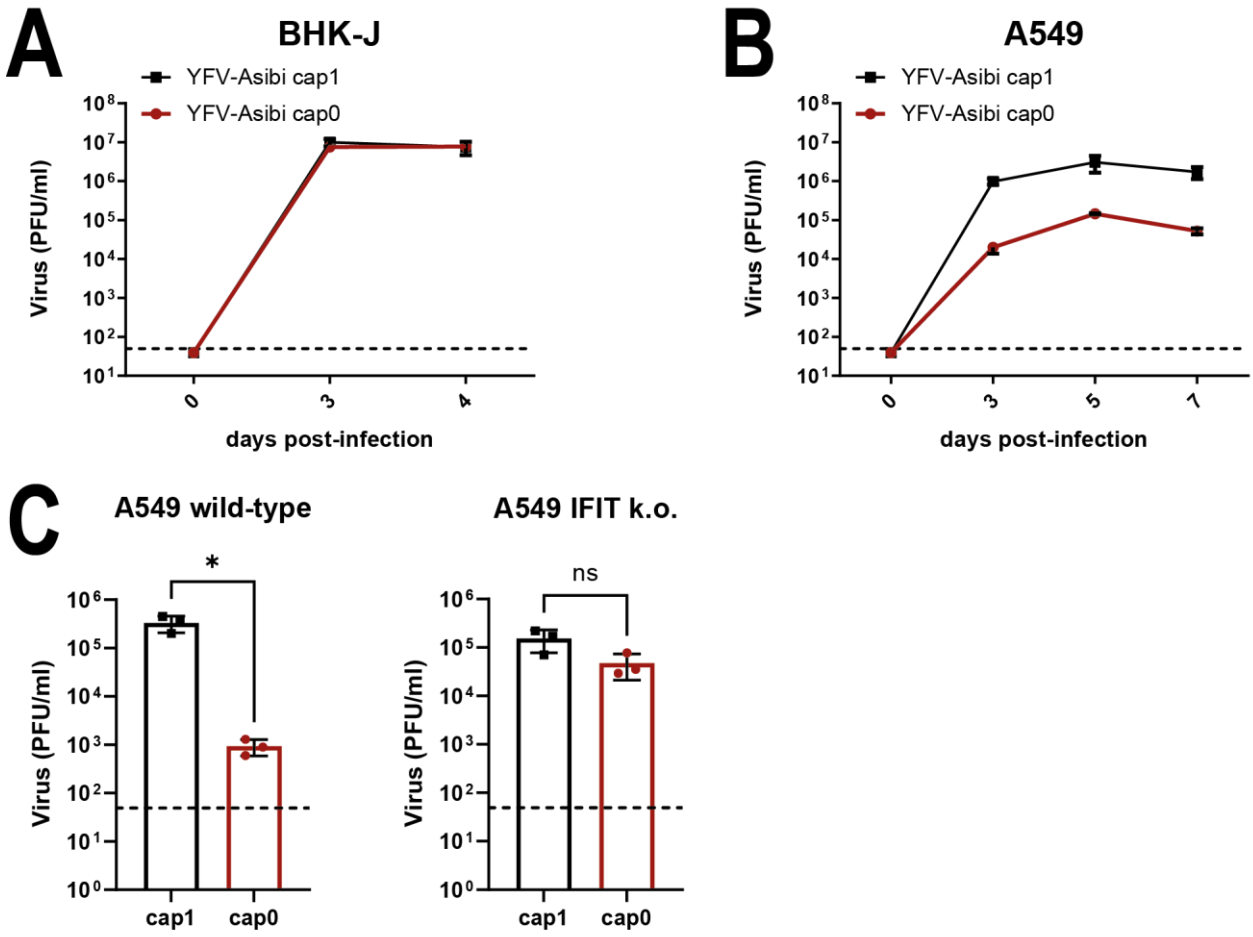

Figure 11: Growth kinetics of YFV-Asibi cap1 and cap0 in different vertebrate cells. A-B) Growth kinetics of YFV-Asibi cap1 and cap0 in BHK-21/J (A) and A549 (B) cells. C) Replication of YFV-Asibi cap1 and cap0 at 3 days post-infection in A549 wild-type and IFIT1 k.o cells. Cells were infected at an MOI of 0.01 and viral titers were measured at 3 days (A549 wild-type, A549 IFIT1 k.o.), at 0, 3, and 4 days (BHK-21/J) or at 0, 3, 5, and 7 days (A549) post-infection by titration on BHK-21/J cells. Data represent Mean ± SD of duplicates (BHK-21/J) or triplicates (A549, A549 wild-type, IFIT1 k.o cells). Dashed lines: detection limit.

In a previous experiment, the greatest replication difference for YFV-17D cap1 and cap0 was observed in the *Aedes albopictus*-derived cell line C6/36 cells (Figure 9B). Due to this, it was of great interest to analyze how the YFV-Asibi cap0 virus replicates in this cell line. Upon infection of C6/36 cells with YFV-Asibi cap1 and cap0 (MOI 0.01), viral titers of the cap0 virus were undetectable until day three (Figure 12A). In contrast, the cap1 virus rapidly replicated to high titers and peaked three days post-infection (3.8×10^6 PFU/ml). Hereafter, the cap1 viral titer decreased due to a cytopathic effect. Viral replication of YFV-Asibi cap0 exceeded the detection limit of 50 PFU/ml after day three and increased continuously until day ten (d5: 550 PFU/ml; d10: 1.4×10^4 PFU/ml). In total, viral replication of YFV-Asibi cap1 was increased by 5 $\log_{10}$ on day three, 3.7 $\log_{10}$ on day five, 2.8 $\log_{10}$ on day seven, and 1 $\log_{10}$ on day ten compared to cap0.

Following infection of the *Aedes aegypti*-derived cell line Aag2 with YFV-Asibi cap1 and cap0 (MOI 0.01), YFV-Asibi cap0 produced 1 $\log_{10}$ lower viral titers than the cap1 virus on day three post-infection (Figure 12B). This difference neglected itself over time because YFV-Asibi cap1 replication peaked on day five post-infection (8.8×10^5 PFU/ml) and decreased until day ten (3.1×10^4 PFU/ml). In contrast, replication of YFV-Asibi cap0 remained nearly constant between day five and day seven (d5: 4.3×10^5 PFU/ml; d7: 3.6×10^5 PFU/ml) and started to decrease between day seven and day ten.

Collectively, YFV-Asibi cap1 and cap0 showed similar replication behavior in the immune-deficient vertebrate cell line BHK-21/J, whereas replication of the cap0 virus was reduced in immune-competent A549 cells. Since no reduction of YFV-Asibi cap0 was observed in A549 IFIT1 k.o cells, it was indirectly confirmed that the introduction of the E218A mutation results in the production of a methyltransferase deficient cap0 virus, which is recognized in an IFIT1-dependent manner.

Further, replication of YFV-Asibi cap0 was reduced in C6/36 cells but to a lower extent than the reduction of the respective YFV-17D counterpart. This data indicates that YFV-Asibi counteracts the cap0 recognition in mosquitoes to a different extent than YFV-17D. In Aag2 cells, the level of inhibition for the cap0 variants was only observed at early time points, indicating that the mechanism involved in discriminating between cap0 and cap1 is differentially active in various mosquito cells.

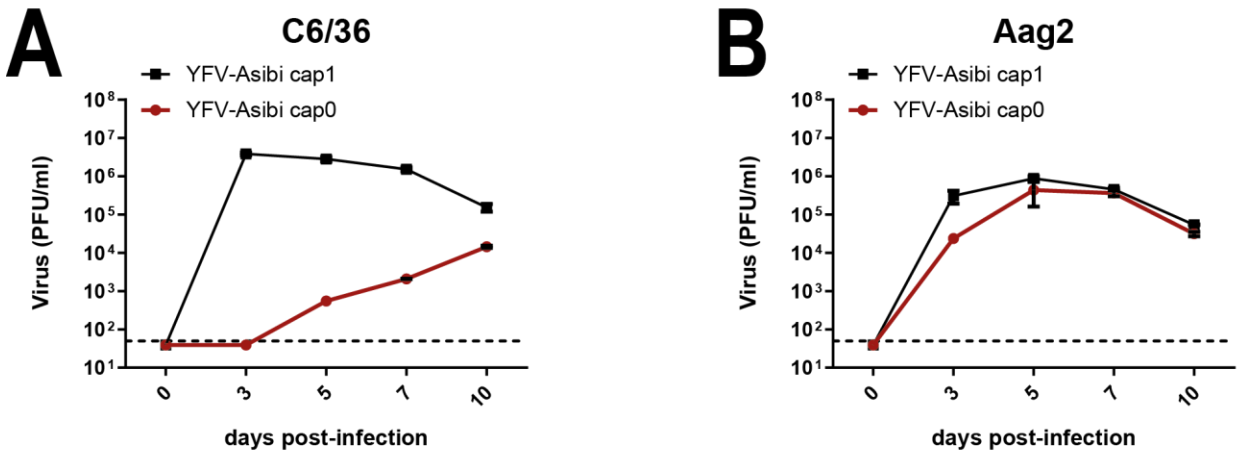

Figure 12: Growth kinetics of YFV-Asibi cap1 and cap0 in different insect cells. A-B) Growth kinetics of YFV-Asibi cap1 and cap0 in C6/36 (A) and Aag2 (B) cells. Cells were infected at an MOI of 0.01 and viral titers were measured at 0, 3, 5, 7, and 10 days post-infection by titration on BHK-21/J cells. Data represent Mean ± SD of triplicates. Dashed lines: detection limit.

3.3 Effect of cap0 priming on the replication of YFV cap1 virus

Immunostimulatory RNAs, such as viral dsRNAs, are recognized by RIG-I-like receptors (RLRs) in the cytosol of mammalian cells. This recognition activates signaling cascades, leading to the transcriptional induction of genes encoding type I interferons and other genes (Rehwinkel *et al.*, 2020). Type I interferons are well known for their antiviral effect, and priming of A549 cells with interferon-alpha led to reduced replication of various viruses (Basu *et al.*, 2006). These data led to the hypothesis that infected cells produce secretory antiviral factors that can be transferred to new cells by transferring the cell culture supernatant, providing an antiviral effect against a second infection.

Even though no orthologues for the well-known interferons in vertebrates were found in mosquitoes, several secretory proteins with potential antiviral effects were described in mosquitoes (Riedel *et al.*, 1979; Cheng *et al.*, 2009). One of those proteins is Vago, which is induced by Dcr-2 and activates the JAK/STAT pathway in *Culex* cells (Paradkar *et al.*, 2012, 2014; Altinli *et al.*, 2022). Despite the antiviral effect of Vago in *Culex* cells, Vago seemed not to be induced in the *Aedes aegypti*-derived cell line Aag2 (Russell *et al.*, 2020). Nevertheless, it was aimed to investigate if secretory factors secreted by mosquito cells can prime uninfected cells. The transfer of potential antiviral factors from cell culture supernatant to fresh cells will be called priming in the following.

3.3.1 Construction of yellow fever virus reporter replicon particles

A previous study using the YFV-17D cap0 virus showed reduced replication of the respective virus in A549 cells (Schuberth-Wagner *et al.*, 2015). Along with the reduced replication of the virus, the cells' immune system was activated, leading to an increased type I interferon response. As it is well known that soluble products like interferon-α can be secreted as a response to a viral infection, it was presumed that the supernatant of infected cells contains soluble factors that can be transferred onto fresh cells to prevent or reduce infection of the cells (priming). To determine the priming effect of YFV-17D cap1 and cap0 infected cells, yellow fever virus replicon particles (YF-VRPs) containing a fluorescent protein were established (Figure 13A). Virus replicon particles express the non-structural proteins of the respective virus but lack the structural proteins. The latter are provided in *trans* to mimic viral entry and to allow single-round infection. YF-VRPs allow efficient self-replication but cannot form progeny viral particles in cells that do not

express the viral structural proteins (Kümmerer, 2018). Due to the lack of progeny viral particles, the cellular supernatant of YF-VRP cap1 and cap0 infected cells can be transferred without viral contamination.

Site-directed mutagenesis through fusion PCR technology was used to establish a YF replicon harboring a fluorescent mCherry protein. In total, three individual fragments were amplified, which were subsequently fused. First, the 5' end of the YFV genome was amplified from a YFV *Renilla* replicon (Schuberth-Wagner *et al.*, 2015). The resulting fragment contained the SP6 promoter, the 5'UTR, the first 41 codons of the capsid, and the ubiquitin gene. In a second PCR reaction, the mCherry gene was amplified from an infectious CHIKV-mCherry construct (Kümmerer *et al.*, 2012). The third fragment contained the proteolytic peptide from the foot-and-mouth disease virus (FMDV) 2A and the last 23 codons of the envelope protein. The latter fragment was also amplified from the YFV *Renilla* replicon. The resulting PCR fragments were fused and then cut with the restriction enzymes NotI and MluI. The resulting fragment was cloned into the backbone of the YFV *Renilla* replicon previously cut with the same enzymes. The first 41 codons of the capsid and the last 23 codons of the envelope were retained to ensure efficient translation and correct insertion of the NS1 protein into the endoplasmic reticulum (Hahn, Hahn, *et al.*, 1987; Jones *et al.*, 2005). Hereafter, the generated replicon will be referred to as YFVR cap1. A schematic illustration of the construct can be found in the appendix (10.2)

In addition to the YFVR cap1 replicon, a second replicon carrying a mutation at amino acid 218 in the NS5 protein (E218A, GAA → GCA) was established. This mutation abrogated the 2'-O-methylation activity of NS5, leading to a cap0 structure at the replicons' 5' end. For this purpose, the YFV-E218A *Renilla* replicon described by Schuberth-Wagner *et al.* was cut with the restriction enzymes NgoMIV and XhoI (Schuberth-Wagner *et al.*, 2015). The resulting fragment was ligated into the previously established YFVR cap1 cut with the same restriction enzymes. The resulting replicon was named YFVR cap0.

As mentioned above, the structural proteins were provided in *trans* by a so-called packaging construct. The packaging construct used in this study was kindly provided by Beate Kümmerer and was described previously (Lücke *et al.*, 2022). In brief, this construct is based on a noncytopathogenic SINV replicon containing the envelope proteins prM and

E under the first subgenomic promoter and the capsid protein under a second subgenomic promoter.

To confirm the expression of the fluorescent mCherry protein and to produce YF-VRPs, YFVR cap1, cap0, and the packaging construct were linearized with XhoI, precipitated, and *in vitro* transcribed. The generated RNAs (YFVR cap1 + packaging construct; YFVR cap0 + packaging construct) were co-electroporated into BHK-21/J cells using the same amount of RNA for both constructs. The cells were incubated at 32 °C for optimal YF-VRP production and harvested 72 hours post-electroporation (Lücke *et al.*, 2022). Titers were determined by titration on a cell line, stably expressing YFV prM-E/C, resulting in the formation of plaques (data not shown). The functionality of the YF-VRPs was verified by infecting BHK-21/J cells at an MOI of 0.1 for 24 h. Fluorescence microscopy of the YF-VRP cap1 and cap0 infected BHK-21/J cells showed efficient replication 24 h post-infection (Figure 13B, C).

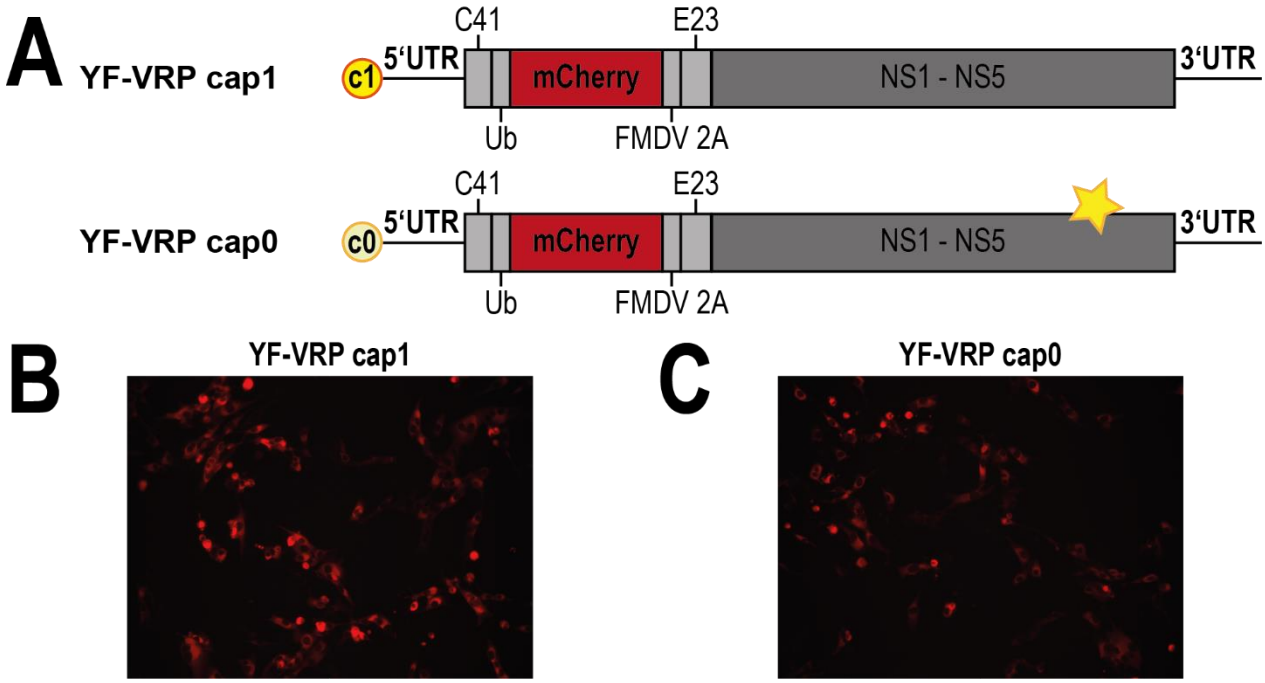

Figure 13: Schematic representation and characterization of YFVR cap1 and cap0. A) Schematic representation of mCherry expressing YFV replicons. The mCherry protein (depicted in red) was inserted between the first 41 amino acids of the capsid protein (C41) and the last 23 amino acids of the envelope protein (E23). Boxes in light grey represent the structural proteins, boxes in dark grey the NS proteins, and black lines the UTRs. The yellow dots represent the cap structures and the yellow star represents the E218A exchange in the NS5 protein. BHK-21/J cells were infected with YF-VRP cap1 (B) or YF-VRP cap0 (C) at an MOI of 0.1. The fluorescence was analyzed 24 h post-infection.

3.3.2 Priming of mosquito cells with YFV-17D replicons

A priming experiment was performed to investigate whether insect cells release transferrable secretory factors into the cell culture supernatant as an immune response to infection. Since YFV-17D cap1 and cap0 showed the most significant replication difference in the cell line C6/36 (Figure 9B), these cells were used for the priming experiments.

To this end, C6/36 cells were infected with YF-VRP cap1 or YF-VRP cap0 at an MOI of 1 for 24 h to allow sufficient replication. The infection status was examined by fluorescence microscopy. As shown in Figure 14A, 24 h post-infection YF-VRP cap1 uniformly infected C6/36 cells, whereas mCherry fluorescence was only spotted for individual cells when infected with YF-VRP cap0. As expected, no fluorescence was visible in uninfected control cells. The fluorescence was also detected 72 h post YF-VRP infection (Figure 14B) to verify efficient replication during the experiment. The amount of mCherry fluorescent positive cells was highly increased for YF-VRP cap1 infected cells. Again, only single cells were fluorescence positive after infection with YF-VRP cap0, and the uninfected control cells were negative.

YF-VRP supernatants were harvested 24 h post-infection, centrifuged, and transferred to new C6/36 cells to prime them for 24 h. Following cap1 or cap0 priming, the cells were infected with full-length YFV-17D cap1 containing a *Renilla* luciferase. Replication of YFV-17D cap1 *Renilla* was examined 48 h post-infection by lysing the cells and measuring the luciferase activity. Luciferase activity was equally high in the unprimed as well as in the YF-VRP cap1 and cap0 primed cells (Figure 14C).

Besides priming, the effect of superinfection was investigated in C6/36 cells. Superinfection describes a phenomenon in which a second viral infection is reduced because the cells were already infected with a closely related virus (Tscherne *et al.*, 2007; Glover *et al.*, 2020). For this purpose, the previously YF-VRP cap1 and YF-VRP cap0 infected cells were superinfected with YFV-17D cap1 *Renilla* for 48 h. As shown in Figure 14D, the luciferase activity of the cells primarily infected with YF-VRP cap0 was equally high to the non-infected cells. In contrast, the luciferase activity of YF-VRP cap1 primed cells was reduced by 0.5 $\log_{10}$ compared to the non-primed cells (Figure 14D). Nevertheless, this reduction was not significant.

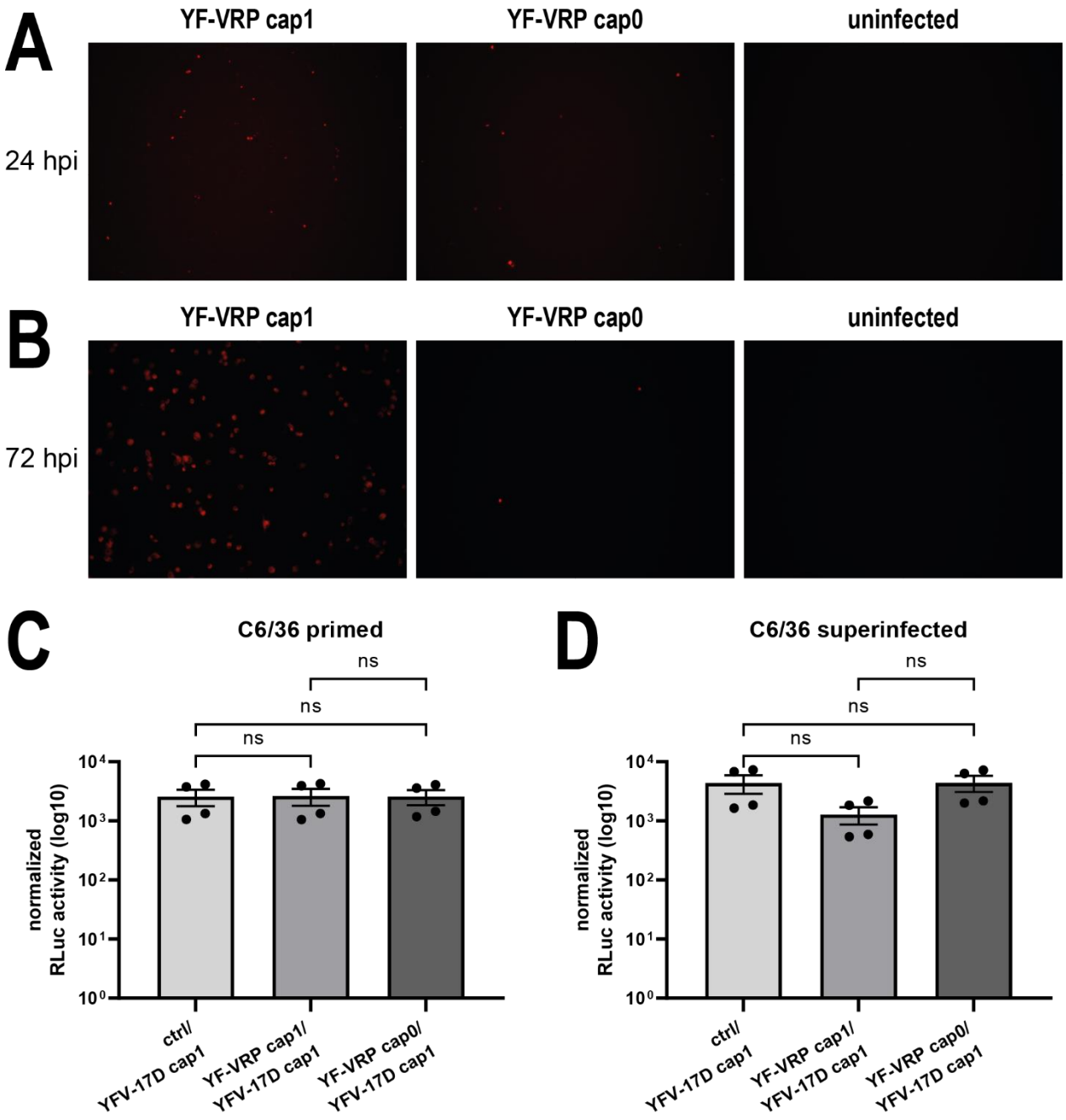

Figure 14: Priming experiment of the insect cells C6/36.
C6/36 cells were infected with YF-VRP cap1 or YF-VRP cap0 at an MOI of 1. The expression of mCherry was examined by immunofluorescence at 24 h (A) or 72 h (B) post-infection. C) Supernatant of YF-VRP cap1 infected, cap0 infected, or uninfected cells was transferred to C6/36 cells. Following priming, the cells were infected with YFV-17D cap1 *Renilla* at an MOI of 1 for 48 h. D) YFVR cap1 infected, cap0 infected, or uninfected C6/36 cells were superinfected with YFV-17D cap1 *Renilla* at an MOI of 1 for 48 h. At 48 h post-infection, relative luciferase activity (Rluc) was determined and normalized to control cells. Data represent Mean ± SD of duplicate infection experiments. Significance was determined by Student's t-test (ns = not significant).

3.3.3 Priming of mosquito cells with YFV-Asibi

The previously obtained priming data revealed that the supernatant of YF-VRP cap1 or cap0 infected C6/36 cells did not reduce the replication capacity of YFV-17D cap1. Moreover, following sequential infection with YF-VRP cap0 and YFV-17D cap1, replication of YFV-17D cap1 remained unchanged. In contrast, sequential infection with YF-VRP cap1 and YFV-17D cap1 led to slightly reduced replication of the latter virus, but this reduction was not significant.

So far, all priming experiments were performed in C6/36 cells, as these cells showed the most significant replication difference between YFV-17D cap1 and cap0. However, previous studies demonstrated that C6/36 cells have a dysfunctional RNAi response due to a truncated Dcr-2 gene (Brackney *et al.*, 2010; Morazzani *et al.*, 2012). The Dcr-2 gene encoded by *Aedes albopictus* comprises a DExD/H-box domain, a domain of unknown function (DUF), a PAZ domain, and two RNase III domains. The Dcr-2 gene encoded by C6/36 cells contains a frameshift mutation, leading to a premature stop codon. Due to this, the PAZ domain and the two RNase III domains are missing in the C6/36 Dcr-2 gene (Morazzani *et al.*, 2012). Nevertheless, 21 nt small RNAs with strong U1 and A10 characteristics were found upon alphavirus infection in C6/36 cells, indicating a functional ping-pong-dependent pathway (Morazzani *et al.*, 2012; Gestuveo *et al.*, 2022).

Due to the dysfunctional siRNA response in C6/36 cells, it was aimed to investigate the immune response in immune-competent Aag2 cells upon sequential viral infection. To study the potential role of Dcr-2 simultaneously, not only Aag2 wild-type cells were sequentially infected, but also Aag2 Dcr-2 k.o. cells. YFV-Asibi cap1 and cap0 replicated more efficiently in Aag2 cells than YFV-17D cap1 and cap0, so YFV-Asibi was chosen for this experiment. To this end, Aag2 wild-type cells and Aag2 Dcr-2 k.o. cells were either infected with YFV-Asibi cap1, cap0, or were left uninfected. Infection was performed at an MOI of 1 for 24 h. Following the first infection, the cells were sequentially infected with YFV-Asibi cap1 containing a *Gaussia* luciferase. Measurement of the luciferase activity allowed precise monitoring of the YFV-Asibi cap1 replication used for the sequential infection virus over time.

YFV-Asibi cap1 efficiently replicated in Aag2 wild-type cells when a single infection was performed (Figure 15A, grey line). In contrast, replication of YFV-Asibi cap1 was highly

impaired when the cells were previously infected with YFV-Asibi cap0 (red line). This effect was even more substantial when the first infection was performed with YFV-Asibi cap1 (black line). At 56 h post-infection, the peak titer of YFV-Asibi cap0/cap1 infected cells was highly reduced compared to the single infection, and the peak titer of YFV-Asibi cap1/cap1 infected cells was even reduced by 2.4 $\log_{10}$. In order to assess whether Dcr-2 is responsible for the reduced replication of YFV-Asibi cap1 when sequentially infected, the same experiment was conducted in Dcr-2 k.o. cells. Here, replication of YFV-Asibi cap1 was again highest when a single infection was performed (Figure 15B, grey line). Similarly, replication of YFV-Asibi cap1 was highly impaired when sequentially infected. YFV-Asibi cap1/cap1 (black line) infection resulted in a higher replication reduction than YFV-Asibi cap0/cap1 (red line) infection. Overall, the titers of the YFV-Asibi cap1/cap1 and the YFV-Asibi cap0/cap1 group were comparable in both cell lines, indicating an effect independent from Dcr-2. The replication of the second virus was most likely reduced due to a superinfection exclusion.

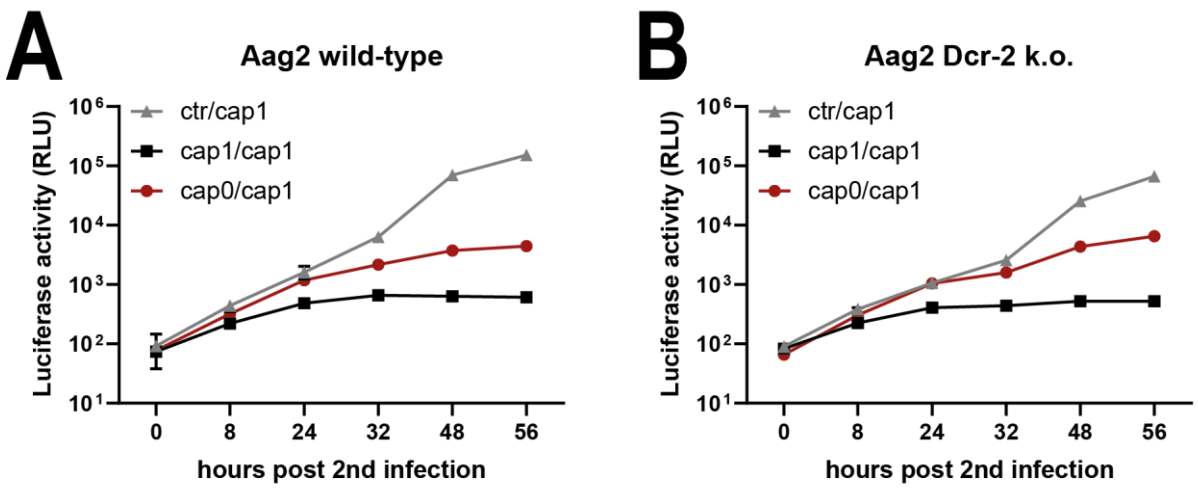

Figure 15: Priming of Aag2 wild-type and Aag2 Dcr-2 k.o. cells through sequential infection.
Aag2 wild-type cells (A) or Aag2 Dcr-2 k.o. cells (B) were infected with YFV-Asibi cap1 or cap0 at an MOI of 1 or were left uninfected. 24 h post first infection, cells were sequentially infected with YFV-Asibi cap1 *Gaussia* at an MOI of 0.01. YFV-Asibi cap1 replication was assessed by measuring the *Gaussia* luciferase released into the cell culture supernatant at 0, 8, 24, 32, 48, and 56 h post-second infection. Data represent Mean ± SD of triplicate infection experiments.

3.4 Analysis of Dcr-2 involvement in recognition of cap0 viruses

Viral dsRNA is not only recognized in the cytosol of vertebrate cells but also in the cytosol of mosquito cells. This recognition is mediated by the DExD/H-box domain expressing receptor Dcr-2, an essential component of the siRNA pathway (Figure 6). Dcr-2 cleaves long dsRNA into short 21 nt small virus-derived RNA duplexes (Galiana-Arnoux *et al.*, 2006). The short dsRNA molecules activate the siRNA pathway, which ends with the sequence-specific degradation of complementary RNAs. Interestingly, Dcr-2 belongs like the vertebrate receptor RIG-I to the DExD/H-box helicases, and both receptors interact with RNA through their DExD/H-box domain (Ahmad *et al.*, 2015). Previous studies reported the production of antiviral factors such as Vago following viral infection in a Dcr-2-dependent manner in *Culex* cells (Deddouche *et al.*, 2008; Paradkar *et al.*, 2014). Since the specific antiviral role of Dcr-2 is well described in the literature, it was tempting to speculate that Dcr-2 also plays an essential role in the differentiation between cap1 and cap0 orthoflaviviruses similar to RIG-I.

In order to study the potential cap1 and cap0 discrimination activity of the receptor Dcr-2 in more detail, viral replication levels of YFV-17D cap1 and cap0 were determined in Dcr-2 k.o. cells. The previously described Aag2 Dcr-2 k.o. cells and the corresponding parental control cells were infected with YFV-17D cap1 and cap0 (MOI 0.01) (Varjak, Maringer, *et al.*, 2017). At different time points, the amount of virus released into the cell culture supernatant was determined using plaque assay. As expected from previous experiments (Figure 9C), YFV-17D cap0 showed reduced replication compared to YFV-17D cap1 in the parental cells (Figure 16A). The replication difference between YFV-17D cap1 and cap0 increased over time and peaked at day seven post-infection, where the replication of YFV-17D cap1 was increased by 1.7 $\log_{10}$ compared to the cap0 virus.

Both viruses also showed increasing replication over time in the Dcr-2 k.o. cell line (Figure 16B). Again, the overall replication of YFV-17D cap0 was distinctly reduced compared to cap1 (Figure 16B, C). YFV-17D cap1 and cap0 replication levels continuously increased until day ten, reaching titers of 8.5×10^6 PFU/ml for YFV-17D cap1 and 7.6×10^5 PFU/ml for cap0 (Figure 16B).

Comparing the replication kinetics of the cap1 and cap0 viruses in the two cell lines revealed a similar reduction of the cap0 virus compared to the cap1 virus in both cell lines

(Figure 16C). In summary, these data imply that Dcr-2 does not play an essential role in recognizing YFV-17D cap0. If Dcr-2 would be necessary for the differentiation between cap1 and cap0 RNAs, the replication efficiency of YFV-17D cap0 should have been significantly increased in the Dcr-2 k.o. cells compared to the parental cells.

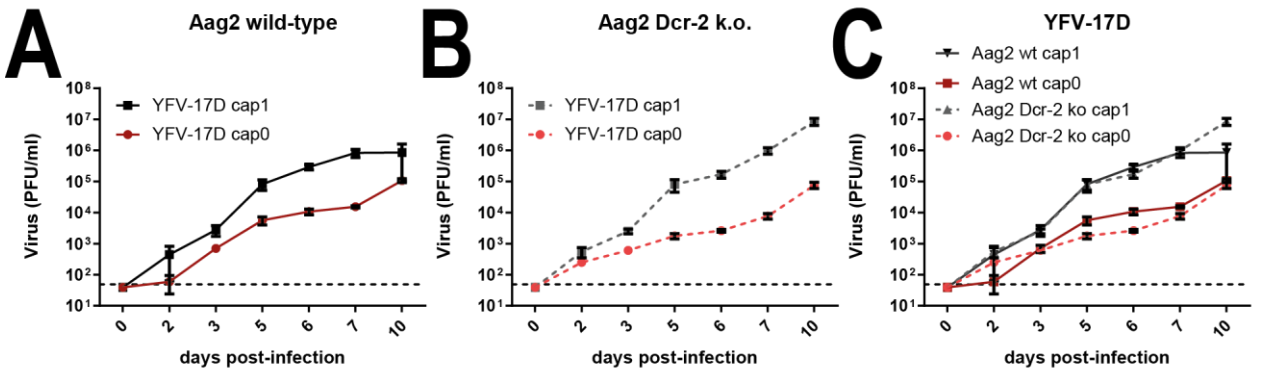

Figure 16: Viral replication of YFV-17D cap1 and cap0 in Aag2 wild-type and Dcr-2 k.o. cells.
Parental Aag2 cells (A) or Dcr-2 k.o. cells (B) were infected with YFV-17D cap1 and cap0 at an MOI of 0.01. C) Merged growth kinetics of the cap1 and cap0 viruses on parental and k.o. cells. Viral titers were measured at 0, 2, 3, 5, 6, 7, and 10 days post-infection by titration on BHK-21/J cells. Data represent Mean ± SD of triplicates (day 2, 5, 6, 7, and 10 post-infection) or six replicates (day 0 and 3 post-infection). Dashed lines: detection limit.

Since YFV-17D cap0 and YFV-Asibi cap0 showed different replication levels in insect cells, especially in C6/36 cells, it was next investigated whether Dcr-2 affected the replication of YFV-Asibi cap0. For this purpose, Dcr-2 k.o. cells and the parental cells were infected with YFV-Asibi cap1 and cap0 (MOI 0.01). Replication was measured at different time points to establish replication kinetics of the viruses in both cell types. YFV-Asibi cap1 replicated faster in the parental cell line than YFV-17D cap1 and reached its replication peak as early as day five with a titer of 1.5 x 10^5 PFU/ml (Figure 16A, Figure 17A) before plateauing. Replication of YFV-Asibi cap0 increased until day seven before reaching its plateau with a peak titer of 9.5 x 10^4 PFU/ml. At early time points, a difference in the replication rate of YFV-Asibi cap1 and cap0 was apparent in the parental cells, but this difference decreased over time.

The difference in the replication rates between YFV-Asibi cap1 and cap0 was likewise present at early time points in the Dcr-2 k.o. cells (Figure 17B). In contrast to the parental cells, this replication difference stayed stable until ten days post-infection. YFV-Asibi cap1

replicated to slightly higher titers in the k.o. cells and did not reach a plateau. Both viruses reached their replication peak ten days post-infection with a titer of 4.8 x 10^5 PFU/ml and 1.4 x 10^5 PFU/ml for cap1 and cap0 viruses, respectively. YFV-Asibi cap1 and cap0 showed no significant replication differences in the Dcr-2 k.o. and parental cells (Figure 17C).

In summary, the obtained data indicate that the absence of Dcr-2 neither positively nor negatively affects the replication of YFV-17D cap0 or YFV-Asibi cap0. Thus, the replication difference between YFV cap1 and cap0 is not solely mediated by the receptor Dcr-2.

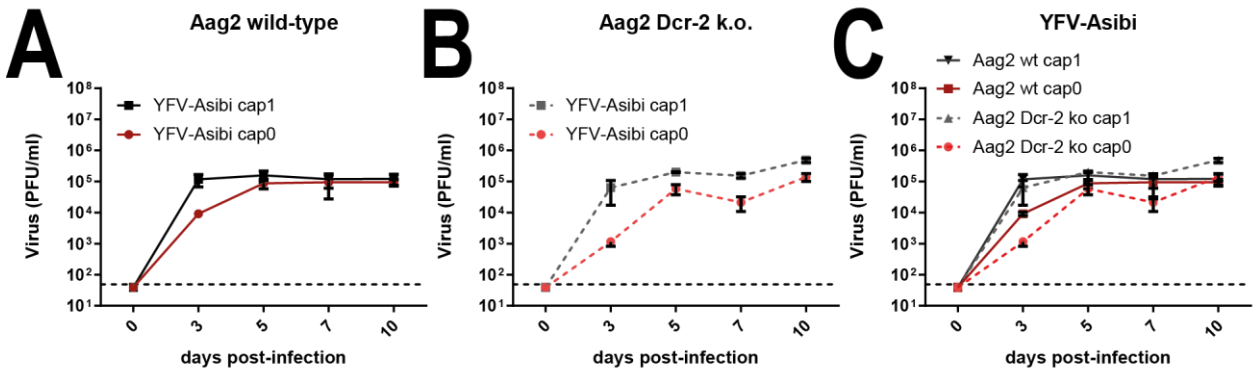

Figure 17: Viral replication of YFV-Asibi cap1 and cap0 in Aag2 wild-type and Dcr-2 k.o. cells.
Parental Aag2 cells (A) or Dcr-2 k.o. cells (B) were infected with YFV-Asibi cap1 and cap0 at an MOI of 0.01. C) Merged growth kinetics of the cap1 and cap0 viruses on parental and k.o. cells. Viral titers were measured at 0, 3, 5, 7, and 10 days post-infection by titration on BHK-21/J cells. Data represent Mean ± SD of triplicates. Dashed lines: detection limit.

3.4.1 Gene expression of innate immune defense genes

The previously obtained data indicate that the discrimination mechanism between YFV cap1 and cap0 RNA is independent of Dcr-2. Due to this, it was aimed to investigate whether other immune pathways are involved in this mechanism. Therefore, qPCR assays were established to measure the activation of the siRNA pathway, the Toll pathway, the JAK/STAT pathway, and the miRNA pathway. One representative gene was selected for each pathway, and the relative expression was measured in three different conditions. In order to detect the activation of the siRNA pathway, the expression of Ago2 was measured (Figure 18A), while for the Toll pathway MyD88 (Figure 18B), for the JAK/STAT pathway vir-1 (Figure 18C), and for the miRNA pathway Dcr-1 (Figure 18D) was chosen.

C6/36 cells were either infected with YFV-Asibi cap1, cap0, or mock-infected at an MOI of 0.1 for 24 h. After incubation, the total RNA was extracted, and the expression of the four genes was measured via RT-qPCR.

The RNA endonuclease Ago2 is an essential component of the siRNA pathway, acting downstream of Dcr-2 (Blair *et al.*, 2015). Expression of Ago2 was slightly increased in C6/36 cells upon infection with YFV-Asibi cap1 (Figure 18A), while the expression remained nearly unchanged upon infection with YFV-Asibi cap0. Nevertheless, the induction of Ago2 upon YFV-Asibi cap1 infection was not significant. Previous studies showed that silencing of MyD88 led to increased levels of DENV particles in *Aedes aegypti*, indicating that the Toll pathway exhibits an antiviral role mediated via MyD88 (Ramirez *et al.*, 2010). Expression of MyD88 was only marginally increased by 1-fold in C6/36 cells upon infection with YFV-Asibi cap1 and cap0 (Figure 18B), indicating that both viruses do not interfere with this gene. Vir-1 is an effector gene downstream of the JAK/STAT pathway whose expression is induced upon viral infection (Dostert *et al.*, 2005; Almire *et al.*, 2021). While vir-1 expression was minimally increased in YFV-Asibi cap1 infected cells, the expression was significantly reduced in YFV-Asibi cap0 infected cells by 2-fold (Figure 18C). This data suggests that YFV-Asibi cap0 may inhibit the JAK/STAT pathway or the gene expression downstream of the JAK/STAT pathway, allowing it to replicate in C6/36 cells, unlike YFV-17D cap0. Lastly, the activation of the miRNA pathway was investigated by measuring the expression of the RNase III-like enzyme Dcr-1 (Figure 18D). In neither YFV-Asibi cap1 nor cap0 infected cells, the

expression of Dcr-1 was reduced. However, the reduction was still insignificant. None of the tested genes gave a distinct hint of whether one or more antiviral pathways were activated upon infection with YFV-Asibi cap1 or cap0 in C6/36 cells.

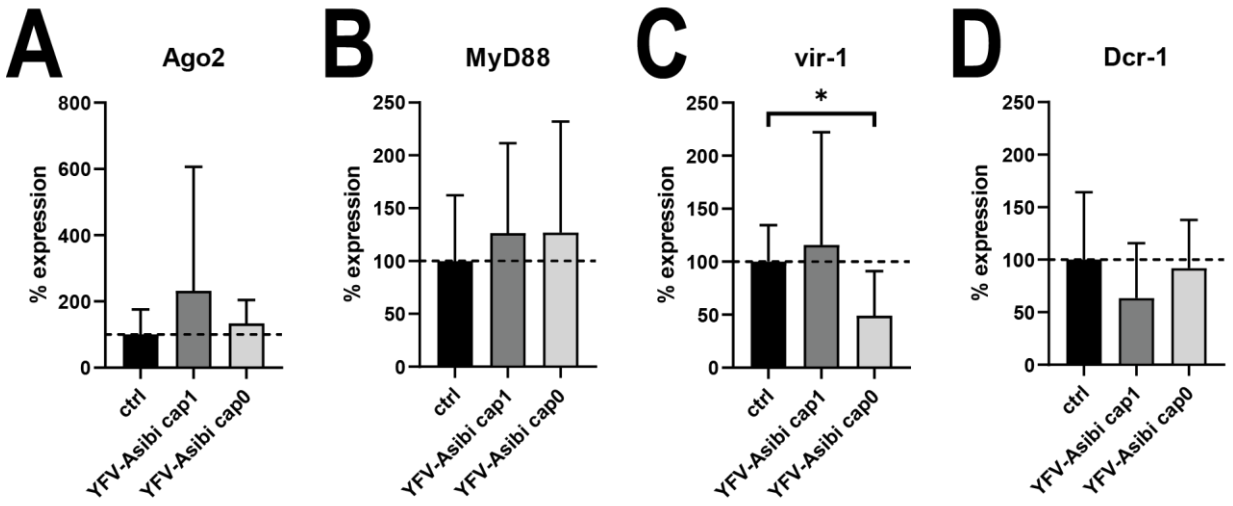

Figure 18: RT-qPCR assays measuring the siRNA, Toll, JAK/STAT, and miRNA pathway activation.
Expression of Ago2 in uninfected or YFV-Asibi cap1 or cap0 infected cells. B) Expression of MyD88 in uninfected or YFV-Asibi cap1 or cap0 infected cells. C) Expression of vir-1 in uninfected or YFV-Asibi cap1 or cap0 infected cells. D) Expression of Dcr-1 in uninfected or YFV-Asibi cap1 or cap0 infected cells. Infected cells were normalized to uninfected cells, and uninfected cells were set to 100%. Data represent Mean ± SD of three independent infection experiments performed in triplicates. Stars (*) indicate significance by Student's t-test (* $p \leq 0.05$).

3.5 Replication analysis of YFV-Asibi cap1 and cap0 *in vivo*

The previous experiments showed that the replication of YFV-17D cap0 and YFV-Asibi cap0 were especially down-regulated in the insect cells C6/36 compared to their respective cap1 viruses. These data suggest a potential mechanism discriminating between cap1 and cap0 viruses in insects. To further characterize the discrimination mechanism, *in vivo* experiments were performed. Since *Aedes aegypti* is the primary vector of YFV, experiments were performed with this mosquito species (McElroy *et al.*, 2006b).

3.5.1 Oral infection of *Aedes aegypti*

Female *Aedes aegypti* were orally infected with YFV-Asibi cap1 (Figure 19A) or cap0 (Figure 20A) to analyze the replication of the viruses *in vivo*. The mosquitoes were orally infected with a blood meal spiked with virus to a final concentration of 1×10^7 PFU/ml. At least 30 mosquitoes were collected at each time point and dissected within three hours post-infection (d0) or on days 3, 5, 7, 10, 14, or 21. The mosquitoes were dissected into the carcass to examine the infection rate and into legs plus wings to analyze the dissemination rate of the respective virus. Lastly, the mosquitoes' saliva was collected for YFV-Asibi cap1 infected mosquitoes to analyze the transmission rate and efficiency. The amount of viral RNA was assessed by measuring viral RNA quantity over time by RT-qPCR.

Analysis of the YFV-Asibi cap1 viral loads in the carcass on day zero revealed an infection rate of 100% and a median viral titer of 1×10^6 RNA copies/carcass (Figure 19B, Table 31). Interestingly, the average titer of the cap1 virus decreased between day zero and day three post-infection by 1 $\log_{10}$ to a median titer of 7×10^4 RNA copies/carcass; however, the infection rate stayed nearly stable at 98%. From day three on, the cap1 viral titers in the carcasses increased steadily over time. The viral replication significantly increased between day zero and day 21 post-infection by 0.5 $\log_{10}$ (Figure 19B). The infection rates were stable throughout the experiments, ranging from 94% to 98% (Table 31).

Next, the viral RNA of YFV-Asibi cap1 in the secondary organs was examined at different time points. Therefore, legs plus wings of every single mosquito were pooled, the RNA was extracted, and viral loads were analyzed via RT-qPCR. While little viral RNA was detected at early time points, the amount increased significantly until day 21 (Figure 19C).

The highest median titer in legs plus wings was measured 21 days after infection with a value of 3.1 x 10^5 RNA copies/legs plus wings. On days three and five post-infection, the cap1 dissemination rate varied between 26% and 36%, respectively (Table 31). From day five, the dissemination rate increased and reached its highest level ten days after infection (89%). After this time point, the amount of viral RNA continued to increase, but the dissemination rate remained broadly stable (84% - 86%).

Even though YFV-Asibi cap1 could successfully infect carcasses (Figure 19B) and secondary organs such as legs plus wings (Figure 19C), saliva was only positive in single mosquitoes at all tested time points (Figure 19D). Due to the few mosquitoes positive in saliva, the transmission rate only reached a maximum of 14% on day three post-infection (Table 31). Accordingly, transmission efficiency ranged from 0% to 7%.

These data indicate that after oral infection, YFV-Asibi cap1 can successfully establish an infection in *Aedes aegypti* carcasses, legs, and wings. Nevertheless, the virus required time to overcome the midgut barrier and to establish an efficient infection in secondary organs. The low transmission efficiency, on the contrary, suggests that YFV-Asibi cap1 could not establish an infection in the salivary glands.

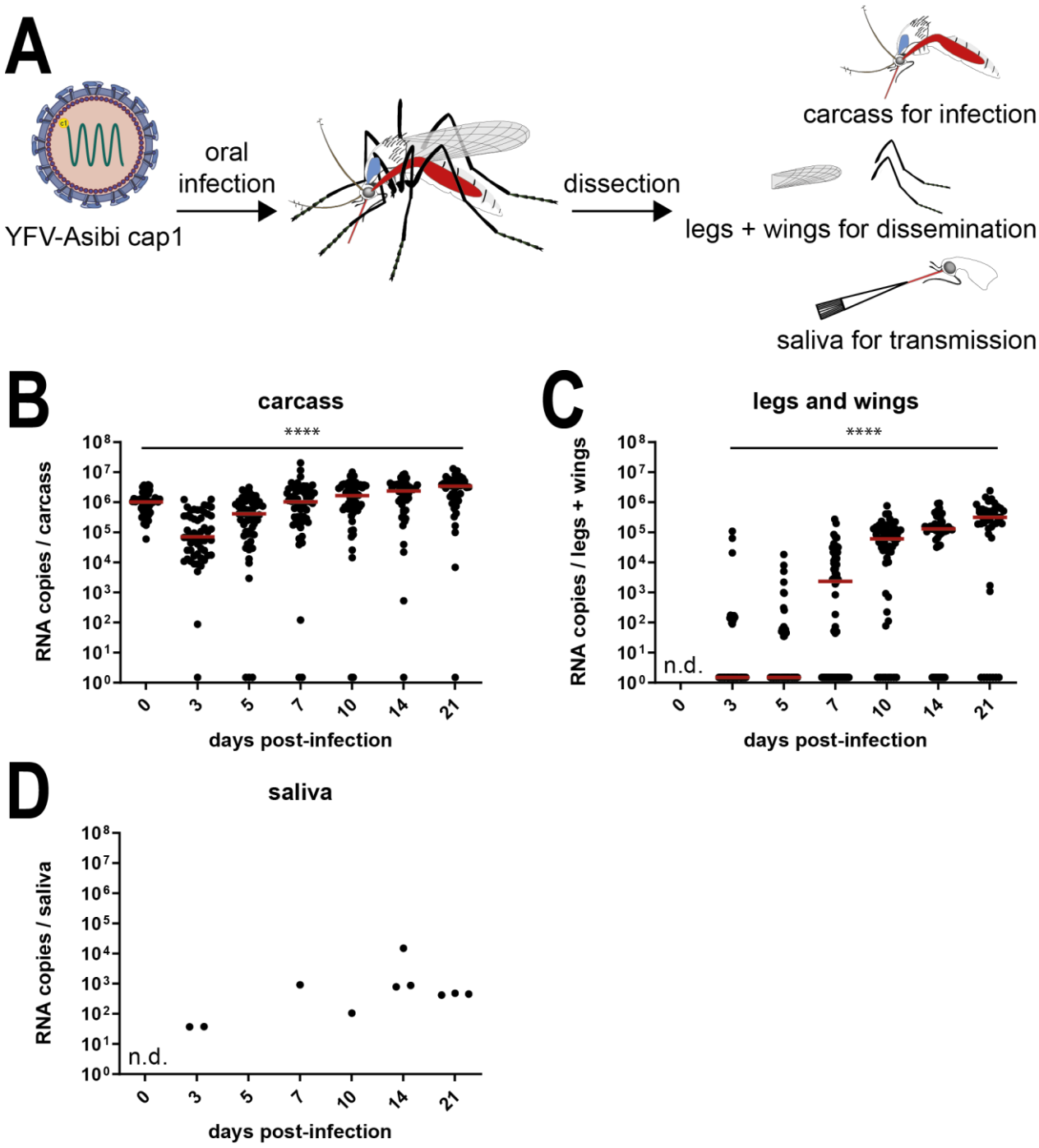

Figure 19: Oral infection of *Aedes aegypti* with YFV-Asibi cap1.
A) Schematic overview of the experimental setup. Female mosquitoes were fed with an infectious blood meal containing 1 x 10^7 PFU/ml virus. Engorged mosquitoes were kept at 28 °C and 80% humidity. The mosquitoes were dissected on days 0, 3, 5, 7, 10, 14, or 21 post-infection. The viral RNA copies in the carcass, legs plus wings, and saliva were determined by RT-qPCR. B) RNA copies of YFV-Asibi cap1 per carcass (B), legs plus wings (C), and saliva (D) at different time points post-infection. Each point represents a single female mosquito. The red line indicates the median titers and stars (*) the significance by Mann-Whitney U-test (**** $p \leq 0.0001$).

Table 31: Infection, dissemination, transmission rates, and transmission efficiencies for YFV-Asibi cap1 and cap0 at different time points post-infection.
Minus (-) indicates values that were not measured. Infection rate: mosquitoes positive in the carcasses in relation to the total number of examined mosquitoes; dissemination rate: mosquitoes containing viral RNA in legs plus wings in relation to the number of positive carcasses; transmission rate: mosquitoes containing viral RNA in the saliva in relation to the number of positive legs plus wings; transmission efficiency: mosquitoes containing viral RNA in the saliva in relation to the total number of tested mosquitoes.

Virus	Days post-infection	Infection rate (%)	Dissemination rate (%)	Transmission rate (%)	Transmission efficiency (%)
cap1	0	53/53 100%	-	-	-
	3	53/54 98%	14/53 26%	2/14 14%	2/54 4%
	5	50/53 94%	18/50 36%	0/18 0%	0/53 0%
	7	53/55 96%	35/53 66%	1/35 3%	1/55 2%
	10	55/57 96%	49/55 89%	1/49 2%	1/57 2%
	14	44/45 98%	37/44 84%	3/37 8%	3/45 7%
	21	44/45 98%	38/44 86%	3/38 8%	3/45 7%
cap0	0	33/33 100%	-	-	-
	3	11/33 33%	2/11 18%	-	-
	5	6/31 19%	0/6 0%	-	-
	7	6/30 20%	1/6 17%	-	-
	10	7/30 23%	1/7 14%	-	-
	14	7/31 23%	2/7 29%	-	-
	21	9/37 24%	1/9 11%	-	-

Next, the same experimental setup was chosen to orally infect *Aedes aegypti* mosquitoes with YFV-Asibi cap0 (Figure 20A). Again, the blood meal contained a final titer of 1 x 10^7 PFU/ml, and mosquitoes were dissected within three hours post-infection (d0) or on days 3, 5, 7, 10, 14, or 21.

YFV-Asibi cap0 could not establish an efficient infection in the mosquito carcasses (Figure 20B). The median viral titer reached 6.7 x 10^5 RNA copies/carcass on day zero, indicating an efficient viral uptake by the mosquitoes. However, the viral RNA titers significantly decreased from day zero until day 21 post-infection. Most mosquitoes were negative for YFV RNA, indicating no efficient replication of YFV-Asibi cap0 in the mosquito carcasses. The infection rate on day zero resulted in 100% but decreased to 33% on day three and 24% on day 21 post-infection.

The replication efficiency of YFV-Asibi cap0 in secondary tissues was again measured by determining the amount of viral RNA in legs plus wings. Consistent with the data for the carcasses, the cap0 virus was unable to replicate in secondary tissues except for single mosquitoes (Figure 20C), resulting in dissemination rates of less than 30% (Table 31). Due to the low dissemination rates, the transmission rate and efficiency were not further evaluated.

These findings demonstrate that YFV-Asibi cap0 could not establish an infection in the mosquito midgut after oral infection. Additionally, with a few exceptions, the virus could not overcome the midgut barrier to replicate in secondary tissues. Accordingly, the data suggest a mechanism within the mosquito that differentiated between cap1 and cap0 viruses that is mainly localized in the midgut barrier.

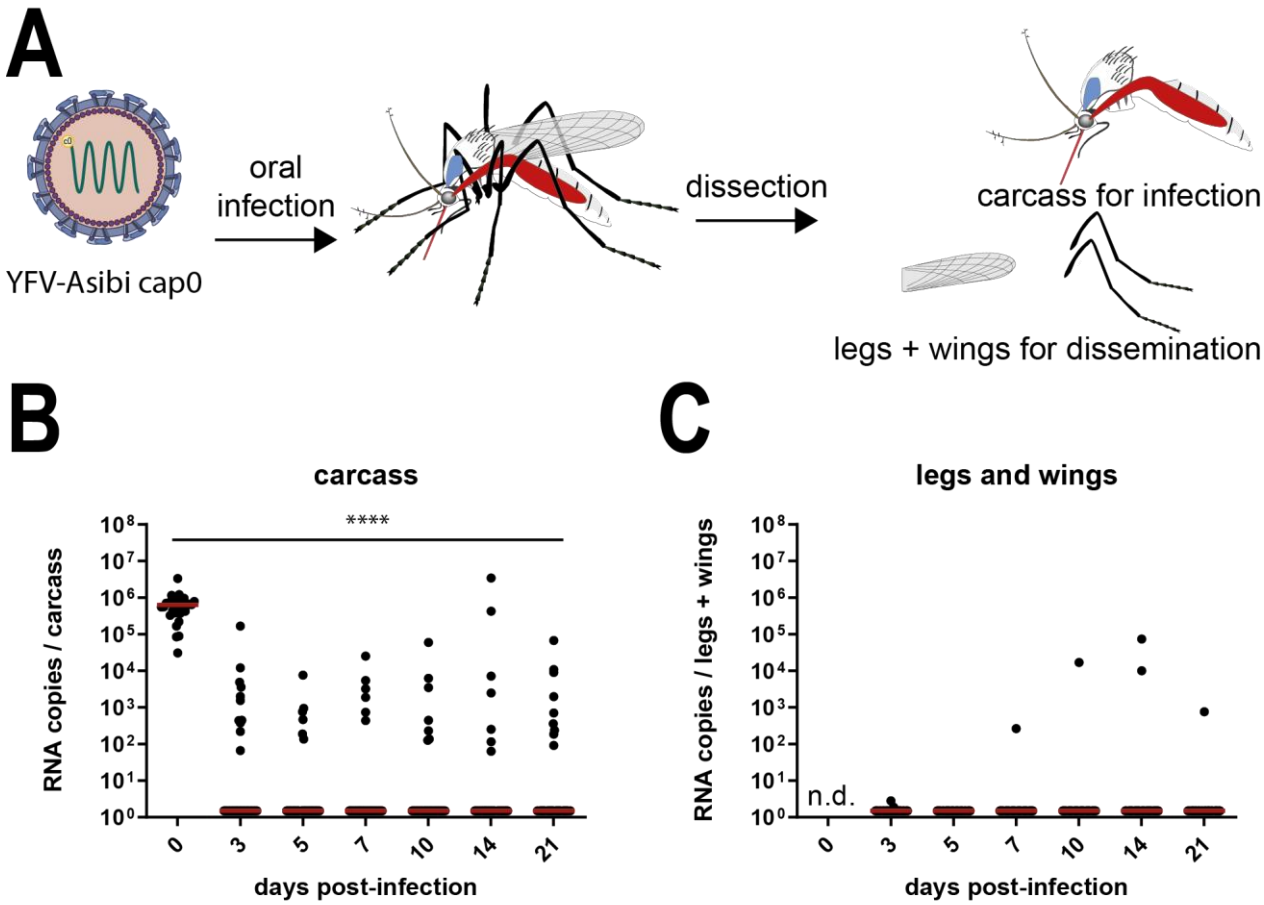

Figure 20: Oral infection of *Aedes aegypti* with YFV-Asibi cap0.
A) Schematic overview of the experimental setup. Female mosquitoes were fed with an infectious blood meal containing 1 x 10^7 PFU/ml virus. Engorged mosquitoes were kept at 28 °C and 80% humidity. The mosquitoes were dissected on days 0, 3, 5, 7, 10, 14, or 21 post-infection. The viral RNA copies in the carcass, legs plus wings were determined by RT-qPCR. RNA copies of YFV-Asibi cap0 per carcass (B) and legs plus wings (C) at different time points post-infection. Each point represents a single female mosquito. The red line indicates the median titers, and stars (*) indicate significance by Mann-Whitney U-test (**** $p \leq 0.0001$).

3.5.2 Intrathoracic infection of *Aedes aegypti*

The previously obtained data indicate that YFV-Asibi cap0 replication was specifically restricted after oral infection. However, it was not analyzed whether it was a distinct downregulation of the cap0 virus or whether the cap0 virus had some defect that prevented efficient replication *in vivo*. To investigate the general replication ability of YFV-Asibi cap0 *in vivo*, female *Aedes aegypti* were intrathoracically infected with YFV-Asibi cap1 and cap0. This method was applied to assess the replication ability of YFV-Asibi cap0 when delivered via a non-oral route. To this end, female mosquitoes were injected with 300 PFU YFV-Asibi cap1 or cap0 virus (Figure 21A). Whole mosquitoes were sampled on days zero and seven post-infection to analyze the viral replication via RT-qPCR.

Intrathoracic injection with YFV-Asibi cap1 resulted in a median input titer of 4.5×10^3 RNA copies/mosquito (Figure 21B). Analysis of viral replication on day seven post-infection revealed efficient virus replication. The amount of virus increased significantly to a median titer of 3.98×10^6 RNA copies/mosquito. Next, *Aedes aegypti* were intrathoracically injected with YFV-Asibi cap0 virus to assess the replication efficiency as well (Figure 21C). The median input titer of the cap0 virus was 7×10^3 RNA copies/mosquito, which was quite similar to the median input titer of the cap1 virus.

Interestingly, YFV-Asibi cap0 replicated also efficiently at day seven post-infection in the mosquitoes, reaching a median titer of 1.76×10^6 RNA copies/mosquito. Although the median titer of YFV-Asibi cap0 was lower at seven days post-injection than that of YFV-Asibi cap1, the data show that YFV-Asibi cap0 can replicate efficiently in mosquitoes when circumventing the midgut barrier. Hence, the replication of YFV-Asibi cap0 is primarily restricted at the midgut barrier.

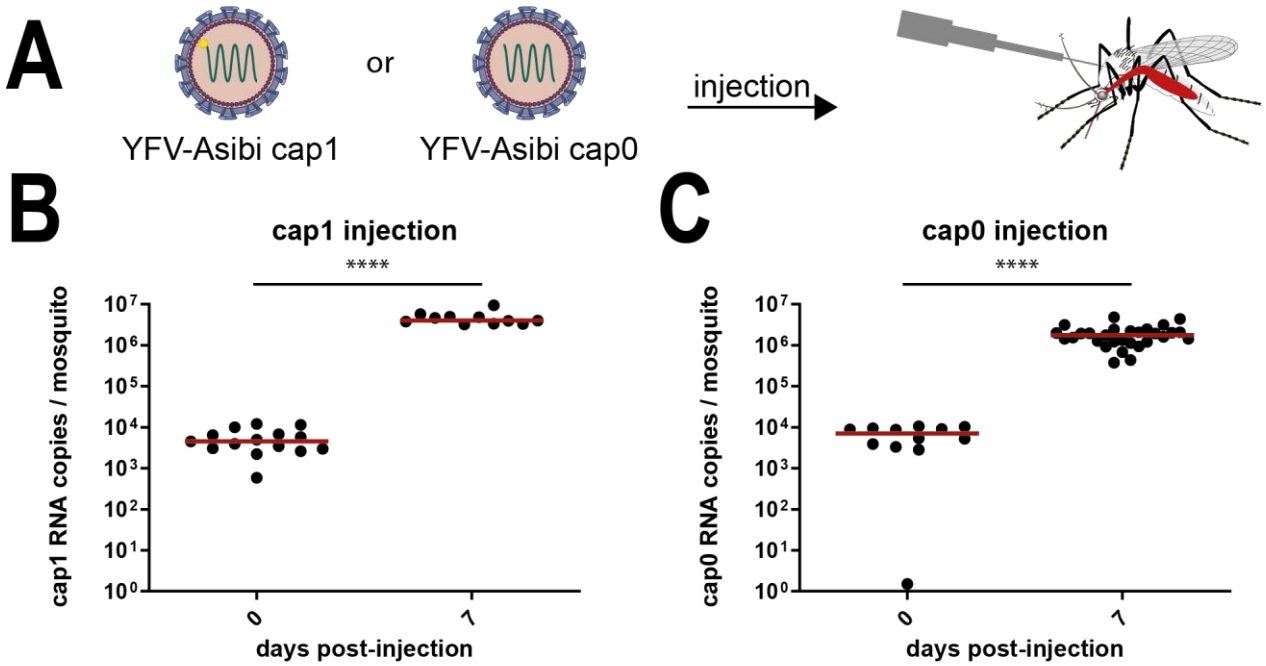

Figure 21: Intrathoracic injection of *Aedes aegypti* with YFV-Asibi cap1 and cap0. A) Experimental setup of an intrathoracic injection experiment. Female mosquitoes were injected with 300 PFU YFV-Asibi cap1 or cap0 in a total volume of 26.7 nl. B) RNA copies of YFV-Asibi cap1 per mosquito at days 0 and 7 post-infection. C) RNA copies of YFV-Asibi cap0 per mosquito at days 0 and 7 post-infection. Each point represents a single female mosquito. The red line indicates the median titers, and stars (*) indicate significance by unpaired t-test with Welch's correction (**** $p \leq 0.0001$).

3.6 Recognition of different cap0 orthoflaviviruses

The YFV methyltransferase encoded in the NS5 protein is highly conserved between different YFV strains and different orthoflaviviruses. The active site of the methyltransferase consisting of the amino acids K-D-K-E is conserved among all orthoflaviviruses (Egloff *et al.*, 2002). To examine whether the mosquito immune system can differentiate other cap1 and cap0 orthoflaviviruses besides YFV, the E218A mutation was also introduced into ZIKV and DENV.

3.6.1 Growth analysis of ZIKV cap0

The infectious cDNA clone pCCI-SP6-ZIKV, based on the ZIKV isolate BeH19015 from Brazil, was used as the starting point for establishing the ZIKV-E218A mutant (ZIKV cap0) (Mutso *et al.*, 2017). For this purpose, the codon GAG was mutated to GCC using site-directed mutagenesis through fusion PCR technology (2.2.3.2). The resulting PCR fragment was cut with the restriction enzymes RsrII and BstBI and ligated into the pCCI-SP6-ZIKV backbone cut with the same set of enzymes. A schematic illustration of the construct can be found in the appendix (10.2). Following establishing the ZIKV cap0 infectious cDNA clone, ZIKV cap1 and cap0 virus were rescued in parallel. Therefore, both infectious cDNA clones were linearized with AgeI, precipitated, and *in vitro* transcribed using an SP6 RNA polymerase. The resulting RNA was transfected into Vero E6 cells, and the cells were incubated for ten days before the progeny virus was harvested (P0 virus). P0 virus was used for all subsequent experiments.

ZIKV cap1 and cap0 formed plaques on Vero B4 cells of variable sizes four days post-titration (Figure 22A). The plaques formed by ZIKV cap0 were smaller than the ones formed by ZIKV cap1.

In order to study whether ZIKV cap0 was lacking the 2'-O-methylation, A549 IFIT1 k.o. cells and parental A549 cells were infected with ZIKV cap1 and cap0 at an MOI of 0.001. The amount of virus released into the supernatant was determined 72 h post-infection using plaque assay (Figure 22B). While ZIKV cap1 showed modest replication in the A549 wild-type cells, ZIKV cap0 replication was significantly attenuated compared to ZIKV cap1. Interestingly, replication of ZIKV cap0 was also reduced compared to ZIKV cap1 in the A549 IFIT1 k.o. cells. However, this reduction was not significant due to the high variability of the individual samples.

Schuberth-Wagner and colleagues reported similar growth behavior of YFV-17D cap1 and cap0 on Vero B4 cells due to the dysfunctional type I interferon response (Schuberth-Wagner *et al.*, 2015). In contrast, they saw reduced replication of YFV-17D cap0 in immune-competent A549 cells. In order to characterize the established ZIKV cap1 and cap0 virus, Vero B4 and A549 cells were infected with both viruses at an MOI of 0.001. The growth characteristics of ZIKV cap1 and cap0 virus released into the cell culture medium of the infected cells were compared at six days post-infection by titration on Vero B4 cells. Replication of ZIKV cap1 was highly increased by 2 $\log_{10}$ compared to replication of ZIKV cap0 in Vero B4 cells (Figure 22C). Similarly, the replication of ZIKV cap0 was highly attenuated in A549 cells, while ZIKV cap1 replicated comparable in A549 and Vero B4 cells (Figure 22C).

Next, the growth characteristics of ZIKV cap1 and cap0 were determined in C6/36 cells over time. Therefore, C6/36 cells were infected with both viruses at an MOI of 0.001, and viruses released in the supernatant were harvested on days 0, 3, 5, 7, and 10 post-infection (Figure 22D). Replication of ZIKV cap1 rapidly increased in C6/36 cells between day zero and five post-infection. After day five, the replication entered a plateau and peaked on day seven with a titer of 2.6×10^6 PFU/ml. In contrast, ZIKV cap0 required more time to exceed the detection limit, and efficient replication was detectable from day three post-infection onwards. Compared to ZIKV cap1, ZIKV cap0 also peaked at seven days post-infection with a titer of 6.8×10^4 PFU/ml, but the viral titers of ZIKV cap0 were reduced compared to cap1 throughout the experiment.

Due to the high standard deviations of ZIKV cap1 and cap0 in all tested cell lines, all cap0 viruses from day six (Vero B4, A549) or day ten (C6/36) post-infection were sequenced to verify the stability of the introduced E218A mutation. All viruses tested stably contained the GCC codon, and no spontaneous revision of the introduced mutations occurred (data not shown).

Taken together, the infection experiments could not reveal a clear picture of the ZIKV methylation status due to the inconsistency in the obtained data. ZIKV cap1 replicated to high titers in all vertebrate and insect cells, while the replication of ZIKV cap0 was highly impaired in all tested cell lines.

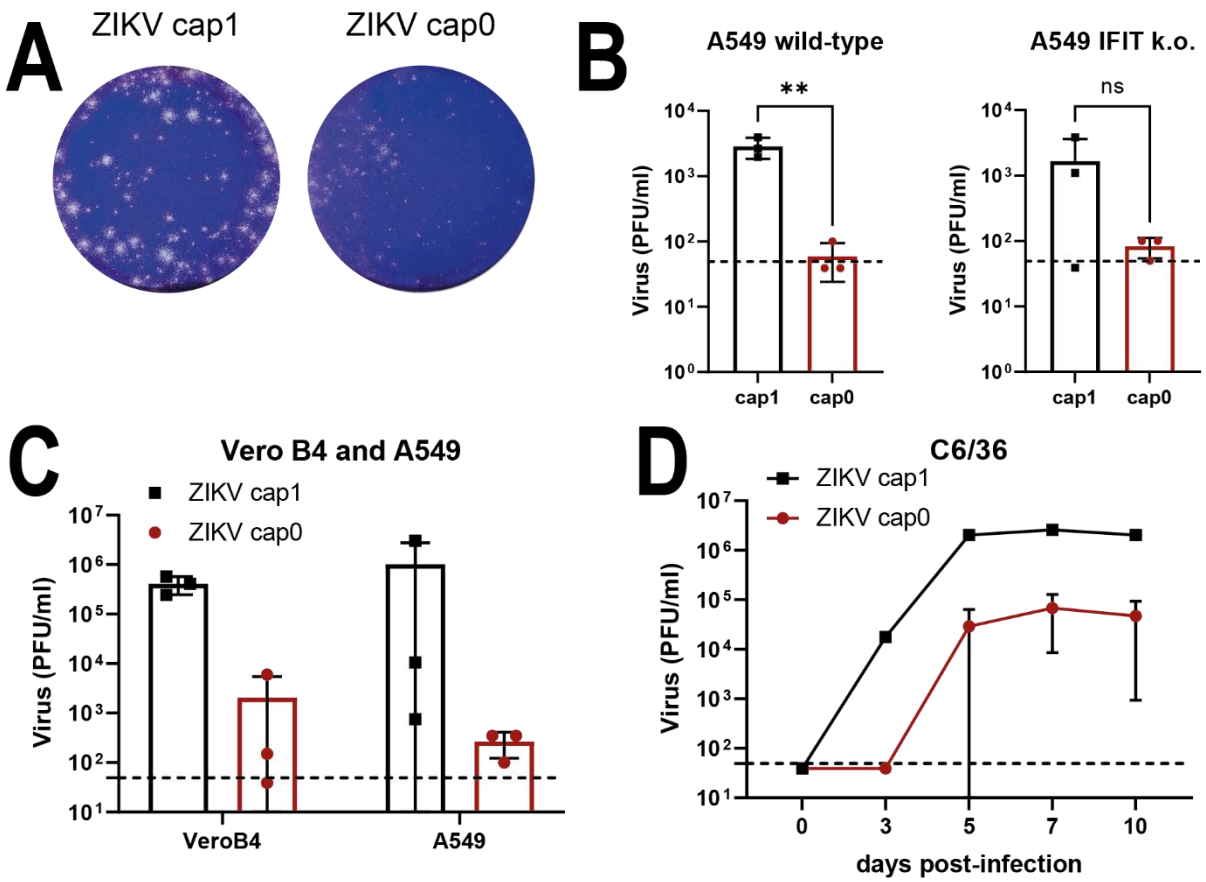

Figure 22: Characterization of ZIKV cap1 and cap0.
A) Plaque phenotypes of ZIKV cap1 and cap0 were characterized in Vero B4. Cells were infected with the cap1 and cap0 viruses that were previously passaged once in Vero B4 cells. At 4 days post-titration, cells were fixed and stained with crystal violet. B) Replication of ZIKV cap1 and cap0 3 days post-infection in A549 wild-type and A549 IFIT1 k.o. cells. C) Replication of ZIKV cap1 and cap0 6 days post-infection in Vero B4 and A549 cells. D) Growth kinetics of ZIKV cap1 and cap0 in C6/36 cells. Viral titers were measured at 0, 3, 5, 7, and 10 days post-infection. All cells were infected at an MOI of 0.001 and viral titers were measured by titration on Vero B4 cells. Data represent Mean ± SD of triplicates (Vero B4, A549, A549 wild-type, A549 IFIT1 k.o.) or duplicates (C6/36). Dashed lines: detection limit.

3.6.2 Growth analysis of DENV cap0

The tetrad consisting of the four amino acids K-D-K-E is not only highly conserved in ZIKV but also in all other orthoflaviviruses (Egloff *et al.*, 2002). Accordingly, these amino acids can also be found in the NS5 protein of DENV, but here the position of the glutamine is 217 and not 218 (Züst *et al.*, 2013).

To analyze the influence of the E217A mutation on the replication efficiency of DENV cap0 in mosquito cells, the infectious cDNA clone pD2/IC-30P-A was mutated using site-directed mutagenesis through fusion PCR technology (2.2.3.2) (Kinney *et al.*, 1997). The resulting PCR fragment, harboring the codon exchange GAG to GCC, was cut with the restriction enzymes NheI and BsrGI. This fragment was ligated into the pD2/IC-30P-A backbone, digested with the same enzymes. A schematic illustration of the construct can be found in the appendix (10.2). To be able to establish comparative growth curve analyses of DENV cap1 and cap0, the viruses were rescued in parallel. Therefore, the plasmids were linearized with XbaI to generate an authentic 3' end of the viral genome upon transcription. The linearized DNA was precipitated and *in vitro* transcribed. The resulting RNA was then electroporated into BHK-21/J cells for virus production. Since it was known that DENV does not cause a cytopathic effect in BHK-21/J cells, no infectious center assay was performed. The virus (P0 virus) was harvested three days post-electroporation and propagated once in Vero B4 cells for five days. These viral stocks (P1) were used for all subsequent experiments.

At day seven post-infection, DENV cap1 and cap0 produced plaques in Vero B4 cells (Figure 23A). The plaque sizes of the two DENVs were heterogeneous, with the DENV cap1 plaques showing greater diameters than the DENV cap0 plaques.

The 2'-O-methylation status of DENV cap1 and cap0 was indirectly verified by infecting A549 wild-type and IFIT1 k.o. cells with the two viruses at an MOI of 0.01. At 72 h post-infection, the amount of virus released into the cell culture supernatant was determined using plaque assay. Compared to DENV cap1, the replication of DENV cap0 was significantly reduced in the A549 wild-type cells (Figure 23B) due to IFIT1 binding to 2'-O-unmethylated RNA. In contrast, DENV cap1 and cap0 replicated to comparable levels in the IFIT1 k.o. cells (Figure 23B).

In line with the results shown in Figure 23B, replication of DENV cap0 was also reduced in A549 when performing growth curve analysis over six days (Figure 23C). Both viruses steadily replicated over time in A549 cells, but replication of DENV cap0 (8.7×10^3 PFU/ml) was suppressed compared to DENV cap1 (5.5×10^4 PFU/ml) from day three post-infection onwards (Figure 23C). This difference became more prominent by day six post-infection, with cap1 replicating 1.8 $\log_{10}$ more efficiently than cap0. Together with the data generated in the A549 IFIT1 k.o. cells, these data demonstrate that DENV cap0 replication was distinctly reduced in cells with a functional interferon response, indicating that the 2'-O-methylation is important for the immune escape of DENV. This viral reduction might be due to a RIG-I-induced immune response.

To further characterize the replication of the DENV mutant in vertebrate cells, Vero B4 cells were infected with DENV cap1 and cap0 (MOI 0.01) to perform a growth curve over six days. For DENV cap1 and cap0, similar RNA copies/ml were detectable in Vero B4 cells (Figure 23D). DENV cap1 and cap0 reached titers of 3.2×10^7 and 3.7×10^7 RNA copies/ml on day six, respectively. Both viruses did not reach their plateau within the course of the experiment.

Since the viral titers of YFV cap1 and cap0 profoundly differed in C6/36 cells (Figure 9B, Figure 12A), DENV cap1 and cap0 growth curve analysis was also performed in this cell line. For this purpose, C6/36 cells were infected in an analogous procedure (MOI 0.01). In this cell line, DENV cap1 and DENV cap0 grew with equal efficacy throughout the experiment (Figure 23E). Six days post-infection, DENV cap1 reached mean titers of 1.1×10^7 PFU/ml and DENV cap0 achieved 5.2×10^6 PFU/ml. Overall, DENV cap1 replicated only marginally higher than DENV cap0, and the profound difference, as seen for YFV, was not detectable for DENV.

In agreement with the results presented in Figure 23E, DENV cap1 and cap0 also replicated with comparable titers in the *Aedes aegypti*-derived Aag2 cells (Figure 23F). Both viruses did not reach their plateau within the course of the experiment. DENV cap1 and cap0 reached titers of 3.2×10^6 RNA copies/ml on day five post-infection. Following day five post-infection, the replication speed of DENV cap1 and cap0 declined.

Taken together, the data underline that DENV requires its cap1 methylation to escape the vertebrate immune recognition. At the same time, replication of DENV cap0 is not impaired in vertebrate cells with a dysfunction type I interferon response. On the contrary, DENV cap1 and cap0 replicated with comparable titers in different mosquito cell lines, implying that DENV does not require its cap1 methylation to escape the mosquito immune recognition. DENV might encode one or more proteins that counteract cap0 recognition by the insect immune system.

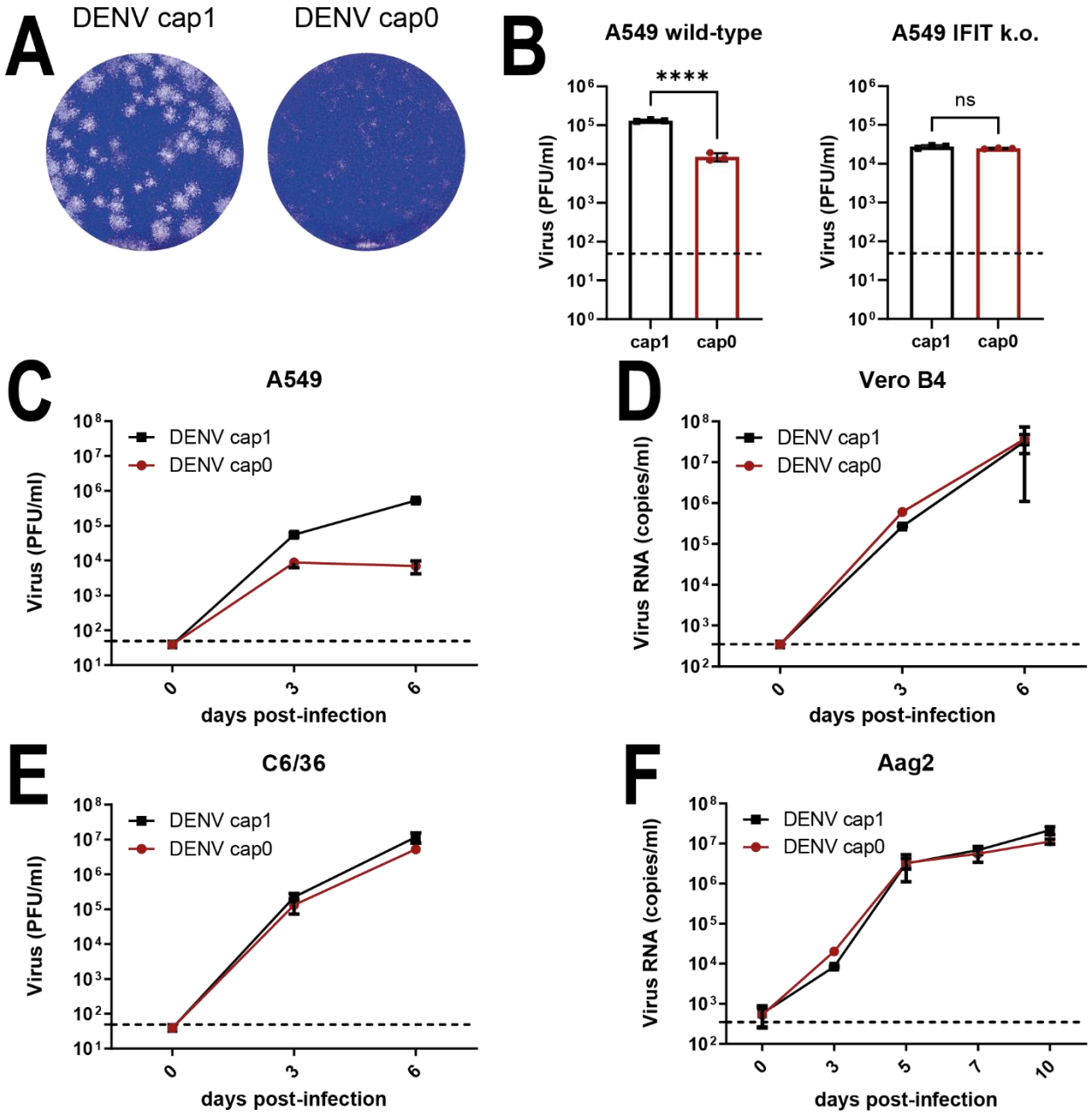

Figure 23: Characterization of DENV cap1 and cap0.
A) Plaque phenotypes of DENV cap1 and cap0 were characterized in Vero B4. Cells were infected with the cap1 and cap0 viruses that were previously passaged once in Vero B4 cells. At 7 days post-infection, cells were fixed and stained by crystal violet. B) DENV cap1 and cap0 replication in A549 wild-type and A549 IFIT1 k.o. cells three days post-infection. C - F) DENV cap1 and cap0 growth kinetics in A549, Vero B4, C6/36, and Aag2 cells. Cells were infected at an MOI of 0.01. Viral titers were measured at 3 days (A549 wild-type, A549 IFIT1 k.o.), at 0, 3, and 6 days (A549, C6/36, Vero B4) or at 0, 3, 5, 7, and 10 days post-infection (Aag2) by titration on Vero B4 cells (A549, C6/36, A549 wild-type, A549 IFIT1 k.o. cells) or by RT-qPCR (Vero B4, Aag2). Data represent Mean ± SD duplicates. Dashed lines: detection limit.

3.7 Analysis of YFV-Asibi counteraction of cap0 recognition in mosquitoes

The obtained data indicate that YFV-17D, YFV-Asibi, and DENV counteract the inhibition of cap0 replication in mosquitoes to different extents. DENV was found to strongly counteract the cap0 recognition, while YFV-Asibi had a slight counteractive effect, and YFV-17D did not have any counteractive effect *in vitro*. Thus, it was aimed to construct chimeras between the viruses to further elucidate the counteracting mechanism. Previous studies mainly described chimeras between DENV and YFV in which prM and E of DENV were inserted into the backbone of YFV (Guirakhoo *et al.*, 2000; Shustov *et al.*, 2010). However, the individual non-structural proteins could not be exchanged between the two viruses. In contrast, replication-competent chimeras between YFV-Asibi and YFV-17D are described in the literature (McElroy *et al.*, 2006b). Due to this, chimeras between the two YFV strains were established, even though the previous data indicate that DENV counteracted the cap0 recognition more strongly.

In the first approach, the structural proteins of YFV-Asibi were introduced into YFV-17D (SP Asibi in 17D) (Figure 24A), and the structural proteins of YFV-17D were introduced into YFV-Asibi (SP 17D in Asibi) (Figure 24B). For both chimeras, the corresponding cap1 and cap0 viruses were established. After successfully rescuing the four viruses, C6/36 cells were infected (MOI 0.01) with the two chimera sets. The SP Asibi in 17D cap1 chimera reached its replication peak five days after infection with a titer of 1.9×10^6 PFU/ml (Figure 24A). After this time point, the viral titers of the cap1 chimera slowly decreased. The corresponding cap0 chimera was unable to exceed the detection limit. Insertion of the structural proteins of YFV-17D into YFV-Asibi led to fast replication of the associated cap1 chimera (Figure 24B). The cap1 chimera replication peaked five days post-infection with a titer of 4.3×10^6 PFU/ml. The associated cap0 chimera, SP 17D in Asibi cap0, was readily detectable from day seven post-infection. Nevertheless, this replication was reduced compared to the parental YFV-Asibi cap0 (Figure 12A vs. Figure 24B). These data indicate that the structural proteins for Asibi are not mainly responsible for promoting cap0 replication.

The orthoflaviviral 3'UTR plays an essential role in producing sfRNAs, which have a broad antiviral effect in mosquitoes (Schnettler *et al.*, 2012; Göertz *et al.*, 2016; Pompon *et al.*, 2017). Since the 3'UTRs of YFV-Asibi and YFV-17D differ from each other in 5

nucleotides, the non-structural proteins of YFV-Asibi were next inserted into YFV-17D (Figure 24C). Again, the corresponding cap1 and cap0 chimeras were rescued, and C6/36 cells were infected with the chimeras (MOI 0.01). The cap1 chimera rapidly replicated in the insect cells and reached a titer of 2×10^6 PFU/ml on day three post-infection. The replication increased slightly until day five post-infection, where it peaked (4×10^6 PFU/ml). The associated cap0 chimera exceeded the detection limit five days post-infection and reached a titer of 1.1×10^3 PFU/ml on day ten post-infection. Again, the overall replication of the cap0 chimera was reduced compared to the parental YFV-Asibi cap0 (Figure 12A vs. Figure 24B). These data further support the hypothesis that the non-structural proteins of YFV-Asibi were mainly involved in promoting replication of the cap0 virus.

Next, the non-structural proteins of Asibi were further examined to determine whether one or more proteins were involved in counteracting the cap0 recognition. The infectious cDNA clones of YFV-Asibi and YFV-17D contain unique NgoMIV and XhoI restriction sites, allowing an easy exchange of the 3' end of NS4A (NS4A*) until the end of the 3'UTR. Thus, NS4A*-3'UTR Asibi was cloned into YFV-17D (NS4A*-3'UTR Asibi in YFV-17D) (Figure 24D). The replication speed of the NS4A*-3'UTR Asibi in 17D cap1 chimera showed a steep increase from day zero to day three post-infection. This increase in speed was comparable to the increase of the NS Asibi in 17D cap1 chimera (Figure 24C vs. Figure 24D). Likewise, the NS4A*-3'UTR Asibi in 17D cap1 chimera reached its replication maximum five days post-infection (5.9×10^6 PFU/ml). From day five post-infection, the associated cap0 chimera exceeded the detection limit, but the replication was severely limited compared to the parental YFV-Asibi cap0 (Figure 12A vs. Figure 24D). Nevertheless, the data indicate that one or more proteins of interest are located between NS4A* and the 3'UTR.

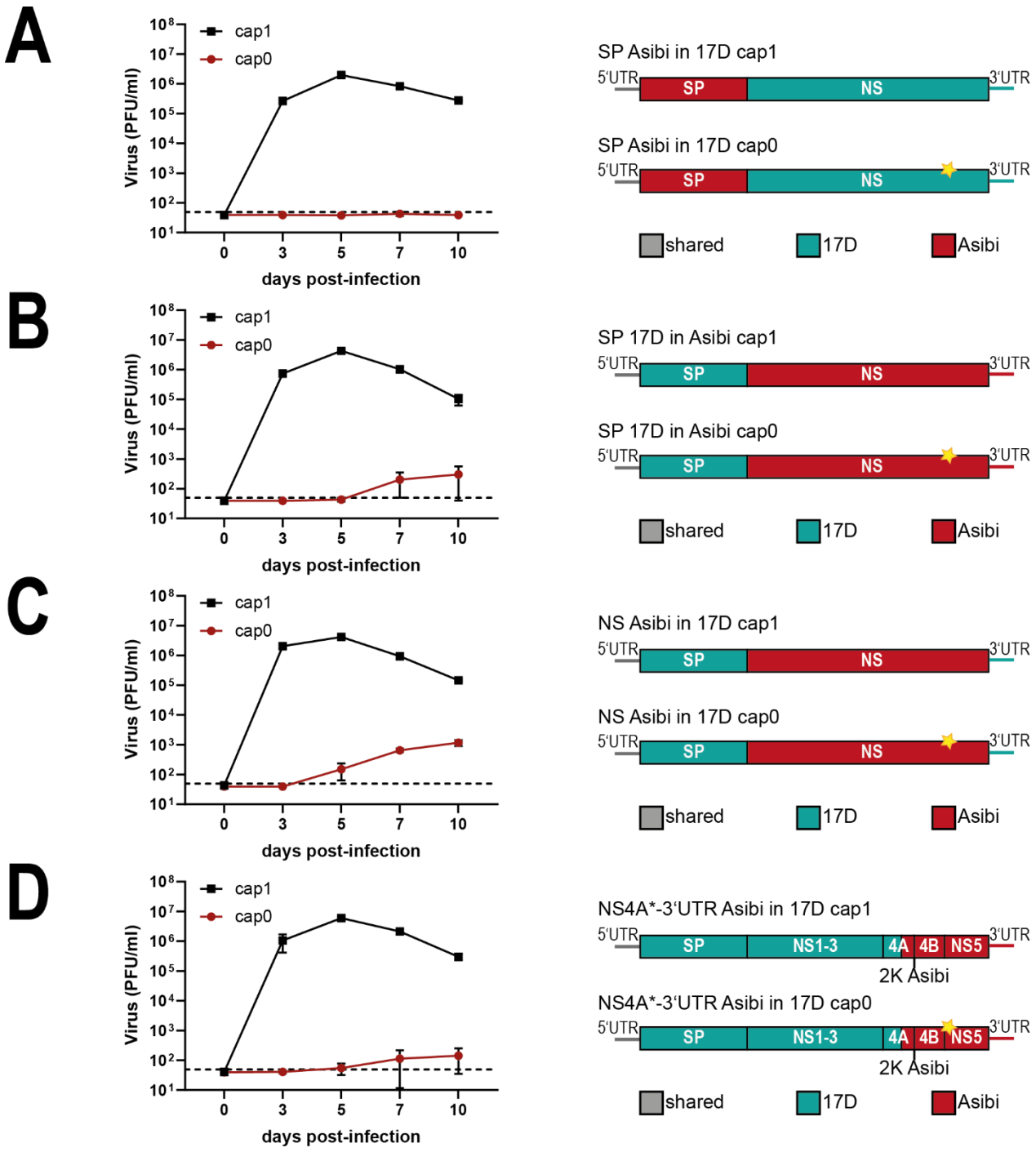

Figure 24: Growth kinetics of the chimeric viruses in C6/36 cells (left) and the corresponding schematic presentations (right).
The colors represent the sequence source (green: YFV-17D; red: YFV-Asibi), and shared sequences are those that do not differ between Asibi and 17D (grey). The yellow star represents the E218A exchange in the NS5 protein. A) Growth kinetics of SP Asibi in 17D cap1 and cap0 in C6/36 cells. B) Growth kinetics of SP 17D in Asibi cap1 and cap0 in C6/36 cells. C) Growth kinetics of NS Asibi in 17D cap1 and cap0 in C6/36 cells. D) Growth kinetics of NS4A*-3'UTR Asibi in 17D cap1 and cap0 in C6/36 cells. The cells were

infected in technical triplicates in one experiment (A-C) or in technical triplicates in two independent experiments (D) at an MOI of 0.01. Viral titers were measured at 0, 3, 5, 7, and 10 days post-infection by titration on BHK-21/J cells. Data represent Mean ± SD of at least triplicates. Dashed lines: detection limit.

Since the methyltransferase is encoded in the NS5 protein and the antiviral function of NS5 is well described in vertebrates, the NS5 protein of YFV-Asibi was next inserted into YFV-17D and vice versa (Figure 25A, B). After successfully rescuing the associated cap1 and cap0 chimeras, C6/36 cells were infected with the two chimera sets (MOI 0.01). Interestingly, the NS5 Asibi in 17D cap1 chimera showed a reduced replication speed at early time points compared to the NS5 17D in Asibi cap1 chimera (Figure 25A vs. Figure 25B). The peak titer of NS5 Asibi in 17D cap1 was reached at seven days post-infection with a titer of 2.8×10^6 PFU/ml. The corresponding cap0 chimera did not exceed the detection limit at any time point (Figure 25A). In contrast, the NS5 17D in Asibi cap1 chimera showed a steep increase in replication speed from day zero to day three post-infection (Figure 25B). After this time point, replication only marginally increased, reaching a peak titer of 2.8×10^6 PFU/ml on day five post-infection. The corresponding cap0 chimera (NS5 17D in Asibi cap0) exceeded the detection limit as early as day three post-infection, and replication increased continuously until day ten (1.2×10^3 PFU/ml). These results hint that NS5 was - at least not exclusively - responsible for the replication of the NS4A*-3'UTR Asibi in 17D cap0 chimera (Figure 24D).

The previous data indicate that the non-structural proteins NS4A* to NS5 of YFV-Asibi enabled the cap0 variant to replicate. However, the replication was not only promoted by the NS5 protein of Asibi. Due to this, the impact of NS4B on the level of the cap0 replication was investigated. Since 2K acts as a signal sequence for the translocation of NS4B into the ER lumen, 2K and NS4B were co-exchanged (Miller *et al.*, 2007). Thus, 2K-NS4B Asibi in 17D cap1 and cap0 chimeras were constructed (Figure 25C). Following the rescue of both viruses, C6/36 cells were infected with the chimeras (MOI 0.01). The cap1 chimera showed a steady increase in replication until day five post-infection (1.5×10^7 PFU/ml). At the same time, the corresponding cap0 chimera failed to exceed the detection limit, indicating that YFV-Asibi 2K and NS4B did not exclusively counteract the inhibition of cap0 replication.

In the next set of chimeras, 2K to NS5 from YFV-Asibi were introduced into the YFV-17D backbone (Figure 25D) or NS4A to NS5 (Figure 25E). Again, the corresponding cap1 and cap0 chimeras were established and successfully rescued. C6/36 cells were infected with the two chimera sets (MOI 0.01) to generate growth curves. While the 2K-NS5 Asibi in 17D cap1 chimera efficiently replicated in C6/36 cells, the corresponding cap0 chimera showed no replication at any time point (Figure 25D). By contrast, the NS4A-NS5 Asibi in 17D cap1 and cap0 chimera replicated in C6/36 cells (Figure 25E). The NS4A-NS5 cap1 chimera peaked with a titer of 5.5×10^6 PFU/ml as early as five days post-infection. The corresponding cap0 chimera exceeded the detection limit as early as day five post-infection and continuously increased until day ten post-infection (260 PFU/ml). Nevertheless, the overall replication of the NS4A-NS5 Asibi in 17D cap0 chimera was reduced compared to the parental YFV-Asibi cap0 (Figure 12A vs. Figure 25E). In summary, the data indicate that not a single protein was responsible for enabling the cap0 virus to replicate but rather a combination of several proteins.

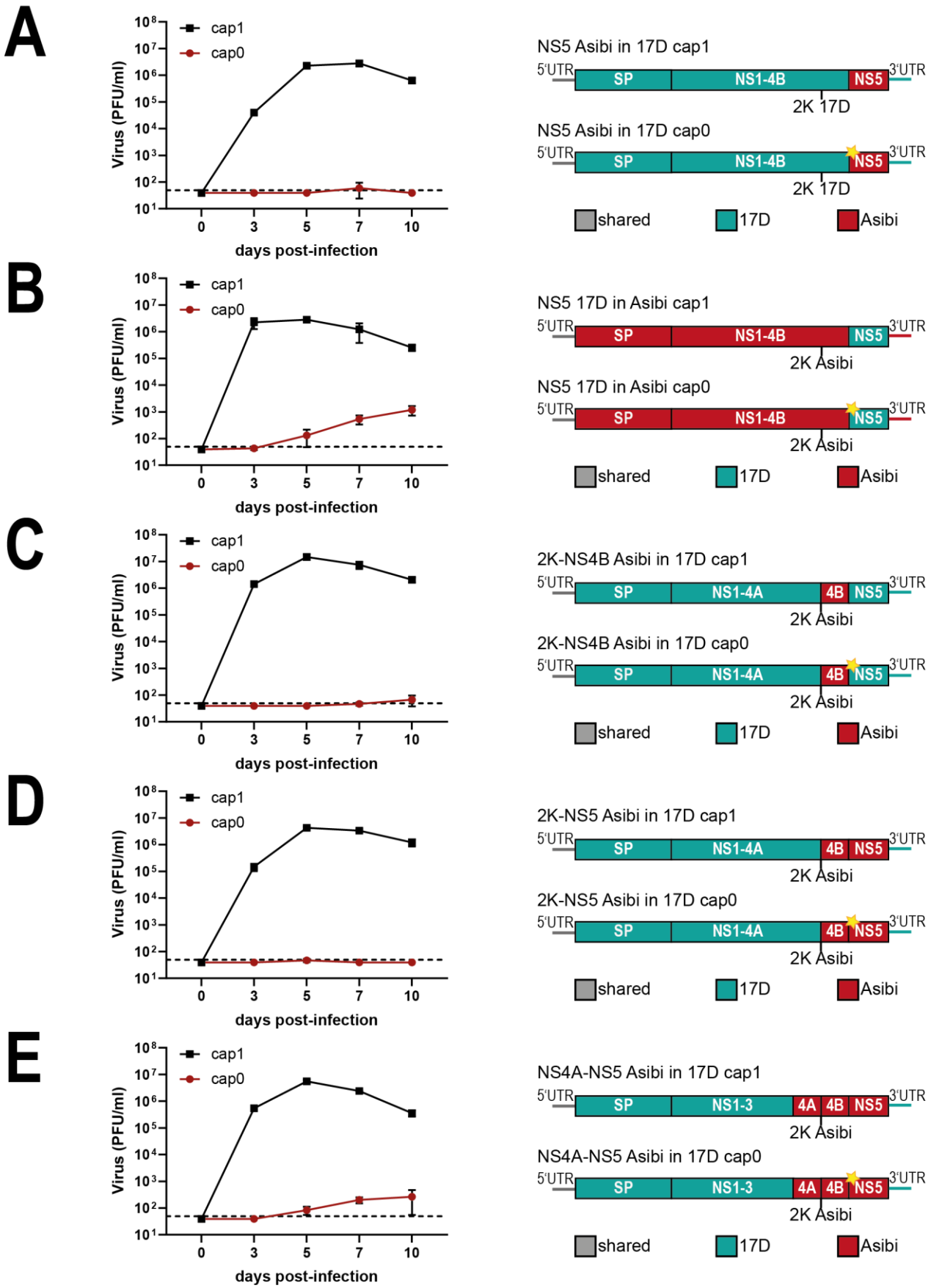
A
B
C
D
E
cap1
cap0
Virus (PFU/ml)
days post-infection
NS5 Asibi in 17D cap1
NS5 Asibi in 17D cap0
NS5 17D in Asibi cap1
NS5 17D in Asibi cap0
2K-NS4B Asibi in 17D cap1
2K-NS4B Asibi in 17D cap0
2K-NS5 Asibi in 17D cap1
2K-NS5 Asibi in 17D cap0
NS4A-NS5 Asibi in 17D cap1
NS4A-NS5 Asibi in 17D cap0
5'UTR
SP
NS1-4B
NS1-4A
NS1-3
4A
4B
NS5
3'UTR
2K 17D
2K Asibi
shared
17D
Asibi

Figure 25: Growth kinetics of the chimeric viruses in C6/36 cells (left) and the corresponding schematic presentations (right).
The colors represent the sequence source (green: YFV-17D; red: YFV-Asibi), and shared sequences are those that do not differ between Asibi and 17D (grey). The yellow star represents the E218A exchange in the NS5 protein. A) Growth kinetics of NS5 Asibi in 17D cap1 and cap0 in C6/36 cells. B) Growth kinetics of NS5 17D in Asibi cap1 and cap0 in C6/36 cells. C) Growth kinetics of 2K-NS4B Asibi in 17D cap1 and cap0 in C6/36 cells. D) Growth kinetics of 2K-NS5 Asibi in 17D cap1 and cap0 in C6/36 cells. E) Growth kinetics of NS4A-NS5 Asibi in 17D cap1 and cap0 in C6/36 cells. The cells were infected in technical triplicates in one experiment (A, C-E) or in technical triplicates in two independent experiments (B) at an MOI of 0.01. Viral titers were measured at 0, 3, 5, 7, and 10 days post-infection by titration on BHK-21/J cells. Data represent Mean ± SD of at least triplicates. Dashed lines: detection limit.

Interestingly, there was a tendency for the cap0 chimera to exceed the detection limit whenever the initial growth rate of the associated cap1 chimera was particularly high between day zero and day three post-infection (Figure 26A). To test whether a high initial growth rate was critical to allow the cap0 variant to replicate above the detection level, the replication of YFV-Asibi cap1, YFV-17D cap1, and DENV cap1 was examined at early time points in C6/36 cells (MOI 0.01) (Figure 26B). DENV was included in this experimental setup because the replication characteristics of the DENV cap0 variant was comparable to the corresponding cap1 variant in the insect cell line C6/36, suggesting that DENV also counteracts the cap0 recognition. No significant increase in viral replication was measured until 24 h post-infection, but the replication increased markedly from 24 h to 48 h for all viruses. While YFV-Asibi cap1 already reached a titer of 3.3×10^5 PFU/ml at 48 h post-infection, the replication of YFV-17D cap1 and DENV cap1 was reduced by at least 1 $\log_{10}$ (YFV-17D cap1: 9.1×10^3 PFU/ml, DENV cap1: 3.2×10^4 PFU/ml). Overall, YFV-Asibi cap1 exhibited the highest initial growth rate, but the initial replication of YFV-17D cap1 and DENV cap1 were comparable. This indicated that, at least for DENV, the initial growth rate was not essential for counteracting the cap0 recognition. However, a high initial growth rate might be important for YFV-Asibi to counteract the cap0 recognition.

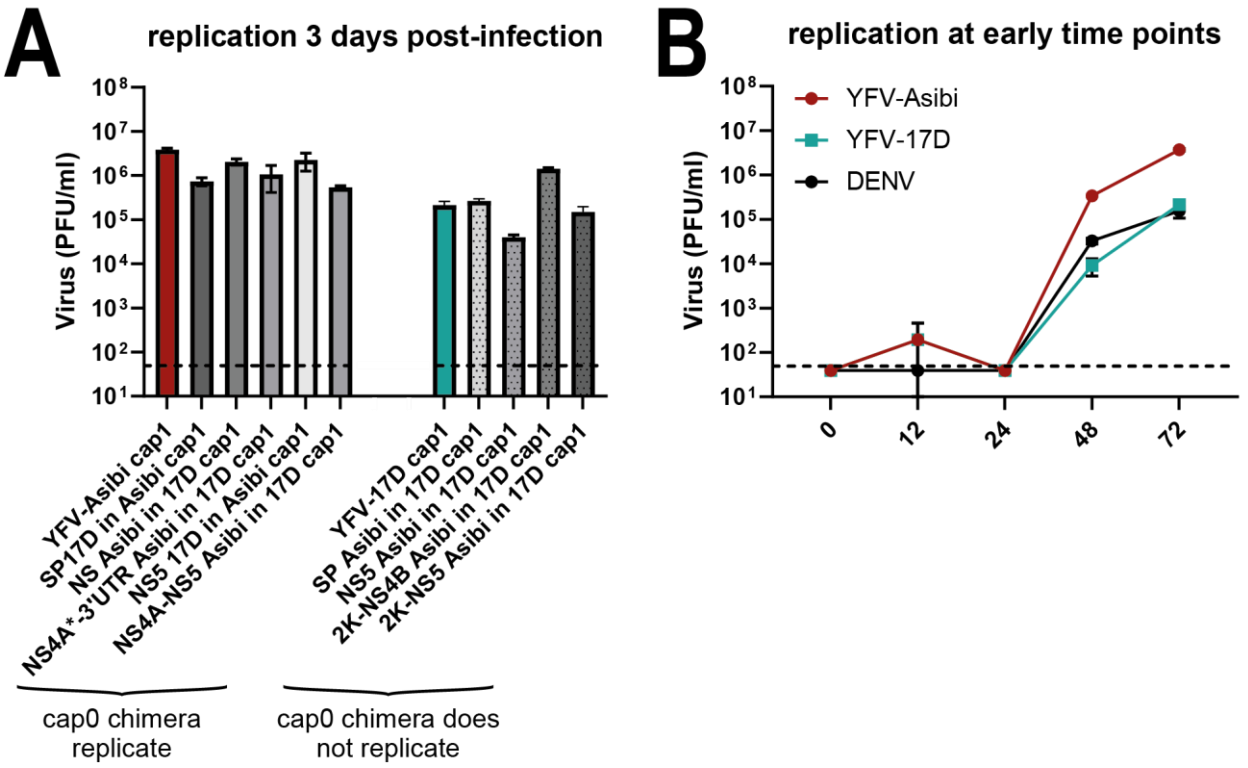

Figure 26: Chimera and wild-type virus replication at early time points.
A) Replication of the different YFV-Asibi/YFV-17D cap1 chimeras three days post-infection. The chimeras are grouped into clusters depending on the replication ability of the corresponding cap0 chimera. On the left are the cap1 chimeras where the cap0 chimera exceeded the detection limit, and on the right are the cap1 chimeras where the cap0 chimera did not exceed the detection limit. B) Replication of YFV-Asibi, YFV-17D, and DENV cap1 at early time points post-infection. C6/36 cells were infected at an MOI of 0.01. Viral titers were measured at 0, 12, 24, 48, and 72 hours post-infection by titration on BHK-21/J cells. Data represent Mean ± SD of at least triplicates. Dashed lines: detection limit.

3.8 DENV viral suppressor of RNAi

For invertebrate organisms, the RNAi pathway is believed to be one of the main components of the immune response against invading viruses. Viruses have evolved mechanisms to antagonize the RNAi pathway to circumvent the recognition of the invertebrate immune systems. One mechanism is that viruses encode VSRs, which inhibit the elimination of viral RNAs, leading to their accumulation. A recent study using three different insect RNA viruses (Culex Y virus, Drosophila X virus, and Drosophila C virus) showed that VSRs protect dsRNAs from Dcr-2 recognition by almost irreversibly binding with dsRNAs (Fareh *et al.*, 2018). Qiu and colleagues described that DENV NS2A has a VSR activity in mammalian and mosquito cells, and they could show that introducing a point mutation into the NS2A protein reduced the VSR activity (Qiu *et al.*, 2020). In the mutant virus, a lysine at position 135 of NS2A was replaced by an alanine. Comparative growth curve analysis revealed that DENV wild-type replicated to higher titers in the RNAi-competent Aag2 cells compared to DENV-NS2A-K135A, indicating suppression of the RNAi pathway (Qiu *et al.*, 2020). These data suggested that NS2A might functions as an antagonist of the antiviral immune response in mosquitoes. Hence, it was tempting to speculate that NS2A is also involved in promoting replication of DENV cap0.

To investigate whether DENV-NS2A is also involved in preventing recognition of DENV cap0 and whether the amino acid K135 plays a critical role in a potential antagonistic function, the NS2A-K135A mutation was introduced into the infectious cDNA clone pD2/IC-30P-A using site-directed mutagenesis through fusion PCR technology (2.2.3.2) (Figure 27A). The resulting fragment carrying the AAA to GCG exchange was cut with the restriction enzymes SphI plus EagI and was ligated into the pD2/IC-30P-A backbone, previously cut with the same enzymes. The newly generated plasmid was named DENV-NS2A-K135A cap1. In order to establish the cap0 variant harboring both the NS2A-K135A and the NS5-E218A mutation, DENV-NS2A-K135A cap1 was again cut with the enzymes SphI plus EagI. This fragment was ligated into the DENV cap0 backbone (described in 3.6.2) cut with the same pair of enzymes. The resulting virus was named DENV-NS2A-K135A cap0. A schematic illustration of the construct can be found in the appendix (10.2). In order to perform comparable growth curve analyses, DENV cap1, DENV cap0, DENV-NS2A-K135A cap1, and DENV-NS2A-K135A cap0 were rescued in parallel. Therefore, the plasmids were linearized with XbaI, precipitated, and *in vitro* transcribed. The RNA

was electroporated into BHK-21/J cells for virus propagation. The virus (P0 virus) was harvested three days post-infection, and viral titers were determined via $TCID_{50}$ in Vero B4 cells, as the DENV-NS2A-K135A cap0 mutant showed no cytopathic effect in Vero B4 cells. Due to the low titers after electroporation, the P0 virus was passaged once in Vero B4 cells by infecting them at a low MOI (0.001) for seven days. The resulting P1 viral titers were again determined via $TCID_{50}$ in Vero B4 and used for all subsequent experiments.

C6/36 cells were infected with the four different DENV viruses at an MOI of 0.001 to perform growth curve kinetics over ten days. Due to the non-cytopathic effect of DENV-NS2A-K135A cap0, the growth curve was analyzed via RT-qPCR. All four viruses rapidly replicated from day 0 post-infection and peaked ten days post-infection (Figure 27B). The replication of DENV-NS2A-K135A cap1 was comparable throughout the experiment to the replication of DENV cap1. Contrary to expectations, DENV cap0 replicated to slightly lower titers in this experimental setup as DENV cap1 but comparable to DENV-NS2A-K135A cap0. At day ten post-infection, the peak titers for DENV cap1 and DENV cap0 were 5×10^7 copies/ml and 1×10^7 copies/ml, respectively. The peak titers of DENV-NS2A-K135A cap1 and cap0 at this time point were 3×10^7 copies/ml and 2×10^7 copies/ml, respectively. As DENV cap0 and DENV-NS2A-K135A cap0 replicated comparable throughout the experiment, this data indicates that the VSR activity of NS2A did not promote replication of DENV cap0.

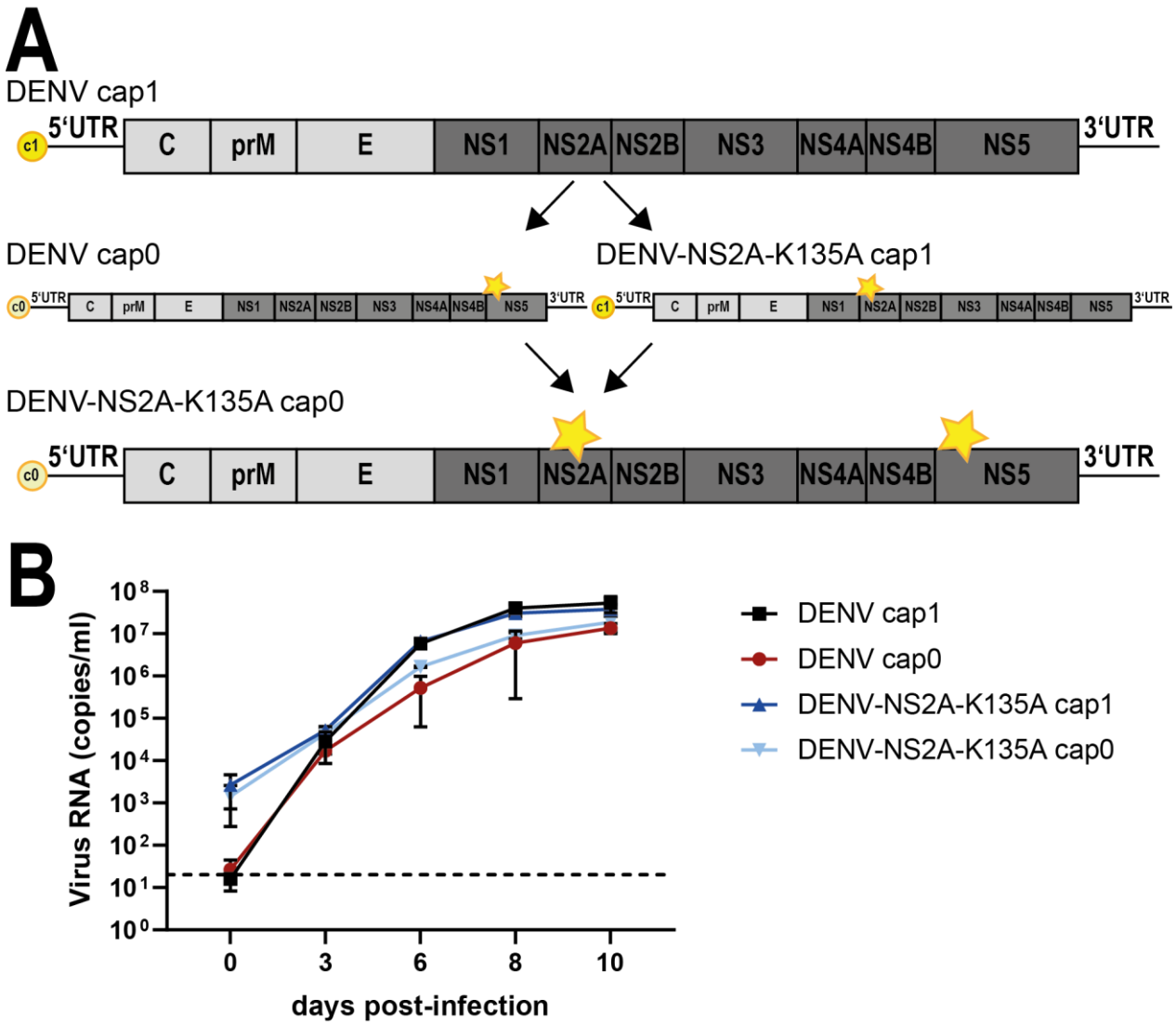

Figure 27: Characterization of DENV-NS2A-K135A cap1 and cap0.
A) Schematic presentation of DENV-NS2A-K135A cap1 and cap0. B) Growth kinetics of DENV cap1, cap0, DENV-NS2A-K135A cap1, and DENV-NS2A-K135A cap0 in C6/36 cells. The cells were infected at an MOI of 0.001. Viral titers were measured at 0, 3, 6, 8, and 10 days post-infection by RT-qPCR. Data represent Mean ± SD of triplicates. Dashed line: detection limit.

4. Discussion

4.1 YFV-17D cap0 replication is reduced to different extents in mosquito cells

Orthoflaviviruses transmitted between mosquitoes and vertebrates must be able to replicate efficiently in both organisms. The orthoflaviviral replication efficiency primarily relies on their ability to suppress the host immune system. Various mechanisms on how orthoflaviviruses suppress the vertebrate immune system are known, but relatively little is known about their interaction with the mosquito immune system. One crucial mechanism orthoflaviviruses use to escape the vertebrate immune system is the 2'-O cap methylation of their RNA (Wu *et al.*, 2022). Since orthoflavivirus replication occurs in the cytosol, but the vertebrate capping machinery is localized in the nucleus, orthoflaviviruses encode their own viral methyltransferase in the NS5 protein. The amino acids K-D-K-E form the active site of the 2'-O-MTase (Egloff *et al.*, 2002). Previous studies using WNV demonstrated that all four amino acids from the tetrad are relevant for the 2'-O-MTase activity, but only the amino acid D146 for N-7-MTase activity (Ray *et al.*, 2006; Zhou *et al.*, 2007).

Previously, an intact YFV-17D 2'-O-MTase was shown to be crucial for RIG-I escape. Mutation of E218 to A in the NS5 protein of YFV-17D abolished the 2'-O-methylation of the viral RNA (cap0 formation) and restricted viral immune escape in a type I interferon-dependent manner (Schuberth-Wagner *et al.*, 2015). Since not only vertebrate cellular mRNAs carry a 5' cap structure, but all higher eukaryotes do, and because RIG-I has a DExD/H-box helicase domain just like Dcr-2, it was tempting to speculate that YFV-17D also escapes the invertebrate immune system by capping its viral RNA.

This thesis successfully confirmed that the replication of YFV-17D cap0 was reduced in vertebrate cells such as A549 and further showed that the replication of YFV-17D cap0 was also reduced in various mosquito cells. Testing four mosquito cell lines, two *Aedes aegypti*-derived (Aag2, CCL-125) and two *Aedes albopictus*-derived cell lines (C6/36, U4.4), revealed that replication of YFV-17D cap0 was reduced in all tested mosquito cell lines, but to different degrees (Figure 9). The Aag2 cell line, in contrast to C6/36 cells, produces all three types of small RNAs (siRNA, piRNA, miRNA) and is therefore considered immunocompetent (Miesen, Ivens, *et al.*, 2016). C6/36 cells contain a frameshift mutation in the Dcr-2 gene, resulting in a premature stop codon. Thus, C6/36

Dcr-2 only expresses the DExD/H-box domain and DUF, and the cells cannot produce siRNAs (Morazzani *et al.*, 2012). The cells are considered to be immunodeficient. However, replication of YFV-17D cap0 was less reduced in Aag2 cells than in C6/36 cells. These data provide preliminary evidence that the reduced replication of YFV-17D cap0 might occur independently of Dcr-2 and the siRNA pathway. This hypothesis was confirmed through comparative growth curve analyses of YFV-17D cap1 and cap0 in Aag2 Dcr-2 k.o. cells and in the parental cell line. Since the loss of Dcr-2 neither promoted nor inhibited replication of YFV-17D cap0, the differentiation of YFV-17D cap1 and cap0 is most likely independent from Dcr-2. Interestingly, the loss of Dcr-2 also did not promote the replication of YFV-17D cap1. An increased YFV-17D cap1 replication was expected since previous studies observed enhanced ZIKV and Semliki Forest Virus (SFV) replication in Dcr-2 k.o. cells (Varjak, Donald, *et al.*, 2017; Varjak, Maringer, *et al.*, 2017).

Even though C6/36 cells do not produce siRNAs, they can still produce 21 nt small RNAs with a preference for U1 and A10 characteristics after infection with alphaviruses (Morazzani *et al.*, 2012; Gestuveo *et al.*, 2022). Thus, a distinct antiviral immune response could also be induced by a different immune pathway, leading to reduced replication of YFV-17D cap0.

4.2 Recognition of YFV-Asibi cap0 *in vivo*

The previously obtained data revealed that insect cells distinguish between YFV-17D cap1 and cap0 RNA. Thus, it was aimed to study whether such differentiation also occurred *in vivo*. Many publications reported that YFV-17D could establish an infection in the mosquito midgut but did not disseminate (Whitman, 1939; Miller *et al.*, 1988; Danet *et al.*, 2019). Presumably, the restriction of YFV-17D replication already occurs in the epithelial cells of the midgut and prevents the virus from replicating in secondary organs like the salivary glands (Danet *et al.*, 2019). Viral transmission can only occur when the virus efficiently replicates in the salivary gland and saliva. Due to these difficulties, this thesis aimed to establish an infectious cDNA clone of the YFV wild-type Asibi to study viral replication *in vivo*.

On the contrary, it has been shown that YFV-Asibi successfully replicates in mosquitoes and also passes to secondary organs (Lorenz *et al.*, 1984; Hahn, Dalrymple, *et al.*, 1987; Miller *et al.*, 1988). However, the susceptibility of *Aedes aegypti* mosquitoes to the

infection with YFV-Asibi was highly dependent on the origin of the mosquitoes used (Tabachnick *et al.*, 1985). In addition to successfully infecting *Aedes aegypti* with YFV-Asibi isolates, McElroy and colleagues demonstrated that their infectious YFV-Asibi clone replicated and disseminated as efficiently as the parental YFV-Asibi virus 14 days post oral infection of *Aedes aegypti* (McElroy *et al.*, 2005). Based on this data, an infectious cDNA clone for YFV-Asibi was successfully established in this thesis. The “original” YFV-Asibi strain is unavailable today, and no sequence exists (Davis *et al.*, 2021). Most YFV-Asibi studies are based on the sequence reported by Hahn *et al*., but this strain was passaged at least 45 times in monkeys prior to sequencing (Hahn, Dalrymple, *et al.*, 1987; Davis *et al.*, 2021). Depending on the laboratory and the number of passages, the currently available sequences of YFV-Asibi clones differ to varying degrees, resulting in no unique YFV-Asibi sequence. The Asibi sequences differ in their nucleotide and amino acid levels (Davis *et al.*, 2021). For example, the YFV-Asibi clone used in this thesis differed in two amino acids compared to the YFV-Asibi-Yale clone (GenBank accession number: MT956628).

The sequence of the YFV-Asibi strain described by Hahn *et al*. was used as a reference for the infectious YFV-Asibi clone established in this thesis (Hahn, Dalrymple, *et al.*, 1987). In a first attempt, several nucleotides of the plasmid pPseAsibi were exchanged via site-directed mutagenesis through fusion PCR technology to result in a sequence identical to the Asibi sequence described by Hahn and colleagues. No virus could be rescued from the infectious clone (data not shown). Therefore, the exchanges at nucleotide positions 2142 and 7319 were reversed. Viruses rescued from this new YFV-Asibi plasmid formed infectious particles and showed plaques in the infectious center assay (Figure 10C). After the successful rescue of YFV-Asibi, infection experiments were performed to test whether the established virus showed similar behavior to YFV-Asibi in the literature. In the infectious center assay, the virus exhibited homogenous plaque morphology, with the plaques of YFV-Asibi having a smaller diameter than YFV-17D (Figure S 1). In line with these findings, other groups reported the plaque diameters of YFV-Asibi as mainly small when the virus was not passaged (Miller *et al.*, 1988; McElroy *et al.*, 2006b). The homogenous plaque sizes vanished after the first passage of YFV-Asibi, and the virus population exhibited a mixture of small and large plaque morphologies (Barrett *et al.*,

1990). Likewise, passaging YFV-Asibi established in this thesis resulted in a heterogeneous plaque morphology with large and small plaques (data not shown).

No significant difference in replication was observed between YFV-Asibi and YFV-17D three days post-infection in vertebrate cells (Figure 10D). However, cells infected with YFV-17D showed an extensive cytopathic effect at this point, which may indicate that the two viruses replicated differently early during infection. Other studies also observed higher replication titers of YFV-17D (Fernandez-Garcia *et al.*, 2016; Collins *et al.*, 2018). Higher replication of YFV-17D might correlate with the different entry mechanisms of the two viruses. While YFV-Asibi infects host cells exclusively by clathrin-dependent endocytosis, YFV-17D uses a clathrin-independent mechanism (Fernandez-Garcia *et al.*, 2016). In contrast to the described higher replication of YFV-17D in vertebrate cells, YFV-Asibi replicated to higher titers in insect cells.

Even though YFV is a constant threat to the human population, the number of studies using an infectious YFV-Asibi clone to infect *Aedes aegypti* mosquitoes is very limited. This thesis demonstrated that virus derived from the established YFV-Asibi cDNA clone successfully infected the *Aedes aegypti* Liverpool strain. This strain was chosen for infection experiments because it has previously been shown to be susceptible to intrathoracic infection with YFV (Samuel *et al.*, 2016). YFV-Asibi cap1 displayed a distinct eclipse phase characterized by decreased viral titers in the carcass between days one and three following oral infection. The virus production phase followed the eclipse phase, in which the viral titers steadily increased. In line with these findings, McElroy and colleagues previously described a similar replication pattern for their established YFV-Asibi infectious clone (McElroy *et al.*, 2006b; Danet *et al.*, 2019).

Similar to the high infection rates, YFV-Asibi cap1 efficiently disseminated in secondary organs, leading to high dissemination rates. Initially, viral RNA was only detectable in single legs plus wings, but viral titers increased significantly over time, reaching a dissemination rate of 86% (Table 31). In line with these findings, McElroy and colleagues extracted and analyzed salivary glands of YFV-Asibi-infected mosquitoes, revealing a dissemination rate of 83% (McElroy *et al.*, 2005). Despite the high infection and dissemination rates, only a low transmission rate and efficiency could be detected in this thesis (Table 31). Viral RNA was only detectable in the saliva of individual mosquitoes. In

order to be transmitted, the virus needs to bypass the salivary gland infection barrier and needs to replicate in the saliva. From the data presented in this thesis, it was not possible to differentiate whether YFV-Asibi cap1 was unable to infect the salivary glands or whether it was unable to escape from the salivary gland infection barrier. However, since secondary organs such as legs plus wings were successfully infected, as reflected by a high dissemination rate, it is more likely that YFV-Asibi cap1 can infect the salivary glands but fails to overcome the salivary gland escape barrier.

The susceptibility of mosquitoes to viral infection highly depends on the mosquito's origin. In particular, Caribbean populations, Central-South American, and East African populations are more susceptible to infection with YFV-Asibi than West African sylvatic populations (Tabachnick *et al.*, 1985). The origin of the *Aedes aegypti* strain Liverpool used in this thesis is unknown. Initially, the strain was thought to be first held in a laboratory between 1935 and 1938 and originated from West Africa, Sierra Leone (Kuno, 2010). A recent study examined single nucleotide polymorphisms (SNPs) to investigate the differences and similarities between laboratory colonies. The authors discovered that the genetic diversity in laboratory colonies was significantly lower than in field populations, that colonies with the same names may be highly divergent, and that the genetic composition of the Liverpool strain suggests an Asian rather than a West African origin (Gloria-Soria *et al.*, 2019). Already in 1984, Lorenz *et al*. suggested that colonization of mosquito strains had an impact on genetic and phenotypic variance, altering the susceptibility of *Aedes aegypti* to YFV infection (Lorenz *et al.*, 1984). These genetic divergences may be one reason YFV-Asibi cap1 achieved a high infection and dissemination rate but only a low transmission rate of 8%.

Compared to the high infection and dissemination rate of YFV-Asibi cap1, YFV-Asibi cap0 failed to establish a successful infection in *Aedes aegypti* in the carcass. Following the expected eclipse phase (days 1-3), the amount of viral RNA did not increase but continued to decrease. The infection rates varied around 20%, and the virus was solely able to escape the midgut infection barrier in single mosquitoes to replicate in secondary tissues. Two different hypotheses might explain the inability of the YFV-Asibi cap0 virus to establish efficient infections *in vivo* following oral infection: I) The virus was replication-incompetent due to the defective methyltransferase, leading to almost no replication *in*

vivo. II) An unknown receptor or transcription factor discriminated between cap1 and cap0 viruses, thereby down-regulating cap0 virus replication and restricting replication to the midgut. To test those hypotheses, mosquitoes were intrathoracically infected with the cap1 and cap0 viruses. This data revealed that the median replication of YFV-Asibi cap0 increased between day zero and seven post-infection when circumventing the midgut barrier but to a lower extent than the replication of YFV-Asibi cap1. Nevertheless, the replication of YFV-Asibi cap0 distinctly increased, ruling out replication incompetence and confirming hypothesis II. Mosquitoes might express a potential receptor or gene in the midgut or midgut escape barrier, differentiating between cap1 and cap0 viral. To further characterize this receptor or gene, transcriptomic analysis after YFV-Asibi cap1 and cap0 infection might be useful. A previous study identified specific up-and down-regulated genes upon infection with several orthoflaviviruses (Colpitts *et al.*, 2011). Comparing the transcriptome data of YFV-Asibi cap1 with the ones of cap0 might help to discern specific up- and down-regulations.

Earlier reports demonstrated a critical role of ROS in limiting DENV infection. One study observed a *Wolbachia*-induced upregulation of ROS, resulting in the activation of the Toll pathway and the expression of AMPs. The AMPs, in turn, downregulated DENV infection (Pan *et al.*, 2012). Another study also observed an upregulation of ROS in C6/36 cells upon infection with DENV (Santana-Román *et al.*, 2021). Interestingly, the ROS system is not only important *in vitro* but also *in vivo*. Inhibition of ROS activity by vitamin C resulted in a higher susceptibility of mosquitoes to DENV, while activation of ROS by uracil led to reduced susceptibility (Liu *et al.*, 2016). While some interactions between DENV and ROS are already described, there is little information on whether and how ROS and YFV interact. It might be possible that YFV cap0 led to increased ROS induction in mosquitoes, resulting in attenuated infection rates *in vivo*. Additionally, one *Wolbachia* strain was described to limit YFV replication *in vivo*, but in this study, the role of ROS was not investigated (van den Hurk *et al.*, 2012). Therefore, future experiments should include the potential role of ROS on YFV cap1 and cap0 replication *in vivo*.

4.3 Effect of cap0 priming on the replication of YFV cap1 virus

Like in vertebrates and *Drosophila*, the JAK/STAT pathway is also conserved in mosquitoes (Tikhe *et al.*, 2021). While various secretory cytokines and growth factors lead

to the activation of the JAK/STAT pathway in vertebrates, little is known about activating cytokines in insects. In *D. melanogaster*, Upd cytokines were identified as ligands for the JAK/STAT pathway, but homologs have not been found in mosquitoes (Harrison *et al.*, 1998). So far, only the antiviral factor Vago was described for mosquitoes, which was produced in a Dcr-2-dependent manner in *Culex* cells after WNV infection. Secreted Vago activated the JAK/STAT pathway and led to JAK/STAT-dependent reduction of viral infection (Paradkar *et al.*, 2012, 2014). However, the primary activator of the JAK/STAT pathway in vertebrates is interferon, for which no orthologues are known in insects (Cheng *et al.*, 2009, 2016).

Priming experiments were, on the one hand, performed to test whether insect cells can secrete antiviral factors, similar to type I interferons, into the cell culture supernatant. On the other hand, it was aimed to investigate whether the cap0 virus leads to a higher production of antiviral factors than the cap1 virus because replication of the YFV-17D cap0 virus was more strongly reduced than the replication of the cap1 virus. Therefore, immune priming experiments were performed in C6/36 cells. Immune priming was previously successfully reported in various *in vitro* and *in vivo* studies. In *in vivo* experiments, immune priming is defined as an antiviral immune response in which insects can survive a potentially lethal infection after treatment with a sublethal dose of a pathogen (Sheehan *et al.*, 2020). No such clear definition exists for *in vitro* experiments.

A previous study reported an inhibitory low-molecular-weight peptide produced by mosquito cells persistently infected with SINV. This peptide was transferrable to new cells and reduced SINV replication in these cells upon infection. However, the replication reduction was time-dependent (only after 48 h) and virus-specific (Riedel *et al.*, 1979). C6/36 cells persistently infected with DENV also produced peptides that were transferrable to new cells and protected them from infection with DENV (Sheehan *et al.*, 2020).

In this thesis, C6/36 cells were first infected with YF-VRP cap1 and cap0 to trigger an antiviral immune response without generating progeny virus. The virus-free supernatants with potentially secreted antiviral factors were then added to fresh cells for 24 h to initiate an immune response. Subsequently, the primed cells were infected with YFV-17D cap1 to test whether the potential priming led to reduced viral replication. Contrary to

expectations, the data provided in this thesis showed that replication of YFV-17D cap1 was not reduced upon YF-VRP cap1 or cap0 priming, suggesting no transferable antiviral factors were produced (Figure 14C). A possible explanation for the unchanged replication upon priming might be that an infection period of 24 hours was not long enough to produce an efficient amount of antiviral factors, as Riedel and Brown describe the production of a potentially antiviral peptide after persistent viral infection (Riedel *et al.*, 1979). Apparently, insect cells require a persistent infection with orthoflaviviruses or alphaviruses to secrete transferrable antiviral peptides.

Previously published data showed a priming effect in cell culture and *in vivo* with orthoflaviviruses. *Aedes aegypti* mosquitoes orally primed with inactivated DENV showed a lower viral load when infected a second time with active DENV (Serrato-Salas *et al.*, 2018). The small seven-day interval between priming and infection was essential in this study. Mosquitoes have an effective innate immune defense but no adaptive immune defense. Due to the missing adaptive immune response, it was assumed that immune priming was only effective for short periods (Serrato-Salas *et al.*, 2018). However, in a more recent study, 3rd instar larvae were treated with inactivated DENV and infected with active DENV at the adult stage. Following oral infection, mosquitoes primed in the larval stage exhibited lower viral replication than non-primed larvae. In addition, the relative expression of the immune markers Dcr-2 and Ago2 was significantly increased in DENV-primed and infected mosquitoes (Vargas *et al.*, 2020). This study demonstrated that *in vivo* immune priming increased the antiviral immune response for an extended period and that priming was maintained across different developmental stages.

The *in vivo* data of Vargas *et al*. indicate that the observed immune priming was dependent on the siRNA pathway because essential genes of this pathway were significantly upregulated (Vargas *et al.*, 2020). Due to its truncated Dcr-2 gene, C6/36 cells are considered immunodeficient and exhibit a dysfunctional siRNA pathway (Morazzani *et al.*, 2012). Secretory factors may be produced more rapidly in mosquito cells when the siRNA pathway is functional. Thus, the experimental outcome might have been different if another cell line would have been used. Eventually, the experiments should be repeated in two ways: I) Persistent infection with YFV cap1 and cap0 should be performed to test whether antiviral factor production requires a longer time. II) Repetition of the priming

experiment with immunocompetent Aag2 cells to test whether mosquito cells need a functional siRNA pathway to produce antiviral factors.

In another study, *Culex quincefacius* mosquitoes were treated intrathoracically with inactivated WNV before they were orally infected with WNV seven days after injection. The number of mosquitoes with detectable WNV in the saliva was significantly reduced in previously primed mosquitoes compared to mock-primed mosquitoes. Subsequent RNA sequencing showed that priming increased the expression of various effectors, such as antimicrobial peptides. In addition, the hypothetical protein CPIJ005651, an orthologue of the *D. melanogaster* cap-binding protein 80, was upregulated in primed WNV-infected mosquitoes (Blagrove *et al.*, 2021). These data might suggest that the priming of mosquitoes is related to the cap structure of orthoflaviviral RNA.

In this thesis, the identical priming experiment was also performed in vertebrate cells (data not shown). Briefly, immunocompetent A549 cells were either YF-VRP cap1, cap0, or mock primed for 24 h. Subsequently, the virus-free supernatants were transferred to new A549 for 24 h before the cells were infected with YFV-17D cap1. The replication of YFV-17D cap1 was measured 48 h after infection. It was expected that YFV-17D cap1 replication would be significantly reduced in cells primed with cap0 RNA due to the more robust immune response elicited by cap0 RNA (Schuberth-Wagner *et al.*, 2015). However, replication of YFV-17D cap1 was reduced to a greater extent in the cap1 primed cells than in the cap0 primed cells. The presented data indicate that priming in vertebrates is a complex process. Supernatants containing antiviral factors should be collected earlier in vertebrates as the secretion of these factors may peak earlier than the secretion of antiviral factors secreted by mosquito cells. In the study conducted by Schuberth-Wagner *et al*., high amounts of antiviral factors were measured as early as 8 h after infection (Schuberth-Wagner *et al.*, 2015).

Besides the priming experiments, superinfections were performed. In these experiments, C6/36 cells were first infected with the VRPs and 24 h later with the full-length YFV-17D cap1 virus. Again, replication of the second virus was not significantly reduced (Figure 14D). Replication of YFV-17D cap1 was only slightly reduced when cells were previously infected with YF-VRP cap1 but not when cells were first infected with YF-VRP cap0. In conclusion, it was impossible to differentiate whether the reduced replication of YFV-17D

cap1 was due to an antiviral immune response or superinfection exclusion. The latter describes a phenomenon in which infection with a second (closely related) pathogen is reduced due to the first infection interfering with infection of the second virus (Tscherne *et al.*, 2007; Glover *et al.*, 2020). This phenomenon was described between DENV and YFV in C6/36 cells, suggesting that two YFV infections might be mutually exclusive (Abrao *et al.*, 2016). With this data, it could not be excluded that cells can generate an antiviral immune response against a second infection, even with a truncated Dcr-2 gene.

Since the previous data could not exclude an involvement of Dcr-2 in the reduction of a second infection, superinfection experiments were also performed in Aag2 wild-type and Dcr-2 k.o. cells. Thus, a direct comparison between cells with a functional and a dysfunctional siRNA pathway was possible. Again, cells first infected with the cap1 virus restricted replication of the second virus more strongly. These data suggest that Dcr-2 is not relevant for reducing a secondary infection and indicate that a functional Piwi pathway is sufficient. In line with these findings, Léger *et al*. demonstrated that the vpiRNAs produced by Rift Valley Fever virus infected C6/36 cells were sufficient to establish an antiviral immune response against a superinfecting virus (Léger *et al.*, 2013). The question of why YFV-Asibi cap1 leads to a more robust reduction of the secondary virus than YFV-Asibi cap0 remains unanswered. One possible explanation might be that the low replication of YFV-Asibi cap0 leads to a reduced immune response compared to YFV-Asibi cap1. In order to further answer this question, the expression of antiviral factors should be measured over time to receive a deeper insight into the antiviral immune response against YFV cap1 and cap0 viruses in insects. With an optimized priming time, it might be possible that cap0 viruses elicit a more robust immune response than cap1 viruses and thus inhibit the replication of a secondary virus more strongly.

4.4 Activation of immune pathways upon YFV cap0 viral infection

While the collected data in this thesis indicate that Dcr-2 was not relevant for the reduced replication of a superinfected orthoflavivirus, it has yet not been tested whether Dcr-2 had a crucial role in discriminating YFV-Asibi cap1 and cap0. By performing parallel infection experiments with YFV-Asibi cap1 and cap0 in Aag2 wild-type and Dcr-2 k.o. cells, it was possible to show that Dcr-2 had no crucial role in differentiating YFV-Asibi cap1 and cap0 (Figure 17). Replication of YFV-Asibi cap0 was slightly reduced in the Dcr-2 k.o. compared

to the wild-type cells. However, if Dcr-2 would be relevant for the differentiation of YFV-Asibi cap1 and cap0, replication of the cap0 virus should have been increased. Interestingly, a recent study demonstrated that YFV-Asibi replicated to higher titers in *Dcr-2* null mutant compared to wild-type sibling *Aedes aegypti*, which was in contrast to the observed *in vitro* data in this study (Samuel *et al.*, 2023). Thus, it would be of great interest to elucidate whether YFV-Asibi cap0 replicates differently in *Dcr-2* null mutant mosquitoes.

The assumption that Dcr-2 is not relevant for distinguishing YFV cap1 and cap0 RNA was supported by the fact that YFV-17D cap0 and YFV-Asibi cap0 showed no or reduced replication in C6/36 cells, respectively. As mentioned earlier, the piRNA pathway was repeatedly described as an essential component of antiviral immune defense in mosquitoes (Morazzani *et al.*, 2012; Schnettler *et al.*, 2013; Varjak, Maringer, *et al.*, 2017). Since C6/36 cells have a functional piRNA pathway, this pathway might be involved in the cap1/cap0 discrimination (Morazzani *et al.*, 2012; Gestuveo *et al.*, 2022).

Other critical antiviral pathways that may play a role in the differentiation between YFV-Asibi cap1 and cap0 were investigated by establishing an antiviral panel. Activation of the siRNA pathway was examined by measuring the expression of Ago2, which acts downstream of Dcr-2. Ago2 is an RNA endonuclease that cleaves dsRNA molecules produced by Dcr-2 (Matranga *et al.*, 2005). In YFV-Asibi cap1 and cap0 infected cells, Ago2 was upregulated, but this difference was insignificant (Figure 18A). Previous experiments showed increased alpha-and bunyaviruses replication but no increased ZIKV replication upon gene silencing of Ago2 (Scherer *et al.*, 2021). These data indicate that Ago2 is not effective against ZIKV. In contrast, Ago2 knockdown led to increased DENV replication (Scott *et al.*, 2010). Whether the unaltered replication of ZIKV in Ago2 k.o. cells was a specific effect only for ZIKV or whether Ago2 is not antiviral against other orthoflaviviruses except DENV remains open.

Activated Toll recruits adaptor proteins, including MyD88, which leads to a down signaling cascade, resulting in the expression of AMPs (Russell *et al.*, 2020; Tikhe *et al.*, 2021). Ramirez and colleagues silenced MyD88 in *Aedes aegypti*, which resulted in increased DENV virus particles upon infection (Ramirez *et al.*, 2010). In this thesis, MyD88 expression was also minimally increased after viral infection with YFV-Asibi cap1 and

cap0. Since this difference was not significant, it was assumed that the Toll pathway was not involved in cap1 and cap0 RNA discrimination.

In contrast, vir-1 expression was significantly downregulated after infection with YFV-Asibi cap0 compared to uninfected cells. Vir-1 is a gene produced in a JAK/STAT-dependent manner (Dostert *et al.*, 2005; Almire *et al.*, 2021). YFV-Asibi cap0 may inhibit the production of genes downstream of JAK/STAT more strongly than YFV-17D cap0, allowing replication of YFV-Asibi cap0 in C6/36 cells.

Dcr-1, like Dcr-2, is an RNase III-like enzyme that plays a central role in miRNA signaling (Donald *et al.*, 2012; Blair *et al.*, 2015). In cap1 and cap0 infected cells, the expression of Dcr-1 was downregulated, whereby an association between the miRNA pathway and the discrimination between YFV-Asibi cap1 and cap0 was unlikely.

The data indicate that YFV cap1 and cap0 RNA discrimination is probably not related to the siRNA pathway but to the piRNA pathway. A possible role of the JAK/STAT pathway cannot be excluded. Small RNA sequencing should be performed in future experiments to gain further insight into which pathways might be relevant for differentiation. Since all RNAi pathways generate RNA molecules of different lengths, this can help to determine which pathways are activated by YFV cap1 or cap0 (Scott *et al.*, 2010; Hess *et al.*, 2011; Scherer *et al.*, 2021).

4.5 Recognition of different cap0 orthoflaviviruses

The infection experiments performed in this thesis illustrate the existence of an innate 5’ RNA-modification recognizing effector protein in mosquito cells and *in vivo*. Since the methyltransferase is highly conserved among YFV strains and all other orthoflaviviruses, cap0 mutants were established for additional orthoflaviviruses and studied in infection experiments. The active site, consisting of amino acids K-D-K-E, can also be found in WNV, DENV, and ZIKV (Züst *et al.*, 2013). In previous studies, glutamine at position 218 in the NS5 protein of WNV was mutated to alanine, resulting in the formation of a cap0 structure at the 5’ end of the viral genome. While WNV cap1 and cap0 replicated equally in Vero cells, WNV cap0 showed reduced replication in C6/36 cells (Zhou *et al.*, 2007).

Likewise, it was described that the ZIKV MTase methylates the RNA at the N-7 position of the cap and at the 2’-O position on the ribose of the first nucleotide (Coutard *et al.*,

2017). Moreover, ZIKV requires its MTase to restrict the RIG-I-induced immune defense by directly suppressing the K63-linked polyubiquitination of RIG-I. In this process, the amino acid D146 of the active site is essential (Li *et al.*, 2020).

In this thesis, the E218A mutation was introduced into an infectious ZIKV cDNA clone to study the replication of cap1 methylated and cap0 unmethylated ZIKV in mosquito cells. After successfully introducing the mutation, the PCR amplified region was sequenced up to and across cloning junctions. To validate that ZIKV cap0, similar to YFV-17D cap0 and WNV cap0, replicated with comparable growth characteristics as ZIKV cap1 in cells lacking type I interferon, Vero cells were infected with ZIKV cap1 and cap0. Contrary to expectations, replication of ZIKV cap0 was strongly reduced in Vero cells. This reduction might indicate that the viral stocks produced in Vero E6 cells contained cytokines that led to a reduced replication of ZIKV cap0 even though Vero E6 cells are assumed to not produce interferons (Desmyter *et al.*, 1968; Schmid *et al.*, 2015). ZIKV cap0 also replicated reduced in immunocompetent A549 cells and in insect C6/36 cells compared to ZIKV cap1. In addition, the technical triplicates showed very high standard deviations.

Other possibilities for the inconsistent results and the high standard deviations are problems with the virus derived from the infectious clone. A major difficulty in establishing orthoflaviviral cDNA clones is the low stability of large infectious cDNA clones during propagation in bacteria (Lai *et al.*, 1991; Mandl *et al.*, 1997; Shan *et al.*, 2016). This problem was first circumvented by Rice *et al*. by *in vitro* ligation of RNAs from two separate cDNA segments (Rice *et al.*, 1989). The infectious ZIKV cDNA clone established by Widman and colleagues consisted of four high-copy plasmids (Widman *et al.*, 2017). In contrast, the infectious clone used in this study consists of one low-copy plasmid (Mutso *et al.*, 2017). As a cloning vector (pCC1BAC), a single-copy vector was used to increase stability by low replication numbers. The same vector was also used to successfully establish infectious clones of DENV-4 and SARS-CoV-2 (Xie *et al.*, 2020; Ayers *et al.*, 2021). Thus, the instability of the used plasmid seems unlikely to explain the high divergence in the infection experiment.

Nevertheless, mutations can occur not only during plasmid propagation in the bacteria due to low stability but also during viral passaging in cell culture. Due to this, Mutso and colleagues sequenced the virus after rescuing and passing it from the infectious cDNA

clone to identify potential cell culture adaptations. A single point mutation in the NS2A protein was identified, present from P1 onwards but not in the initially rescued virus (Mutso *et al.*, 2017). This data indicates that the emergence of mutations is not unlikely in the rescued virus. Likewise, the long viral rescue time of ten days increases the probability of cell culture adaptations. Hence, avoiding excessive passaging of viruses derived from the infectious cDNA is crucial. Different cell culture-adaptive mutations were also described following excessive passaging of ZIKV isolates, resulting in increased infectivity (Grass *et al.*, 2022). Reasons for the high mutation rate of RNA viruses in cell culture are their adaptations to the used cell line and the existence of quasispecies. RNA viruses harbor their own RNA-dependent RNA polymerase without proofreading activity in the NS5 protein. The lack of proofreading activity quickly leads to mutations and the parallel existence of different viral populations, so-called quasispecies (Drake *et al.*, 1999). Since the standard deviations were very high after the infection experiments, quasispecies might have been present in the individual triplicates. The virus populations need to be sequenced to further investigate the existence of quasispecies. So far, only the NS5 protein was partially sequenced at defined time points to verify the stability of the E218A mutation introduced into ZIKV cap0. In all tested samples, the mutation was stable on day seven (Vero B4, A549) or day ten (C6/36) post-infection (data not shown).

Even though sequencing validated that the E218A mutation was stably incorporated into the infectious clone, conclusive evidence that the ribose-2'-O position of the first nucleotide is methylated needed to be included. The methylation status was indirectly verified by infecting A549 wild-type and IFIT1 k.o. cells with equal amounts of ZIKV cap1 and cap0. Here, ZIKV cap0 replication was significantly reduced compared to the cap1 virus in the wild-type cells, but the overall replication of ZIKV cap0 was attenuated at the tested time point (Figure 22B). The replication of the cap0 virus was also reduced in the IFIT1 k.o. cells, but this difference was not significant. Again, the standard deviations were relatively high in this experimental setup, and thus, it was difficult to discern whether IFIT1 proteins specifically bound to ZIKV lacking 2'-O-methylation (Habjan *et al.*, 2013). Russ *et al*. recently described another method to test the enzymatic function of a viral methyltransferase. They abrogated the enzymatic activity of the SARS-CoV-2 methyltransferase by mutation and tested the activity in an *in vitro* methyltransferase assay. For this, cellular RNAs harvested from SARS-CoV-2 wt and SARS-CoV-2 ΔMTase

infected cells were used to measure the methylation status of the isolated RNA after incubation with the recombinant vaccinia virus methyltransferase VP39. The vaccinia virus methyltransferase VP39 methylated RNA isolated from SARS-CoV-2 ΔMTase infected cells with a higher efficiency, suggesting a lower amount of 2'-O-methylated RNA in these cells (Russ *et al.*, 2022). An analogous experiment would shed light on the enzymatic activity of the ZIKV cap0 methyltransferase.

In total, infection experiments performed with ZIKV cap1 and cap0 revealed no clear picture of the ZIKV methylation status and thus, the importance of the ZIKV cap1 methylation in mosquitoes remains open.

While the methyltransferase in most orthoflaviviruses consists of the tetrad K61-D146-K182-E218, it is K61-D146-K181-E217 in DENV (Egloff *et al.*, 2002; Liu *et al.*, 2010). Likewise, the glutamine was at position 217 in the infectious DENV-2 clone used in this thesis (16681) and not 218, as in YFV and ZIKV (Kinney *et al.*, 1997). Thus, the glutamine at position 217 was mutated to alanine using site-directed-mutagenesis through fusion PCR. The resulting fragment was sequenced up to and across cloning junctions to validate that it harbored no PCR-derived accidental errors before DENV cap1 and cap0 were rescued. The viral titers of the resulting cap1 and cap0 viruses were relatively low and required passaging to increase titers, similar to what was previously shown for viruses derived from the 16681 infectious clones (Kinney *et al.*, 1997). Several previous studies demonstrated that viral RNAs lacking 2'-O-methylation are targeted by the restriction factor IFIT1 (Daffis *et al.*, 2010; Habjan *et al.*, 2013). Based on this, infection experiments with A549 wild-type and A549 IFIT1 k.o. cells were performed in this thesis to verify the methylation status of DENV cap0 indirectly. While the replication of DENV cap0 was significantly reduced in the wild-type cells, it showed comparable growth characteristics in the IFIT1 k.o. cells. These data indirectly confirm that DENV cap0 lacked its 2'-O-methylation of the 5'-terminal nucleotide (N1).

Further infection experiments performed with DENV cap1 and cap0 in cells with a functional and a dysfunctional type I interferon response indicate that the induction of type I interferons was crucial to control a DENV cap0 infection (Figure 23). In line with these findings, Schuberth-Wagner *et al*. observed that a functional type I interferon

immune response was also relevant to control infection with YFV-17D cap0 (Schuberth-Wagner *et al.*, 2015).

The importance of the DENV methyltransferase for the escape of the insect immune recognition was evaluated by infecting the mosquito cell lines C6/36 and Aag2 with DENV cap1 and cap0. Unlike YFV cap1 and cap0, DENV cap1 and cap0 replicated with comparable efficiency in both insect cell lines and thus behaved differently than YFV. Besides YFV cap0, WNV cap0 replicated to reduced titers in C6/36 cells compared to the associated cap1 virus, indicating that an intact methyltransferase is not only crucial for the replication of YFV in insect cells (Zhou *et al.*, 2007). DENV might escape recognition by the invertebrate immune system through another mechanism, resulting in identical DENV cap1 and cap0 replication efficiencies. In *in vivo* studies, the silencing of MyD88, an important Toll pathway component, increased DENV levels (Ramirez *et al.*, 2010). In addition, overexpression of Hop and Dome resulted in reduced DENV replication (Jupatanakul *et al.*, 2017). These data suggest that DENV counteracts several invertebrate immune pathways to promote its replication. Thus, it is tempting to speculate that DENV counteracts the cap1/cap0 discrimination mechanism in insects with unknown means.

Other groups also investigated the replication of DENV-2 cap1 and cap0 viruses with different infectious clones. Züst and colleagues used an infectious clone based on the TSV01 isolate to study the replication of DENV cap1 and cap0 in Vero and C6/36 cells. Contrary to the data presented in this thesis, Züst and colleagues observed slightly reduced DENV cap0 replication in Vero and C6/36 cells (Züst *et al.*, 2013). Since they did not assess viral replication at early points post-infection, it was difficult to determine whether the input viral titer was identical for both viruses. Different input titers might support the replication of one virus over another, resulting in different growth of DENV cap1 and cap0, and this might explain the different viral growth observed in this thesis and observed by Züst and colleagues (Züst *et al.*, 2013).

Another explanation for the diverse viral replication of DENV cap0 might be the different origins of the infectious clones. The infectious clone established by Züst *et al*. was based on the isolate TSV01, originating from Australia (Züst *et al.*, 2013). The infectious clone used in this thesis was based on the isolate 16681, which originated from Thailand (Kinney

et al., 1997). A direct comparison of TSV01 and 16681 showed that 16681 replicated more robustly than TSV01 (Wirtz *et al.*, 1992). In addition, TSV01 infection induced greater activation of type I antiviral genes, and it was less efficient at suppressing STAT-1 and STAT-2 than other DENV-2 isolates (Umareddy *et al.*, 2008).

In addition to the *in vitro* data, Züst *et al*. performed *in vivo* infection experiments with *Aedes aegypti*. They orally infected mosquitoes with 1 x 10^5 PFU/ml DENV cap1 or cap0 and separated the abdomen from the thorax 15 days after infection. Abdomens with measurable DENV RNA reflected the infection, and positive thoraxes reflected dissemination. While DENV cap0 neither infected nor disseminated in the mosquitoes, DENV cap1 infected 29% and disseminated in 24%. Mosquitoes were also intrathoracically injected to test whether DENV cap0 can, in principle, replicate *in vivo*. The results showed that the genome copies of DENV cap1 were approximately 35% higher than those of DENV cap0. Based on these findings, the authors concluded a reduced vector fitness of DENV cap0 (Züst *et al.*, 2013). Of note, the number of mosquitoes used for oral infection was difficult to compare, as 82 mosquitoes were used for DENV cap1, and 42 were used for DENV cap0. The difference in the groups' size may have contributed to the observed infection of 0% for DENV cap0 infected mosquitoes. Although the authors saw increased genome copies for DENV cap1 after intrathoracic infection, this difference was not significant. For future experiments, the *in vivo* data should be repeated in *Aedes aegypti* mosquitoes using the infectious 16681 clone to test whether DENV cap0 exhibits reduced fitness in mosquitoes.

Besides the 2'-O-methylation of the cap structure, the orthoflaviviral NS5 protein also catalyzes the methylation of internal nucleotides at the 2'-OH position of adenosine. Similar to cap methylation, the active site of the internal methylation activity is formed by the K61-D146-K181-E217 tetrad (Dong *et al.*, 2012). Dong and colleagues treated *in vitro* transcribed DENV-1 replicons RNA either with a wild-type MTase or an E217A MTase. The latter MTase lacked the 2'-O-methylation activity and was unable to perform internal methylation on the replicon RNA. Electroporation of the treated RNAs resulted in attenuated RNA replication and translation of the replicons with internal methylations (Dong *et al.*, 2012). Combining the findings of Schmid and Dong, it might be possible that the missing internal methylations of DENV cap0 led to a faster viral replication at very

early time points and earlier induction of type I interferons. Conversely, DENV cap0 replicated fast within the first hours post-infection, but after the induction of type I interferons, the replication was attenuated (Dong *et al.*, 2012; Schmid *et al.*, 2015). Future experiments should include the precise role of internal orthoflaviviral methylation on viral replication in vertebrate and insect cells.

Similar to the data of Züst *et al*., other researchers reported that insertion of the E216A mutation in DENV-1, which is equivalent to the E217A mutation in DENV-2, caused a decrease in the replication capacity of the cap0 mutant at early time points in BHK-21 cells (Chang *et al.*, 2016). Similar to Vero cells, BHK-21 cells do not produce type I interferons. Nevertheless, Chang and colleagues also observed that the replication difference between DENV-1 and DENV-E216A decreased over time in Vero cells, while the replication difference between the viruses was notable in A549 cells (Chang *et al.*, 2016). These data strengthen the hypothesis that a functional type I interferon response was crucial for controlling the mutant at later time points. In support of this, Chang *et al*. measured increased levels of immune genes in A549 cells at early time points after cap0 infection, and thus, viral replication was reduced (Chang *et al.*, 2016). Levels of immune genes after cap1 infection were only increased at later time points, suggesting that DENV-1 cap0 triggered an early immune response and thereby impaired its replication (Chang *et al.*, 2016).

To summarize, the DENV infection experiments in vertebrate and mosquito cells were only partially supported by the findings in the literature. While previous studies found reduced viral fitness for DENV cap0, the viral replication but not the fitness of DENV cap0 was attenuated in this thesis when cells with a functional type I interferon response were infected. However, experiments performed in this thesis and by others strongly indicated that the methyltransferase-deficient mutant was susceptible to type I interferon (Züst *et al.*, 2013; Chang *et al.*, 2016). In contrast to the data generated in vertebrate cells, an active methyltransferase seemed not to be crucial for DENV to replicate in insect cells. Most likely, DENV acted against the insect immune system by an unknown mechanism independently from the methyltransferase. Apparently, this mechanism did not counteract the siRNA pathway, as DENV cap1 and cap0 replicated to the same extent in C6/36 cells that lack Dcr-2.

4.6 Analysis of YFV-Asibi counteraction of mosquito cap0 recognition

The data presented in this thesis show that YFV-Asibi and DENV counteracted the mosquito immune system with an unknown mechanism but to different extents. While DENV strongly counteracted the mosquito immune system, resulting in comparable replication of DENV cap1 and cap0, YFV-Asibi counteracted the immune system to a lower extent, allowing slight viral replication. Therefore, it was attempted to pinpoint the viral genes responsible for YFV-Asibi cap0 and DENV cap0 replication by establishing chimeras. As shown by others, replication-competent chimeras between YFV and DENV were only possible when the prM and E structural proteins of DENV were inserted into the backbone of YFV (Guirakhoo *et al.*, 2000; Shustov *et al.*, 2010). In contrast, several replication-competent YFV-Asibi/YFV-17D chimeras are documented that replicated *in vivo* (McElroy *et al.*, 2006a, 2006b; Collins *et al.*, 2018). However, the authors did not use these chimeras to study viral genes that act against the mosquitoes' cap1/cap0 discrimination mechanism.

In a first attempt, the influence of the structural proteins on the discrimination mechanism was investigated in this thesis by inserting the structural proteins of YFV-Asibi into YFV-17D and vice versa. Replacing the structural proteins did not change the replication ability of the corresponding cap0 chimeras, indicating that the structural proteins of Asibi are not mainly responsible for promoting cap0 replication. Since modifications in the 3'UTR of YFV and DENV were associated with reduced viral growth in vertebrate and mosquito hosts and since the orthoflaviviral 3'UTR plays an essential role in producing sfRNAs, which have a broad antiviral effect in mosquitoes, it was assumed that the 3'UTR might influence the cap1/cap0 discrimination mechanism (Bredenbeek *et al.*, 2003; Cologna *et al.*, 2003; Bryant *et al.*, 2005; Schnettler *et al.*, 2012; Göertz *et al.*, 2016; Pompon *et al.*, 2017). Since the SP 17D in Asibi cap0 chimera showed some replication in C6/36 cells, the influence of the 3'UTR of Asibi was further investigated. For this purpose, the NS proteins of Asibi were inserted into 17D, resulting in a chimera with a 3'UTR belonging to 17D (Figure 24C). The associated cap0 chimera replicated in C6/36 cells to relatively high titers, yet nearly 0.5 $\log_{10}$ reduced compared to YFV-Asibi cap0. Nevertheless, the data provide strong evidence that the NS proteins might act against the cap1/cap0 discrimination mechanism.

Next, additional chimeras were established to identify the specific viral NS gene(s) responsible for the replication of YFV-Asibi cap0. Due to the availability of restriction sites, the 5' end of the NS4A-3'UTR of Asibi was inserted into 17D. The corresponding cap0 chimera replicated upon infection but clearly reduced compared to YFV-Asibi cap0. This data indicated that the exchanged region might be essential for the discrimination mechanism.

The previously exchanged fragment still contained the NS5 protein, which was shown to interact with the vertebrate and mosquito immune systems. In addition to the methyltransferase encoded in the NS5 protein, it was demonstrated that in *Aedes albopictus* mosquitoes infected with DENV, vpiRNAs were produced mainly from the 3' end of the NS5 protein (Wang *et al.*, 2018). Moreover, the E3 ubiquitin ligase Cullin4 was induced by WNV NS5, leading to STAT degradation in *Culex* mosquitoes (Paradkar *et al.*, 2015). Therefore, it was assumed that the NS5 protein might be particularly important in suppressing the discrimination mechanism. However, the NS5 Asibi in 17D cap0 chimera failed to replicate, while the NS5 17D in Asibi cap0 chimera replicated. Thus, Asibi NS5 was not solely responsible for the replication of the cap0 virus.

The potential VSR activity of the orthoflaviviral NS4B protein is currently under discussion. While Schnettler and colleagues could not see any RNAi suppressive effect in mammals or plants for the non-structural proteins of WNV, Kakumani suggested a VSR activity for DENV NS4B (Schnettler *et al.*, 2012; Kakumani *et al.*, 2013). Since NS4B is a small transmembrane protein that interferes with the vertebrates' interferon response, it is not unlikely that it also interacts with the insect immune system (Pijlman, 2014). However, the NS4B Asibi in 17D cap0 chimera failed to replicate in C6/36 cells, indicating that NS4B is not mainly responsible for promoting cap0 replication. Likewise, the 2K-NS5 Asibi in 17D cap0 chimera did not exceed the detection limit, and no replication was observed. Only the combination of NS4A-NS5 Asibi in 17D resulted in the replication of the cap0 chimera, indicating that multiple Asibi NS proteins were necessary to overcome the discrimination mechanism.

Based on the chimera results presented in this thesis, it was hypothesized that a fast initial replication rate of the cap1 chimera would positively correlate with the replication ability of the corresponding cap0 chimera. The obtained data showed that if the cap1 chimera

replicated rapidly at early time points and reached a high titer three days after infection, it was likely that the cap0 chimera could also replicate (Figure 26A).

Due to the above-stated hypothesis, it was of interest to analyze whether DENV also showed a high initial growth rate. Comparative growth curve kinetics of YFV-Asibi, YFV-17D, and DENV at early time points revealed that all three viruses replicated comparably fast during the first 12 h of the experiment. After 12 h, YFV-Asibi replicated faster than YFV-17D and DENV. Throughout the experiment, DENV and YFV-17D replicated to comparable growth rates, indicating that the initial replication speed of DENV was probably not responsible for promoting DENV cap0 replication. It seems more likely that one or more structural or non-structural protein(s) of DENV might act against the cap1/cap0 discrimination mechanism, leading to equal replication of DENV cap1 and cap0 in all tested mosquito cells.

Taking together, no single Asibi NS protein was responsible for suppressing the cap1/cap0 discrimination mechanism, but a synergy of several proteins. The present data suggest that NS4A to NS5 were mainly responsible for this suppression.

4.7 Analysis of DENV counteraction of mosquito cap0 recognition

DENV-2 NS2A has been reported to be a viral suppressor of RNAi in mammalian and mosquito cells, and through mutational analysis, K135 was identified as a critical residue for the VSR activity (Qiu *et al.*, 2020). The introduction of the mutation K135A resulted in significantly reduced replication of DENV-K135A in Aag2 cells but not in C6/36. These results indicated that K135 is essential to act against the RNAi pathway in Aag2 cells. (Qiu *et al.*, 2020).

Considering the importance of DENV NS2A, it was interesting to analyze whether DENV NS2A might also act independently from the RNAi pathway against the cap1/cap0 discrimination mechanism in mosquitoes. Therefore, two viral mutants were established, namely DENV-NS2A-K135A cap1 and DENV-NS2A-K135A cap0. While DENV cap1, cap0, and DENV-NS2A-K135A cap1 formed plaques in Vero B4 cells, the DENV-NS2A-K135A cap0 double mutant failed to form plaques (data not shown). The loss of the ability to form plaques might display attenuated infectivity of the virus. The viral titers were evaluated via $TCID_{50}$ and immunofluorescence after passaging the viruses once in Vero B4 cells. The positive immunofluorescence of the DENV-NS2A-K135A cap0 mutant

indicated that infectious particles were formed. Due to the availability of a well-established qPCR, the growth curve was analyzed with this method.

As expected, the growth curve in C6/36 cells showed identical replication of DENV cap1 and DENV-NS2A-K135A cap1. The replication of DENV cap0 and DENV-NS2A-K135A cap0 were comparable to each other but slightly reduced compared to the two cap1 viruses. Since DENV-NS2A-K135A cap0 and DENV cap0 showed comparable replication rates, DENV NS2A does not seem to be responsible for promoting DENV cap0 replication. The growth curve revealed a slight discrepancy in the replication efficiency of DENV cap0 compared to DENV cap1. The obtained data did not align with the previously acquired DENV growth curve results (Figure 23C): here, DENV cap1 and cap0 replicated with equal efficiency in C6/36 cells. However, it needs to be considered that different evaluation methods were used to analyze the two growth curve kinetics.

The growth curve evaluated by qPCR showed a high amount of residual infectivity, meaning the inoculum input could not be reduced to the point of being undetectable. In the previous experiment, the input inoculum could be removed by extensive washing, which was described to be essential to remove residual infectivity (Lindenbach *et al.*, 1999).

Future experiments should aim to narrow down DENV proteins that support the replication of cap1 unmethylated YFV RNAs. As previously mentioned, superinfection exclusion in C6/36 cells has been reported for YFV and DENV, eliminating superinfection experiments as one possibility to identify important DENV proteins (Abrao *et al.*, 2016). Another possibility to identify the DENV proteins that may be suppressing the cap1/cap0 discrimination mechanism might be the expression of the individual DENV NS proteins in *trans*. With this experimental setup, it might be possible to test whether the expression of single DENV proteins leads to enhanced replication of YFV cap0. A suitable expression plasmid would be one with an *Aedes aegypti* polyubiquitin promoter (Pub promoter) (Anderson *et al.*, 2010). Numerous studies successfully used this promoter to efficiently express different constructs in mosquito cells (Varjak, Maringer, *et al.*, 2017; Fredericks *et al.*, 2019; Gestuveo *et al.*, 2022). One limitation of this approach is that the potential influence of the UTRs cannot be co-investigated.

Ultimately, no conclusion can be drawn regarding which DENV proteins are responsible for suppressing the cap1/cap0 discrimination mechanism. The 17D/Asibi chimera data indicated that the 3'UTR of YFV-Asibi was not mainly responsible for the replication of YFV-Asibi cap0. However, such an exclusion cannot be made for DENV. In recent years, several studies showed that degradation of viral RNA by the exoribonuclease Pacman in insect cells stalls on the highly structured 3'UTR of orthoflaviviruses (Göertz *et al.*, 2016). The stalling produces so-called sfRNAs, whose antiviral effect has been described several times (Schnettler *et al.*, 2012; Moon *et al.*, 2015; Göertz *et al.*, 2019). Thus, sfRNA has also been shown to bind to the DEAD/H-box helicase ME31B, thereby promoting orthoflaviviral replication (Göertz *et al.*, 2019). Given the general antiviral effect of sfRNA, future experiments should further investigate the potential role of sfRNA in counteracting the DENV cap1/cap0 differentiation mechanism.

5. Abstract

Various infectious diseases are caused by mosquito-borne orthoflaviviruses affecting people worldwide. Efficient transmission of these viruses highly depends on the pathogen's ability to overcome the host immune system. Previous studies showed that orthoflaviviruses evade the vertebrate immune system by capping their viral genome via a cap-N1-2'-O-methyltransferase encoded in the non-structural protein NS5. This thesis aimed to analyze whether orthoflaviviruses also escape the insect immune system by modulating their 5' cap structure via 2'-O-methylation.

Using the yellow fever virus (YFV) vaccine strain (YFV-17D cap1) and a methyltransferase deficient mutant (YFV-17D cap0), this thesis demonstrates that the replication of YFV-17D cap0 is also impaired in mosquito cells. Since YFV-17D is unable to replicate in mosquitoes, a YFV-Asibi cDNA clone was additionally established to compare the respective cap1 and cap0 variants *in vitro* and *in vivo*. Similar to YFV-17D cap0, YFV-Asibi cap0 was suppressed in mosquito cells in a Dicer-2 independent manner but to a slightly lower extent. These data indicate that YFV-Asibi counteracts the insect antiviral discrimination mechanism of cap0 RNA. Studies comparing chimeras between YFV-Asibi and YFV-17D aimed to pinpoint the viral genes responsible for counteracting the discrimination mechanism. The results suggest that a synergy of several non-structural proteins is involved in this mechanism. In the case of YFV, the counteraction seems to be linked to a faster viral replication at early time points.

Furthermore, after oral infection of *Aedes aegypti* mosquitoes, YFV-Asibi cap1 replicated in the mosquito midgut and secondary tissues like legs plus wings. Conversely, replication of YFV-Asibi cap0 was suppressed in the midgut and nearly blocked in secondary tissues. Intriguingly, efficient replication of YFV-Asibi cap0 occurred after intrathoracic infection, indicating the existence of a potential receptor or protein discriminating between cap1 and cap0 RNAs in the midgut or the midgut barrier.

Since the methyltransferase is highly conserved between orthoflaviviruses, DENV cap0 was established as well. Comparative growth curve kinetics revealed that DENV cap0 replication is not suppressed in mosquito cells, implying that DENV also counteracts the insect antiviral discrimination mechanism of cap0 RNA but more strongly than YFV-Asibi.

In summary, the obtained results suggest the existence of an innate 5’ RNA-modification recognizing effector protein in mosquito cells and mosquitoes. Further, orthoflaviviruses counteract this effector protein by different means, leading to different levels of cap0 virus replication.

6. List of figures

7. List of tables

8. References

Abrao, E.P. and Da Fonseca, B.A.L. (2016) 'Infection of Mosquito Cells (C6/36) by Dengue-2 Virus Interferes with Subsequent Infection by Yellow Fever Virus', *Vector-Borne and Zoonotic Diseases*, 16(2), pp. 124–130

Adelman, Z.N., Anderson, M.A.E., Liu, M., Zhang, L. and Mylesa, K.M. (2012) 'Sindbis virus induces the production of a novel class of endogenous siRNAs in Aedes aegypti mosquitoes', *Insect Mol Biol.*, 21(3), pp. 357–368

Ahmad, S. and Hur, S. (2015) 'Helicases in Antiviral Immunity: Dual Properties as Sensors and Effectors', *Trends in Biochemical Sciences*, 40(10), pp. 576–585

Almire, F., Terhzaz, S., Terry, S., McFarlane, M., Gestuveo, R.J., Szemiel, A.M., Varjak, M., McDonald, A., Kohl, A. and Pondeville, E. (2021) 'Sugar feeding protects against arboviral infection by enhancing gut immunity in the mosquito vector Aedes aegypti', *PLoS Pathogens*, 17(9), pp. 1–26

Altinli, M., Leggewie, M., Badusche, M., Gyanwali, R., Scherer, C., Schulze, J., Sreenu, V.B., Fegebank, M., Zibrat, B., Fuss, J., Junglen, S. and Schnettler, E. (2022) 'Antiviral RNAi Response against the Insect-Specific Agua Salud Alphavirus', *mSphere*, 7(1), pp. 1–13

Ammerman, N.C., Beier-Sexton, M. and Azad, A.F. (2009) 'Growth and maintenance of Vero cell lines', *Curr Protoc Microbiol*, pp. 1–10

Anderson, M.A.E., Gross, T.L., Myles, K.M. and Adelman, Z.N. (2010) 'Validation of novel promoter sequences derived from two endogenous ubiquitin genes in transgenic Aedes aegypti', *Insect Molecular Biology*, 19(4), pp. 441–449

Angleró-Rodríguez, Y.I., MacLeod, H.J., Kang, S., Carlson, J.S., Jupatanakul, N. and Dimopoulos, G. (2017) 'Aedes aegypti molecular responses to Zika Virus: Modulation of infection by the toll and Jak/Stat immune pathways and virus host factors', *Frontiers in Microbiology*, 8(OCT), pp. 1–12

Ayers, J.B., Xie, X., Coatsworth, H., Stephenson, C.J., Waits, C.M., Shi, P.Y. and Dinglasan, R.R. (2021) 'Infection Kinetics and Transmissibility of a Reanimated Dengue Virus Serotype 4 Identified Originally in Wild Aedes aegypti From Florida', *Frontiers in Microbiology*, 12

Barrett, A.D.T., Monath, T.P., Cropp, C.B., Adkins, J.A., Ledger, T.N., Gould, E.A., Schlesinger, J.J., Kinney, R.M. and Trent, D.W. (1990) 'Attenuation of wild-type yellow fever virus by passage in HeLa cells', *Journal of General Virology*, 71(10), pp. 2301–2306

Barrows, N.J., Campos, R.K., Liao, K.C., Prasanth, K.R., Soto-Acosta, R., Yeh, S.C., Schott-Lerner, G., Pompon, J., Sessions, O.M., Bradrick, S.S. and Garcia-Blanco, M.A. (2018) 'Biochemistry and Molecular Biology of Flaviviruses', *Chemical Reviews*, 118(8), pp. 4448–4482

Bartholomeusz, A. and Thompson, P. (1999) 'Flaviviridae polymerase and RNA replication', *Journal of Viral Hepatitis*, 6(4), pp. 261–270

Basu, M., Maitra, R.K., Xiang, Y., Meng, X., Banerjee, A.K. and Bose, S. (2006) 'Inhibition of vesicular stomatitis virus infection in epithelial cells by alpha interferon-induced soluble secreted proteins', *Journal of General Virology*, 87(9), pp. 2653–2662

Bhatt, S., Gething, P.W., Brady, O.J., Messina, J.P., Farlow, A.W., Moyes, C.L., Drake, J.M., Brownstein, J.S., Hoen, A.G., Sankoh, O., Myers, M.F., George, D.B., Jaenisch, T., Wint, G.R.W., Simmons, C.P., Scott, T.W., Farrar, J.J. and Hay, S.I. (2013) 'The global distribution and burden of dengue', *Nature*, 496(7446), pp. 504–507

Blagrove, M. and Barribeau, S.M. (2021) 'Immune priming can prevent WNV establishment in Culex quinquefasciatus mosquitoes: evidence for immune priming based reversal of WNV-mediated immune suppression', *bioRxiv*, p. 2021.05.05.442826

Blair, C. (2011) 'Mosquito RNAi is the major innate immune pathway controlling arbovirus infection and transmission', *Future Microbiology*, 6(3), pp. 265–277

Blair, C.D. and Olson, K.E. (2015) 'The role of RNA interference (RNAi) in arbovirus-vector interactions', *Viruses*, 7(2), pp. 820–843

Boo, S.H. and Kim, Y.K. (2020) 'The emerging role of RNA modifications in the regulation of mRNA stability', *Experimental and Molecular Medicine*, 52(3), pp. 400–408

Brackney, D.E., Scott, J.C., Sagawa, F., Woodward, J.E., Miller, N.A., Schilkey, F.D., Mudge, J., Wilusz, J., Olson, K.E., Blair, C.D. and Ebel, G.D. (2010) 'C6/36 Aedes albopictus cells have a dysfunctional antiviral RNA interference response', *PLoS Neglected Tropical Diseases*, 4(10), pp. 24–27

Bredenbeek, P.J., Kooi, E.A., Lindenbach, B., Huijkman, N., Rice, C.M. and Spaan, W.J.M. (2003) 'A stable full-length yellow fever virus cDNA clone and the role of conserved RNA elements in flavivirus replication', *Journal of General Virology*, 84(5), pp. 1261–1268

Bronkhorst, A.W. and van Rij, R.P. (2014) 'The long and short of antiviral defense: Small RNA-based immunity in insects', *Current Opinion in Virology*, 7(1), pp. 19–28

Bryant, J.E., Vasconcelos, P.F.C., Rijnbrand, R.C.A., Mutebi, J.P., Higgs, S. and Barrett, A.D.T. (2005) 'Size Heterogeneity in the 3′ Noncoding Region of South American Isolates of Yellow Fever Virus', *Journal of Virology*, 79(6), pp. 3807–3821

Campbell, C.L., Black IV, W.C., Hess, A.M. and Foy, B.D. (2008) 'Comparative genomics of small RNA regulatory pathway components in vector mosquitoes', *BMC Genomics*, 9

Carpenter, A. and Clem, R.J. (2023) 'Factors Affecting Arbovirus Midgut Escape in Mosquitoes', *Pathogens*, 12(2)

Chambers, T.J., Hahn, C.S., Galler, R. and Rice, C.M. (1990) 'Flavivirus genome organization, expression, and replication', *Annual Review of Microbiology*, 44, pp. 649–688

Chang, D.C., Hoang, L.T., Mohamed Naim, A.N., Dong, H., Schreiber, M.J., Hibberd, M.L., Tan, M.J.A. and Shi, P.Y. (2016) 'Evasion of early innate immune response by 2′-O-methylation of dengue genomic RNA', *Virology*, 499, pp. 259–266

Cheng, G., Liu, Y., Wang, P. and Xiao, X. (2016) 'Mosquito Defense Strategies against Viral Infection', *Trends in Parasitology*, 32(3), pp. 177–186

Cheng, G., Zhao, X., Li, Z., Liu, X., Yan, W., Zhang, X., Zhong, Y. and Zheng, Z. (2009) 'Identification of a putative invertebrate helical cytokine similar to the ciliary neurotrophic factor/Leukemia inhibitory factor family by PSI-BLAST-Based approach', *Journal of Interferon and Cytokine Research*, 29(8), pp. 461–468

Chiu, W., Kinney, R.M. and Dreher, T.W. (2005) 'Control of Translation by the 5'- and 3'-Terminal Regions of the Dengue Virus Genome', *American Society for Microbiology.*, 79(13), pp. 8303–8315

Christophides, G.K., Zdobnov, E., Barillas-Mury, C., Birney, E., Blandin, S., Blass, C., Brey, P.T., Collins, F.H., Danielli, A., Dimopoulos, G., Hetru, C., Hoa, N.T., Hoffmann, J.A., Kanzok, S.M., Letunic, I., Levashina, E.A., Loukeris, T.G., Lycett, G., Meister, S., Michel, K., Moita, L.F., Müller, H.M., Osta, M.A., Paskewitz, S.M., Reichhart, J.M., Rzhetsky, A., Troxler, L., Vernick, K.D., Vlachou, D., Volz, J., Von Mering, C., Xu, J., Zheng, L., Bork, P. and Kafatos, F.C. (2002) 'Immunity-related genes and gene families in Anopheles gambiae', *Science*, 298(5591), pp. 159–165

Collins, N.D., Beck, A.S., Widen, S.G., Wood, T.G., Higgs, S. and Barrett, A.D.T. (2018) 'Structural and nonstructural genes contribute to the genetic diversity of RNA viruses', *mBio*, 9(5), pp. 1–13

Cologna, R. and Rico-Hesse, R. (2003) 'American Genotype Structures Decrease Dengue Virus Output from Human Monocytes and Dendritic Cells', *Journal of Virology*, 77(7), pp. 3929–3938

Colpitts, T.M., Cox, J., Vanlandingham, D.L., Feitosa, F.M., Cheng, G., Kurscheid, S., Wang, P., Krishnan, M.N., Higgs, S. and Fikrig, E. (2011) 'Alterations in the aedes aegypti transcriptome during infection with west nile, dengue and yellow fever viruses', *PLoS Pathogens*, 7(9)

Condreay, L.D. and Brown, D.T. (1986) 'Exclusion of Superinfecting Homologous Virus by Sindbis Virus- Infected Aedes albopictus (Mosquito) Cells', *J Virol*, 58(1), pp. 81–86

Coutard, B., Barral, K., Lichière, J., Selisko, B., Martin, B., Aouadi, W., Lombardia, M.O., Debart, F., Vasseur, J.-J., Guillemot, J.C., Canard, B. and Decroly, E. (2017) 'Zika Virus Methyltransferase: Structure and Functions for Drug Design Perspectives', *Journal of Virology*, 91(5)

Cui, Y. and Franz, A.W.E. (2020) 'Heterogeneity of midgut cells and their differential responses to blood meal ingestion by the mosquito, Aedes aegypti', *Insect Biochemistry and Molecular Biology*, 127, pp. 1–25

Czech, B., Malone, C., Zhou, R., Stark, A., Schlingeheyde, C., Dus, M., Perrimon, N., Kellis, M., Wohlschlegel, J., Sachidanandam, R., Hannon, G. and Brennecke, J. (2008) 'An endogenous small interfering RNA pathway in Drosophila', *Nature*, 453(7196), pp. 1–7

Daffis, S., Szretter, K.J., Schriewer, J., Li, J., Youn, S., Errett, J., Lin, T.Y., Schneller, S., Zust, R., Dong, H., Thiel, V., Sen, G.C., Fensterl, V., Klimstra, W.B., Pierson, T.C., Buller, R.M., Gale Jr, M., Shi, P.Y. and Diamond, M.S. (2010) '2′-O methylation of the viral mRNA cap evades host restriction by IFIT family members', *Nature*, 468(7322), pp. 452–456

Danet, L., Beauclair, G., Berthet, M., Moratorio, G., Gracias, S., Tangy, F., Choumet, V. and Jouvenet, N. (2019) 'Midgut barriers prevent the replication and dissemination of the yellow fever vaccine in Aedes aegypti', *PLoS Neglected Tropical Diseases*, 13(8)

Davis, E.H., Beck, A.S., Strother, A.E., Thompson, J.K., Widen, S.G., Higgs, S., Wood, T.G. and Barrett, A.D.T. (2019) 'Attenuation of live-attenuated yellow fever 17D vaccine virus is localized to a high-fidelity replication complex', *mBio*, 10(5), pp. 1–14

Davis, E.H., Thompson, J.K., Widen, S.G. and Barrett, A.D.T. (2021) 'Genome Characterization of Yellow Fever Virus Wild-Type Strain Asibi, Parent to Live-Attenuated 17D Vaccine, from Three Different Sources', *Viruses*, 13(7)

Decroly, E., Ferron, F., Lescar, J. and Canard, B. (2012) 'Conventional and unconventional mechanisms for capping viral mRNA', *Nature Reviews Microbiology*, 10(1), pp. 51–65

Deddouche, S., Matt, N., Budd, A., Mueller, S., Kemp, C., Galiana-Arnoux, D., Dostert, C., Antoniewski, C., Hoffmann, J.A. and Imler, J.L. (2008) 'The DExD/H-box helicase Dicer-2 mediates the induction of antiviral activity in drosophila', *Nature Immunology*, 9(12), pp. 1425–1432

Desmyter, J., Melnick, J.L. and Rawls, W.E. (1968) 'Defectiveness of Interferon Production and of Rubella Virus Interference in a Line of African Green Monkey Kidney Cells (Vero)', *Journal of Virology*, 2(10), pp. 955–961

Donald, C.L., Kohl, A. and Schnettler, E. (2012) 'New insights into control of arbovirus replication and spread by insect RNA interference pathways', *Insects*, 3(2), pp. 511–531

Dong, H., Chang, D.C., Hua, M.H.C., Lim, S.P., Chionh, Y.H., Hia, F., Lee, Y.H., Kukkaro, P., Lok, S.M., Dedon, P.C. and Shi, P.Y. (2012) '2′-O methylation of internal adenosine by flavivirus NS5 methyltransferase', *PLoS Pathogens*, 8(4)

Dong, H., Fink, K., Züst, R., Lim, S.P., Qin, C.F. and Shi, P.Y. (2014) 'Flavivirus RNA methylation', *Journal of General Virology*, 95(PART 4), pp. 763–778

Dostert, C., Jouanguy, E., Irving, P., Troxler, L., Galiana-Arnoux, D., Hetru, C., Hoffmann, J.A. and Imler, J.L. (2005) 'The Jak-STAT signaling pathway is required but not sufficient for the antiviral response of drosophila', *Nature Immunology*, 6(9), pp. 946–953

Drake, J.W. and Holland, J.J. (1999) 'Mutation rates among RNA viruses', *Proceedings of the National Academy of Sciences of the United States of America*, 96(24), pp. 13910–13913

Duc, C., Yoth, M., Jensen, S., Mouniée, N., Bergman, C.M., Vaury, C. and Brasset, E. (2019) 'Trapping a somatic endogenous retrovirus into a germline piRNA cluster immunizes the germline against further invasion', *Genome Biology*, 20(1), pp. 1–14

Egloff, M.P., Benarroch, D., Selisko, B., Romette, J.L. and Canard, B. (2002) 'An RNA cap (nucleoside-2′-O-)-methyltransferase in the flavivirus RNA polymerase NS5: Crystal structure and functional characterization', *EMBO Journal*, 21(11), pp. 2757–2768

van den Elsen, K., Quek, J.P. and Luo, D. (2021) 'Molecular insights into the flavivirus replication complex', *Viruses*, 13(6), pp. 1–28

Fareh, M., Van Lopik, J., Katechis, I., Bronkhorst, A.W., Haagsma, A.C., Van Rij, R.P. and Joo, C. (2018) 'Viral suppressors of RNAI employ a rapid screening mode to discriminate viral RNA from cellular small RNA', *Nucleic Acids Research*, 46(6), pp. 3187–3197

Feng, X., Zhou, S., Wang, J. and Hu, W. (2018) 'microRNA profiles and functions in mosquitoes', *PLoS Neglected Tropical Diseases*, 12(5), pp. 1–19

Fernandez-Garcia, M.D., Meertens, L., Chazal, M., Hafirassou, M.L., Dejarnac, O., Zamborlini, A., Despres, P., Sauvonnet, N., Arenzana-Seisdedos, F., Jouvenet, N. and Amara, A. (2016) 'Vaccine and wild-type strains of yellow fever virus engage distinct entry mechanisms and differentially stimulate antiviral immune responses', *mBio*, 7(1), pp. 1–15

Figueiredo, L.T.M. (2019) 'Human urban arboviruses can infect wild animals and jump to sylvatic maintenance cycles in South America', *Frontiers in Cellular and Infection Microbiology*, 9(JUL), pp. 1–6

Fishburn, A.T., Pham, O.H., Kenaston, M.W., Beesabathuni, N.S. and Shah, P.S. (2022) 'Let's Get Physical: Flavivirus-Host Protein–Protein Interactions in Replication and Pathogenesis', *Frontiers in Microbiology*, 13(March)

Fredericks, A.C., Russell, T.A., Wallace, L.E., Davidson, A.D., Fernandez-Sesma, A. and Maringer, K. (2019) 'Aedes aegypti (Aag2)-derived clonal mosquito cell lines reveal the effects of pre-existing persistent infection with the insect-specific bunyavirus Phasi Charoen-like virus on arbovirus replication', *PLoS Neglected Tropical Diseases*, 13(11), pp. 1–25

Furuichi, Y., LaFiandra, A. and Shatkin, A.J. (1977) '5′-Terminal structure and mRNA stability', *Nature*, 266(5599), pp. 235–239

Furuichi, Y. and Shatkin, A.J. (1976) 'Differential synthesis of blocked and unblocked 5' termini in reovirus mRNA: Effect of pyrophosphate and pyrophosphatase', *Proceedings of the National Academy of Sciences of the United States of America*, 73(10), pp. 3448–3452

Galiana-Arnoux, D., Dostert, C., Schneemann, A., Hoffmann, J.A. and Imler, J.L. (2006) 'Essential function in vivo for Dicer-2 in host defense against RNA viruses in drosophila', *Nature Immunology*, 7(6), pp. 590–597

Gershman, M.D. and Staples, J.E. (2012) *Yellow Fever*, *Netter's Infectious Disease*. Elsevier Inc.

Gestuveo, R.J., Parry, R., Dickson, L.B., Lequime, S., Sreenu, V.B., Arnold, M.J., Khromykh, A.A., Schnettler, E., Lambrechts, L., Varjak, M. and Kohl, A. (2022) 'Mutational analysis of Aedes aegypti Dicer 2 provides insights into the biogenesis of antiviral exogenous small interfering RNAs', *PLoS Pathogens*, 18(1), pp. 1–29

Giard, D.J., Aaronson, S.A., Todaro, G.J., Arnstein, P., Kersey, J.H. and Parks, W.P. (1973) 'In vitro cultivation of human tumors: Establishment of cell lines derived from a series of solid tumors', *Journal of the National Cancer Institute*, 51(5), pp. 1417–1423

Girard, Y.A., Klingler, K.A. and Higgs, S. (2004) 'West Nile virus dissemination and tissue tropisms in orally infected Culex pipiens quinquefasciatus', *Vector-Borne and Zoonotic Diseases*, 4(2), pp. 109–122

Gloria-Soria, A., Soghigian, J., Kellner, D. and Powell, J.R. (2019) 'Genetic diversity of laboratory strains and implications for research: The case of Aedes aegypti', *PLoS Negl Trop Dis*, 13(12), pp. 1–17

Glover, A. and White, A. (2020) 'A vector-host model to assess the impact of superinfection exclusion on vaccination strategies using dengue and yellow fever as case studies', *Journal of Theoretical Biology*, 484, p. 110014

Göertz, G.P., van Bree, J.W.M., Hiralal, A., Fernhout, B.M., Steffens, C., Boeren, S., Visser, T.M., Vogels, C.B.F., Abbo, S.R., Fros, J.J., Koenraadt, C.J.M., van Oers, M.M. and Pijlman, G.P. (2019) 'Subgenomic flavivirus RNA binds the mosquito DEAD/H-box helicase ME31B and determines Zika virus transmission by Aedes aegypti', *Proceedings of the National Academy of Sciences of the United States of America*, 116(38), pp. 19136–19144

Göertz, G.P., Fros, J.J., Miesen, P., Vogels, C.B.F., van der Bent, M.L., Geertsema, C., Koenraadt, C.J.M., van Rij, R.P., van Oers, M.M. and Pijlman, G.P. (2016) 'Noncoding Subgenomic Flavivirus RNA Is Processed by the Mosquito RNA Interference Machinery and Determines West Nile Virus Transmission by Culex pipiens Mosquitoes', *Journal of Virology*, 90(22), pp. 10145–10159

Goic, B., Stapleford, K.A., Frangeul, L., Doucet, A.J., Gausson, V., Blanc, H., Schemmel-Jofre, N., Cristofari, G., Lambrechts, L., Vignuzzi, M. and Saleh, M.C. (2016) 'Virus-derived DNA drives mosquito vector tolerance to arboviral infection', *Nature Communications*, 7, pp. 1–10

Grass, V., Hardy, E., Kobert, K., Talemi, S.R., Décembre, E., Guy, C., Markov, P. V., Kohl, A., Paris, M., Böckmann, A., Muñoz-González, S., Sherry, L., Höfer, T., Boussau, B. and Dreux, M. (2022) 'Adaptation to host cell environment during experimental evolution of Zika virus', *Communications Biology*, 5(1), pp. 1–14

Grivna, S.T., Beyret, E., Wang, Z. and Lin, H. (2006) 'A novel class of small RNAs in mouse spermatogenic cells', *Genes and Development*, 20(13), pp. 1709–1714

Guirakhoo, F., Weltzin, R., Chambers, T.J., Zhang, Z.-X., Soike, K., Ratterree, M., Arroyo, J., Georgakopoulos, K., Catalan, J. and Monath, T.P. (2000) 'Recombinant Chimeric Yellow Fever-Dengue Type 2 Virus Is Immunogenic and Protective in Nonhuman Primates', *Journal of Virology*, 74(12), pp. 5477–5485

Habjan, M., Hubel, P., Lacerda, L., Benda, C., Holze, C., Eberl, C.H., Mann, A., Kindler, E., Gil-Cruz, C., Ziebuhr, J., Thiel, V. and Pichlmair, A. (2013) 'Sequestration by IFIT1 Impairs Translation of 2′O-unmethylated Capped RNA', *PLoS Pathogens*, 9(10)

Hahn, C.S., Dalrymple, J.M., Strauss, J.H. and Rice, C.M. (1987) 'Comparison of the virulent Asibi strain of yellow fever virus with the 17D vaccine strain derived from it', *Proceedings of the National Academy of Sciences of the United States of America*, 84(7), pp. 2019–2023

Hahn, C.S., Hahn, Y.S., Rice, C.M., Lee, E., Dalgarno, L., Strauss, E.G. and Strauss, J.H. (1987) 'Conserved elements in the 3′ untranslated region of flavivirus RNAs and potential cyclization sequences', *Journal of Molecular Biology*, 198(1), pp. 33–41

Harrison, D.A., McCoon, P.E., Binari, R., Gilman, M. and Perrimon, N. (1998) 'Drosophila unpaired encodes a secreted protein that activates the JAK signaling pathway', *Genes and Development*, 12(20), pp. 3252–3263

He, Y., Wang, M., Chen, S. and Cheng, A. (2020) 'The role of capsid in the flaviviral life cycle and perspectives for vaccine development', *Vaccine*, 38(44), pp. 6872–6881

Hess, A.M., Prasad, A.N., Ptitsyn, A., Ebel, G.D., Olson, K.E., Barbacioru, C., Monighetti, C. and Campbell, C.L. (2011) 'Small RNA profiling of Dengue virus-mosquito interactions implicates the PIWI RNA pathway in anti-viral defense', *BMC Microbiology*, 11, pp. 24–30

Hoffmann, J.A. and Reichhart, J.M. (2002) 'Drosophila innate immunity: An evolutionary perspective', *Nature Immunology*, 3(2), pp. 121–126

van den Hurk, A.F., Hall-Mendelin, S., Pyke, A.T., Frentiu, F.D., McElroy, K., Day, A., Higgs, S. and O'Neill, S.L. (2012) 'Impact of Wolbachia on Infection with Chikungunya and Yellow Fever Viruses in the Mosquito Vector Aedes aegypti', *PLoS Neglected Tropical Diseases*, 6(11)

Issur, M., Geiss, B.J., Bougie, I., Picard-Jean, F., Despins, S., Mayette, J., Hobdey, S.E. and Bisaillon, M. (2009) 'The flavivirus NS5 protein is a true RNA guanylyltransferase that catalyzes a two-step reaction to form the RNA cap structure', *Rna*, 15(12), pp. 2340–2350

Jones, C.T., Patkar, C.G. and Kuhn, R.J. (2005) 'Construction and applications of yellow fever virus replicons', *Virology*, 331(2), pp. 247–259

Jupatanakul, N., Sim, S., Angleró-Rodríguez, Y.I., Souza-Neto, J., Das, S., Poti, K.E., Rossi, S.L., Bergren, N., Vasilakis, N. and Dimopoulos, G. (2017) 'Engineered Aedes aegypti JAK/STAT Pathway-Mediated Immunity to Dengue Virus', *PLoS Neglected Tropical Diseases*, 11(1), pp. 1–24

Kakumani, P.K., Ponia, S.S., S, R.K., Sood, V., Chinnappan, M., Banerjea, A.C., Medigeshi, G.R., Malhotra, P., Mukherjee, S.K. and Bhatnagar, R.K. (2013) 'Role of RNA Interference (RNAi) in Dengue Virus Replication and Identification of NS4B as an RNAi Suppressor', *Journal of Virology*, 87(16), pp. 8870–8883

Kinney, R.M., Butrapet, S., Chang, G.J., Tsuchiya, K.R., Roehrig, J.T., Bhamarapravati, N. and Gubler, D.J. (1997) 'Construction of infectious cDNA clones for dengue 2 virus: strain 16681 and its attenuated vaccine derivative, strain PDK-53', *Virology*, 230(2), pp. 300–308

Kuhn, R., Zhang, W., Rossmann, M., Pletnev, S., Corver, J., Lenches, E., Jones, C., Mukhopadhyay, S., Chipman, P., Strauss, E., Baker, T. and Strauss, J. (2002) 'Structure of Dengue Virus: Implications for Flavivirus Organization, Maturation, and Fusion', *Cell*, 108(5), pp. 717–725

Kümmerer, B.M. (2018) 'Establishment and Application of Flavivirus Replicons', *Advances in Experimental Medicine and Biology*, 1062, pp. 165–173

Kümmerer, B.M., Grywna, K., Gläsker, S., Wieseler, J. and Drosten, C. (2012) 'Construction of an infectious Chikungunya virus cDNA clone and stable insertion of mCherry reporter genes at two different sites', *Journal of General Virology*, 93(PART 9), pp. 1991–1995

Kuno, G. (2010) 'Early history of laboratory breeding of Aedes aegypti (Diptera: Culicidae) focusing on the origins and use of selected strains', *Journal of Medical Entomology*, 47(6), pp. 957–971

Lai, C.J., Zhao, B., Hori, H. and Bray, M. (1991) 'Infectious RNA transcribed from stably cloned full-length cDNA of dengue type 4 virus', *Proceedings of the National Academy of Sciences of the United States of America*, 88(12), pp. 5139–5143

Lambrechts, L. and Scott, T.W. (2009) 'Mode of transmission and the evolution of arbovirus virulence in mosquito vectors', *Proceedings of the Royal Society B: Biological Sciences*, 276(1660), pp. 1369–1378

Lee, W.S., Webster, J.A., Madzokere, E.T., Stephenson, E.B. and Herrero, L.J. (2019) 'Mosquito antiviral defense mechanisms: A delicate balance between innate immunity and persistent viral infection', *Parasites and Vectors*, 12(1), pp. 1–12

Léger, P., Lara, E., Jagla, B., Sismeiro, O., Mansuroglu, Z., Coppée, J.Y., Bonnefoy, E. and Bouloy, M. (2013) 'Dicer-2- and Piwi-Mediated RNA Interference in Rift Valley Fever Virus-Infected Mosquito Cells', *Journal of Virology*, 87(3), pp. 1631–1648

van Leur, S.W., Heunis, T., Munnur, D. and Sanyal, S. (2021) 'Pathogenesis and virulence of flavivirus infections', *Virulence*, 12(1), pp. 2814–2838

Li, A., Wang, W., Wang, Y., Chen, K., Xiao, F., Hu, D., Hui, L., Liu, W., Feng, Y., Li, G., Tan, Q., Liu, Y., Wu, K. and Wu, J. (2020) 'NS5 Conservative Site Is Required for Zika Virus to Restrict the RIG-I Signaling', *Frontiers in Immunology*, 11(February), pp. 1–14

Li, H., Clum, S., You, S., Ebner, K.E. and Padmanabhan, R. (1999) 'The Serine Protease and RNA-Stimulated Nucleoside Triphosphatase and RNA Helicase Functional Domains of Dengue Virus Type 2 NS3 Converge within a Region of 20 Amino Acids', *Journal of Virology*, 73(4), pp. 3108–3116

Lin, C.C., Chou, C.M., Hsu, Y.L., Lien, J.C., Wang, Y.M., Chen, S.T., Tsai, S.C., Hsiao, P.W. and Huang, C.J. (2004) 'Characterization of two mosquito STATs, AaSTAT and CtSTAT: Differential regulation of tyrosine phosphorylation and DNA binding activity by lipopolysaccharide treatment and by Japanese encephalitis virus infection', *Journal of Biological Chemistry*, 279(5), pp. 3308–3317

Lindbo, J.A. and Dougherty, W.G. (2005) 'Plant pathology and RNAi: A brief history', *Annual Review of Phytopathology*, 43, pp. 191–204

Lindenbach, B.D. and Rice, C.M. (1997) 'trans-Complementation of yellow fever virus NS1 reveals a role in early RNA replication', *Journal of Virology*, 71(12), pp. 9608–9617

Lindenbach, B.D. and Rice, C.M. (1999) 'Genetic Interaction of Flavivirus Nonstructural Proteins NS1 and NS4A as a Determinant of Replicase Function', *Journal of Virology*, 73(6), pp. 4611–4621

Liu, J., Liu, Y., Nie, K., Du, S., Qiu, J., Pang, X., Wang, P. and Cheng, G. (2016) 'Flavivirus NS1 protein in infected host sera enhances viral acquisition by mosquitoes', *Nature Microbiology*, 1(9), pp. 1–11

Liu, J., Swevers, L., Kolliopoulou, A. and Smagghe, G. (2019) 'Arboviruses and the challenge to establish systemic and persistent infections in competent mosquito vectors: The interaction with the RNAi mechanism', *Frontiers in Physiology*, 10(JUL), pp. 1–29

Liu, L., Dong, H., Chen, H., Zhang, J., Ling, H., Li, Z., Shi, P.-Y. and Li, H. (2010) 'Flavivirus RNA cap methyltransferase: structure, function, and inhibition', *Front Biol*, 5(4), pp. 286–303

Liu, Q., Rand, T.A., Kalidas, S., Du, F., Kim, H.E., Smith, D.P. and Wang, X. (2003) 'R2D2, a bridge between the initiation and effector steps of the Drosophila RNAi pathway', *Science*, 301(5641), pp. 1921–1925

Lorenz, I.C., Allison, S.L., Heinz, F.X. and Helenius, A. (2002) 'Folding and Dimerization of Tick-Borne Encephalitis Virus Envelope Proteins prM and E in the Endoplasmic Reticulum', *Journal of Virology*, 76(11), pp. 5480–5491

Lorenz, L., Beaty, B.J. and Aitken, T.H.G. (1984) 'The effect of colonization upon Aedes aegypti susceptibility to oral infection with yellow fever virus', *American Journal of Tropical Medicine and Hygiene*, 33(4), pp. 690–694

Lücke, A.C., vom Hemdt, A., Wieseler, J., Fischer, C., Feldmann, M., Rothenfusser, S., Drexler, J.F. and Kümmerer, B.M. (2022) 'High-Throughput Platform for Detection of Neutralizing Antibodies Using Flavivirus Reporter Replicon Particles', *Viruses*, 14(2)

Machado, S.R., Qu, J., Koopman, W.J.H. and Miesen, P. (2022) 'The DEAD-box RNA helicase Dhx15 controls glycolysis and arbovirus replication in Aedes aegypti mosquito cells', *PLoS Pathogens*, 18(11)

Mandl, C.W., Ecker, M., Holzmann, H., Kunz, C. and Heinz, F.X. (1997) 'Infectious cDNA clones of tick-borne encephalitis virus European subtype prototypic strain Neudoerfl and high virulence strain Hypr', *Journal of General Virology*, 78(5), pp. 1049–1057

Matranga, C., Tomari, Y., Shin, C., Bartel, D.P. and Zamore, P.D. (2005) 'Passenger-strand cleavage facilitates assembly of siRNA into Ago2-containing RNAi enzyme complexes', *Cell*, 123(4), pp. 607–620

McElroy, K.L., Girard, Y.A., McGee, C.E., Tsetsarkin, K.A., Vanlandingham, D.L. and Higgs, S. (2008) 'Characterization of the antigen distribution and tissue tropisms of three phenotypically distinct yellow fever virus variants in orally infected Aedes aegypti mosquitoes', *Vector-Borne and Zoonotic Diseases*, 8(5), pp. 675–687

McElroy, K.L., Tsetsarkin, K.A., Vanlandingham, D.L. and Higgs, S. (2005) 'Characterization of an infectious clone of the wild-type yellow fever virus Asibi strain that is able to infect and disseminate in mosquitoes', *Journal of General Virology*, 86(6), pp. 1747–1751

McElroy, K.L., Tsetsarkin, K.A., Vanlandingham, D.L. and Higgs, S. (2006a) 'Manipulation of the yellow fever virus non-structural genes 2A and 4B and the 3′non-coding region to evaluate genetic determinants of viral dissemination from the Aedes Aegypti midgut', *American Journal of Tropical Medicine and Hygiene*, 75(6), pp. 1158–1164

McElroy, K.L., Tsetsarkin, K.A., Vanlandingham, D.L. and Higgs, S. (2006b) 'Role of the yellow fever virus structural protein genes in viral dissemination from the Aedes aegypti mosquito midgut', *Journal of General Virology*, 87(10), pp. 2993–3001

McGee, C.E., Tsetsarkin, K.A., Guy, B., Lang, J., Plante, K., Vanlandingham, D.L. and Higgs, S. (2011) 'Stability of yellow fever virus under recombinatory pressure as compared with chikungunya virus', *PLoS ONE*, 6(8)

Miesen, P., Ivens, A., Buck, A.H. and van Rij, R.P. (2016) 'Small RNA Profiling in Dengue Virus 2-Infected Aedes Mosquito Cells Reveals Viral piRNAs and Novel Host miRNAs', *PLoS Neglected Tropical Diseases*, 10(2), pp. 1–22

Miesen, P., Joosten, J. and van Rij, R.P. (2016) 'PIWIs Go Viral: Arbovirus-Derived piRNAs in Vector Mosquitoes', *PLoS Pathogens*, 12(12), pp. 1–17

Miller, B. and Adkins, A. (1988) 'Biological characterization of plaque-size variants of yellow fever virus in mosquitoes and mice', *Acta Virologica*, 32(3), pp. 227–234

Miller, S., Kastner, S., Krijnse-Locker, J., Bühler, S. and Bartenschlager, R. (2007) 'The non-structural protein 4A of dengue virus is an integral membrane protein inducing membrane alterations in a 2K-regulated manner', *Journal of Biological Chemistry*, 282(12), pp. 8873–8882

Moon, S.L., Dodd, B.J.T., Brackney, D.E., Wilusz, C.J., Ebel, G.D. and Wilusz, J. (2015) 'Flavivirus sfRNA suppresses antiviral RNA interference in cultured cells and mosquitoes and directly interacts with the RNAi machinery', *Virology*, 485, pp. 322–329

Morazzani, E.M., Wiley, M.R., Murreddu, M.G., Adelman, Z.N. and Myles, K.M. (2012) 'Production of virus-derived ping-pong-dependent piRNA-like small RNAs in the mosquito soma', *PLoS Pathogens*, 8(1)

Mukhopadhyay, S., Kuhn, R.J. and Rossmann, M.G. (2005) 'A structural perspective of the Flavivirus life cycle', *Nature Reviews Microbiology*, 3(1), pp. 13–22

Mutso, M., Saul, S., Rausalu, K., Susova, O., Žusinaite, E., Mahalingam, S. and Merits, A. (2017) 'Reverse genetic system, genetically stable reporter viruses and packaged subgenomic replicon based on a Brazilian zika virus isolate', *Journal of General Virology*, 98(11), pp. 2712–2724

Netzband, R. and Pager, C.T. (2020) 'Epitranscriptomic marks: Emerging modulators of RNA virus gene expression', *Wiley Interdisciplinary Reviews: RNA*, 11(3), pp. 1–25

Okamura, K., Balla, S., Martin, R., Liu, N. and Lai, E. (2008) 'Two distinct mechanisms generate endogenous siRNAs from bidirectional transcription in Drosophila melanogaster', *Nat Struct Mol Biol*, 15(6), pp. 581–590

Ong, R.Y., Lum, F.M. and Ng, L.F.P. (2014) 'The fine line between protection and pathology in neurotropic flavivirus and alphavirus infections', *Future Virology*, 9(3), pp. 313–330

Pan, X., Zhou, G., Wu, J., Bian, G., Lu, P., Raikhel, A.S. and Xi, Z. (2012) 'Wolbachia induces reactive oxygen species (ROS)-dependent activation of the Toll pathway to control dengue virus in the mosquito Aedes aegypti', *Proceedings of the National Academy of Sciences of the United States of America*, 109(1)

Paradkar, P.N., Duchemin, J.B., Rodriguez-Andres, J., Trinidad, L. and Walker, P.J. (2015) 'Cullin4 Is Pro-Viral during West Nile Virus Infection of Culex Mosquitoes', *PLoS Pathogens*, 11(9), pp. 1–21

Paradkar, P.N., Duchemin, J.B., Voysey, R. and Walker, P.J. (2014) 'Dicer-2-Dependent Activation of Culex Vago Occurs via the TRAF-Rel2 Signaling Pathway', *PLoS Neglected Tropical Diseases*, 8(4)

Paradkar, P.N., Trinidad, L., Voysey, R., Duchemin, J.B. and Walker, P.J. (2012) 'Secreted Vago restricts West Nile virus infection in Culex mosquito cells by activating the Jak-STAT pathway', *Proceedings of the National Academy of Sciences of the United States of America*, 109(46), pp. 18915–18920

Patterson, E.I., Khanipov, K., Rojas, M.M., Kautz, T.F., Rockx-brouwer, D., Golovko, G., Albayrak, L., Fofanov, Y. and Forrester, N.L. (2018) 'Mosquito bottlenecks alter viral mutant swarm in a tissue and time-dependent manner with contraction and expansion of variant positions and diversity', *Virus Evol*, 15(4), pp. 1–11

Peleg, J. (1968) 'Growth of Arboviruses in Primary Tissue Culture of Aedes Aegypti Embryos', *The American Journal of Tropical Medicine and Hygiene*, 17(2), pp. 219–223

Pfaffl, M.W. and Bustin, S.A. (2004) 'Quantification strategies in real-time PCR', *The Real-Time PCR Encyclopedia A–Z of Quantitative PCR*, pp. 87–112

Pijlman, G.P. (2014) 'Flavivirus RNAi suppression: Decoding non-coding RNA', *Current Opinion in Virology*, 7(1), pp. 55–60

Pompon, J., Manuel, M., Ng, G.K., Wong, B., Shan, C., Manokaran, G., Soto-Acosta, R., Bradrick, S.S., Ooi, E.E., Missé, D., Shi, P.Y. and Garcia-Blanco, M.A. (2017) 'Dengue subgenomic flaviviral RNA disrupts immunity in mosquito salivary glands to increase virus transmission', *PLoS Pathogens*, 13(7), pp. 1–27

Postler, T.S., Beer, M., Blitvich, B.J., Bukh, J., de Lamballerie, X., Drexler, J.F., Imrie, A., Kapoor, A., Karganova, G.G., Lemey, P., Lohmann, V., Simmonds, P., Smith, D.B., Stapleton, J.T. and Kuhn, J.H. (2023) 'Renaming of the genus Flavivirus to Orthoflavivirus and extension of binomial species names within the family Flaviviridae', *Archives of Virology*, 168(9), pp. 1–7

Qiu, Y., Xu, Y.P., Wang, M., Miao, M., Zhou, H., Xu, J., Kong, J., Zheng, D., Li, R.T., Zhang, R.R., Guo, Y., Li, X.F., Cui, J., Qin, C.F. and Zhou, X. (2020) 'Flavivirus induces and antagonizes antiviral RNA interference in both mammals and mosquitoes', *Science Advances*, 6(6), pp. 1–14

Ramanathan, A., Robb, G.B. and Chan, S.H. (2016) 'mRNA capping: Biological functions and applications', *Nucleic Acids Research*, 44(16), pp. 7511–7526

Ramirez, J.L. and Dimopoulos, G. (2010) 'The Toll immune signaling pathway control conserved anti-dengue defenses across diverse Ae. aegypti strains and against multiple dengue virus serotypes', *Developmental and Comparative Immunology*, 34(6), pp. 625–629

Randall, R.E. and Griffin, D.E. (2017) 'Within host RNA virus persistence: mechanisms and consequences', *Current Opinion in Virology*, 23(August), pp. 35–42

Ray, D., Shah, A., Tilgner, M., Guo, Y., Zhao, Y., Dong, H., Deas, T.S., Zhou, Y., Li, H. and Shi, P.-Y. (2006) 'West Nile Virus 5′-Cap Structure Is Formed by Sequential Guanine N-7 and Ribose 2′-O Methylations by Nonstructural Protein 5', *Journal of Virology*, 80(17), pp. 8362–8370

Rehwinkel, J. and Gack, M.U. (2020) 'RIG-I-like receptors: their regulation and roles in RNA sensing', *Nature Reviews Immunology*, 20(9), pp. 537–551

Rice, C., Grakoui, A., Galler, R. and Chambers, T. (1989) 'Transcription of infectious yellow fever RNA from full-length cDNA templates produced by in vitro ligation', *The new biologist*, 1(3), pp. 285–296

Rice, C.M., Lenches, E.M., Eddy, S.R., Shin, S.J., Sheets, R.L. and Strauss, J.H. (1985) 'Nucleotide sequence of yellow fever virus: implications for flavivirus gene expression and evolution', *Science*, 229(4715), pp. 726–733

Riedel, B. and Brown, D.T. (1979) 'Novel antiviral activity found in the media of Sindbis virus-persistently infected mosquito (Aedes albopictus) cell cultures', *Journal of Virology*, 29(1), pp. 51–60

Rückert, C. and Ebel, G.D. (2018) 'How Do Virus–Mosquito Interactions Lead to Viral Emergence?', *Trends in Parasitology*, 34(4), pp. 310–321

Ruggieri, A., Helm, M. and Chatel-Chaix, L. (2021) 'An epigenetic "extreme makeover": the methylation of flaviviral RNA (and beyond)', *RNA Biology*, 18(5), pp. 696–708

Russ, A., Wittmann, S., Tsukamoto, Y., Herrmann, A., Deutschmann, J., Lagisquet, J., Ensser, A., Kato, H. and Gramberg, T. (2022) 'Nsp16 shields SARS–CoV-2 from efficient MDA5 sensing and IFIT1-mediated restriction', *EMBO reports*, 23(12), pp. 1–15

Russell, T.A., Ayaz, A., Davidson, A.D., Fernandez-Sesma, A. and Maringer, K. (2020) 'Imd pathway-specific immune assays reveal NF-κB stimulation by viral RNA PAMPs in Aedes aegypti Aag2 cells', *PLoS Neglected Tropical Diseases*, 15(2), pp. 1–23

Sacchetto, L., Drumond, B.P., Han, B.A., Nogueira, M.L. and Vasilakis, N. (2020) 'Re-emergence of yellow fever in the neotropics - Quo vadis?', *Emerging Topics in Life Sciences*, 4(4), pp. 411–422

Saeedi, B.J. and Geiss, B.J. (2013) 'Regulation of flavivirus RNA synthesis and capping', *Wiley Interdisciplinary Reviews: RNA*, 4(6), pp. 723–735

Samuel, G.H., Pohlenz, T., Dong, Y., Coskun, N., Adelman, Z.N., Dimopoulos, G. and Myles, K.M. (2023) 'RNA interference is essential to modulating the pathogenesis of mosquito-borne viruses in the yellow fever mosquito Aedes aegypti', *Proceedings of the National Academy of Sciences of the United States of America*, 120(11)

Samuel, G.H., Wiley, M.R., Badawi, A., Adelman, Z.N. and Myles, K.M. (2016) 'Yellow fever virus capsid protein is a potent suppressor of RNA silencing that binds double-stranded RNA', *Proceedings of the National Academy of Sciences of the United States of America*, 113(48), pp. 13863–13868

Sang, W.S., Kokoza, V., Bian, G., Cheon, H.M., Yu, J.K. and Raikhel, A.S. (2005) 'REL1, a homologue of Drosophila dorsal, regulates toll antifungal immune pathway in the female mosquito Aedes aegypti', *Journal of Biological Chemistry*, 280(16), pp. 16499–16507

Santana-Román, M., Maycotte, P., Uribe-Carvajal, S., Uribe-Alvarez, C., Alvarado-Medina, N., Khan, M., Siddiqui, A. and Pando-Robles, V. (2021) 'Monitoring Mitochondrial Function in Aedes albopictus C6/36 Cell Line during Dengue Virus Infection', *Insects*, 12(10)

Saucereau, Y., Wilson, T.H., Tang, M.C.K., Moncrieffe, M.C., Hardwick, S.W., Chirgadze, D.Y., Soares, S.G., Marcaida, M.J., Gay, N.J. and Gangloff, M. (2022) 'Structure and dynamics of Toll immunoreceptor activation in the mosquito Aedes aegypti', *Nature communications*, 13(1), p. 5110

van der Schaar, H.M., Rust, M.J., Chen, C., van der Ende-Metselaar, H., Wilschut, J., Zhuang, X. and Smit, J.M. (2008) 'Dissecting the Cell Entry Pathway of Dengue Virus by Single-Particle Tracking in Living Cells', *PLoS Pathogens*, 4(12)

Scherer, C., Knowles, J., Sreenu, V.B., Fredericks, A.C., Fuss, J., Maringer, K., Fernandez-Sesma, A., Merits, A., Varjak, M., Kohl, A. and Schnettler, E. (2021) 'An aedes aegypti-derived ago2 knockout cell line to investigate arbovirus infections', *Viruses*, 13(6), pp. 1–19

Schmid, B., Rinas, M., Ruggieri, A., Acosta, E.G., Bartenschlager, M., Reuter, A., Fischl, W., Harder, N., Bergeest, J.P., Flossdorf, M., Rohr, K., Höfer, T. and Bartenschlager, R. (2015) 'Live Cell Analysis and Mathematical Modeling Identify Determinants of Attenuation of Dengue Virus 2'-O-Methylation Mutant', *PLoS Pathogens*, 11(12), pp. 1–36

Schnettler, E., Donald, C.L., Human, S., Watson, M., Siu, R.W.C., McFarlane, M., Fazakerley, J.K., Kohl, A. and Fragkoudis, R. (2013) 'Knockdown of piRNA pathway proteins results in enhanced semliki forest virus production in mosquito cells', *Journal of General Virology*, 94(PART7), pp. 1680–1689

Schnettler, E., Sterken, M.G., Leung, J.Y., Metz, S.W., Geertsema, C., Goldbach, R.W., Vlak, J.M., Kohl, A., Khromykh, A.A. and Pijlman, G.P. (2012) 'Noncoding Flavivirus RNA Displays RNA Interference Suppressor Activity in Insect and Mammalian Cells', *Journal of Virology*, 86(24), pp. 13486–13500

Schuberth-Wagner, C., Ludwig, J., Bruder, A.K., Herzner, A.M., Zillinger, T., Goldeck, M., Schmidt, T., Schmid-Burgk, J.L., Kerber, R., Wolter, S., Stümpel, J.P., Roth, A., Bartok, E., Drosten, C., Coch, C., Hornung, V., Barchet, W., Kümmerer, B.M., Hartmann, G. and Schlee, M. (2015) 'A Conserved Histidine in the RNA Sensor RIG-I Controls Immune Tolerance to N1-2'O-Methylated Self RNA', *Immunity*, 43(1), pp. 41–51

Schuster, S., Miesen, P. and van Rij, R.P. (2019) 'Antiviral RNAi in insects and mammals: Parallels and differences', *Viruses*, 11(5)

Scott, J.C., Brackney, D.E., Campbell, C.L., Bondu-Hawkins, V., Hjelle, B., Ebel, G.D., Olson, K.E. and Blair, C.D. (2010) 'Comparison of dengue virus type 2-specific small RNAs from RNA interference-competent and - incompetent mosquito cells', *PLoS Neglected Tropical Diseases*, 4(10)

Serrato-Salas, J., Izquierdo-Sánchez, J., Argüello, M., Conde, R., Alvarado-Delgado, A. and Lanz-Mendoza, H. (2018) 'Aedes aegypti antiviral adaptive response against DENV-2', *Developmental and Comparative Immunology*, 84, pp. 28–36

Shan, C., Xie, X., Muruato, A.E., Rossi, S.L., Roundy, C.M., Azar, S.R., Yang, Y., Tesh, R.B., Bourne, N., Barrett, A.D., Vasilakis, N., Weaver, S.C. and Shi, P.Y. (2016) 'An Infectious cDNA Clone of Zika Virus to Study Viral Virulence, Mosquito Transmission, and Antiviral Inhibitors', *Cell Host and Microbe*, 19(6), pp. 891–900

Sheehan, G., Farrell, G. and Kavanagh, K. (2020) 'Immune priming: the secret weapon of the insect world', *Virulence*, 11(1), pp. 238–246

Shustov, A. V. and Frolov, I. (2010) 'Efficient, trans-complementing packaging systems for chimeric, pseudoinfectious dengue 2/yellow fever viruses', *Virology*, 400(1), pp. 8–17

Sim, S. and Dimopoulos, G. (2010) 'Dengue virus inhibits immune responses in Aedes aegypti cells', *PLoS ONE*, 5(5)

Sim, S., Jupatanakul, N. and Dimopoulos, G. (2014) 'Mosquito immunity against arboviruses', *Viruses*, 6(11), pp. 4479–4504

Simmonds, P., Becher, P., Bukh, J., Gould, E.A., Meyers, G., Monath, T., Muerhoff, S., Pletnev, A., Rico-Hesse, R., Smith, D.B., Stapleton, J.T. and ICTV Report Consortium (2017) 'ICTV virus taxonomy profile: Flaviviridae', *Journal of General Virology*, 98(1), pp. 2–3

Singh, K.R.P. (1967) 'Cell cultures derived from larvae of Aedes Albopictus (Skuse) and Aedes Aegypti (L.)', *Source: Current Science*, 36(19), pp. 506–508

Siomi, M.C., Sato, K., Pezic, D. and Aravin, A.A. (2011) 'PIWI-interacting small RNAs: The vanguard of genome defence', *Nature Reviews Molecular Cell Biology*, 12(4), pp. 246–258

Slonchak, A., Hugo, L.E., Freney, M.E., Hall-Mendelin, S., Amarilla, A.A., Torres, F.J., Setoh, Y.X., Peng, N.Y.G., Sng, J.D.J., Hall, R.A., van den Hurk, A.F., Devine, G.J. and Khromykh, A.A. (2020) 'Zika virus noncoding RNA suppresses apoptosis and is required for virus transmission by mosquitoes', *Nature Communications*, 11(1), pp. 1–14

Slonchak, A., Hussain, M., Torres, S., Asgari, S. and Khromykh, A.A. (2014) 'Expression of Mosquito MicroRNA Aae-miR-2940-5p Is Downregulated in Response to West Nile Virus Infection To Restrict Viral Replication', *Journal of Virology*, 88(15), pp. 8457–8467

Slonchak, A., Parry, R., Pullinger, B., Sng, J.D.J., Wang, X., Buck, T.F., Torres, F.J., Harrison, J.J., Colmant, A.M.G., Hobson-Peters, J., Hall, R.A., Tuplin, A. and Khromykh, A.A. (2022) 'Structural analysis of 3'UTRs in insect flaviviruses reveals novel determinants of sfRNA biogenesis and provides new insights into flavivirus evolution', *Nature Communications*, 13(1), pp. 1–16

Smit, J.M., Moesker, B., Rodenhuis-Zybert, I. and Wilschut, J. (2011) 'Flavivirus cell entry and membrane fusion', *Viruses*, 3(2), pp. 160–171

Souza-Neto, J.A., Sim, S. and Dimopoulos, G. (2009) 'An evolutionary conserved function of the JAK-STAT pathway in anti-dengue defense', *Proceedings of the National Academy of Sciences of the United States of America*, 106(42), pp. 17841–17846

Stapleton, J.T., Foung, S., Muerhoff, A.S., Bukh, J. and Simmonds, P. (2011) 'The GB viruses: A review and proposed classification of GBV-A, GBV-C (HGV), and GBV-D in genus Pegivirus within the family Flaviviridae', *Journal of General Virology*, 92(2), pp. 233–246

Stoker, M. and Macpherson, I. (1964) 'Syrian hamster fibroblast cell line BHK21 and its derivatives', *Nature*, 203(4952), pp. 1355–1357

Stokes, A. and Bauer, J.H. (1928) 'Transmission of yellow fever to Macacas rhesus, preliminary note', *JAMA*, 90(4), pp. 253–254

Tabachnick, W.J., Wallis, G.P., Aitken, T.H.G., Miller, B.R., Amato, G.D., Lorenz, L., Powell, J.R. and Beaty, B.J. (1985) 'Oral infection of Aedes aegypti with yellow fever virus: Geographic variation and genetic considerations', *American Journal of Tropical Medicine and Hygiene*, 34(6), pp. 1219–1224

Theiler, M. and Smith, H. (1937) 'THE EFFECT OF PROLONGED CULTIVATION IN VITRO UPON THE PATHOGENICITY OF YELLOW FEVER VIRUS', *J Exp Med*, 65(6), pp. 767–786

Tikhe, C. V. and Dimopoulos, G. (2021) 'Mosquito antiviral immune pathways', *Developmental and Comparative Immunology*, 116(December 2020)

Tomari, Y., Matranga, C., Haley, B., Martinez, N. and Zamore, P.D. (2004) 'A protein sensor for siRNA asymmetry', *Science*, 306(5700), pp. 1377–1380

Tscherne, D.M., Evans, M.J., von Hahn, T., Jones, C.T., Stamataki, Z., McKeating, J.A., Lindenbach, B.D. and Rice, C.M. (2007) 'Superinfection Exclusion in Cells Infected with Hepatitis C Virus', *Journal of Virology*, 81(8), pp. 3693–3703

Tsukamoto, Y., Hiono, T., Yamada, S., Matsuno, K., Faist, A., Claff, T., Hou, J., Namasivayam, V., vom Hemdt, A., Sugimoto, S., Ng, J.Y., Christensen, M.H., Tesfamariam, Y.M., Wolter, S., Juranek, S., Zillinger, T., Bauer, S., Hirokawa, T., Schmidt, F.I., Kochs, G., Shimojima, M., Huang, Y.-S., Pichlmair, A., Kümmerer, B.M., Sakoda, Y., Schlee, M., Brunotte, L., Müller, C., Igarashi, M. and Kato, H. (2023) 'Inhibition of cellular RNA methyltransferase abrogates influenza virus capping and replication', *Science*, 379(6632), pp. 586–591

Umareddy, I., Tang, K.F., Vasudevan, S.G., Devi, S., Hibberd, M.L. and Gu, F. (2008) 'Dengue virus regulates type I interferon signalling in a strain-dependent manner in human cell lines', *Journal of General Virology*, 89(12), pp. 3052–3062

Vargas, V., Cime-Castillo, J. and Lanz-Mendoza, H. (2020) 'Immune priming with inactive dengue virus during the larval stage of Aedes aegypti protects against the infection in adult mosquitoes', *Scientific Reports*, 10(1), pp. 1–10

Varjak, M., Donald, C.L., Mottram, T.J., Sreenu, V.B., Merits, A., Maringer, K., Schnettler, E. and Kohl, A. (2017) 'Characterization of the Zika virus induced small RNA response in Aedes aegypti cells', *PLoS Neglected Tropical Diseases*, 11(10), pp. 1–18

Varjak, M., Leggewie, M. and Schnettler, E. (2018) 'The antiviral piRNA response in mosquitoes?', *Journal of General Virology*, 99(12), pp. 1551–1562

Varjak, M., Maringer, K., Watson, M., Sreenu, V.B., Fredericks, A.C., Pondeville, E., Donald, C.L., Sterk, J., Kean, J., Vazeille, M., Failloux, A. and Kohl, A. (2017) 'Aedes aegypti Piwi4 Is a Noncanonical PIWI Protein Involved in Antiviral Responses', *American Society for Microbiology*, 2(3), pp. 1–16

Wang, S. and Beerntsen, B.T. (2015) 'Functional implications of the peptidoglycan recognition proteins in the immunity of the yellow fever mosquito, Aedes aegypti', *Insect Molecular Biology*, 24(3), pp. 293–310

Wang, Y., Jin, B., Liu, P., Li, J., Chen, X. and Gu, J. (2018) 'piRNA Profiling of Dengue Virus Type 2-Infected Asian Tiger Mosquito and Midgut Tissues', *Viruses*, 10(4), pp. 1–20

Weaver, S.C. and Barrett, A.D.T. (2004) 'Transmission cycles, host range, evolution and emergence of arboviral disease', *Nature Reviews Microbiology*, 2(10), pp. 789–801

Weaver, S.C., Forrester, N.L., Liu, J. and Vasilakis, N. (2021) 'Population bottlenecks and founder effects: implications for mosquito-borne arboviral emergence', *Nature Reviews Microbiology*, 19(3), pp. 184–195

Welsch, S., Miller, S., Romero-Brey, I., Merz, A., Bleck, C.K.E., Walther, P., Fuller, S.D., Antony, C., Krijnse-Locker, J. and Bartenschlager, R. (2009) 'Composition and Three-Dimensional Architecture of the Dengue Virus Replication and Assembly Sites', *Cell Host and Microbe*, 5(4), pp. 365–375

Wengler, Gerd and Wengler, Gisela (1981) 'Terminal sequences of the genome and replicatioe-form RNA of the flavivirus west nile virus: absence of poly(A) and possible role in RNA replication', *Virology*, 113(2), pp. 544–555

Westaway, E., Brinton, M., Gaidamovich, Sy., Horzinek, M., Igarashi, A., Kääriäinen, L., Lvov, D., Porterfield, J., Russell, P. and Trent, D. (1985) 'Flaviviridae', *Intervirology*, 24(4), pp. 189–192

Whitman, L. (1939) 'Failure of Aedes aegypti to transmit Yellow Fever Cultured Virus (17D)', *American Journal of Tropical Medicine*, 19(1), pp. 19–26

Widman, D.G., Young, E., Yount, B.L., Plante, K.S., Gallichotte, E.N., Carbaugh, D.L., Peck, K.M., Plante, J., Swanstrom, J., Heise, M.T., Lazear, H.M. and Baric, R.S. (2017) 'A reverse genetics platform that spans the Zika virus family tree', *mBio*, 8(2), pp. 1–15

Wirtz, R.A., Sattabongkot, J., Hall, T., Burkot, T.R. and Rosenberg, R. (1992) 'Development and evaluation of an enzyme-linked immunosorbent assay for Plasmodium vivax-VK247 sporozoites.', *Journal of medical entomology*, 29(5), pp. 854–857

Wu, X., Pan, Y., Huang, J., Huang, S., Wang, M., Chen, S., Liu, M., Zhu, D., Zhao, X., Wu, Y., Yang, Q., Zhang, S., Ou, X., Zhang, L., Liu, Y., Yu, Y., Gao, Q., Mao, S., Sun, D., Tian, B., Yin, Z., Jing, B., Cheng, A. and Jia, R. (2022) 'The substitution at residue 218 of the NS5 protein methyltransferase domain of Tembusu virus impairs viral replication and translation and may triggers RIG-I-like receptor signaling', *Poultry Science*, 101(9)

Xi, Z., Ramirez, J.L. and Dimopoulos, G. (2008) 'The Aedes aegypti toll pathway controls dengue virus infection', *PLoS Pathogens*, 4(7)

Xie, X., Muruato, A., Lokugamage, K.G., Narayanan, K., Zhang, X., Zou, J., Liu, J., Schindewolf, C., Bopp, N.E., Aguilar, P. V., Plante, K.S., Weaver, S.C., Makino, S., LeDuc, J.W., Menachery, V.D. and Shi, P.Y. (2020) 'An Infectious cDNA Clone of SARS-CoV-2', *Cell Host and Microbe*, 27(5), pp. 841–848

Yang, J.S. and Lai, E.C. (2011) 'Alternative miRNA Biogenesis Pathways and the Interpretation of Core miRNA Pathway Mutants', *Molecular Cell*, 43(6), pp. 892–903

Yang, Z., Ebright, Y.W., Yu, B. and Chen, X. (2006) 'HEN1 recognizes 21-24 nt small RNA duplexes and deposits a methyl group onto the 2′ OH of the 3′ terminal nucleotide', *Nucleic Acids Research*, 34(2), pp. 667–675

Zhang, G., Hussain, M., O'Neill, S.L. and Asgari, S. (2013) 'Wolbachia uses a host microRNA to regulate transcripts of a methyltransferase, contributing to dengue virus inhibition in Aedes aegypti', *Proceedings of the National Academy of Sciences of the United States of America*, 110(25), pp. 10276–10281

Zhou, Y., Ray, D., Zhao, Y., Dong, H., Ren, S., Li, Z., Guo, Y., Bernard, K.A., Shi, P.-Y. and Li, H. (2007) 'Structure and Function of Flavivirus NS5 Methyltransferase', *Journal of Virology*, 81(8), pp. 3891–3903

Züst, R., Dong, H., Li, X.F., Chang, D.C., Zhang, B., Balakrishnan, T., Toh, Y.X., Jiang, T., Li, S.H., Deng, Y.Q., Ellis, B.R., Ellis, E.M., Poidinger, M., Zolezzi, F., Qin, C.F., Shi, P.Y. and Fink, K. (2013) 'Rational Design of a Live Attenuated Dengue Vaccine: 2′-O-Methyltransferase Mutants Are Highly Attenuated and Immunogenic in Mice and Macaques', *PLoS Pathogens*, 9(8)

9. Acknowledgment

The time has come to express my deepest appreciation to everyone who supported me during my Ph.D.

First of all, I would like to thank Dr. Beate Kümmerer for the exciting topic and the opportunity to work on my thesis in her lab. I would not have been able to complete this thesis without her guidance, patience, and endless conversations we had together.

Further, I would like to acknowledge the other members of my dissertation committee, Prof. Dr. Martin Schlee, Prof. Dr. Anna Maria Eis-Hübinger, and Prof. Dr. Stefanie Becker, for devoting their time to review this thesis.

I am thankful to Prof. Dr. Hendrik Streeck for the opportunity to complete my thesis at the Institute of Virology.

I am thankful for all the great collaborators, Prof. Dr. Hiroki Kato, Dr. Yuta Tsukamoto, Prof. Dr. Florian I. Schmidt, Lea-Marie Jenster, Prof. Dr. Martin Pfeffer, Dr. Yauhen Karliuk, and Dr. Martin Schlee I was allowed to work with. A special word of gratitude goes to Katrin Ciupka, who started the mosquito project with me and has shown friendship and support during the whole time.

I am also grateful for the great team, colleagues, and friends I worked with. Thank you, Janett, Johanna, Hannah, Arlen, Philipp, Franzi, and Alex, for your relentless support during work (and breaks). Every moment with you was noteworthy, and I highly appreciate the time and laughter we shared. I want to emphasize my gratitude to Hannah and Janett: Hannah rocked many experiments for me (or sometimes with me). Her optimistic nature cheered me up even on the most stressful days. Janett taught me every minor and major skill in the lab, was always patient with me, discussed every result, and performed priceless happy dances after a successful experiment.

I am deeply thankful to my family and friends. Especially Mama, Anke, Ansgar, Natalie, and Eric were always there for me and listened carefully when I talked about viruses with and without hats. Thank you, Mama, for being who you are and always having my back. This thesis would not have been possible without your support. Of course, I don’t want to neglect the little ones in my family - even if they don’t understand it, they are the best

distraction. Your laughter is the warmest, and nothing could take my mind off work better than you.

Finally, I would like to thank Fabian. Thank you for your love, for listening to me, for drying my tears, and for laughing with me. Thank you for always being at my side no matter what.

10. Appendix

10.1 Supplementary figures and tables

Table S 1: Summary of differences between pYFV-17D and pYFV-Asibi used in this thesis. Amino acids in bold indicate aa exchanges between YFV-17D and YFV-Asibi.

Protein	Position	nt exchange		aa in the respective virus	
		YFV-17D	YFV-Asibi	YFV-17D	YFV-Asibi
C	304	A	G	T	T
	370	C	T	V	V
prM	854	T	C	**F**	**L**
	883	G	A	T	T
E	1127	A	G	**R**	**G**
	1140	T	C	V	A
	1482	T	C	V	A
	1491	T	C	**I**	**T**
	1572	C	A	**T**	**K**
	1750	T	C	T	T
	1819	T	C	S	S
	1870	A	G	**I**	**M**
	1887	T	C	**F**	**S**
	1946	T	C	**S**	**P**
	1965	G	A	**R**	**K**
	2112	G	C	**R**	**T**
	2219	A	G	**T**	**A**
	2356	T	C	L	L
NS1	2687	T	C	**F**	**L**
	2704	G	A	V	V
	3274	A	G	E	E
	3371	G	A	**V**	**I**
NS2A	3613	A	G	V	V
	3860	G	A	**V**	**M**
	4007	G	A	**A**	**T**
	4013	T	C	**F**	**L**
	4022	G	A	**A**	**T**
	4054	T	C	**N**	**N**
	4056	T	C	**F**	**S**
NS2B	4289	C	A	**L**	**I**
	4387	G	A	G	G
	4505	C	A	**L**	**I**
	4507	C	T	L	L

Table S 1: Summary of differences between pYFV-17D and pYFV-Asibi used in this thesis (continued).

Protein	Position	nt exchange		aa in the respective virus	
		YFV-17D	YFV-Asibi	YFV-17D	YFV-Asibi
NS3	4612	C	T	I	I
	4873	G	T	A	A
	5153	G	A	**V**	**I**
	5194	C	T	F	F
	5362	T	C	A	A
	5431	T	C	I	I
	5473	T	C	A	A
	6013	T	C	P	P
	6023	A	G	**N**	**D**
NS4A	6448	T	G	A	A
	6529	C	T	F	F
	6758	G	A	**V**	**I**
2K	6829	C	T	D	D
	6876	C	T	**A**	**V**
NS4B	7171	G	A	**M**	**I**
	7571	A	C	R	R
	7580	C	T	**H**	**Y**
NS5	7642	C	T	S	S
	7701	G	A	**R**	**Q**
	7945	T	C	F	F
	8008	C	T	I	I
	8629	T	C	Y	Y
	9605	G	A	**D**	**N**
	10142	A	G	**K**	**E**
	10243	A	G	L	L
	10285	C	T	Y	Y
	10312	G	A	R	R
	10338	T	C	**L**	**P**
3’UTR	10367	C	T	-	-
	10418	C	T	-	-
	10550	C	T	-	-
	10800	A	G	-	-
	10847	C	A	-	-

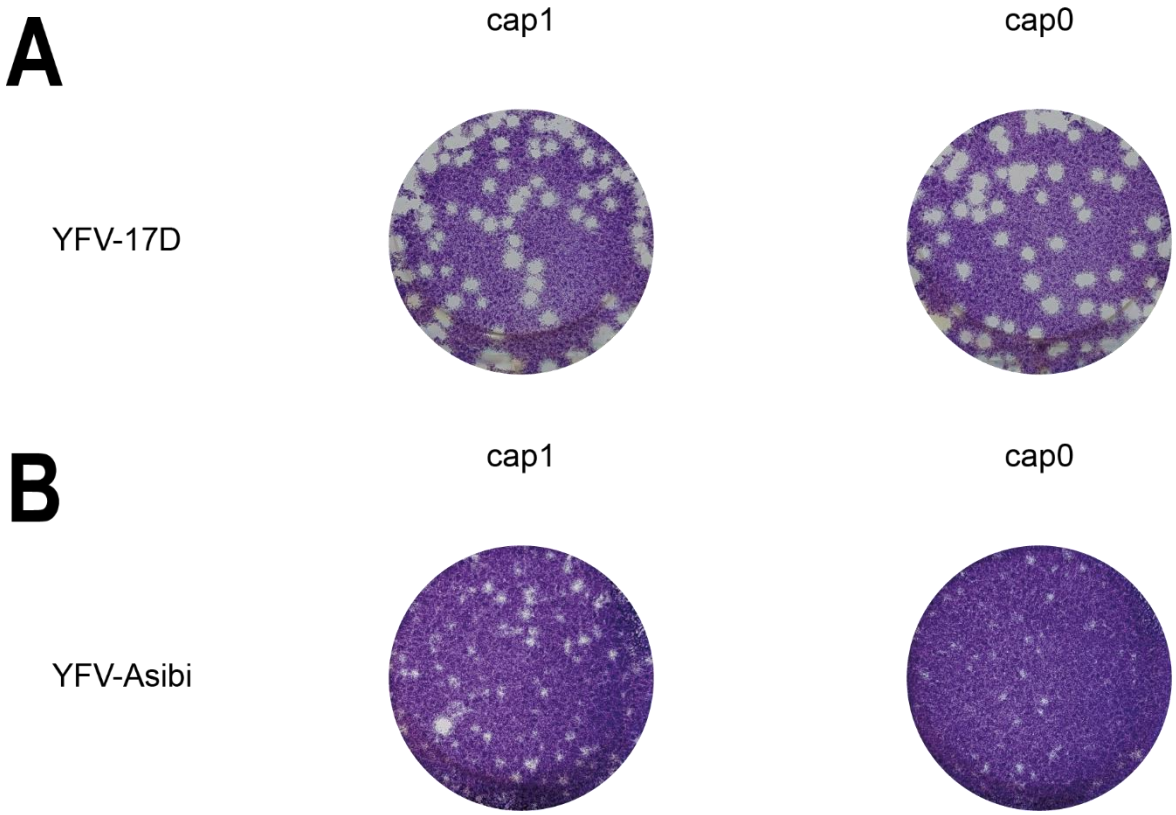

Figure S 1: Plaque morphology of YFV-17D and –Asibi cap1 and cap0.
A) Plaque phenotypes of YFV-17D cap1 and cap0 after passaging the virus once in BHK-J/21 cells. B) Plaque phenotypes of YFV-Asibi cap1 and cap0 after performing an infectious center assay in BHK-21/J cells. At 3 days post-infection, cells were fixed and stained by crystal violet.

10.2 Schematic illustration of constructed plasmids

pYFV-17D cap0

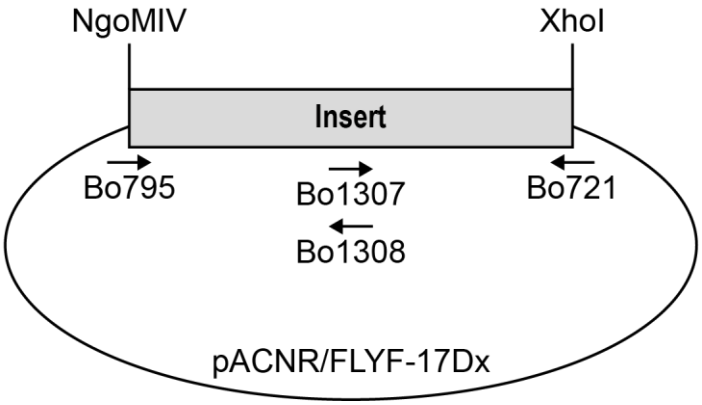

Construct	Insert	Donor/Template	Vector
pYFV-17D cap0	NS5-E218A	pACNR/FLYF-17Dx	pACNR/FLYF-17Dx

pYFVR cap1 (mCherry)

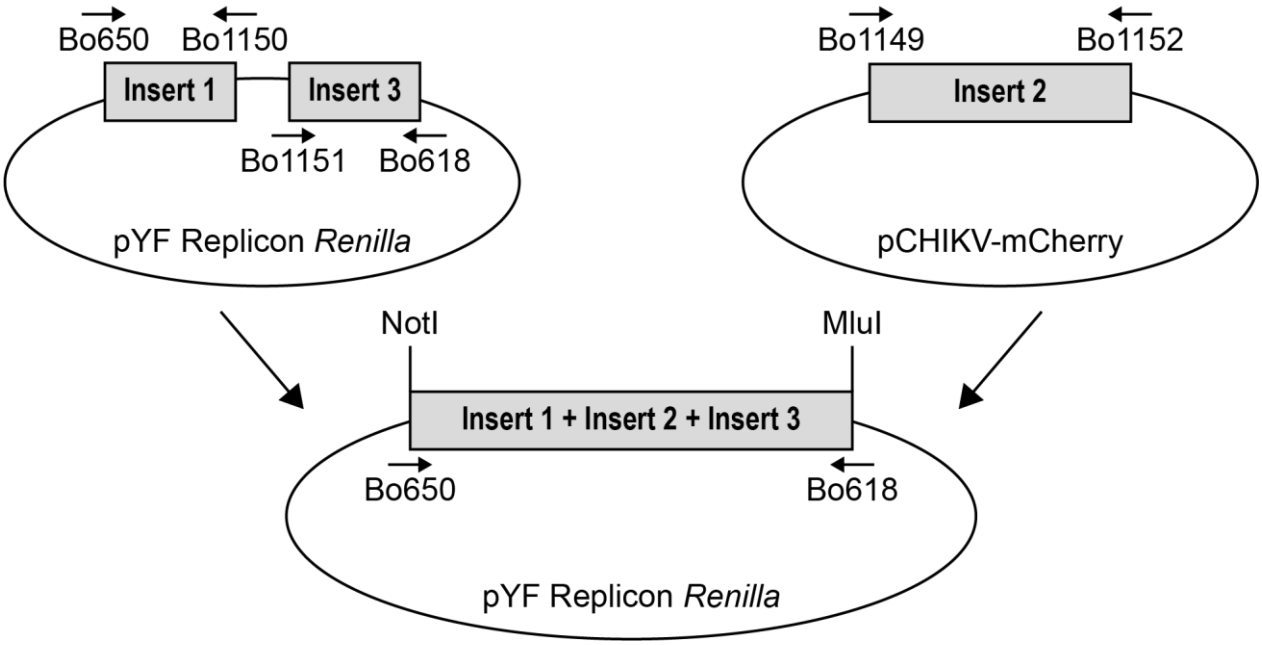

Construct	Insert	Donor/Template	Vector
pYFVR cap1 (mCherry)	C41, Ubi, mCherry, FMDV2A, E23	pYF Replicon *Renilla* / pCHIKV-mCherry	pYF Replicon *Renilla*

pYFVR cap0 (mCherry)

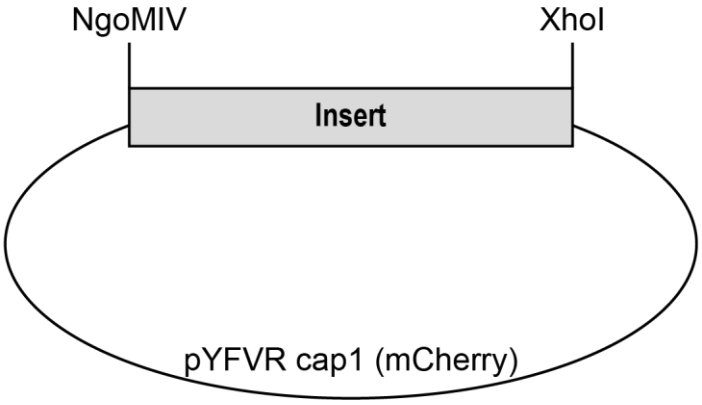

Construct	Insert	Donor/Template	Vector
pYFVR cap0 (mCherry)	NS5-E218A	pYFVR-E218A (Schuberth-Wagner *et al.*, 2015)	pYFVR cap1 (mCherry)

pDENV cap1

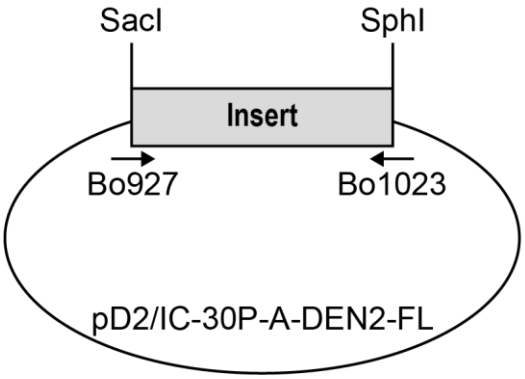

pDENV cap0

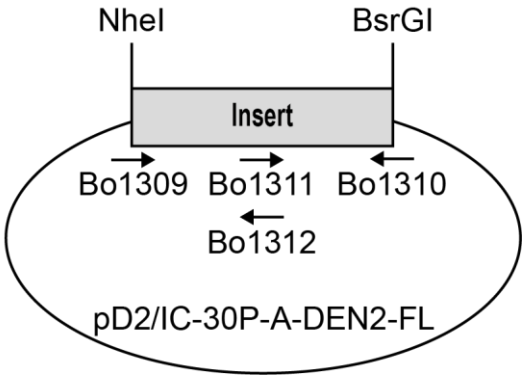

Construct	Insert	Donor/Template	Vector
pDENV cap1	SP6 with G	pD2/IC-30P-A - DEN2-FL (Kinney *et al.*, 1997)	pD2/IC-30P-A - DEN2-FL
pDENV cap0	NS5-E217A	pDENV cap1	pDENV cap1

pDENV-K135A cap1

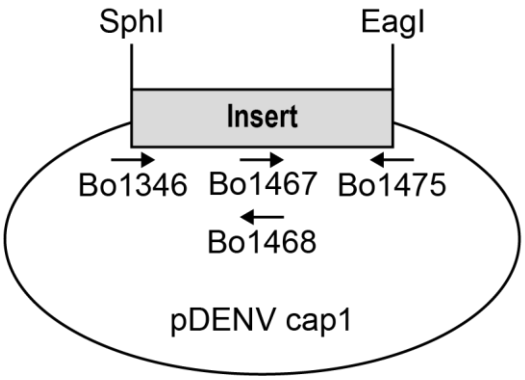

pDENV-K135A cap0

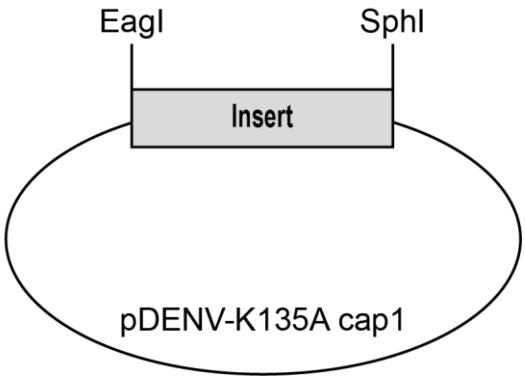

Construct	Insert	Donor/Template	Vector
pDENV-NS2A-K135A cap1	NS2A-K135A	pDENV cap1	pDENV cap1
pDENV-NS2A-K135A cap0	NS5-E217A	pDENV cap0	pDENV-NS2A-K135A cap1

pYFV-Asibi cap1

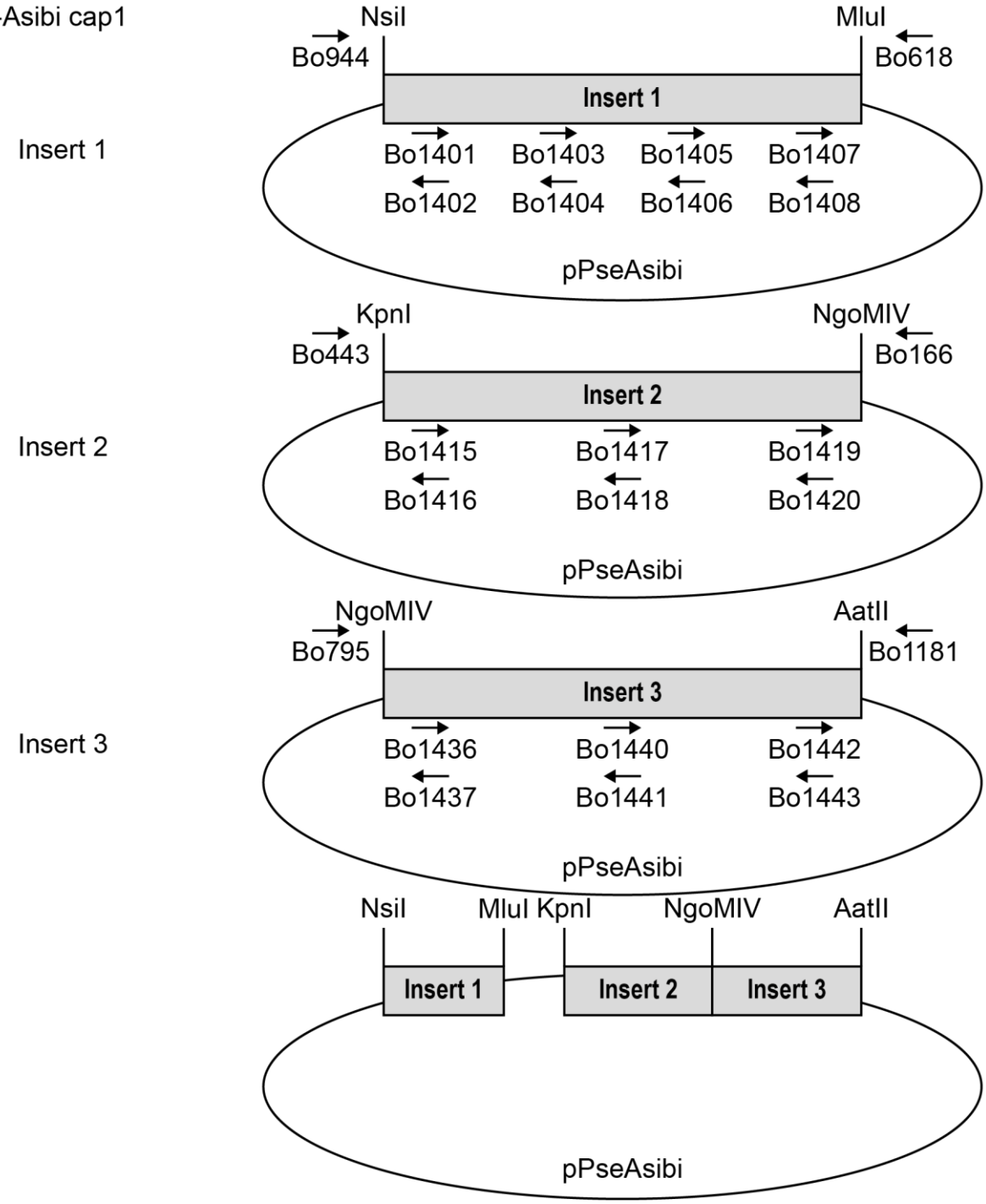

Construct	Insert	Donor/Template	Vector
pYFV-Asibi cap1	E-C2193T, E-G2405C, NS1-G2578T, NS1-G2704A, NS2A-G4025A, NS3-A4864G, NS3-C5926T, 2K-C6829T, NS5-T7945C, NS5-C8008T	pPseAsibi	pPseAsibi

pYFV-Asibi cap0

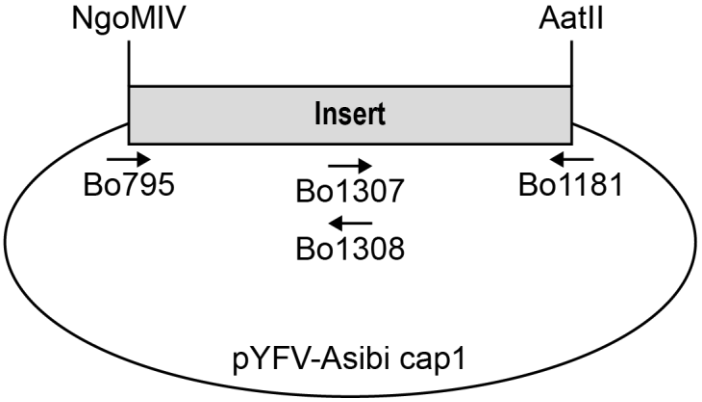

Construct	Insert	Donor/Template	Vector
pYFV-Asibi cap0	NS5-E218A	pYFV-Asibi cap1	pYFV-Asibi cap1

pYFV-Asibi cap1 *Gaussia*

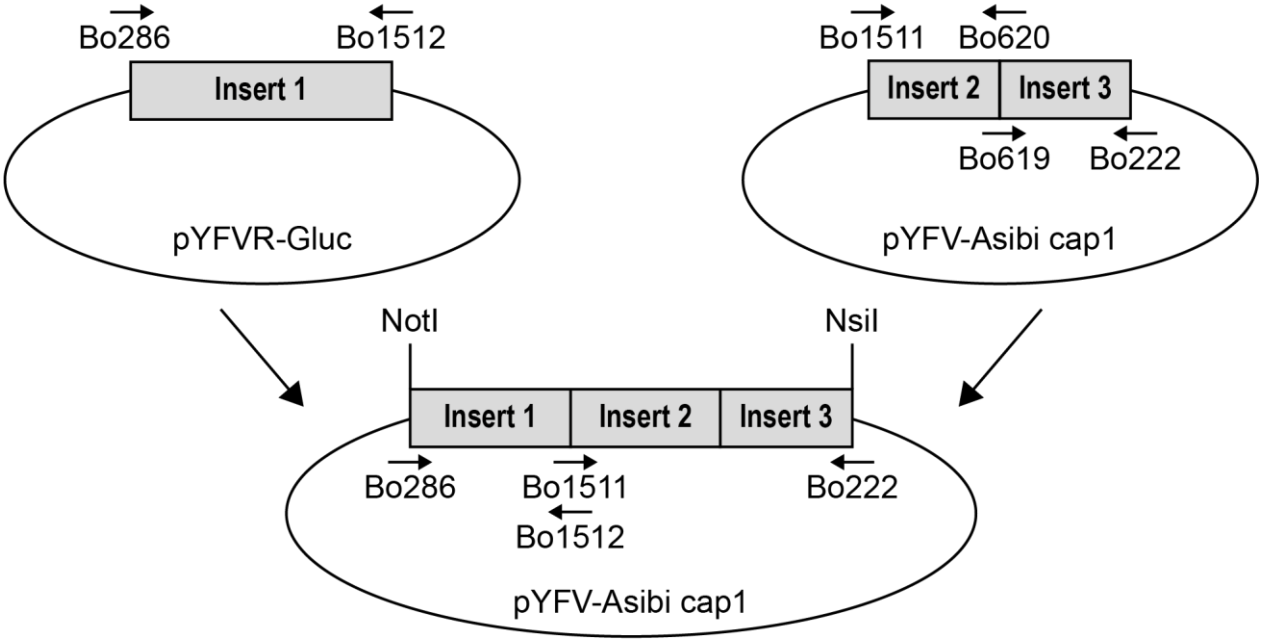

Construct	Insert	Donor/Template	Vector
pYFV-Asibi cap1 *Gaussia*	C25, *Gaussia*, P2A,	pYFV-Asibi cap1, pYFVR Gluc (Lücke *et al.*, 2022)	pYFV-Asibi cap1

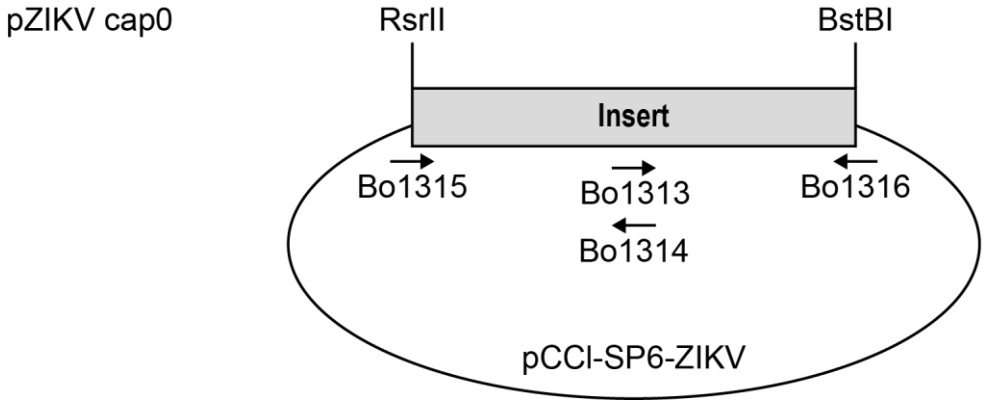

Construct	Insert	Donor/Template	Vector
pZIKV cap0	NS5-E218A	pCCI-SP6-ZIKV	pCCI-SP6-ZIKV

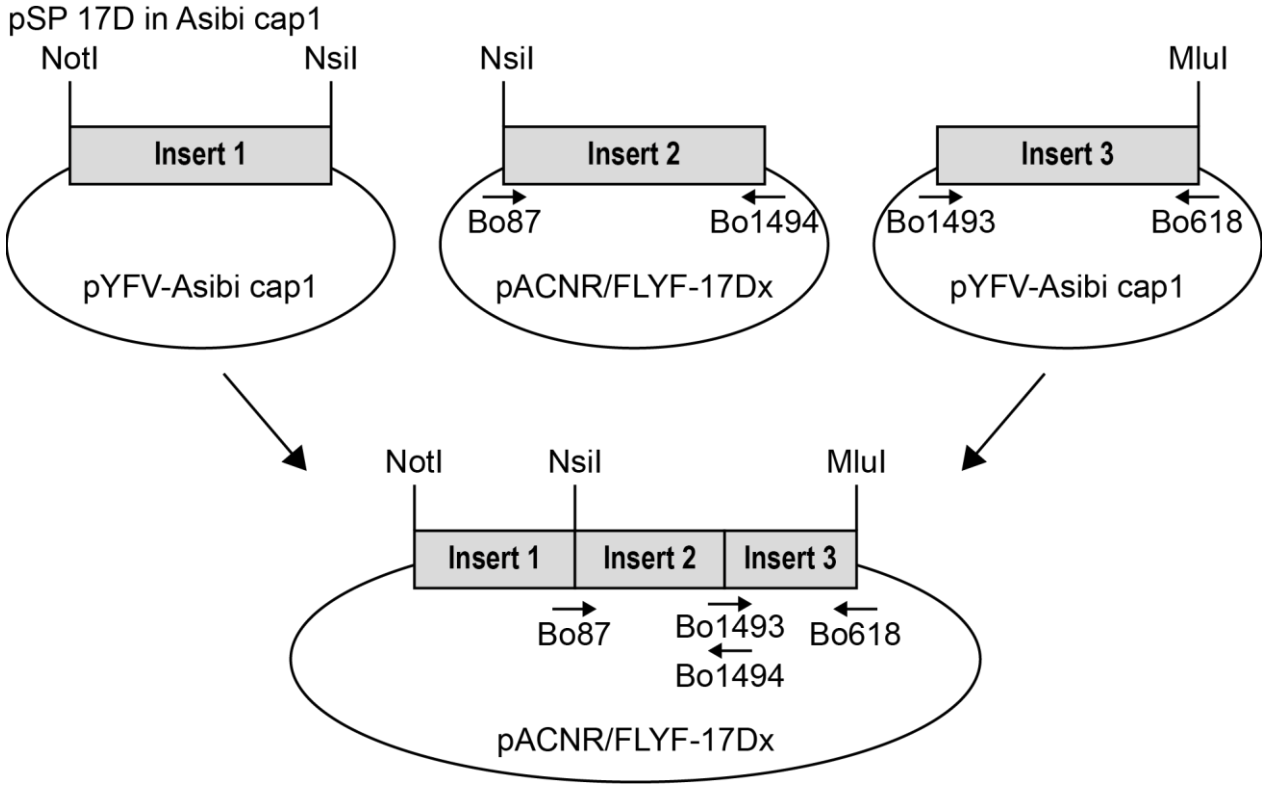

Construct	Insert	Donor/Template	Vector
pSP 17D in Asibi cap1	SP 17D	pACNR/FLYF-17Dx, pYFV-Asibi cap1	pACNR/FLYF-17Dx

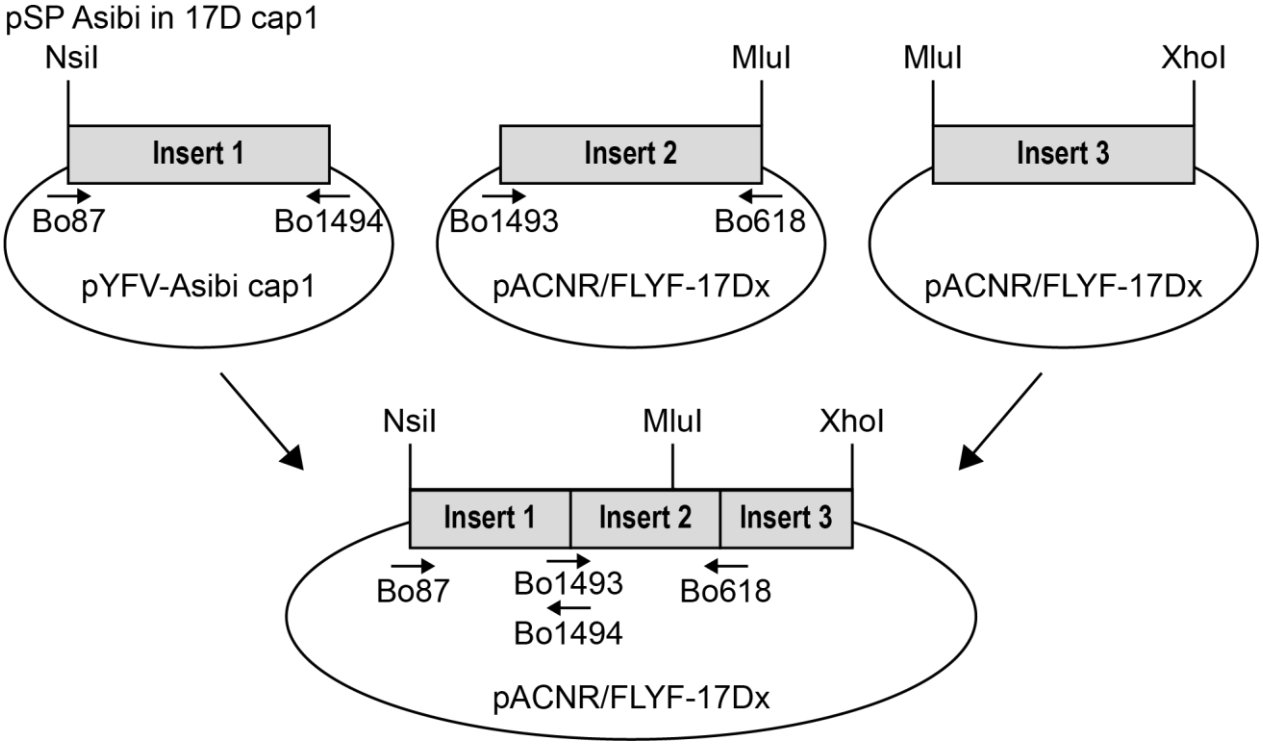

Construct	Insert	Donor/Template	Vector
pSP Asibi in 17D cap1	SP Asibi	pACNR/FLYF-17Dx, pYFV-Asibi cap1	pACNR/FLYF-17Dx

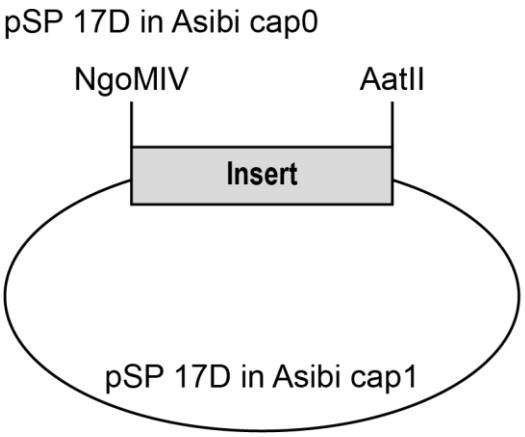

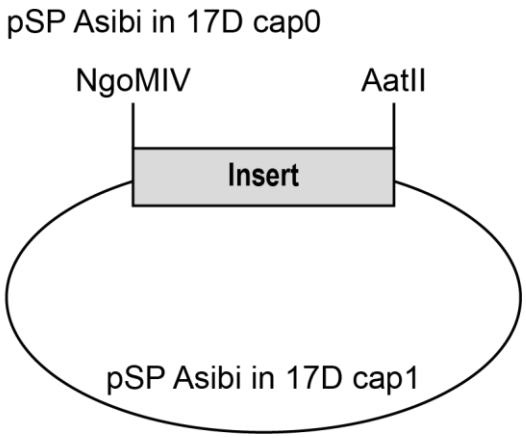

Construct	Insert	Donor/Template	Vector
pSP 17D in Asibi cap0	NS5-E218A	pYFV-Asibi cap0	pSP 17D in Asibi cap1
pSP Asibi in 17D cap0	NS5-E218A	pYFV-17D cap0	pSP Asibi in 17D cap1

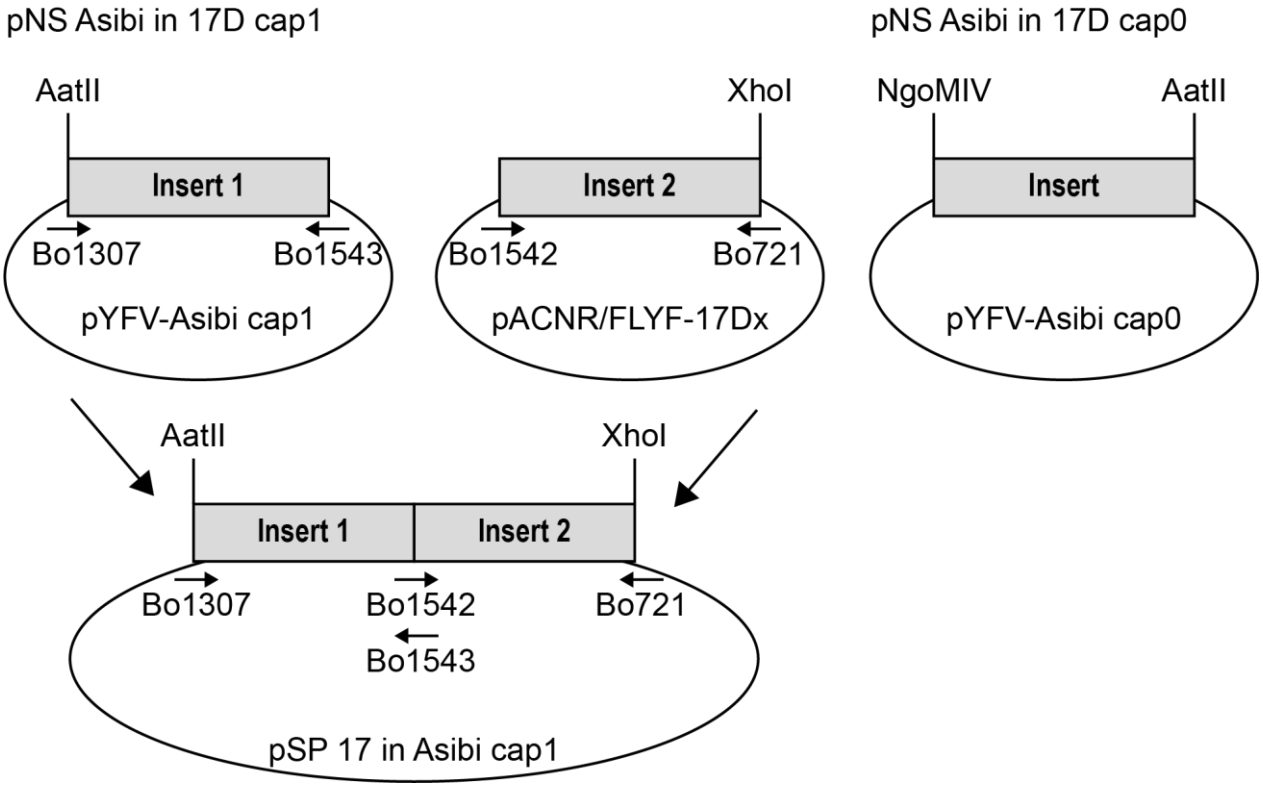

Construct	Insert	Donor/Template	Vector
pNS Asibi in 17D cap1	3'UTR 17D	pYFV-Asibi cap1, pACNR/FLYF-17Dx	pSP 17D in Asibi cap1
pNS Asibi in 17D cap0	NS5-E218A	pYFV-Asibi cap0	pNS Asibi in 17D cap1

pNS4A*-3'UTR Asibi in 17D cap1

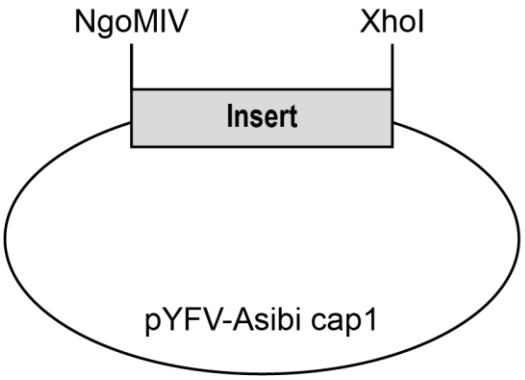

pNS4A*-3'UTR Asibi in 17D cap0

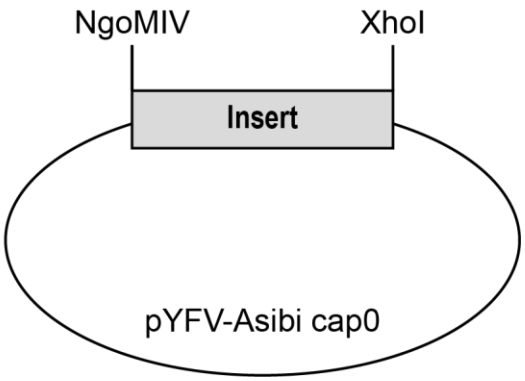

Construct	Insert	Donor/Template	Vector
pNS4A*-3'UTR Asibi in 17D cap1	NS4A*-3'UTR	pYFV-Asibi cap1	pACNR/FLYF-17Dx
pNS4A*-3'UTR Asibi in 17D cap0	NS4A*-3'UTR (incl. E218A)	pYFV-Asibi cap0	pACNR/FLYF-17Dx

pNS5 Asibi in 17D cap1/ pNS5 Asibi in 17D cap0

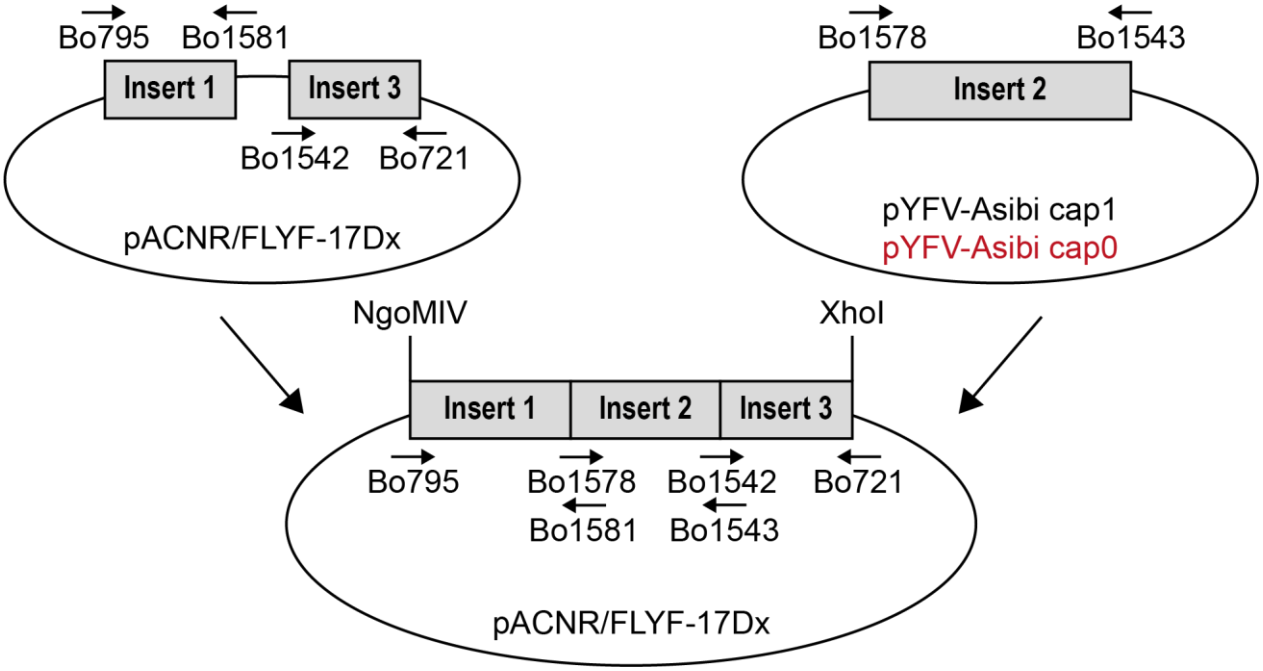

Construct	Insert	Donor/Template	Vector
pNS5 Asibi in 17D cap1	NS5	pACNR/FLYF-17Dx, pYFV-Asibi cap1	pACNR/FLYF-17Dx
pNS5 Asibi in 17D cap0	NS5-E218A	pACNR/FLYF-17Dx, pYFV-Asibi cap0	pACNR/FLYF-17Dx

pNS5 17D in Asibi cap1/ pNS5 17D in Asibi cap0

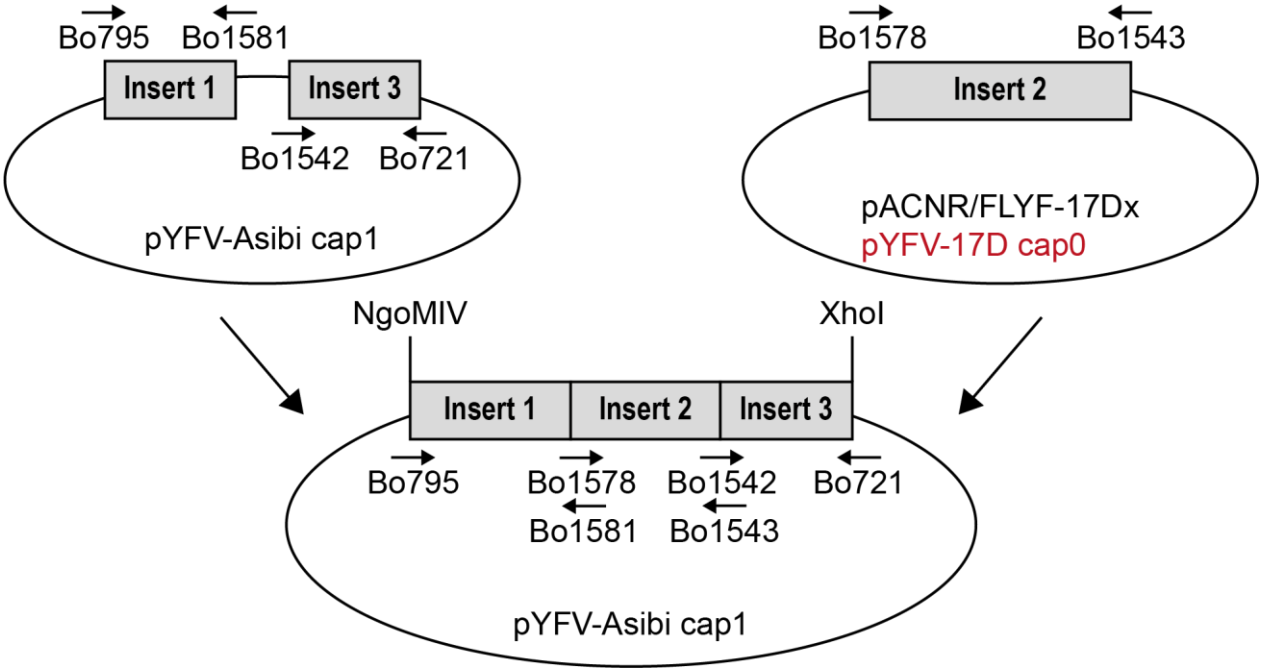

Construct	Insert	Donor/Template	Vector
pNS5 17D in Asibi cap1	NS5	pYFV-Asibi cap1, pACNR/FLYF-17Dx	pYFV-Asibi cap1
pNS5 17D in Asibi cap0	NS5-E218A	pYFV-Asibi cap1, pYFV-17D cap0	pYFV-Asibi cap1

p2K-NS4B Asibi in 17D cap1/ p2K-NS4B Asibi in 17D cap0

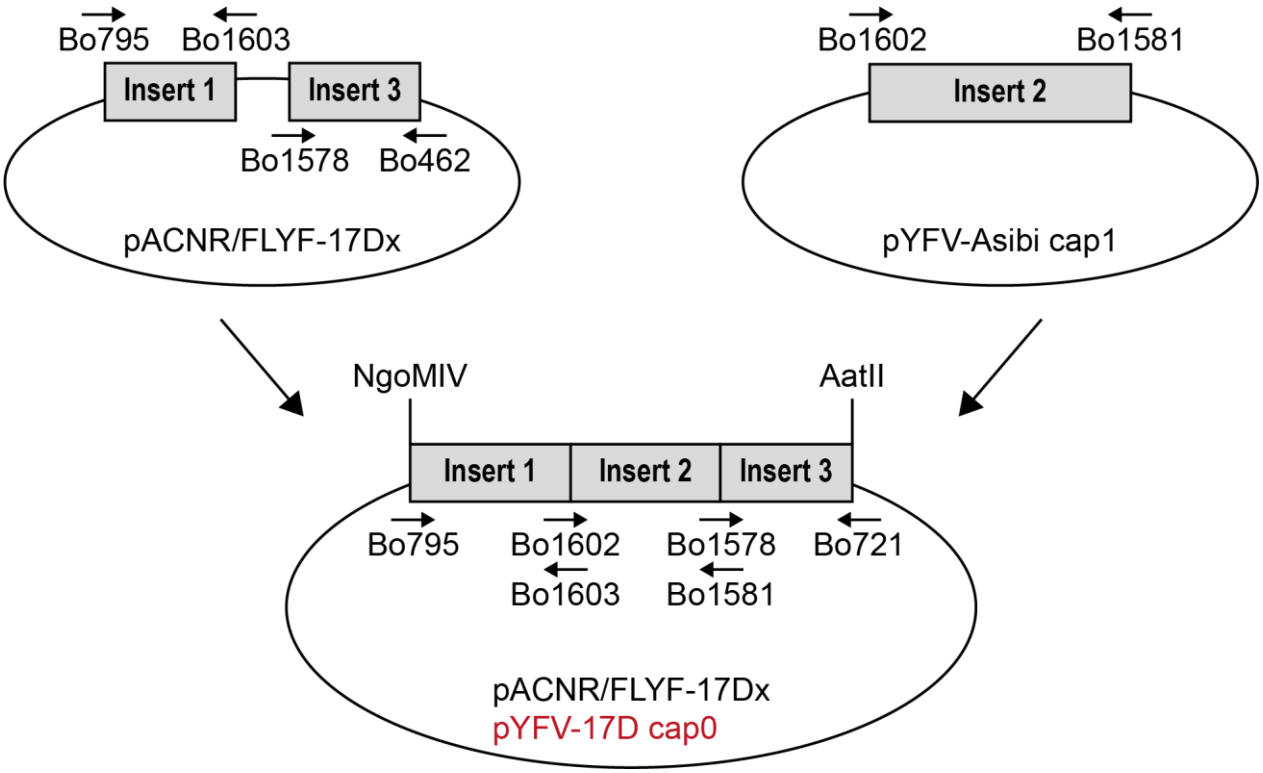

Construct	Insert	Donor/Template	Vector
p2K-NS4B Asibi in 17D cap1	2K-NS4B	pYFV-Asibi cap1, pACNR/FLYF-17Dx	pACNR/FLYF-17Dx
p2K-NS4B Asibi in 17D cap0	2K-NS4B	pYFV-Asibi cap1, pACNR/FLYF-17Dx	pYFV-17D cap0

p2K-NS5 Asibi in 17D cap1/ p2K-NS5 Asibi in 17D cap0

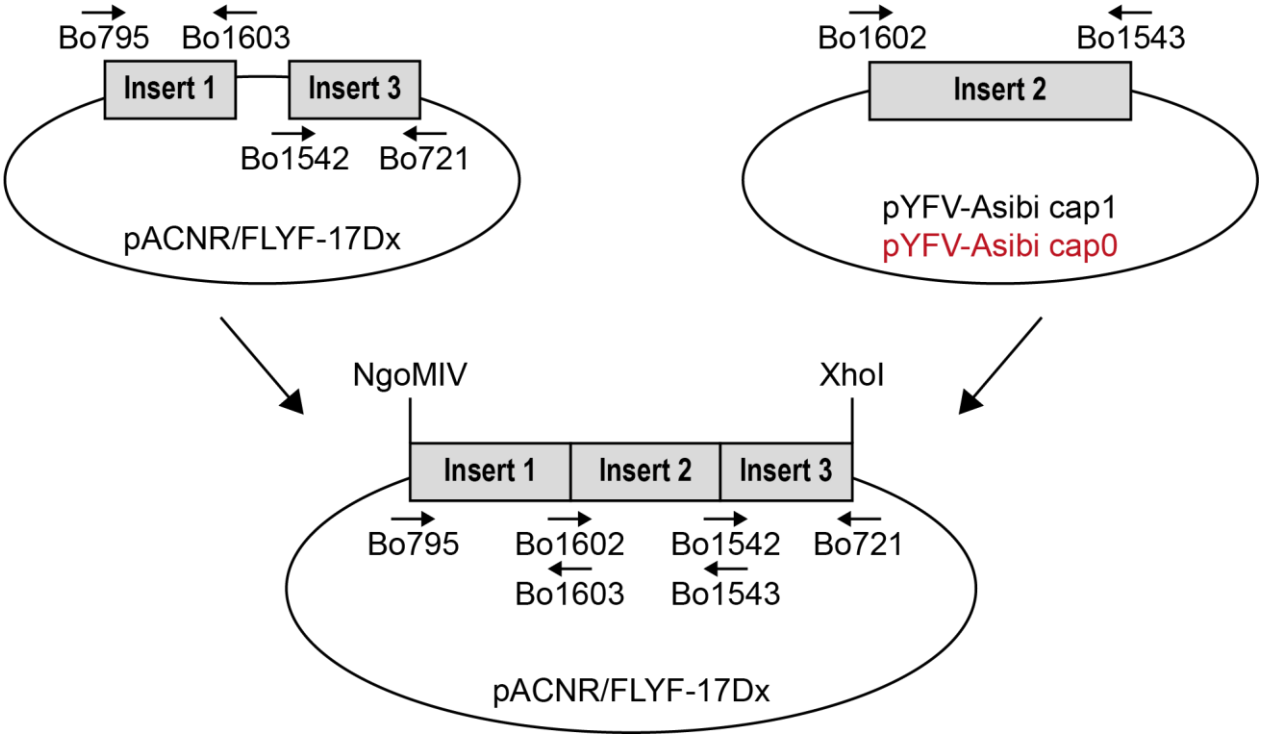

Construct	Insert	Donor/Template	Vector
p2K-NS5 Asibi in 17D cap1	2K-NS5	pACNR/FLYF-17Dx, pYFV-Asibi cap1	pACNR/FLYF-17Dx
p2K-NS5 Asibi in 17D cap0	2K-NS5-E218A	pACNR/FLYF-17Dx, pYFV-Asibi cap0	pACNR/FLYF-17Dx

pNS4A-NS5 Asibi in 17D cap1 / pNS4A-NS5 Asibi in 17D cap0

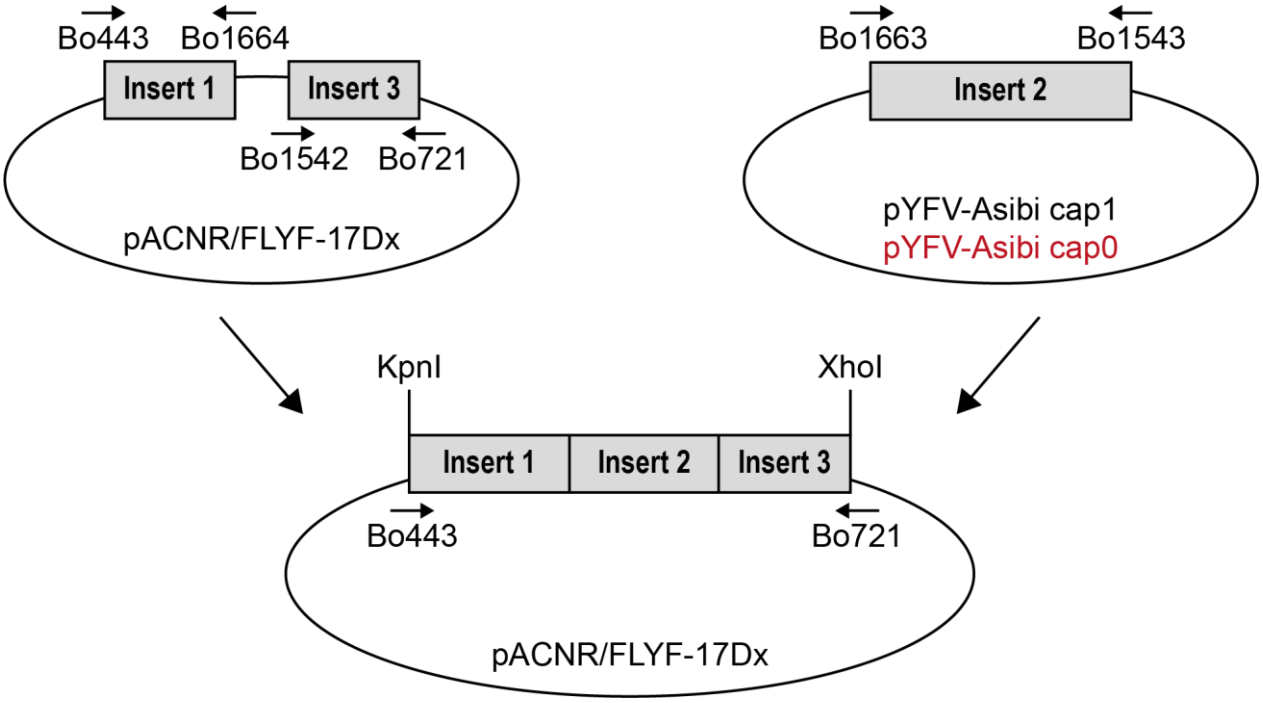

Construct	Insert	Donor/Template	Vector
pNS4A-NS5 Asibi in 17D cap1	NS4A-NS5	pACNR/FLYF-17Dx, pYFV-Asibi cap1	pACNR/FLYF-17Dx
pNS4A-NS5 Asibi in 17D cap0	NS4A-NS5-E218A	pACNR/FLYF-17Dx, pYFV-Asibi cap0	pACNR/FLYF-17Dx